SYNTHESES OF METAL-BINDING POLYMERS TO CREATE FUNCTIONAL FILMS THAT SELECTIVELY CAPTURE PROTEINS

By

Salinda Wijeratne

A DISSERTATION

Submitted to
Michigan State University
in partial fulfillment of the requirements
for the degree of

Chemistry-Doctor of Philosophy

2016

ABSTRACT

**SYNTHESES OF METAL-BINDING POLYMERS TO CREATE FUNCTIONAL FILMS
THAT SELECTIVELY CAPTURE PROTEINS**

By

Salinda Wijeratne

Purification is often the most difficult step in producing proteins for both research and therapeutic applications. Among various protein-purification platforms, modified porous membranes are especially appealing because convective mass transport in small pores overcomes the diffusion limitations characteristic of bead-based columns.

Polymer brushes are attractive for capturing proteins, but their high density may provide steric constraints on protein binding. I designed and synthesized several monomers with long, cleavable side chains. Removal of these side chains after polymerization should reduce brush chain density and provide the space necessary to capture large amounts of protein. Growth of the polymer brushes gave 100 nm-thick films, but unfortunately upon cleaving the side chains, the polymer brushes collapsed to prevent further functionalization. Additionally, synthesis of brush-modified surfaces is cumbersome, frequently requiring deposition of initiator molecules and polymerization under inert conditions. Thus, I developed much simpler methods for creating highly-swollen or porous films for protein binding.

In an initial study, I synthesized the metal-binding polymers poly(*N,N*-dicarboxymethylallyl amine) (PDCMAA) and carboxymethylated polyethyleneimine (CMPEI). These polymers contains iminodiacetic acid groups, which readily form metal-ion complexes that may selectively capture proteins with hexahistindine clusters (His-tags) at their termini. LBL adsorption of multilayer protonated poly(allylamine)

(PAH)/PDCMAA films is a simple, economical method to introduce metal-ion-binding groups onto a surface. Remarkably, 10-bilayer PAH/PDCMAA films are 1 µm thick, and these coatings have a very high Cu^{2+} binding capacity (~2.5 mmol/cm^3 of film, or 2.5 M). However, PAH/PDCMAA films do not swell sufficiently for extensive protein capture. In contrast, sequential adsorption of PAH and CMPEI leads to membranes that bind Ni^{2+} and capture ~60 mg of His-tagged ubiquitin per mL of membrane, which is higher than capacities of commercial beads. Compared to PDCMAA, the more hydrophilic polyethyleneimine in CMPEI might enhance swelling.

In some cases minimizing the metal-ion leaching from membranes is important to avoid contaminating proteins. Therefore, I synthesized another series of polymers containing the stronger metal-ion-binding ligand nitrilotriacetate (NTA). Due to the high cost of commercial NTA derivatization reagents, I established a novel route to synthesize NTA-containing polymers, poly(NTA), at minimal cost. Sequential adsorption of PAH and poly(NTA) yields membranes that bind Ni^{2+} and capture ~40 mg of His-tagged ubiquitin per mL of membrane.

Introduction of porosity may enhance the kinetics of protein binding in polyelectrolyte films. Development of porous films through adsorption of star-poly(dimethylaminoethyl methacrylate) [PDMAEMA] and star-poly(acrylic acid) [PAA], creates highly swollen films that bind as much as 10-20 multilayers of lysozyme. Sequential adsorption of star-PDMAEMA and star-PAA leads to membranes that capture ~120 mg of lysozyme per mL of membrane, which is about 3 times the capacity of commercial ion-exchange membranes.

I dedicate this dissertation to my parents, my wife and my brothers for their love and support......!

ACKNOWLEDGEMENTS

I am yet to fully grasp that I have come to the end of a long, challenging, but rewarding journey through graduate school. I could never have come this far without the guidance, inspiration, and support of many wonderful people.

I sincerely thank my advisors Prof. Merlin L. Bruening and Gregory L. Baker for their guidance, understanding, patience, and support through my graduate studies at Michigan State University. I am forever grateful to them for their continuous motivation and encouragement, and for guiding me to grow as an independent scientist. Without their guidance and persistent help, this dissertation and all the publications would not have been possible.

To the members of my guidance committee, Prof. Robert Maleczka, Prof. Babak Borhan and Prof. William Wulf, I am sincerely thankful to all of you. I thank Prof. Robert Maleczka and Prof. Babak Borhan for their tremendous guidance throughout my graduate career.

I am extremely grateful to current and past Baker and Bruening research group members, and my friends for their help and most of all making grad school an enjoyable experience. I thank my lovely parents without whom I would have not been who I am today. I am fortunate to have such parents for constant source of love, concern, support and strength. I thank my loving wife, for her understanding and constant encouragement. Last, but not least, I owe my success to all who contributed for my journey.

TABLE OF CONTENTS

LIST OF TABLES

LIST OF FIGURES

LIST OF SCHEMES

KEY TO ABBREVIATIONS

Aminobutyl NTA $N\alpha$, $N\alpha$ –bis(carboxymethyl)-L-lysine hydrate

ATR   Attenuated total reflectance

ATRP   Atom-transfer radical polymerization

AAS   Atomic absorption spectroscopy

FTIR   Fourier Transform Infrared

DMF N,N-dimethylformamide

EDC   1-(3-(Dimethylamino)propyl)-3-ethylcarbodiimide hydrochloride

EDTA   Ethylenediaminetetraacetic acid

HEMA   2-hydroxyethyl methacrylate

His-tag   Histidine-tag

HisU   Histidine$_6$-tagged Ubiquitin

HMTETA   1,1,4,7,10,10-Hexamethyltriethylenetetramine

IMAC   Immobilized metal-affinity chromatography

LbL   Layer-by-layer

Me$_6$TREN   Tris(2-(dimethylamino)ethyl)amine

MPA   3-mercaptopropionic acid

MS   Mass spectrometry

NHS   N-Hydroxy succinimide

NTA   Nitrilotriacetate

PAA   Poly(acrylic acid)

PAH	Poly(allylamine)
PEI	Polyethyleneimine
PEMs	Polyelectrolyte multilayers
PNTA	Poly(2,2-(5-acrylamido-1-carboxypentylazanediyl) diacetic acid)
Poly(MES)	Poly(2-(methacryloyloxy)ethyl succinate)
PSS	Poly(sodium styrene sulfonate)
PVAm	Poly(vinyl amine)
PAGE	Polyacrylamide gel electrophoresis
SEM	Scanning electron microscope
SI-ATRP	Surface initiated atom-transfer radical polymerization

CHAPTER 1. INTRODUCTION AND BACKGROUND.

1.1. Introduction.

This dissertation focuses primarily on creating functional polymer films that bind metal ions and in turn selectively capture His-tagged proteins. We are particularly interested in modifying porous membranes to improve protein-binding kinetics and capacities and purify proteins more rapidly and efficiently than current column-based systems. Although the Bruening group previously developed high-performance membranes that capture His-tagged proteins,[1] this study aims to develop metal-ion-binding polymers for direct adsorption in membrane pores to enable more rapid and less expensive membrane modification. The research includes synthesis of initiators, monomers and polymers for creating functionalized films with enhanced protein binding properties. Development of coatings with different metal-ion-binding ligands and architectures in some cases leads to decreased metal-ion leaching and enhanced protein binding. Subsequent chapters will describe the strategies we employ to enhance protein access to metal-ion complexes, decrease metal-ion leaching and simplify film deposition.

To put the work in perspective, this chapter first explains the significance of protein purification and then describes protein-purification methods and their challenges. Subsequent sections present the advantages and limitations of membrane-based protein purification and previous approaches to address the low capacity of protein-adsorbing membranes. Finally, I provide an outline of our strategies for conveniently modifying membranes to rapidly capture large amounts of tagged protein.

1.2. Background.

1.2.1. Significance of Protein Purification.

Protein purification is fundamental to basic protein research as well as the production of therapeutic antibodies,[2-4] and the expanding demand for pure protein[5] challenges current separation methods.[6] Isolation of a particular protein is vital to minimize degradation, remove impurities that might interfere with functionality, and eliminate toxins from proteins used as therapeutics.[7]

1.2.2. Challenges Associate with Obtaining Pure Protein.

Although recent advances in cell culture technology have increased the amount of protein in culture media, purification remains a bottleneck in protein production.[8,9] Figure 1.1 shows a sodium dodecyl sulfate–polyacrylamide gel electrophoresis (SDS-PAGE) analysis of purification of COP 9 signalosome complex subunit 8 (CSN 8). Lane 2, a cell lysate from an organism, shows a myriad of proteins and partially indicates the complexity of the lysate. Thus, isolating only CSN 8 protein from such a complicated mixture is a major challenge. Nevertheless, as Lane 4 suggests remarkable purification is possible when using genetically tagged proteins.
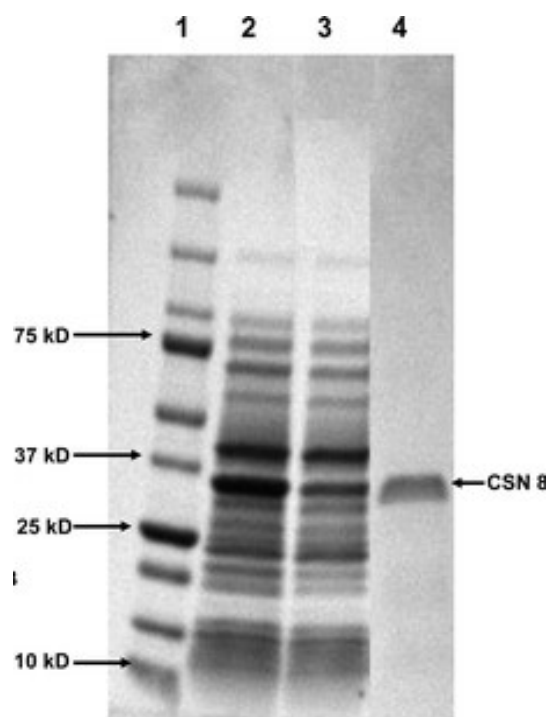
Figure 1.1. SDS-PAGE analysis of purification of polyhistidine-tagged COP 9 signalosome complex subunit 8 (CSN 8) from a cell lysate: (Lane 1) protein ladder, (Lane 2) a cell extract from BL21DE3 cells with tagged CSN 8, (Lane 3) effluent from the membrane loading, and (Lane 4) the eluate. (Figure adapted from reference 1 with permission from the American Chemical Society.)[1]

Several methods are available for protein purification,[2,3,5,10-12] and among these chromatographic techniques are powerful and versatile. In these techniques, various immobilized functional moieties such as ion-exchange groups,[13] hydrophobic molecules or affinity ligands[14] capture the desired proteins. Ion-exchange chromatography[11] isolates proteins based on their charge density (Figure 1.2a), whereas gel-filtration chromatography separates[15] these macromolecules based on their sizes (Figure 1.2b). In affinity purification, scientist design an affinity tag on recombinant proteins, and this

specific tag serves as a "handle" to isolate the protein of interest from the mixture of proteins (Figure 1.2c).[14,16]

(a) Ion-exchange chromatography   **(b) Gel-filtration chromatography**   **(c) Affinity chromatography**

Solvent flow   Solvent flow   Solvent flow

Positively charged beads

Bound negatively charged proteins

Free positively charged proteins pass through

Porous beads

Small proteins

Large proteins pass through

Beads with the affinity ligand

Bound protein

Unbound proteins pass through

Figure 1.2. Different types of chromatographic methods for protein purification.

1.2.3. The Most Powerful Protein Purification Method: Affinity Chromatography.

Because of its high specificity, affinity chromatography[17] is the most powerful method to isolate a single target protein from complex biological fluids. (Affinity adsorption is probably a better name for this technique, which typically occurs in a batch mode.) This method relies on specific interactions between functional groups (ligands attached to a solid surface) and the tag appended to the protein. Common affinity interactions include polyhistidine tags (His-tags) binding to metal-ion complexes,[18]

maltose tags adsorbing to carbohydrate matrices,[19] appended glutathione-s-transferase binding to glutathione[20] and streptavidin capturing proteins with biotin.[21]
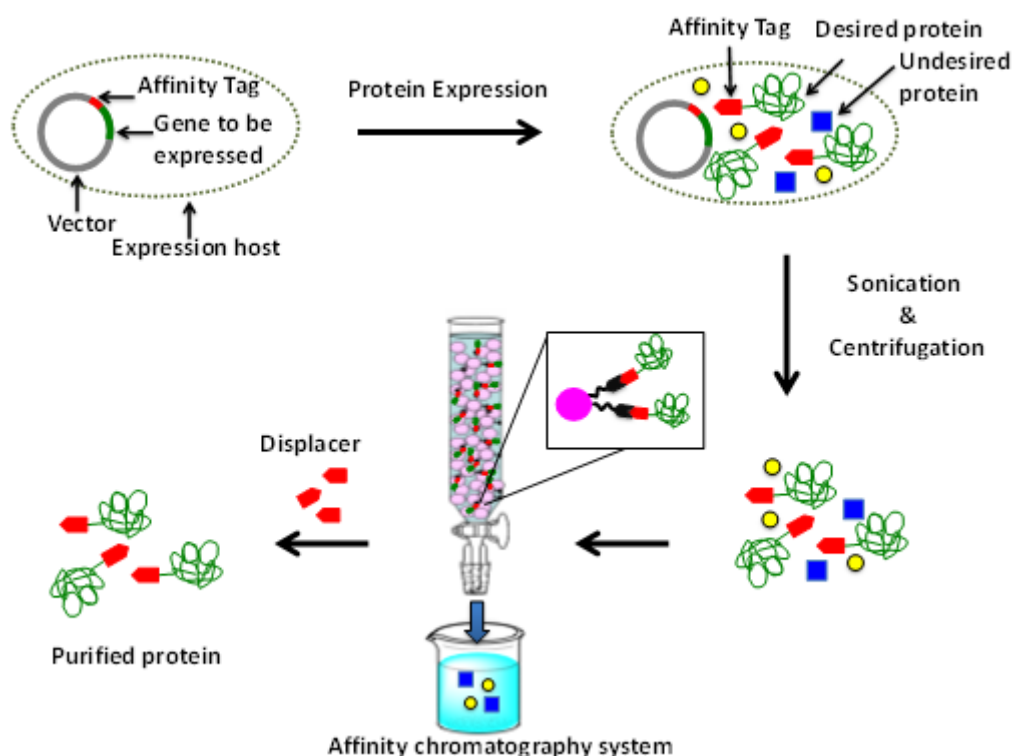
Figure 1.3. Expression and purification of a recombinant, tagged protein.

Figure 1.3 illustrates the general protocol for recombinant protein production and separation, where the specific binding of the protein to the solid surface is vital for obtaining highly pure protein. This research mainly focuses on His-tagged proteins binding to metal-ion complexes, so the following section describes protein purification with this tag.

1.2.4. Immobilized Metal Affinity Chromatography (IMAC) for His-tagged Protein Purification.

Porath et al. introduced the IMAC concept in the mid-1970s.[22] In this technique, metal ions such as Ni^{2+}, Co^{2+} or Cu^{2+} bind to immobilized chelating ligands such as imminodiacetic acid (IDA) or nitrilotriacetic acid (NTA).[23-25] During the purification, these metal-ion complexes bind to a functional group on the protein, frequently a polyhistidine tag, and subsequent rinsing and elution yield predominantly the tagged protein.

Depending on the immobilized metal-ion-ligand complex, histidine, tryptophan or cysteine can serve in tags, but polyhistidine tags are most common.[22,23,26] In His-tagged protein purification, metal-ion complexes will specifically bind to imidazoles of the tag (Figure 1.4).[25] The amount of protein binding depends on the number and position of the histidine residues on the tag. Thus, during the expression of the recombinant protein in bacterial cells, a short DNA sequence for multiple histidine residues (typically 6) is appended to the N- or C-terminus of the gene of the protein of interest.[27,28] This His-tag on the protein binds to the metal complexes[27,29] as shown in Figure 1.4.

Figure 1.4. Models of the interactions between polyhistidine affinity tags and two immobilized metal-ion-ligand complexes: (a) Ni^{2+}–immunodiacetate (Ni^{+2}–IDA) and (b) Ni^{2+}–nitrilotriacetacte (Ni^{+2}–NTA).[30]

The most common metal-ion ligands, IDA and NTA, occupy three or four metal-ion coordination sites, respectively. This typically leaves at least two free coordination sites,[28] so His-tagged proteins coordinate with the metal-ion complexes during the purification process (Figure 1.4). However, most proteins contain one or more native histidine residues, which might cause non-specific binding and decrease the purity of isolated protein. Selection of Ni^{2+} as the coordinating ion leads to relatively weak complexes with single histidine residues and little non-specific adsorption. In contrast, the Histindine$_6$ tag forms very strong complexes with immobilized Ni^{2+} ($K_d = 10^{-13}$ M at pH 8.0 and 10^{-6} to 10^{-8} M at pH 7.0-7.4)[31,32] to efficiently capture the tagged protein. Displacement agents (usually free imidazole) that bind to immobilized metal ions can elute specifically bound His-tagged proteins, and alternative elution strategies include changing pH and ionic strength.[28]

IMAC has many assets such as low cost, high specificity, simplicity and mild elution conditions. This technique can rapidly isolate polyhistidine-tagged proteins with 100-fold enrichment in a single purification step, and purities may exceed 95%.[33] Furthermore, variation of metal-ion-ligand systems and pH and ionic strength allow optimization of selectivity. Reuse of IMAC resins can occur with minimal loss of performance and selectivity.[29] Nevertheless, careful selection of the stationary phase for IMAC is important to achieve high efficiency and low production cost. The following section discusses specific stationary phases.

1.2.5. Common Stationary Phases for IMAC and Their Assets and Limitations.

The most popular IMAC format employs packed-bead columns (Figure 1.3 and Figure 1.5a). In such a system flow of the mobile phase brings the solution to the bead surface, and the target protein selectively binds to immobilized metal-ion complexes while other components pass through the column with the mobile phase. Subsequent rinsing removes remaining impurities, and in the final step target protein elutes from the column upon displacement from the surface by a competitive reagent.[28]

The main limitation of most bead-packed columns is slow diffusion-limited transport of proteins into bead pores.[7,34-36] Additionally, compact stationary phases give rise to large pressure drops across the packed bed and uniform packing of large-scale columns is difficult.[7,12,16,37] Non-porous chromatographic media may overcome diffusion limitations, but these systems are relatively expensive and have a low binding capacity due to low surface area.[38]
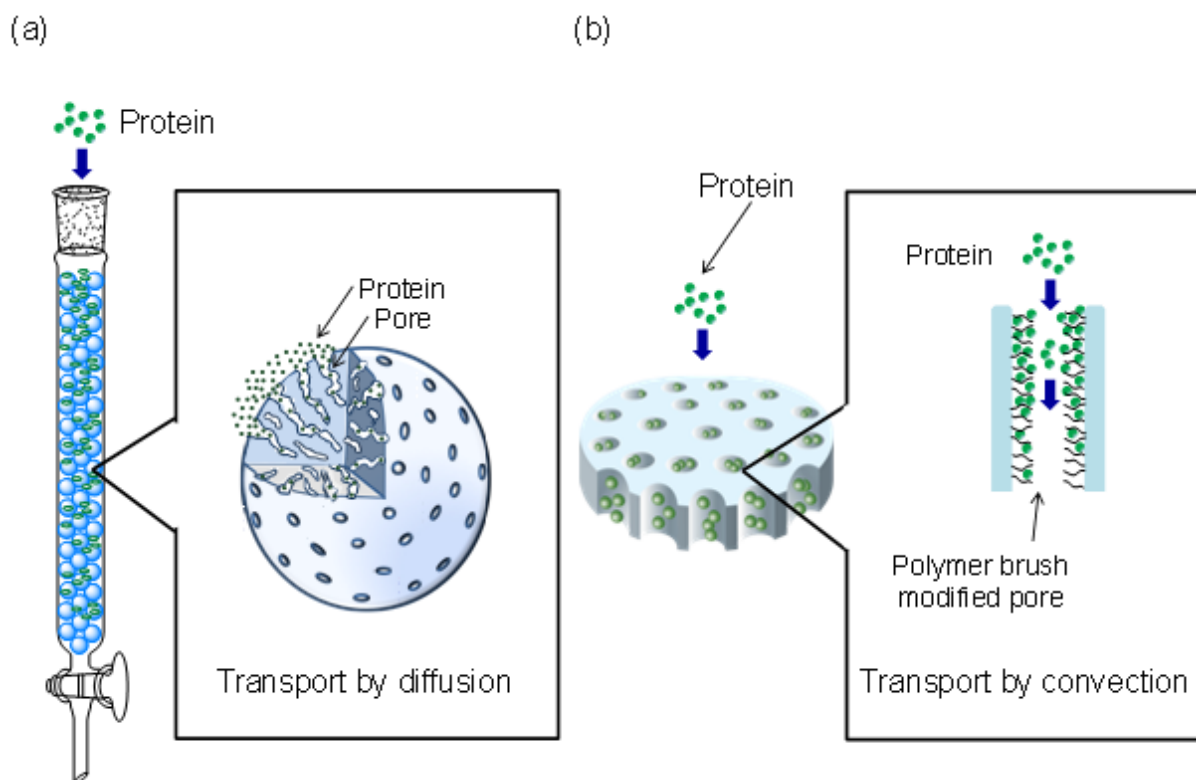
Figure 1.5. Protein transport to affinity sites: (a) diffusion in nanoporous beads; (b) convection in membrane pores.[10, 37]

Porous membranes are emerging as an attractive solid support for IMAC, and various reviews discuss the advantages of membrane adsorbers over packed columns for protein purification.[2,7,21,35,39] In contrast to bead-packed columns, flow through membrane pores (convective transport) brings proteins to binding sites (Figure 1.5b). Convective transport minimizes limitations from diffusional mass-transfer resistance.[37] Additionally, membranes are thinner than packed beds, so the pressure drop across the membrane is significantly lower than that in a packed column. These advantages make membrane purification systems appealing for large-scale, "high-rate" protein purification.[3,7,40]

Although membrane adsorbers are attractive for rapid purification, due to low internal surface area they suffer from low binding capacities. Unmodified membranes typically have specific surface areas of only 10 m^2/g,[41] and they ordinarily bind less than a monolayer of protein in their pores. Grafting polymer brushes in the pores of membranes is a common approach to increase protein capture. In 1990 Müller et al. proposed using polymer brushes containing ion-exchange sites to capture multilayers of protein in membranes.[42] Membrane pores modified with polymer chains bound several layers of a protein with a 10-nm diameter (Figure 1.6).[41]
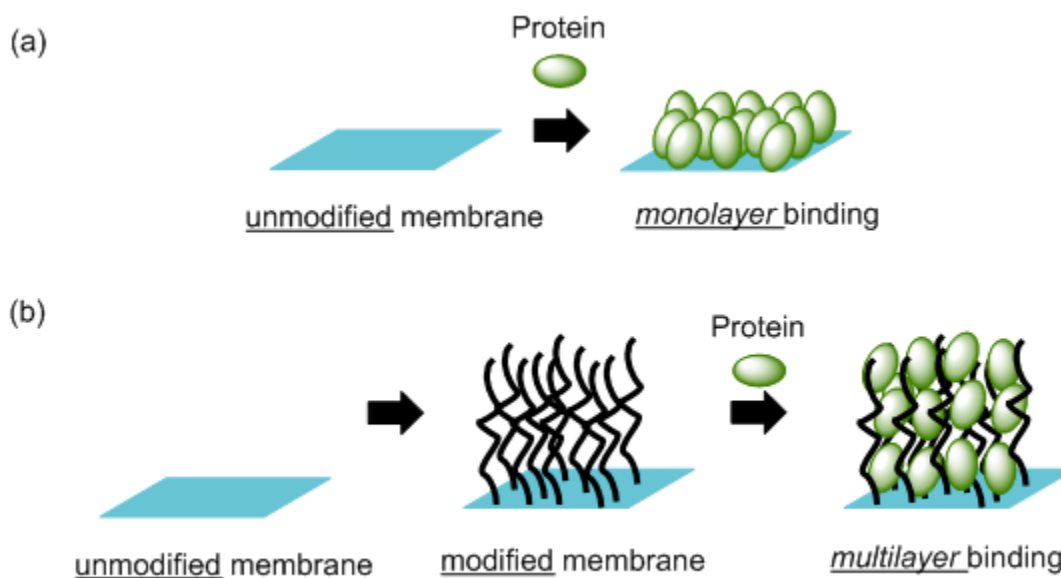
Figure 1.6. Capture of (a) a monolayer of protein on an unmodified membrane surface and (b) a multilayer of protein on a membrane surface modified with a polymer brush.[41]

Much of the ongoing research with membrane adsorbers, including research in this dissertation, focuses on modifying membranes with polymer brushes and polymer films to improve the efficiency and capacity of the membrane matrices. Thus, the next

section discusses methods for modifying the membrane surface to improve protein-binding capacities and kinetics.

1.2.6. Surface-modification Strategies for Increasing Protein-binding Capacities.

1.2.6.1. Polymer Brush-modified Surfaces.

Polymer brushes are assemblies of polymer chains tethered to a substrate (Figure 1.8).[43] When derivatized with suitable ligands, such brushes can immobilize multilayers of proteins (Figure 1.7).
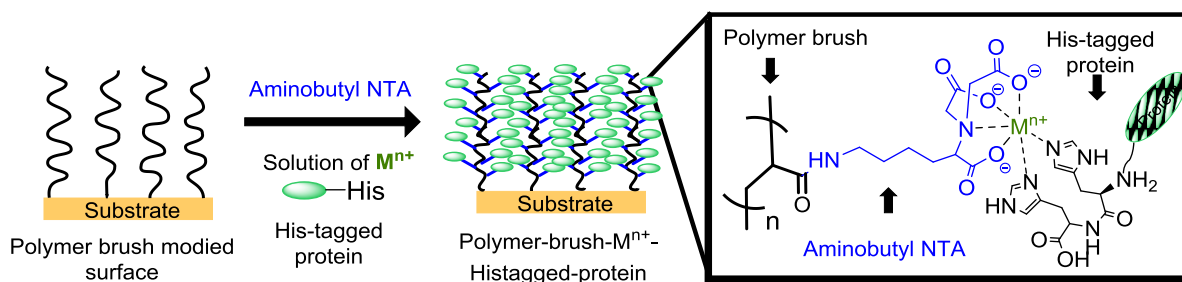
Figure 1.7. Multilayer binding of a His-tagged protein to an acrylic acid brush derivatized with aminobutyl NTA.[44]

1.2.6.1.1.Methods for Growing Polymer Brushes on Surfaces.

There are two primary methods for growing polymer brushes on solid surfaces, physisorption[45,46] (Figure 1.8a) and covalent attachment[47] (Figure 1.8b).
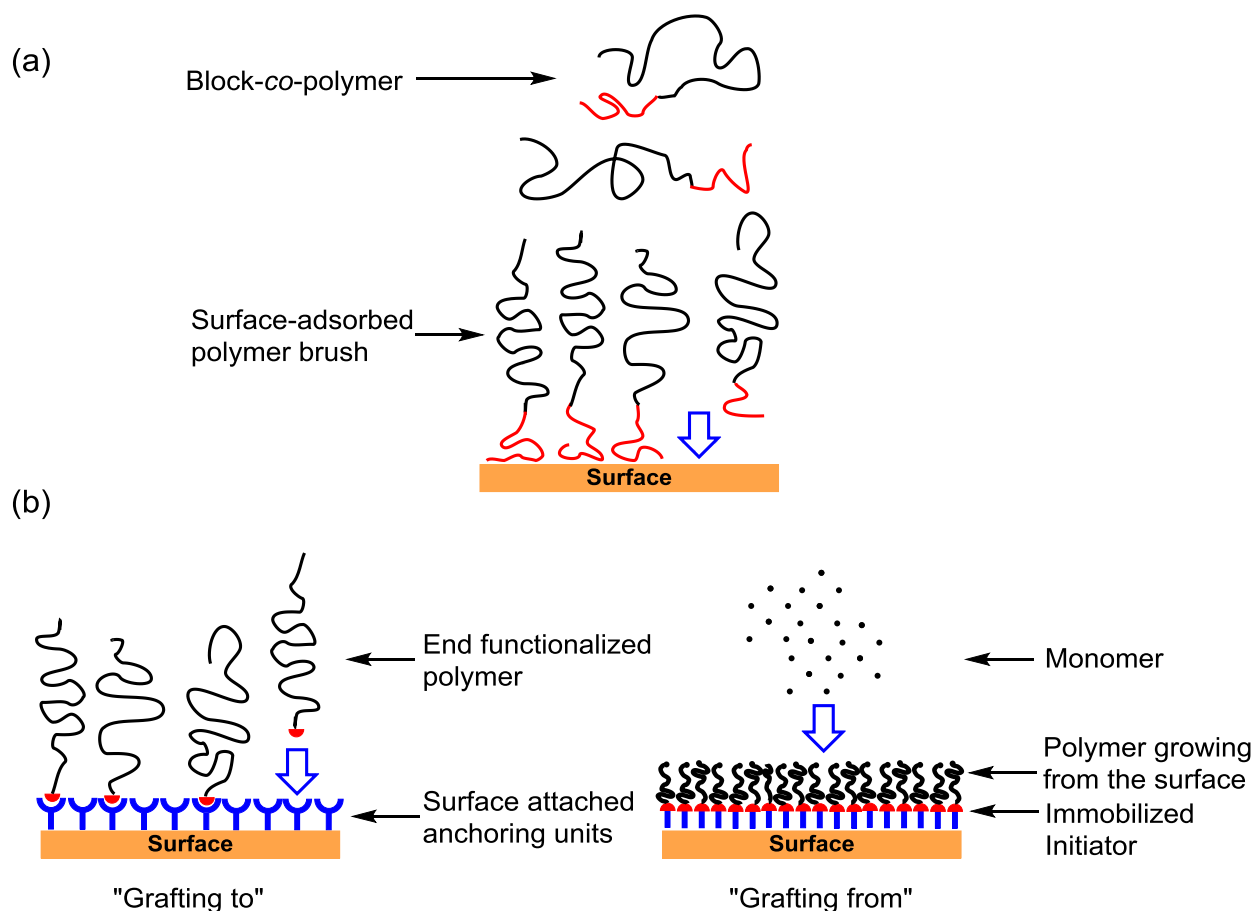
Figure 1.8. Polymer brush formation through (a) physisorption of a block copolymer and (b) covalent attachment via "grafting-to" and "grafting-from" approaches.

In physisorption one end of a block copolymer adsorbs strongly to the surface. Covalent attachment can occur through either "grafting to" [48,49] or "grafting from"[50] methods. In the "grafting to" approach, end-functionalized polymers react with an appropriate functional group on the substrate to form polymer brushes. Alternatively, with the "grafting from"

strategy polymer chains grow directly from initiators covalently attached to the surface. These two covalent methods give different polymer brush densities.

In the "grafting to" method, surface-accessibility limitations for incoming polymer chains lead to relatively low grafting densities and thicknesses. In contrast, the "grafting from" method employs small monomers that readily reach the reactive-growing surface to provide relatively high grafting densities. Furthermore, controlled polymerization from surfaces can create polymer chains with tunable lengths. Polymerization methods used to synthesize polymer brushes include cationic,[47] anionic,[51] TEMPO-mediated radical,[52] atom transfer radical polymerization (ATRP)[53] and ring-opening polymerization. This chapter focuses on ATRP strategies most relevant to the dissertation.

1.2.6.1.2. Biomolecule Immobilization on Polymer Brushes.

Several groups successfully fabricated polymer brushes for biomaterial immobilization.[11,54,55] However, most schemes require a separate derivatization step to introduce a specific functional group for applications such as protein immobilization (e.g. Figure 1.7). Polymer brushes with hydroxyl, carboxylic acid and epoxide groups are common choices for simple derivatization.
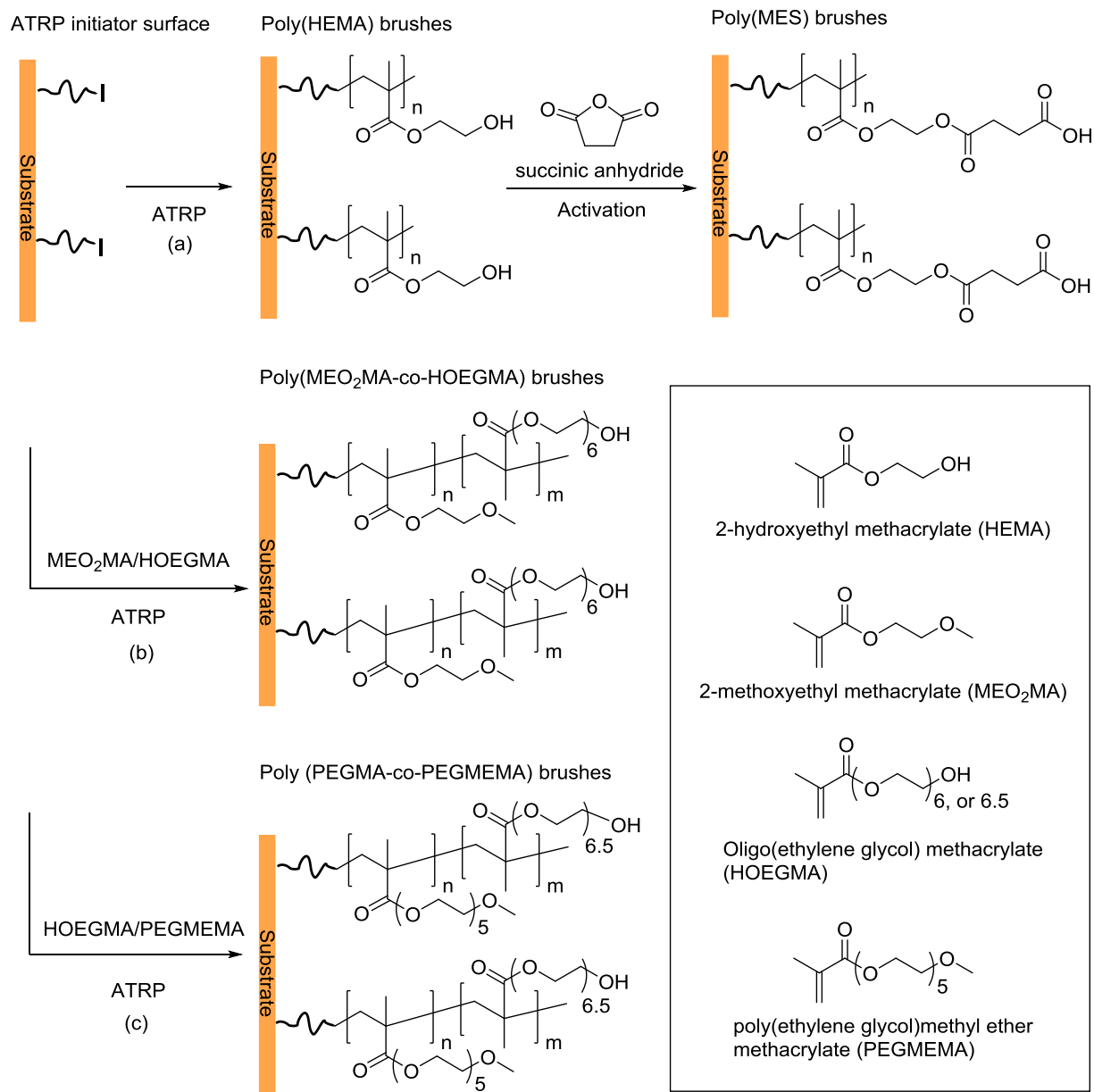
Figure 1.9. Various schemes for preparing hydroxyl group-containing (a) homo-[11,54,55] and (b, c) co-polymer[56-58] brushes. Process (a) also shows the activation of poly(HEMA) with succinic anhydride to obtain poly(MES) brushes.[59]

Surface-initiated ATRP of hydroxyl-containing mononomers yields derivatizable polymer and copolymer brushes on a variety solid substrates (Figure 1.9a).[11,54-57] Functionalization of these polymers often exploits reaction with highly active molecules

including succinic or glutaric anhydride, pentafluropyridine (PFP), 3-chloropropionaldehyde diethylacetal, *p*-nitrophenyl chloroformate, tresyl chloride, oxalyl chloride, cyanuric chloride, carbonyldiimidazole, triflic anhydride, and disuccinimidyl carbonate.[60,61] The negatively charged brushes generated by reaction with glutaric anhydride or succinic anhydride (SA) require subsequent activation via reactions such as *N*-(3-dimethylaminopropyl)-*N'*-ethylcarbodiimide hydrochloride (EDC)/*N*-hydroxysuccinimide (NHS) coupling for further functionalization (Figure 1.10).[62] In contrast, the more active neutral polymer brushes such as the chloro-derivative can directly react with many functional groups (Figure 1.11).

Poly(2-hydroxyethyl methacrylate) [poly(HEMA)] brushes are particularly common in surface functionalization (Figure 1.9).[63] As mentioned, poly(HEMA) contains hydroxyl groups that readily react with succinic anhydride in the presence of a base to give polymer brushes containing terminal carboxylic acid units. These acid-functionalized brushes can bind proteins through ion exchange or undergo further derivatization to incorporate an IMAC ligand such as NTA (Figure 1.10). Reaction of poly(HEMA) with *p*-nitrophenol chloroformate allows covalent immobilization of proteins and peptides.[64-66]
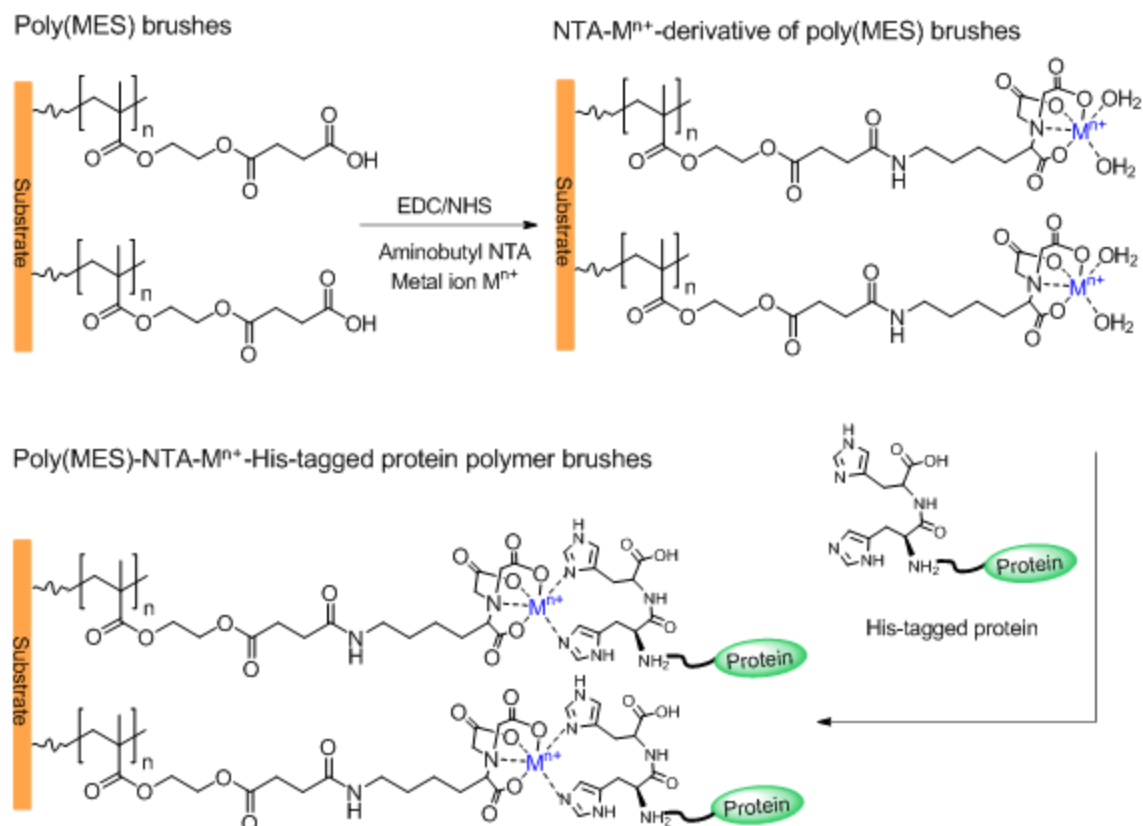
Figure 1.10. Functionalization of poly(MES) brushes with aminobutyl NTA-metal-ion complexes, and His-tagged protein binding to the poly(MES)-NTA-M^{n+} brushes.[59]

Reaction with thionyl chloride can convert the hydroxyl groups on poly(ethylene glycol methacrylate) (Poly(EGMA)) to chloride derivatives for direct protein or carbohydrate immobilization (Figure 1.11). The chloride groups readily react with amines via nucleophilic substitution.[11,67]

16
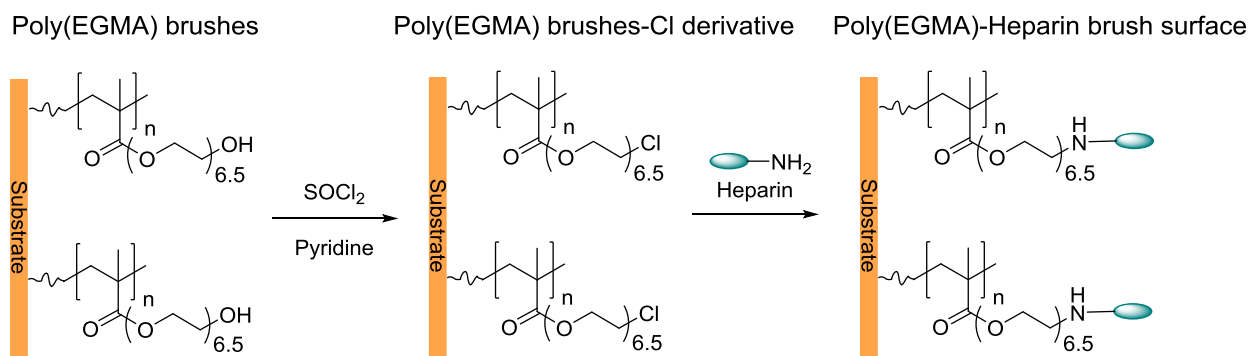
Figure 1.11. Conversion of the hydroxyl groups of poly(EGMA) side chains into a chloride derivative, and heparin immobilization.[11]

Poly(glycidyl methacrylate) (PGMA) brushes are another attractive choice for functionalization of surfaces.[68] Common syntheses of PGMA brushes and their copolymers exploit ATRP from initiator-modified substrates (Figure 1.12). Subsequent ring-opening reactions of the epoxide groups enable brush derivatization without further activation, although this may require hours for completion. Reaction of protein amino groups with epoxides enables direct protein anchoring to poly(GMA) brushes (Figure 1.13a), and functionalization with IMAC ligand such as IDA enables capture through metal-ion affinity (Figure 1.13b).[69]
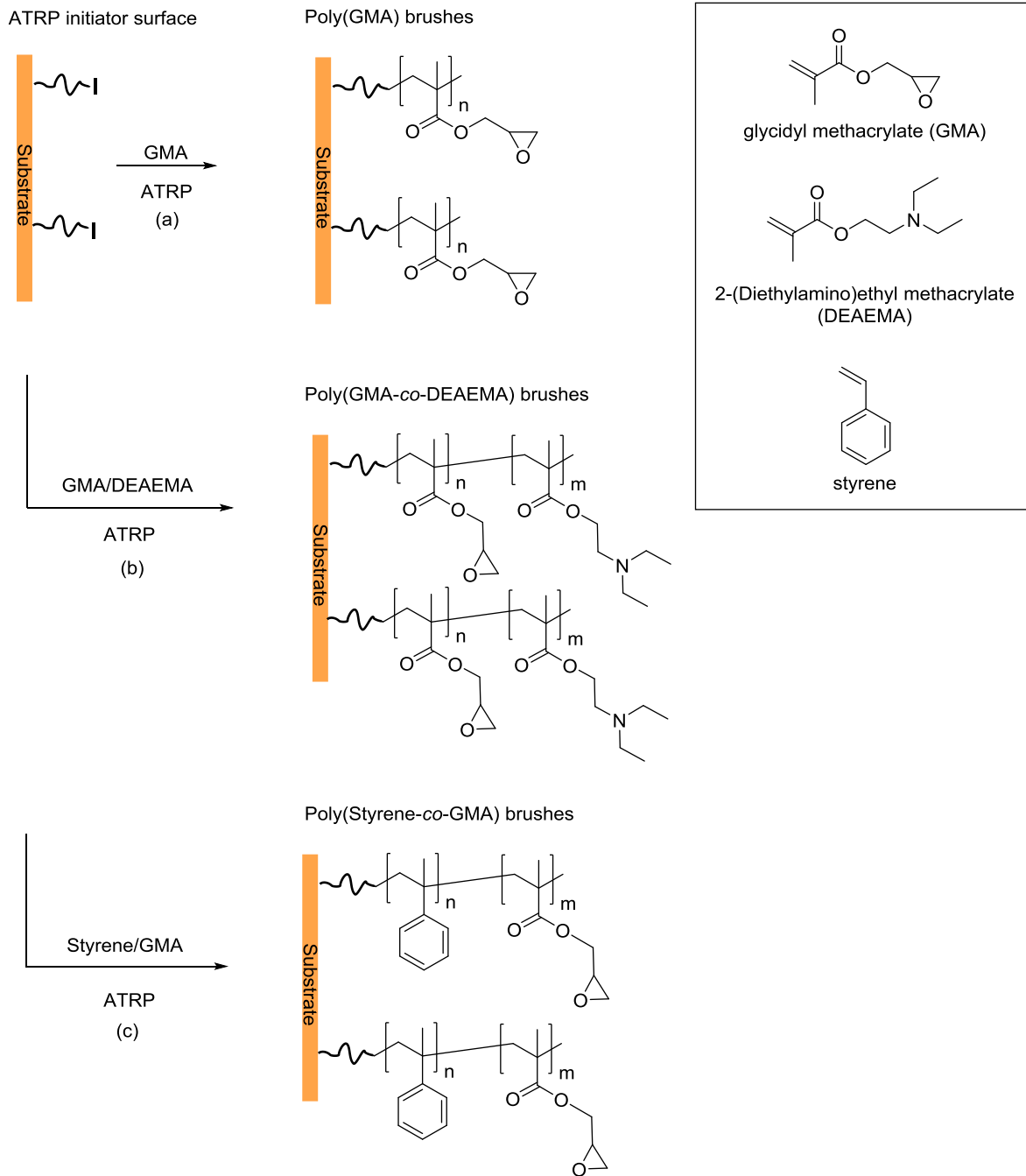
Figure 1.12. Different strategies for preparation of poly(GMA) homo-[6,8,9,70,71] and *co*-polymer[14,16] brushes.
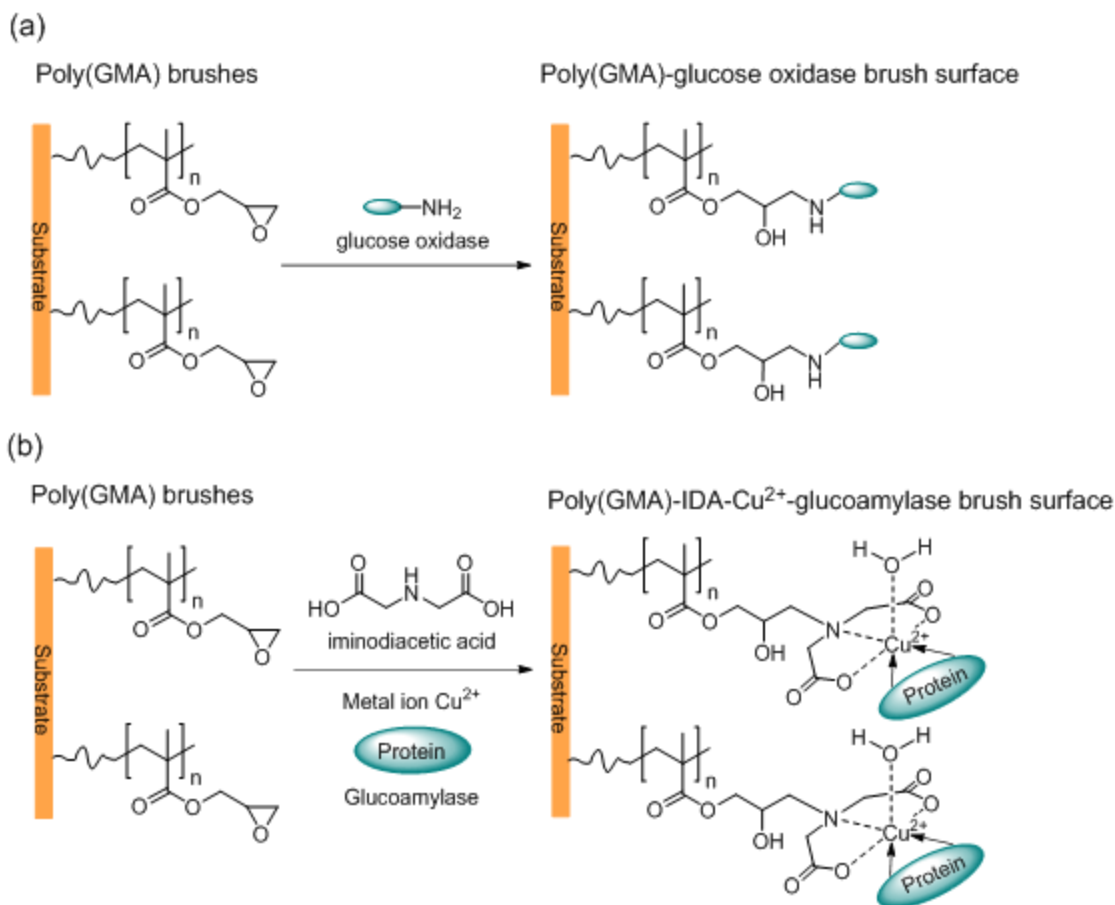
Figure 1.13. Immobilization of protein in poly(GMA) brushes via (a) covalent[11] and (b) affinity[9] techniques.

Carboxylic acid units are especially appealing for immobilization of bio-molecules, and polyacid brushes were grafted to various substrates via UV-photo polymerization and ATRP.[72] Nevertheless, direct ATRP of acrylic acid (AA) or methacrylic acid (MA) monomers is not possible due to their interaction with the ATRP catalyst to form unreactive metal-carboxylates.[73] However, as Figure 1.14a shows, the salts of meth/acrylate are somewhat effective in ATRP.[12,74] Also, polymerization of *tert*-butyl acrylate followed by hydrolysis of the *tert*-butyl esters can lead to the desired polymer brushes (Figure 1.14b).[12,75]
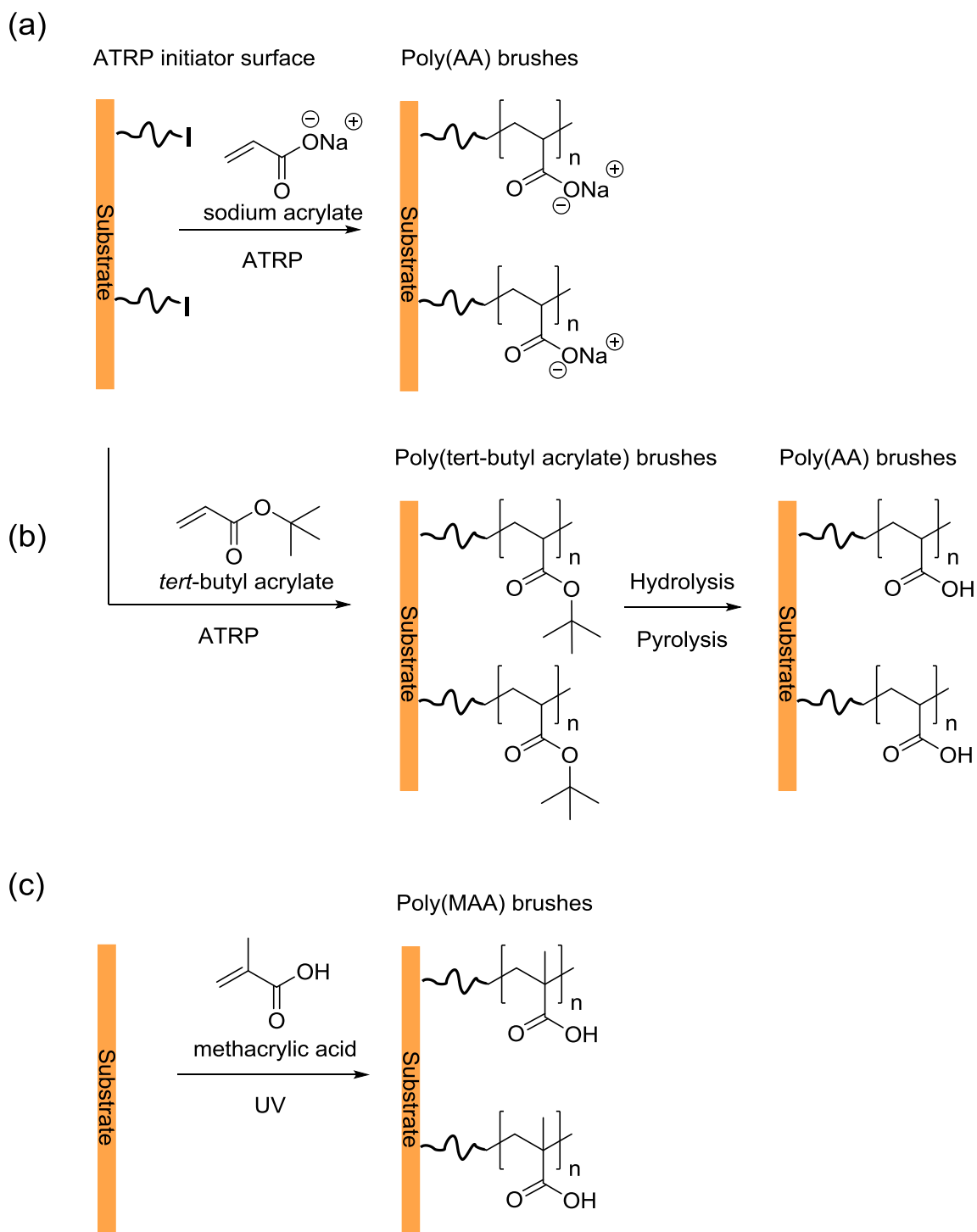
Figure 1.14. Different strategies for preparation of polymer brushes with carboxylic acid groups.[2,5,74,76-78]

Poly(acrylic acid) [poly(AA)], poly(methacrylic acid) [poly(MA)] and poly(2-methacryloyloxy)ethyl succinate) poly[(MES)] enable immobilization of protein through the native polymer carboxylic acid groups.[59,79,80] Deprotonated polyacid brushes electrostatically bind positively charged enzymes such as lysozyme[81] and pectinase.[82] Similar to PMES brushes, activation and functionalization of poly(AA) and poly(MA) is needed for specific protein binding[64] (Figure 1.15b & c) and covalent immobilization of biomolecules (Figure 1.15a).
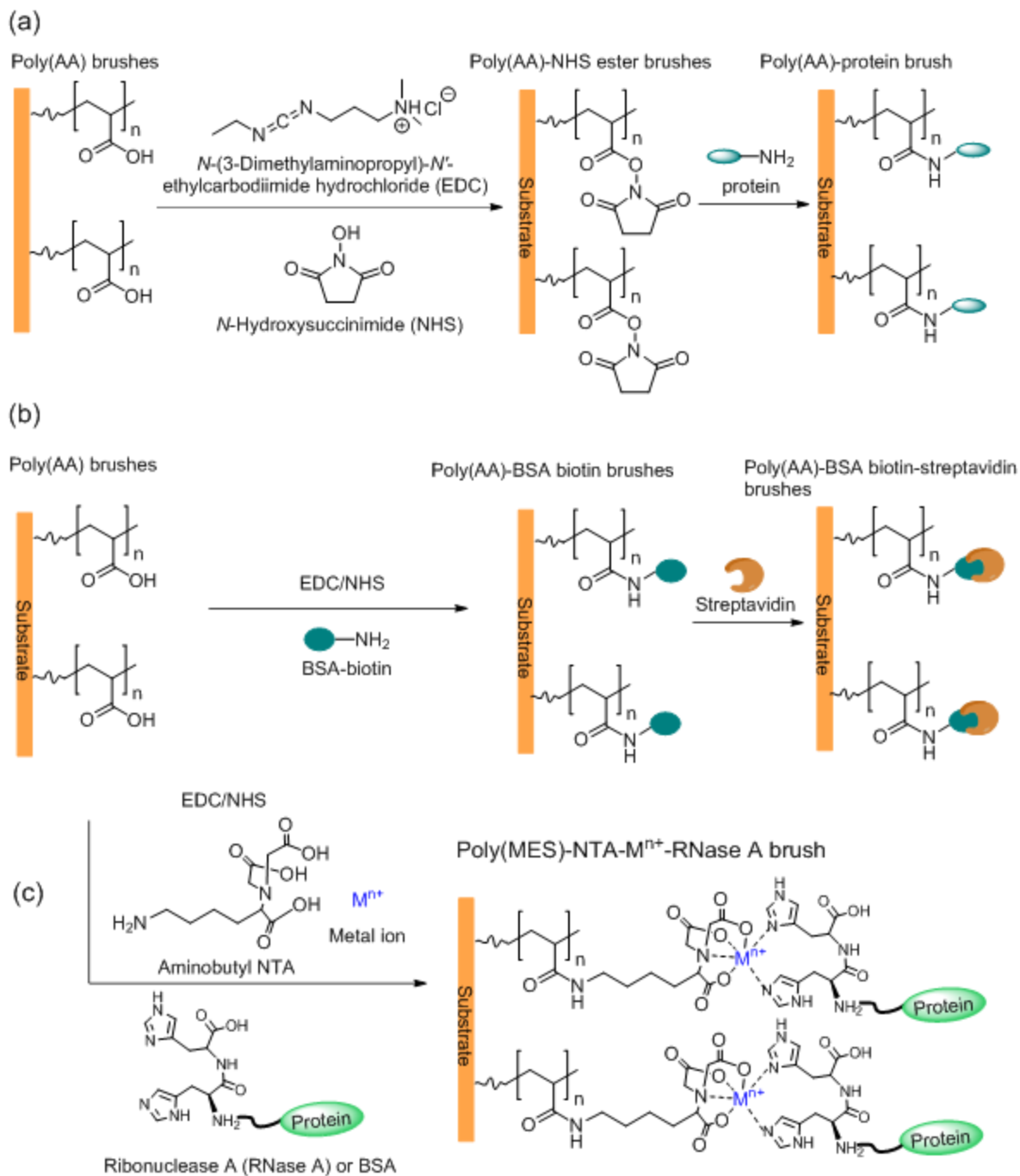
Figure 1.15. Activation and functionalization of poly(AA) brushes for (a) direct immobilization of biomolecules[2] and (b,c) specific protein binding.[64,74]

Membrane modification can occur though brush growth from initiators immobilized in membrane pores (Figure 1.16a). In protein capture via ion-exchange, brush-modified membranes show remarkable protein binding capacities ranging from 80 to 130 mg/cm^3 of membrane (Figure 1.16b).[39,52,83,84]
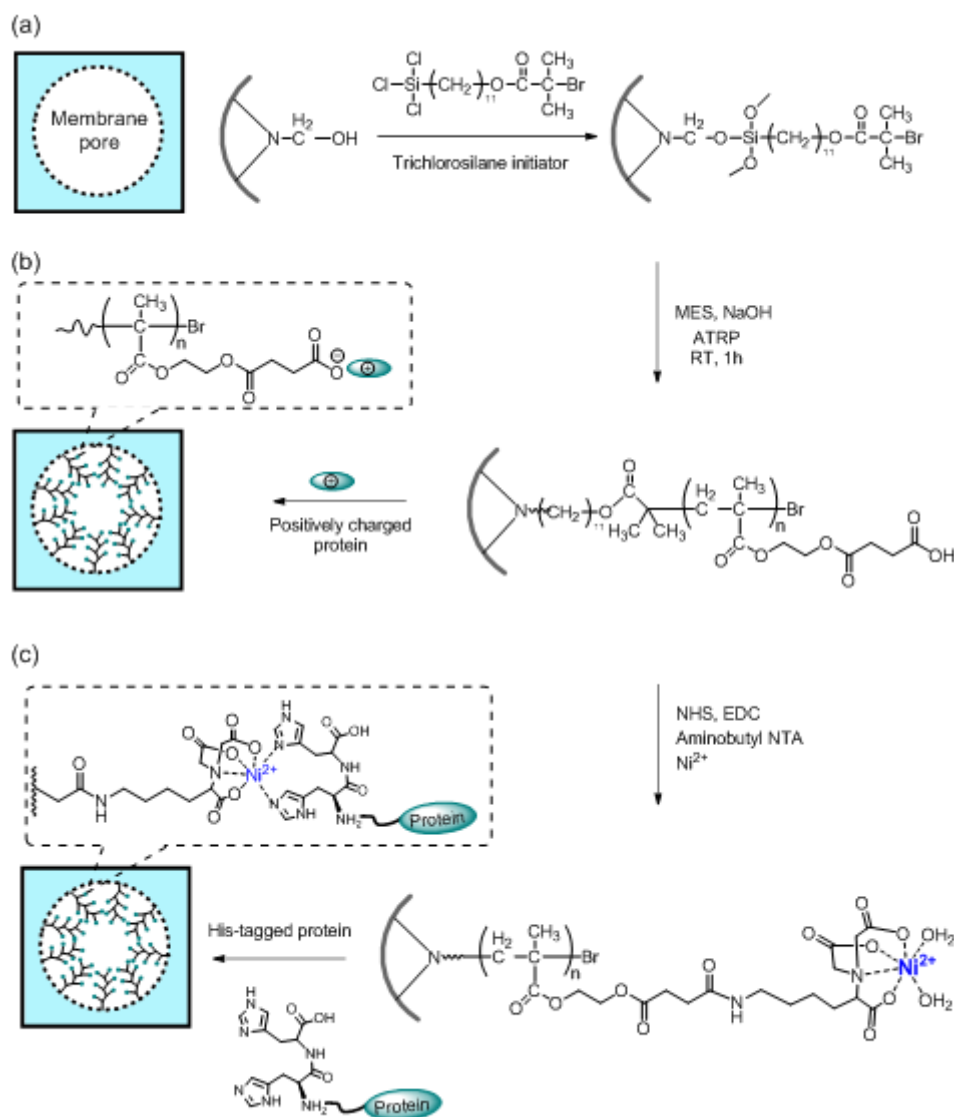
Figure 1.16. Functionalization of membrane pores with poly(HEMA) brushes, activation of poyl(HEMA) to form poly(MES), and binding of His-tagged protein to a poly(MES)-NTA-Ni^{2+} brush inside a membrane pore.[59]

Further functionalization (Figure 1.16c) of brushes enables more selective purification of tagged protein. Jain et al. used PHEMA[65] and Ramstedt et al. used poly (oligoethylene glycol methacrylate)and poly(HEMA)[85] to modify membranes with NTA-Ni^{2+} and selectively bind His-tagged protein. Alumina membranes with PHEMA-NTA-Ni^{2+} bind 120 mg of His-tagged ubiquitin (His U) per cm^3 of membrane. Jain et al. also modified nylon membranes through SI-ATRP of MES and functionalized these brushes with NTA-Ni^{2+} moieties. These membranes have larger pores than alumina but still capture 85 mg of His U per cm^3 of membranes.[59] In addition, these membranes selectively bind His-tagged cellular retinaldehyde binding protein from cellular extracts in less than 10 min.

Even though MES polymerization occurs in water, attachment of the trichlorsilane initiator to membranes takes place in tetrahydrofuran, which is sometimes incompatible with polymeric membranes. To overcome this problem, Anuraj et al. used an aqueous immobilization of a macro-initiator,[86] which adsorbed to the membrane via hydrophobic interactions. Subsequent MES polymerization required less than 5 min and after NTA-Ni^{2+} functionalization, these membranes attain protein-binding capacities as high as those after a 1-h polymerization from membranes modified using a trichlorosilane initiator.

The main disadvantage of membrane modification with polymer brushes is the complexity and inefficiency of brush synthesis and derivation. Brush growth usually includes at least two steps: initiator attachment and polymerization under anaerobic conditions.[44,87] Moreover, most of the monomer does not end up in the brush, and controlling initiator density and polymerization conditions to optimize binding is

challenging.[88]   Derivatization is also inefficient.   To develop simpler methods for modifying membranes, the Bruening group began exploring layer-by-layer (LBL) adsorption, and the following section discusses this technique.

1.2.6.2. Polyelectrolyte Multilayers (PEMs) for Protein Binding.

Polyelectrolyte multilayers form through alternating (layer-by-layer) adsorption of polycations and polyanions. These films can bind multilayers of proteins via electrostatic interactions or capture specific proteins when the polyelectrolytes contain a suitable ligand (Figure 1.17). Such films are versatile materials for binding multilayers of protein on surfaces, including the pores of membranes.
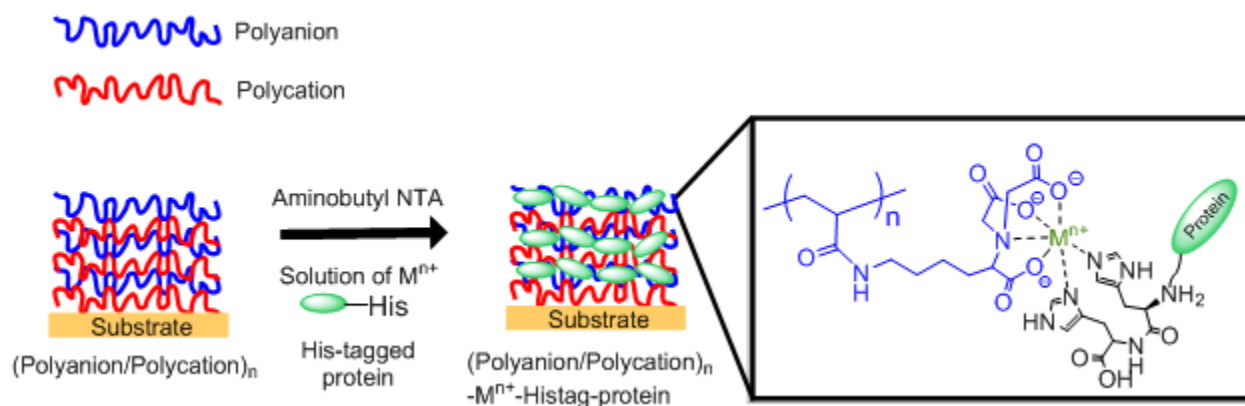
Figure 1.17. Multilayer protein binding in a PEM derivatized with NTA-M^{n+} complexes.

1.2.6.2.1. PEM Film Construction and Growth Mechanisms.

Although spraying of polyelectrolytes provides a rapid method for forming PEMs,[89] adsorption from solution is the most common method for forming these films.[90] In 1990, Hong and Decher[90,91] demonstrated the basic principles of layer-by-layer (LbL) polyelectrolyte adsorption by exposing a charged substrate to alternating solutions of polycations and polyanions (Figure 1.18). After adsorption of either polyelectrolyte (PE), charge reversal take place, and a single quasi-equilibrium adsorption requires only a few minutes.
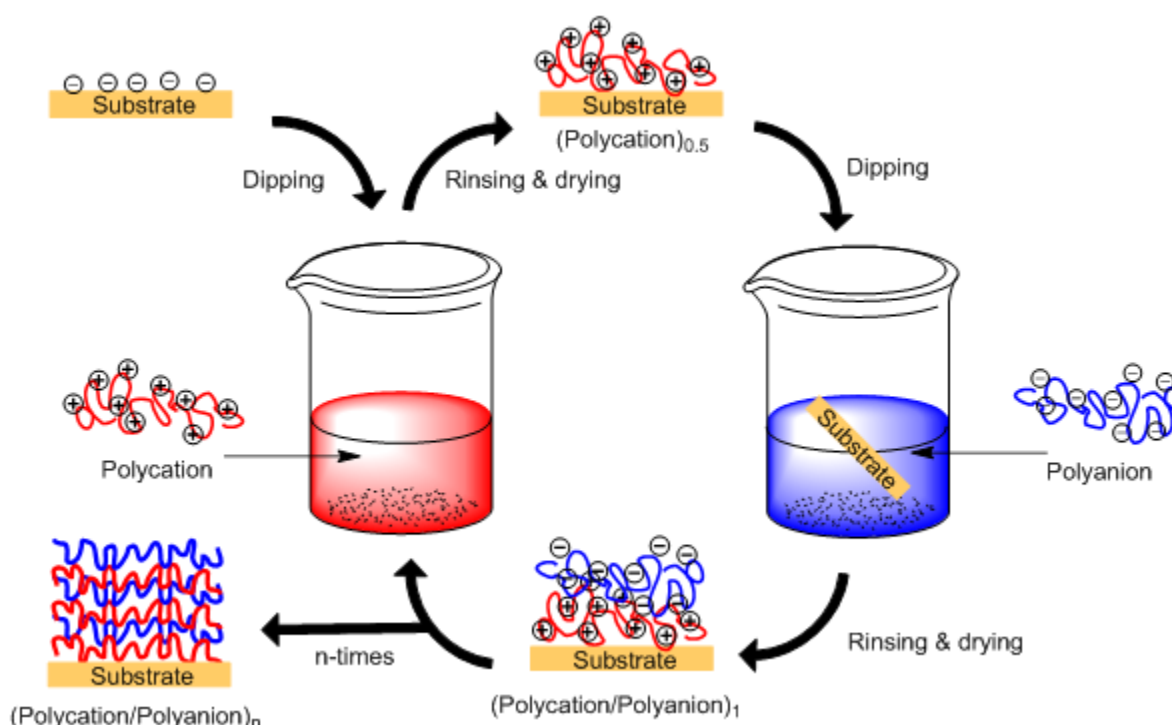
Figure 1.18. Layer-by-layer (LbL) adsorption of polyelectrolyte multilayers (PEMs).

Two current theories, the "ion-exchange model"[92] and the "kinetically controlled model",[93] may describe PEM formation. According to the ion-exchange model PEM formation includes both adsorption and desorption of electrolytes. These phenomena occur simultaneously during PEM formation. When a polycation adsorbs to the negatively charged polyelectrolyte, a significant entropy gain occurs due to desorption of counter ions. This entropic gain likely drives complex formation. Enthalpic changes probably do not contribute greatly to film formation because electrostatically there is minimal difference between polyelectrolyte charge compensation with small counter ions or oppositely charged polyelectrolytes. Also, PEM formation can occur at high ionic strengths where electrostatic interactions are highly screened.

According to the kinetic model, when the screening length of the PEM is small compared to the layer extension, small counterions will compensate some of the charges on the polyelectrolytes. Due to this charge screening, the PEM will adsorb to the surface in a train-loop-train conformation (Figure 1.19). The loop will lead to charge charge reversal at the surface. In the kinetic model, PEM formation is a two-step process.[93,94] First, incoming PE contacts the PEM and forms the PE aggregates. In a second step structural rearrangements of initial aggregates take place via a polyelectrolyte exchange with the PEs in the solution. Dautzenburg et al,[95] first reported and confirmed this type of rearrangement in films of collodial particles. Furthermore, if the PE adsorption from the solution is much faster than the rearrangement of previously adsorbed PE aggregates charge overcompensation will occur in a kinetically hindered manner. Thus, the PEM is not in thermodynamic equilibrium, but a kinetically hindered state.
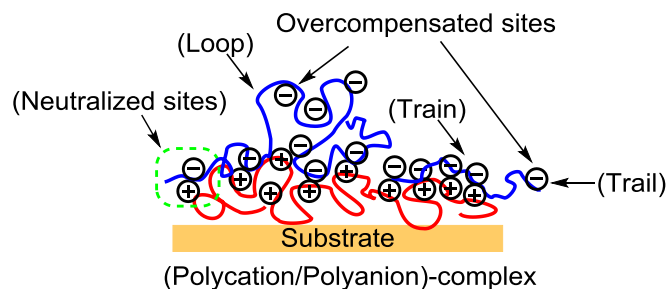
Figure 1.19. Representation of kinetically controlled adsorption of polyelectrolytes and charge overcompensation.

PE adsorption depends on the charge density and structure of the polymer. PEs with essentially a permanent charge, e.g. sodium poly(styrene sulfonate) (PSS)[96] and poly(diallyldimethyl ammonium) (PDDA), are called strong PEs.[97] In contrast, for weak PEs such as poly(vinyl amine) (PVA), poly(L-lysine) (PLL), poly(acrylic acid) (PAA), linear poly(ethylene imine) (LPEI) and poly(allylamine hydrochloride) (PAH), the charge depends on pH and ionic strength. Because both charge density and PE conformation vary with pH and ionic strength, these deposition parameters can dramatically affect film thickness and conformation. Usually PEM thickness increases with an increase in the ionic strength of deposition solutions due to charge screening as well as formation of loops and trains.[98] For weak polyelectrolytes, the thickest films usually form at pH values where the polyelectrolyte has a low charge density.[99]

In addition to common synthetic polyelectrolytes, natural polymers such as nucleic acids and polysaccharides can form multilayer films.[100,101] Moreover, many studies demonstrate LbL adsorption with proteins as constituents of PEMs,[102-106] and proteins may also adsorb throughout previously formed PEMs.[107-111] Binding and release of a protein, or other macromolecule, in a PEM largely depends on the porosity

and mesh size within the film (Figure 1.20).[18,112] Furthermore, film properties such as

hydrophilic-hydrophobic balance and net charge impact protein binding and release.
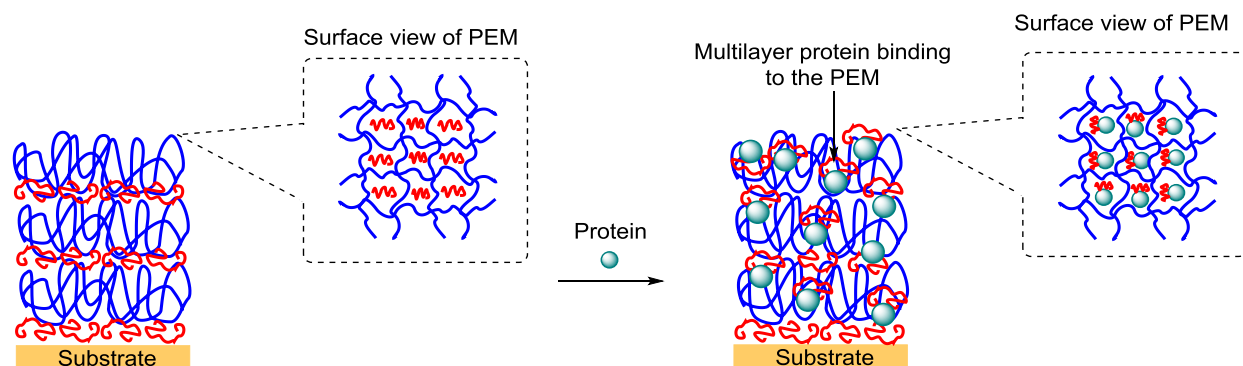
Figure 1.20. Schematic representation of polyelectrolyte matrices tailored for extensive protein binding.[113]

LBL films often resemble a network structure (Figure 1.20), which includes cross-links due to electrostatic interactions of polyanions and polycations. The major factor governing the network porosity is the density of electrostatic complexation sites. A low density of crosslinks leads to a more open film and extensive protein binding, but such films may be unstable. Variation of polyelectrolytes, ionic strength, pH, or temperature can tune the extent of cross-linking and protein binding as well as film stability. Several reviews[114-117] discuss tuning the structural properties and dynamics of PEMs.

1.2.6.2.2. Charge Compensation and Film Growth.

Charge compensation in a PEM can occur due to a neighboring, oppositely charged PE (intrinsic compensation) or due to small counterions (extrinsic compensation). Poly(styrene sulfonate)/poly(allylamine hydrochloride) (PSS/PAH) films show primarily intrinsic compensation, and their thickness increases linearly with the number of adsorption steps.[118] These films are also quite rigid and immobile. Both PAH and PSS have high charge densities, so incoming PEs do not diffuse deeply into the films due to a high density of ionic cross-links.   In contrast, if at least one of the PEs has a low charge density, this PE may diffuse freely inside the film matrix.[119] In these systems, much of the charge compensation is extrinsic. Due to the high mobility of one of the PEs in the film, thickness may increase exponentially with the number of adsorption steps.[117,120] Deposition of the mobile PE may occur throughout the film, whereas this same PE may diffuse to the film surface during adsorption of the oppositely charged PE to further enhance growth.   Compare to PEMs with high densities of cross-links, PEMs that exhibit exponential growth are more flexible and better suited for applications such as protein capture. A common example of a PE system that exhibits exponential growth is   (hyaluronic acid/poly-L-lysine) HA/PLL.[120] Both constituents of this system are weak PEs with low charge densities. Thus, the film has a low density of ionic cross-links.

If supporting electrolyte, i.e. a salt, is present in polyelectrolyte deposition solutions, interactions of polyelectrolytes and counter ions compete with polyelectrolyte/polyelectrolyte ionic cross-linking . Thus, high salt concentrations lead to

more extrinsic charge compensation and fewer ionic cross-links. This effect is more pronounced for ions with low charge densities, e.g. Cs^+ and Br^-.[117] Due to their small hydration shell these counter ions readily interact with oppositely charged PEs. Film deposition from solutions with high salt concentrations leads to increased swelling in water,[121] which is important to create space for binding proteins and other biomolecules.

1.2.6.2.3. Protein Capture in PEMs.

Many studies investigated the interaction of proteins with LBL films,[122,123] and in some cases the films can serve as protein reservoirs with high binding capacities.[124] However, no theory describes the embedding of biomacromolecules within the films or predicts loading. This is mostly due to a lack of experimental tools for precise analysis of the distribution and mobility of the embedded molecules.

Uhlig et al.[113] employed fluorescence recovery after photobleaching to measure protein mobility in μm-thick HA/PLL multilayers on glass fibers. They contacted these PEMs with fluorescently tagged proteins of different sizes and then photobleached 1 μm thick lines along the glass fiber.
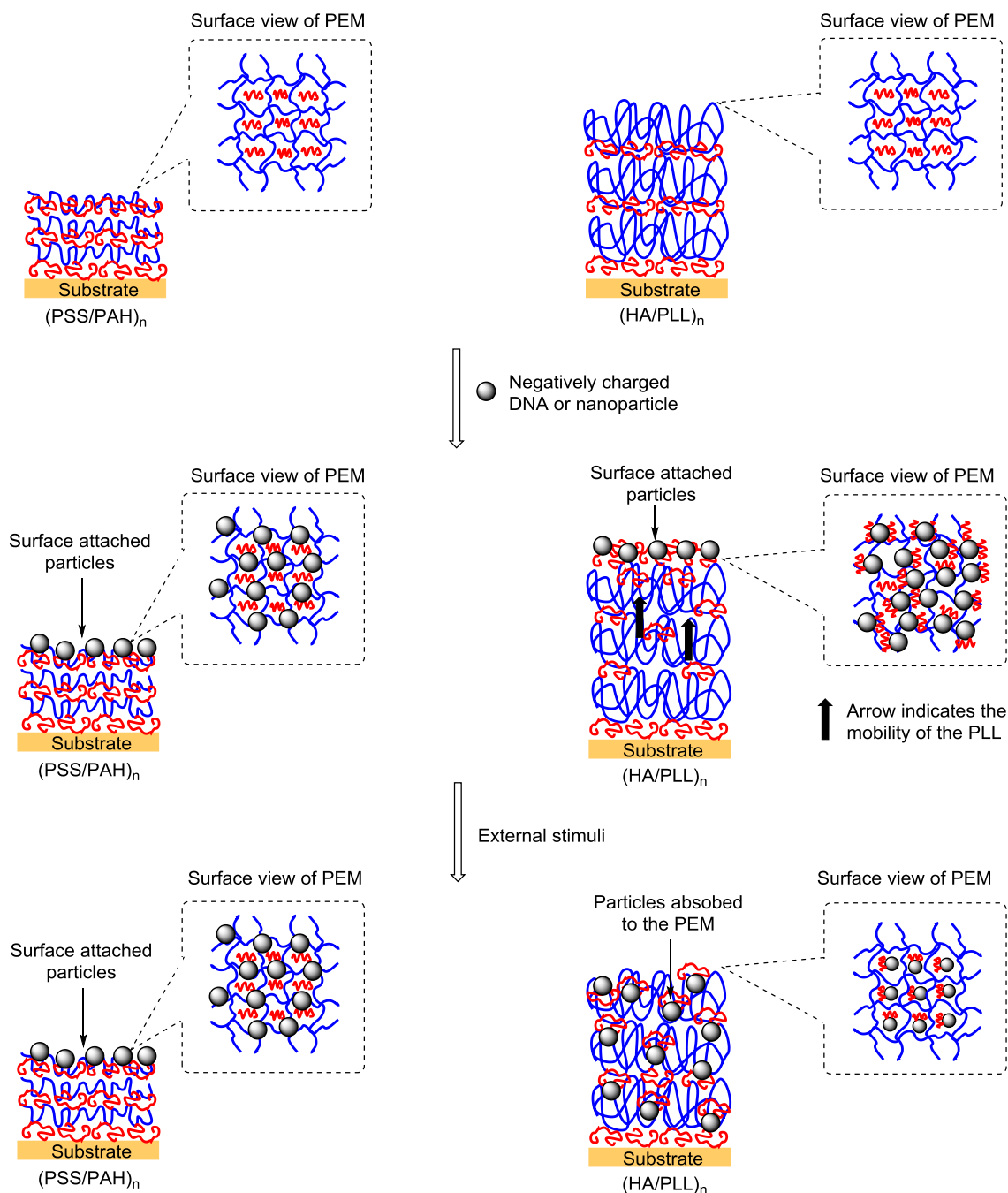
Figure 1.21. Schematic representation of strong, (PSS/PAH)$_n$, and weak, (HA/PLL)$_n$, polyelectrolyte multilayer systems and their interaction with negatively charged nanoparticles or DNA (gray spheres). The particles or DNA only interact with the surface PAH of the PSS/PAH films, but they can accumulate in high quantity as a result of interaction with PLL, which easily diffuses to the surface of the PEM. External stimuli such as an increase in temperature may trigger the diffusion of these particles into the HA/PLL film.

Subsequent determination of the fluorescence recovery from the bleached region gave the diffusion coefficients of proteins inside the PEM. However, this study showed no consistent correlation of diffusion coefficients with protein size or charge. Proteins with a range of diameters (3–11 nm) diffuse relatively quickly through the film (D = 2–4 μm^2 s^{-1}), suggesting that these films have dynamic pores that accommodate a variety of protein sizes. The authors also tried to incorporate dextrans (10 to 500 kDa) in these PEMs, but these uncharged molecules do not diffuse into the film, regardless of their size. This suggests that protein-PEM interactions are mainly electrostatic, although other forces may affect protein capture.

Volodkin et al. prepared two PEM systems to investigate the loading of biomacromolecules (Figure 1.21).[18] The first polyelectrolyte pair, PSS/PAH, shows low PAH diffusivity (10^{-8} to 10^{-6} μm^2 s^{-1}), whereas the second pair, HA/PLL, shows high PLL diffusivity (10^{-1} μm^2 s^{-1}). They contacted both of these PEMs separately with negatively charged DNA and gold nanoparticles. In the PSS/PAH system, immobile PAH at the surface forms a small amount of complexes with negatively charged nanoparticles or DNA. However, for HA/PLL films, PLL film diffuses out from the film interior to make contact with incoming DNA or nanoparticles. Both DNA and nanoparticles form μm-size aggregates at the film surface with charge compensation by PLL. Fluorescence labeling studies shows that PLL chains are inside these aggregates.[125] However, this strong complexation inside the aggregates prevents the diffusion of the materials from the bulk into the film. Nevertheless, the authors showed that increased temperature will trigger the diffusion of the DNA or nanoparticles into the HA/PLL system. The loading capacities for DNA and gold nanoparticles in HA/PLL films are 1%-2% and 100% of the

mass of PLL in the film, respectively. In contrast, PSS/PAH films bind an order of magnitude less material. Srivastava[126] also reported the strong accumulation of 4 nm quantum dots in exponentially growing PDADMAC/PAA films. Thus, with a suitable PEM system, films should bind large amounts of protein.

Salloum and Schlenoff showed that protein capture can occur throughout a PEM (absorption), but the equivalent thickness of absorbed protein was only 35% of the thickness of the dry film.[127] Other studies of protein or nanoparticle sorption in PEMS, especially with films whose thickness grows exponentially, reported similar loadings.[128,129] A recent study of protein binding to a cross-linked polyelectrolyte film with the anion removed revealed absorption of 4−15 monolayers (~30 nm) of human serum albumin.[130] Ma et al.[124] showed that with appropriate deposition conditions, PEMs containing poly(acrylic acid) increase in thickness 4- to 5-fold (as much as 200 nm) upon protein (Lysozyme) binding. However, the aforementioned work was all carried out on flat surfaces.

1.2.6.2.4. LBL Modification of Membranes.

Bhattacharjee et al.[1] employed LBL adsorption followed by derivatization to fabricate functional PEM-modified membranes that readily capture His-tagged protein. Membranes with PAA/BPEI/PAA films binds as much as 100 mg/mL of lysozyme through ion-exchange. Commercial Mustang S ion-exchange membranes show lysozyme-binding capacities of only 45−50 mg/cm^3.[131]
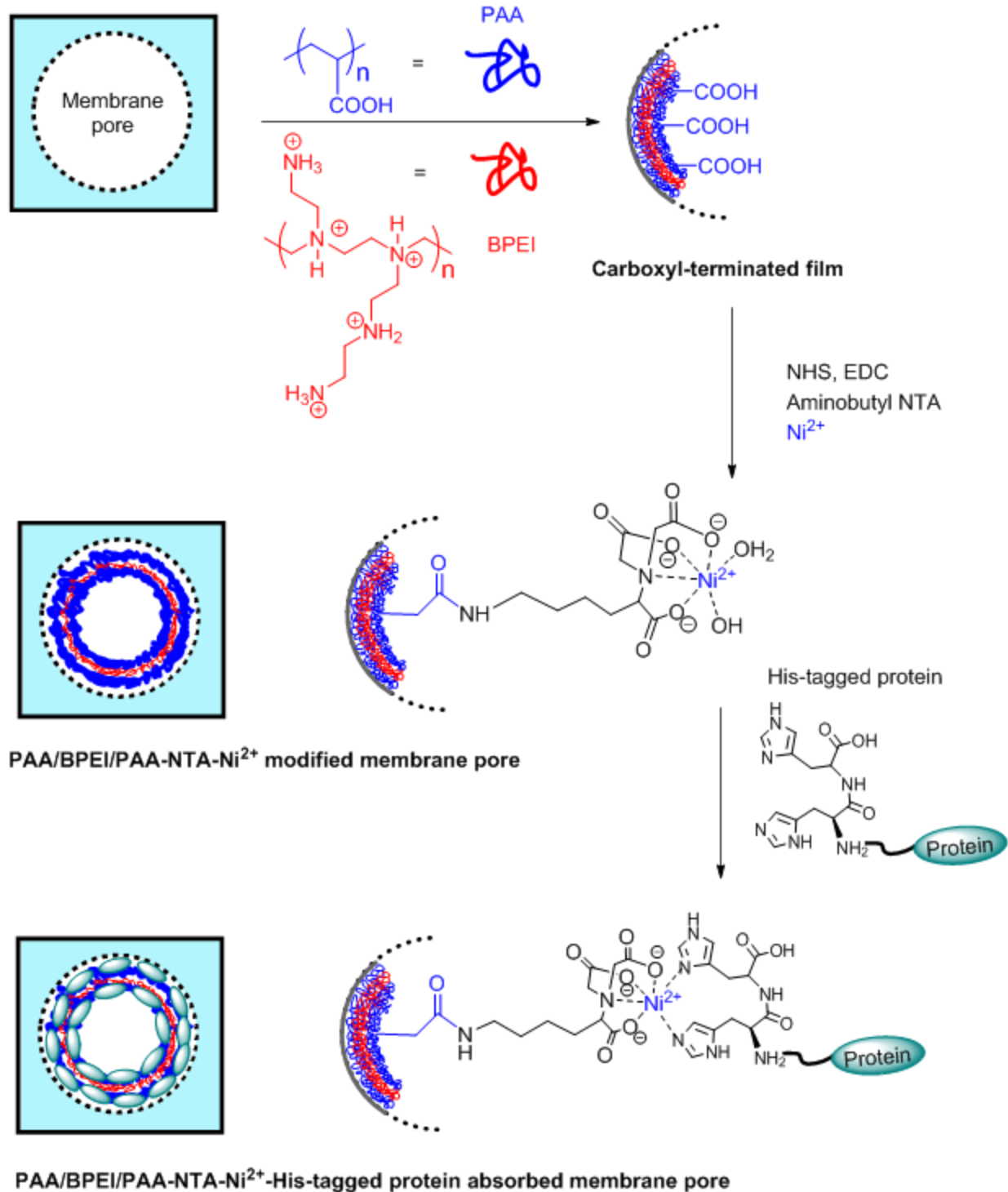
Figure 1.22. Schematic representation of (PAH/PAA)$_n$ adsorption in a membrane pore, functionalization with NTA-Ni^{2+} and multilayer His-tagged protein binding.

After further modification of these layers with NTA-metal-ion complexes (Figure 1.22), membranes bind 70 mg/ml of Concanavalin A (Con A) (a 25-kDa protein as the protomer) and 97 mg/mL of His-tagged Ubiquitin (a 10 kDa protein). Moreover, these membranes selectively capture His-tagged COP9 signalosome complex sub unit 8 from a cell lysate with >95% purity. Remarkably, the whole purification process takes less than 30 min.

Despite the above-mentioned success in modifying membranes through LbL adsorption and derivatization, formation of these films is costly due to the derivatization with aminobutyl NTA, which is expensive to prepare due to protection/deprotection steps.   Moreover, only a small fraction of the aminobutyl NTA attaches to the membrane.

1.3. Outline of the Dissertation.

This research focuses on developing new films with increased protein-binding capacities, with an emphasis on coatings in porous membranes. Chapter 2 describes a simple, rapid and direct procedure to deposit polymer films that bind His-tagged proteins. I synthesized two PEs, poly(*N*,*N*-dicarboxymethylallyl amine) (PDCMAA) and carboxymethylated polyethyleneimine (CMPEI), that contain iminodiacetic acid (IDA) moieties, which can form metal-ion complexes that capture both metal ions and His-tagged proteins. LBL adsorption of these PEs leads to films that capture proteins, and this procedure is much simpler than prior strategies that include LBL adsorption and subsequent derivatization with aminobutyl NTA.[1]

Remarkably, 10-bilayer PAH/PDCMAA films are 1 µm thick, and these coatings have a very high Cu^{2+} binding capacity (~2.5 mmol/cm^3 of film, or 2.5 M). When deposited on the surface of porous membranes, PAH/PDCMAA films function as highly selective facilitated-transport membranes with a Cu^{2+}/Mg^{2+} selectivity around 50. However, binding of a metal ion such as Cu^{2+} or Zn^{2+} is a necessary but not sufficient condition for creating membranes that selectively capture large amounts of polyhistidine-tagged protein. The adsorbed polymer must also swell in water to provide enough space for protein-ligand interactions. Unfortunately, PAH/PDCMAA films do not swell sufficiently for extensive protein capture, perhaps because of the hydrophobic backbone of the polymer.

To create a metal-ion-binding polymer with a more hydrophilic backbone, I allow polyethyleneimine to react with chloro or bromoacetic acid to give carboxymethylated polyethyleneimine (CMPEI). Compared with the dry state, the thicknesses of CMPEI/PAH films increase ~6 fold after immersion in a pH 7 buffer. Thus, these coatings should have sufficient open space for binding proteins. Sequential adsorption of PAH and CMPEI leads to membranes that bind Ni^{2+} and capture ~60 mg of His-tagged ubiquitin per mL of membrane, and this capacity is higher than for commercially available systems. Such membrane can purify His-tagged protein directly from cell extracts.

Minimizing metal-ion leaching is also important in purifying His-tagged protein. Thus, chapter 3 describes synthesis of a series of polymers containing N_α, N_α-bis(carboxymethyl)-L-lysine (tethered NTA). Due to the high cost of commercial NTA derivatization agents, I established a novel route to synthesize these polymers at

minimal cost. I first synthesized the less expensive poly(L-lysine) and carboxymethylated the secondary amine with bromoacetic acid to get NTA functionalities on the polymer. To improve the protein-binding kinetics and capacity of these films, I synthesized poly(NTA-*co*-AA) copolymers, where the AA repeat units promote swelling and improve protein-binding kinetics. Sequential adsorption of PAH and NTA-containing PEs leads to membranes that bind Ni^{2+} and capture ~40 mg of His-tagged ubiquitin per mL of membrane. Moreover, these polymer films show less metal-ion leaching than coatings containing IDA ligands.

Introduction of porosity is another approach to enhance the kinetics of protein binding in polyelectrolyte films. Chapter 4 describes the development of porous films through adsorption of star polymers. I synthesized star polyelectrolytes based on poly(dimethylaminoethyl methacrylate) [PDMAEMA-X] and poly(acrylic acid) [PAA-X], with X=3, 4 and 6 arms. Under appropriate deposition conditions, LBL adsorption of these star polymers leads to highly porous films. The size of surface pores regularly increases (from 200 to 550 nm) when increasing the number of bilayers from 2 to 6. Films with a few bilayers can swell more that 200-300% in water, but swelling decreases with additional bilayers or an increase in the number of arms on the polymers. Highly swollen films bind as much as 10-20 multilayers of lysozyme. Sequential adsorption of PDMAEMA-X and PAA-X leads to membranes that capture ~120 mg of lysozyme per mL of membrane, which is higher than the capacity of commercially available systems (40-50 mg/mL).[131]

Chapter 5 describes efforts to reduce the areal density of polymer-brushes and increase their aqueous swelling, which should enhance the kinetics and amount of

protein binding. To decrease brush density, I designed and synthesized several monomers with long, cleavable side chains. Removal of the side chains after polymerization should reduce brush chain density and provide the space necessary to capture large amounts of protein. Growth of the polymer brushes gave 100 nm-thick films, but unfortunately upon cleaving the side chains, the polymer brushes collapsed to prevent further functionalization. However, this synthetic strategy is an interesting method for fabricating brushes with distinct distances between polymer chains. Nevertheless, synthesis of brushes is cumbersome, frequently requiring deposition of initiator molecules and polymerization under inert conditions. Thus, previously developed methods are simpler for creating highly swollen films.

Finally, chapter 6 summarizes the findings in this dissertation and suggests some future directions. Specially this chapter will discuss a simpler techniques for fabricating porous PEMs, which we discussed in chapter 4, and suggest improvement of these films to absorb His-tagged proteins.

APPENDIX

Figure A1.1. Permission from the American Chemical Society for the figures.

REFERENCES

REFERENCES

(1)   Bhattacharjee, S.; Dong, J. L.; Ma, Y. D.; Hovde, S.; Geiger, J. H.; Baker, G. L.; Bruening, M. L. *Langmuir* **2012**, *28*, 6885-6892.

(2)   Cullen, S. P.; Liu, X.; Mandel, I. C.; Himpsel, F. J.; Gopalan, P. *Langmuir* **2008**, *24*, 913-920.

(3)   Ghosh, R. *J. Chromatogr. A* **2002**, *952*, 13-27.

(4)   Low, D.; O'Leary, R.; Pujar, N. S. *J. Chromatogr. B* **2007**, *848*, 48-63.

(5)   Dai, J.; Bao, Z.; Sun, L.; Hong, S. U.; Baker, G. L.; Bruening, M. L. *Langmuir* **2006**, *22*, 4274-4281.

(6)   Yuan, W.; Li, C.; Zhao, C.; Sui, C.; Yang, W.-T.; Xu, F.-J.; Ma, J. *Adv. Funct. Mater.* **2012**, *22*, 1835-1842.

(7)   Saxena, A.; Tripathi, B. P.; Kumar, M.; Shahi, V. K. *Adv. Colloid Interface Sci.* **2009**, *145*, 1-22.

(8)   Yuan, S.; Xiong, G.; Roguin, A.; Choong, C. *Biointerphases* **2012**, *7*, 30.

(9)   Xu, F. J.; Wang, Z. H.; Yang, W. T. *Biomaterials* **2010**, *31*, 3139-3147.

(10)   Saito, K.; Tsuneda, S.; Kim, M.; Kubota, N.; Sugita, K.; Sugo, T. *Radiat. Phys. Chem* **1999**, *54*, 517-525.

(11)   Xu, F. J.; Li, Y. L.; Kang, E. T.; Neoh, K. G. *Biomacromolecules* **2005**, *6*, 1759-1768.

(12)   Ayres, N.; Boyes, S. G.; Brittain, W. J. *Langmuir* **2007**, *23*, 182-189.

(13)   Liu, G.; Dotzauer, D. M.; Bruening, M. L. *J. Membrane Sci* **2010**, *354*, 198-205.

(14)   Barbey, R.; Kauffmann, E.; Ehrat, M.; Klok, H.-A. *Biomacromolecules* **2010**, *11*, 3467-3479.

(15)   Yang, S.; Zhang, Y.; Wang, L.; Hong, S.; Xu, J.; Chen, Y.; Li, C. *Langmuir* **2006**, *22*, 338-343.

(16)   Karagoz, B.; Bayramoglu, G.; Altintas, B.; Bicak, N.; Arica, M. Y. *Ind. & Eng. Chem. Res* **2010**, *49*, 9655-9665.

(17)   Volodkin, D.; Balabushevitch, N.; Sukhorukov, G.; Larionova, N. *Biochemistry* **2003**, *68*, 236-241.

(18)   Volodkin, D. V.; Madaboosi, N.; Blacklock, J.; Skirtach, A. G.; Möhwald, H. *Langmuir* **2009**, *25*, 14037-14043.

(19)   Cattoli, F.; Sarti, G. C. *Biotechnol. Progr.* **2002**, *18*, 94-100.

(20)   Swaffield, J. C.; Johnston, S. A. In *Current Protocols in Molecular Biology*; John Wiley & Sons, Inc.: 2001.

(21)   Finn, F. M.; Titus, G.; Horstman, D.; Hofmann, K. *P Natl. Acad. Sci-Biol* **1984**, *81*, 7328-7332.

(22)   Porath, J. *TrAC Trend. Anal. Chem* **1988**, *7*, 254-259.

(23)   Arnau, J.; Lauritzen, C.; Petersen, G. E.; Pedersen, J. *Protein. Expres. Purif.* **2006**, *48*, 1-13.

(24)   Porath, J.; Carlsson, J.; Olsson, I.; Belfrage, G. *Nature* **1975**, *258*, 598-599.

(25)   Graslund, S.; Nordlund, P.; Weigelt, J.; Bray, J.; Hallberg, B. M.; Gileadi, O.; Knapp, S.; Oppermann, U.; Arrowsmith, C.; Hui, R.; Ming, J.; Dhe-Paganon, S.; Park, H. W.; Savchenko, A.; Yee, A.; Edwards, A.; Vincentelli, R.; Cambillau, C.; Kim, R.; Kim, S. H.; Rao, Z.; Shi, Y.; Terwilliger, T. C.; Kim, C. Y.; Hung, L. W.; Waldo, G. S.; Peleg, Y.; Albeck, S.; Unger, T.; Dym, O.; Prilusky, J.; Sussman, J. L.; Stevens, R. C.; Lesley, S. A.; Wilson, I. A.; Joachimiak, A.; Collart, F.; Dementieva, I.; Donnelly, M. I.; Eschenfeldt, W. H.; Kim, Y.; Stols, L.; Wu, R.; Zhou, M.; Burley, S. K.; Emtage, J. S.; Sauder, J. M.; Thompson, D.; Bain, K.; Luz, J.; Gheyi, T.; Zhang, F.; Atwell, S.; Almo, S. C.; Bonanno, J. B.; Fiser, A.; Swaminathan, S.; Studier, F. W.; Chance, M. R.; Sali, A.; Acton, T. B.; Xiao, R.; Zhao, L.; Ma, L. C.; Hunt, J. F.; Tong, L.; Cunningham, K.; Inouye, M.; Anderson, S.; Janjua, H.; Shastry, R.; Ho, C. K.; Wang, D. Y.; Wang, H.; Jiang, M.; Montelione, G. T.; Stuart, D. I.; Owens, R. J.; Daenke, S.; Schutz, A.; Heinemann, U.; Yokoyama, S.; Bussow, K.; Gunsalus, K. C.; Consortium, S. G.; Macromol, A. F.; Ctr, B. S. G.; Consortium, C. S. G.; Function, I. C. S.; Ctr, I. S. P.; Genomics, J. C. S.; Genomics, M. C. S.; Ctr, N. Y. S. G. R.; Consortium, N. S. G.; Facility, O. P. P.; Facility, P. S. P.; Med, M. D. C. M.; Proteomics, R. S. G.; Complexes, S. *Nat. Methods* **2008**, *5*, 135-146.

(26)   Porath, J. *Protein. Expres. Purif.* **1992**, *3*, 263-281.

(27)   Crowe, J.; Dobeli, H.; Gentz, R.; Hochuli, E.; Stiiber, D.; Henco, K. In *Protocols for Gene Analysis*; Harwood, A., Ed.; Humana Press: 1994; Vol. 31, p 371-387.

(28)   Petty, K. J. In *Current Protocols in Molecular Biology*; John Wiley & Sons, Inc.: 2001.

(29)   Bornhorst, J. A.; Falke, J. J. In *Methods Enzymol.*; Jeremy Thorner, S. D. E. J. N. A., Ed.; Academic Press: 2000; Vol. 326, p 245-254.

(30)   Porath, J. *Protein. Expres. Purif.* **1992**, *3*, 263-281.

(31)   Schmitt, J.; Hess, H.; Stunnenberg, H. G. *Mol. Biol. Rep* **1993**, *18*, 223-230.

(32)   Ferrer-Miralles, N.; Corchero, J. L.; Kumar, P.; Cedano, J. A.; Gupta, K. C.; Villaverde, A.; Vazquez, E. *Microb. Cell. Fact.* **2011**, *10*.

(33)   Hochuli, E.; Bannwarth, W.; Dobeli, H.; Gentz, R.; Stuber, D. *Nat. Biotech* **1988**, *6*, 1321-1325.

(34)   Boi, C. *J. Chromatogr. B* **2007**, *848*, 19-27.

(35)   Yang, Q.; Adrus, N.; Tomicki, F.; Ulbricht, M. *J. Mater. Chem.* **2011**, *21*, 2783-2811.

(36)   Weaver, J.; Husson, S. M.; Murphy, L.; Wickramasinghe, S. R. *Biotechnol. Bioeng.* **2013**, *110*, 491-499.

(37)   Brandt, S.; Goffe, R. A.; Kessler, S. B.; Oconnor, J. L.; Zale, S. E. *Bio-Technol* **1988**, *6*, 779-782.

(38)   Kalghatgi, K.; Horvath, C. *J. Chromatogr* **1987**, *398*, 335-339.

(39)   Bhut, B. V.; Christensen, K. A.; Husson, S. M. *J. Chromatogr. A* **2010**, *1217*, 4946-4957.

(40)   Thommes, J.; Kula, M. R. *Biotechnol. Progr.* **1995**, *11*, 357-367.

(41)   Tsuneda, S.; Shinano, H.; Saito, K.; Furusaki, S.; Sugo, T. *Biotechnol. Progr.* **1994**, *10*, 76-81.

(42)   Janzen, R.; Unger, K. K.; Muller, W.; Hearn, M. T. W. *J. Chromatogr* **1990**, *522*, 77-93.

(43)   Milner, S. T. *Science* **1991**, *251*, 905-914.

(44)   Jain, P.; Dai, J.; Baker, G. L.; Bruening, M. L. *Macromolecules* **2008**, *41*, 8413-8417.

(45)   Bug, A. L. R.; Cates, M. E.; Safran, S. A.; Witten, T. A. *J. Chem. Phys.* **1987**, *87*, 1824-1833.

(46)   Kelley, T. W.; Schorr, P. A.; Johnson, K. D.; Tirrell, M.; Frisbie, C. D. *Macromolecules* **1998**, *31*, 4297-4300.

(47)   Zhao, B.; Brittain, W. J. *Prog. Polym. Sci* **2000**, *25*, 677-710.

(48)   Halperin, A.; Tirrell, M.; Lodge, T. P. *Adv. Polym. Sci* **1992**, *100*, 31-71.

(49)   Zajac, R.; Chakrabarti, A. *Phys. Rev. E* **1995**, *52*, 6536-6549.

(50)   Yan, M. D. *Chem-Eur. J* **2007**, *13*, 4138-4144.

(51)   Choi, I. S.; Langer, R. *Macromolecules* **2001**, *34*, 5361-5363.

(52)   Yang, H.; Ulbricht, M. *Macromol. Mater. Eng* **2008**, *293*, 419-427.

(53)   Wang, J. S.; Matyjaszewski, K. *J. Am. Chem. Soc* **1995**, *117*, 5614-5615.

(54)   Xu, F. J.; Liu, L. Y.; Yang, W. T.; Kang, E. T.; Neoh, K. G. *Biomacromolecules* **2009**, *10*, 1665-1674.

(55)   Tugulu, S.; Silacci, P.; Stergiopulos, N.; Klok, H.-A. *Biomaterials* **2007**, *28*, 2536-2546.

(56)   Glinel, K.; Jonas, A. M.; Jouenne, T.; Leprince, J.; Galas, L.; Huck, W. T. S. *Bioconjugate Chem.* **2009**, *20*, 71-77.

(57)   Blin, T.; Purohit, V.; Leprince, J.; Jouenne, T.; Glinel, K. *Biomacromolecules* **2011**, *12*, 1259-1264.

(58)   Xu, F. J.; Li, H. Z.; Li, J.; Teo, Y. H. E.; Zhu, C. X.; Kang, E. T.; Neoh, K. G. *Biosens. Bioelectron.* **2008**, *24*, 773-780.

(59)   Jain, P.; Vyas, M. K.; Geiger, J. H.; Baker, G. L.; Bruening, M. L. *Biomacromolecules* **2010**, *11*, 1019-1026.

(60)   Trmcic-Cvitas, J.; Hasan, E.; Ramstedt, M.; Li, X.; Cooper, M. A.; Abell, C.; Huck, W. T. S.; Gautrot, J. E. *Biomacromolecules* **2009**, *10*, 2885-2894.

(61)   Wan, D.; Yuan, S.; Li, G. L.; Neoh, K. G.; Kang, E. T. *ACS Appl. Mater. Inter.* **2010**, *2*, 3083-3091.

(62)   Diamanti, S.; Arifuzzaman, S.; Elsen, A.; Genzer, J.; Vaia, R. A. *Polymer* **2008**, *49*, 3770-3779.

(63)   Barbey, R.; Lavanant, L.; Paripovic, D.; Schuwer, N.; Sugnaux, C.; Tugulu, S.; Klok, H. A. *Chem. Rev.* **2009**, *109*, 5437-5527.

(64)   Sun, L.; Dai, J. H.; Baker, G. L.; Bruening, M. L. *Chem. Mat.* **2006**, *18*, 4033-4039.

(65)   Jain, P.; Sun, L.; Dai, J. H.; Baker, G. L.; Bruening, M. L. *Biomacromolecules* **2007**, *8*, 3102-3107.

(66)   Tugulu, S.; Silacci, P.; Stergiopulos, N.; Klok, H. A. *Biomaterials* **2007**, *28*, 2536-2546.

(67)   Schüwer, N.; Geue, T.; Hinestrosa, J. P.; Klok, H.-A. *Macromolecules* **2011**, *44*, 6868-6874.

(68)   Ko, S.; Jang, J. *Biomacromolecules* **2007**, *8*, 1400-1403.

(69)   Zhao, G.; Wang, J.; Li, Y.; Huang, H.; Chen, X. *Biochem. Eng. J.* **2012**, *68*, 159-166.

(70)   Xu, F. J.; Cai, Q. J.; Li, Y. L.; Kang, E. T.; Neoh, K. G. *Biomacromolecules* **2005**, *6*, 1012-1020.

(71)   Huang, J.; Han, B.; Yue, W.; Yan, H. *J. Mater. Chem.* **2007**, *17*, 3812-3818.

(72)   Jiang, H.; Xu, F.-J. *Chem. Soc. Rev.* **2013**, *42*, 3394-3426.

(73)   Siegwart, D. J.; Oh, J. K.; Matyjaszewski, K. *Prog. Polym. Sci.* **2012**, *37*, 18-37.

(74)   Dong, R.; Krishnan, S.; Baird, B. A.; Lindau, M.; Ober, C. K. *Biomacromolecules* **2007**, *8*, 3082-3092.

(75)   Retsch, M.; Walther, A.; Loos, K.; Müller, A. H. E. *Langmuir* **2008**, *24*, 9421-9429.

(76)   Zhang, C.; Thompson, M. E.; Markland, F. S.; Swenson, S. *Acta Biomater.* **2011**, *7*, 3746-3756.

(77)   Yuan, S.; Xiong, G.; Wang, X.; Zhang, S.; Choong, C. *J. Mater. Chem.* **2012**, *22*, 13039-13049.

(78)   Hutter, N. A.; Steenackers, M.; Reitinger, A.; Williams, O. A.; Garrido, J. A.; Jordan, R. *Soft Matter* **2011**, *7*, 4861-4867.

(79)   Dai, J. H.; Bao, Z. Y.; Sun, L.; Hong, S. U.; Baker, G. L.; Bruening, M. L. *Langmuir* **2006**, *22*, 4274-4281.

(80)   Cullen, S. P.; Liu, X.; Mandel, I. C.; Himpsel, F. J.; Gopalan, P. *Langmuir* **2008**, *24*, 913-920.

(81)   Kusumo, A.; Bombalski, L.; Lin, Q.; Matyjaszewski, K.; Schneider, J. W.; Tilton, R. D. *Langmuir* **2007**, *23*, 4448-4454.

(82)   Lei, Z.; Bi, S. *J. Biotechnol.* **2007**, *128*, 112-119.

(83)   Bhut, B. V.; Husson, S. M. *J. Membr. Sci.* **2009**, *337*, 215-223.

(84)   He, D. M.; Ulbricht, M. *J. Membr. Sci.* **2008**, *315*, 155-163.

(85)   Gautrot, J. E.; Huck, W. T. S.; Welch, M.; Ramstedt, M. *ACS Appl. Mater. Inter.* **2010**, *2*, 193-202.

(86)   Anuraj, N.; Bhattacharjee, S.; Geiger, J. H.; Baker, G. L.; Bruening, M. L. *J. Membr. Sci.* **2012**, *389*, 117-125.

(87)   Jain, P.; Sun, L.; Dai, J.; Baker, G. L.; Bruening, M. L. *Biomacromolecules* **2007**, *8*, 3102-3107.

(88)   Lightfoot, E. N.; Moscariello, J. S. *Biotechnol. Bioeng.* **2004**, *87*, 259-273.

(89)   Schlenoff, J. B.; Dubas, S. T.; Farhat, T. *Langmuir* **2000**, *16*, 9968-9969.

(90)   Decher, G.; Schmitt, J.; Brand, F.; Lehr, B.; Oeser, R.; Losche, M.; Bouwman, W.; Kjaer, K.; Calvert, J.; Geer, R.; Dressik, W.; Shashidhar, R. *Abstr. Pap. Am. Chem. S.* **1997**, *214*, 42.

(91)   Decher, G.; Hong, J. D.; Schmitt, J. *Thin Solid Films* **1992**, *210*, 831-835.

(92)   Lowack, K.; Helm, C. A. *Macromolecules* **1998**, *31*, 823-833.

(93)   Zhao, J. J.; Bradbury, C. R.; Fermin, D. J. *J. Phys. Chem. C* **2008**, *112*, 6832-6841.

(94)   Schwarz, S.; Eichhorn, K. J.; Wischerhoff, E.; Laschewsky, A. *Colloids Surf., A* **1999**, *159*, 491-501.

(95) Dautzenberg, H.; Rother, G. *J. Polym. Sci., Part A: Polym. Phys.* **1988**, *26*, 353-366.

(96) Zhu, H. G.; Srivastava, R.; McShane, M. J. *Biomacromolecules* **2005**, *6*, 2221-2228.

(97) Glinel, K.; Moussa, A.; Jonas, A. M.; Laschewsky, A. *Langmuir* **2002**, *18*, 1408-1412.

(98) Joanny, J. F. *Eur. Phys. J. B* **1999**, *9*, 117-122.
(99) Choi, J.; Rubner, M. F. *Macromolecules* **2005**, *38*, 116-124.

(100) Jewell, C. M.; Lynn, D. M. *Adv. Drug. Deliver. Rev.* **2008**, *60*, 979-999.

(101) Almodóvar, J.; Place, L. W.; Gogolski, J.; Erickson, K.; Kipper, M. J. *Biomacromolecules* **2011**, *12*, 2755-2765.

(102) Lvov, Y.; Ariga, K.; Ichinose, I.; Kunitake, T. *J. Am. Chem. Soc* **1995**, *117*, 6117-6123.

(103) Shutava, T. G.; Kommireddy, D. S.; Lvov, Y. M. *J. Am. Chem. Soc* **2006**, *128*, 9926-9934.

(104) Ladam, G.; Schaaf, P.; Cuisinier, F. J. G.; Decher, G.; Voegel, J. C. *Langmuir* **2001**, *17*, 878-882.

(105) Kepplinger, C.; Lisdat, F.; Wollenberger, U. *Langmuir* **2011**, *27*, 8309-8315.

(106) Saurer, E. M.; Flessner, R. M.; Sullivan, S. P.; Prausnitz, M. R.; Lynn, D. M. *Biomacromolecules* **2010**, *11*, 3136-3143.

(107) Liu, D.; Liu, H. Y.; Hu, N. F. *Electrochim Acta* **2010**, *55*, 6426-6432.

(108) Ladhari, N.; Hemmerle, J.; Haikel, Y.; Voegel, J. C.; Ball, V. *Bio-Med. Mater. Eng.* **2010**, *20*, 217-225.

(109) Liu, Y.; Liu, H. Y.; Guo, X. H.; Hu, N. F. *Electroanal.* **2010**, *22*, 2261-2268.

(110) Muller, M.; Torger, B.; Kessler, B. *Adv. Eng. Mater.* **2010**, *12*, B676-B683.

(111) Ladam, G.; Gergely, C.; Senger, B.; Decher, G.; Voegel, J. C.; Schaaf, P.; Cuisinier, F. J. G. *Biomacromolecules* **2000**, *1*, 674-687.

(112) Volodkin, D.; Von Klitzing, R.; Moehwald, H. *Polymers* **2014**, *6*, 1502-1527.

(113) Uhlig, K.; Madaboosi, N.; Schmidt, S.; Jager, M. S.; Rose, J.; Duschl, C.; Volodkin, D. V. *Soft Matter* **2012**, *8*, 11786-11789.

(114) Decher, G. *Science* **1997**, *277*, 1232-1237.

(115) Schönhoff, M. *Curr. Opin. Colloid & Int. Sci.* **2003**, *8*, 86-95.

(116) v. Klitzing, R. *PCCP Phys. Chem. Ch. Ph.* **2006**, *8*, 5012-5033.

(117) Volodkin, D.; von Klitzing, R. *Curr. Opin. Colloid & Int. Sci.* **2014**, *19*, 25-31.

(118) Nazaran, P.; Bosio, V.; Jaeger, W.; Anghel, D. F.; v. Klitzing, R. *J. Phy. Chem. B* **2007**, *111*, 8572-8581.

(119) Ghostine, R. A.; Markarian, M. Z.; Schlenoff, J. B. *J. Am. Chem. Soc.* **2013**, *135*, 7636-7646.

(120) Lavalle, P.; Picart, C.; Mutterer, J.; Gergely, C.; Reiss, H.; Voegel, J.-C.; Senger, B.; Schaaf, P. *J. Phy. Chem. B* **2004**, *108*, 635-648.

(121) Dodoo, S.; Steitz, R.; Laschewsky, A.; von Klitzing, R. *PCCP Phys. Chem. Ch. Ph.* **2011**, *13*, 10318-10325.

(122) Ladam, G.; Gergely, C.; Senger, B.; Decher, G.; Voegel, J.-C.; Schaaf, P.; Cuisinier, F. J. G. *Biomacromolecules* **2000**, *1*, 674-687.

(123) Richert, L.; Lavalle, P.; Vautier, D.; Senger, B.; Stoltz, J. F.; Schaaf, P.; Voegel, J. C.; Picart, C. *Biomacromolecules* **2002**, *3*, 1170-1178.

(124) Ma, Y. D.; Dong, J. L.; Bhattacharjee, S.; Wijeratne, S.; Bruening, M. L.; Baker, G. L. *Langmuir* **2013**, *29*, 2946-2954.

(125) Volodkin, D.; Madaboosi, N.; Blacklock, J.; Skirtach, A.; Mohwald, H. *Langmuir* **2009**, *25*, 14037-14043.

(126) Srivastava, S.; Ball, V.; Podsiadlo, P.; Lee, J.; Ho, P.; Kotov, N. A. *J. Am. Chem. Soc.* **2008**, *130*, 3748-3749.

(127) Salloum, D. S.; Schlenoff, J. B. *Biomacromolecules* **2004**, *5*, 1089-1096.

(128) Lu, H. Y.; Hu, N. F. *J. Phys. Chem. B* **2006**, *110*, 23710-23718.

(129) Yuan, W. Y.; Lu, Z. S.; Wang, H. L.; Li, C. M. *Adv. Funct. Mater.* **2012**, *22*, 1932-1939.

(130) Dragan, E. S.; Bucatariu, F.; Hitruc, G. *Biomacromolecules* **2010**, *11*, 787-796.

(131) Mustang   Membrane   Chromatography   Starter   Kits. http://www.pall.com/main/Biopharmaceuticals/Product.page?id=33053 (accessed July, 19 2015),

Part of this chapter is adapted from our previous manuscripts (Wijeratne, S.; Bruening, M. L.; Baker, G. L. Layer-by-Layer Assembly of Thick, Cu^{2+}-Chelating Films, *Langmuir* **2013**, *29,* 12720 and Ning, W.; Wijeratne, S**.**; Dong, J.; Bruening, M. L. Immobilization of Carboxymethylated Polyethyleneimine-Metal Ion Complexes in Porous Membranes to Selectively Capture His-tagged Protein, *ACS Appl. Mater. Interfaces* **2015**, *7*, 2575.) Wenjing Ning prepared the protein binding membranes.

CHAPTER 2. SYNTHESIS, CHARACTERIZATION AND DIRECT DEPOSITION OF IMMINODIACETIC ACID (IDA)-CONTAINING POLYMERS FOR PROTEIN BINDING APPLICATIONS.

2.1. Introduction.

Compared to the synthesis of polymer brushes, which is a relatively cumbersome process that frequently requires initiator immobilization and subsequent polymerization under anaerobic conditions, LbL deposition is quite simple. Our group previously employed LbL adsorption of poly(acrylic acid) (PAA)/(polyethyleneimine) (PEI) films followed by derivatization with aminobutyl nitrilotriacetate (NTA) and Ni^{2+} to form NTA-Ni^{2+} complexes that capture His-tagged proteins.[1] However, derivatization represents more than 95% of the cost of chemicals and materials for creating these protein-binding membranes, and most of the aminobutyl NTA does not couple to the membrane. Moreover, in addition to NTA these membranes contain residual PAA -COOH groups that bind metal ions only weakly, which leads to metal-ion leaching.

This study examines whether direct adsorption of relatively inexpensive polyelectrolytes containing chelating groups effectively modifies porous membranes or flat surfaces to bind metal ions and capture His-tagged protein. Specifically, we synthesized the two IDA-containing metal-ion-binding polymers in Figure 2.1 and examined metal-ion and protein binding in LbL films containing these polymers. In addition to protein capture,[2,3] these and similar films may be attractive for applications such as ion capture and separation,[4-6] catalysis,[7,8] and fluorescence sensing.[9] Some films containing metal-ion complexes also exhibit antimicrobial properties.[10]

(Carboxymethylated branched polyethyleneimine) (CMPEI)

poly[(N,N-dicarboxymethyl)allylamine] (PDCMAA)
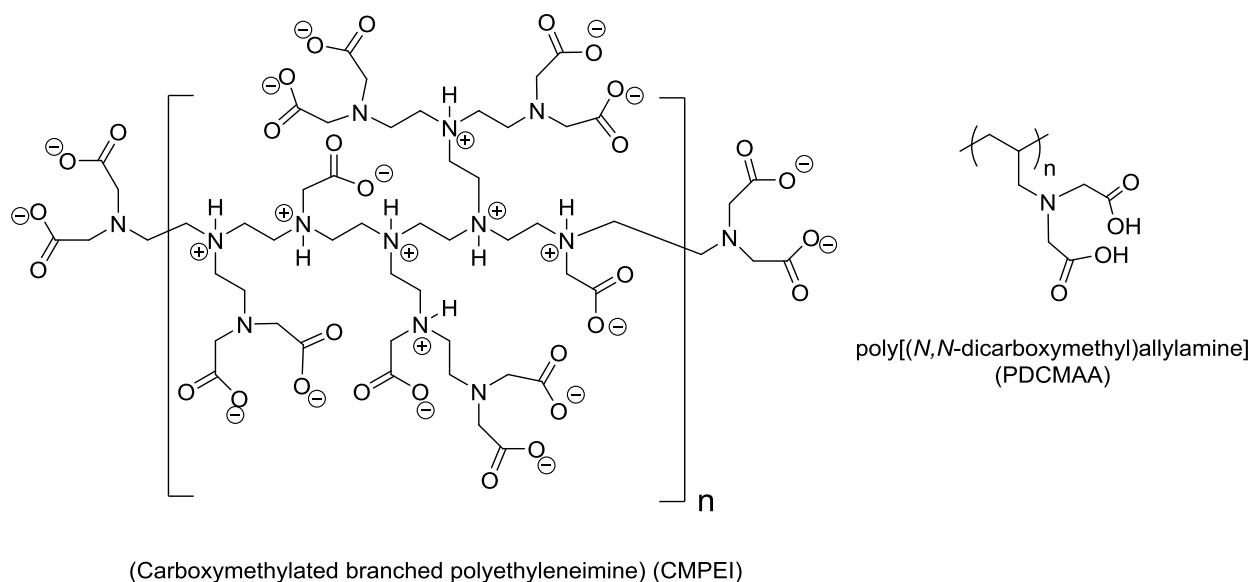
Figure 2.1. Structures of CMPEI and PDCMAA.

A number of papers described the incorporation of metal-ion complexes in LBL films, but the formation of thick films that strongly bind metal ion is challenging. One form of LBL assembly directly employs metal-ion coordination to connect neighboring

polymers.[9,11-14] However, the thicknesses of such films are typically <3 nm/per bilayer,[12] and elution of the metal ion delaminates the film unless it is cross-linked. In a second LBL method for creating metal-ion-containing films, functional groups in the film, e.g. carboxylates, bind metal ions after film formation.[2,8,15] Subsequent reduction of these ions leads to metal nanoparticles.[16] Polymer-metal ion complexes can also serve as the polyelectrolytes for LBL assembly.[17] However, most metal-ion binding polyelectrolytes exploit carboxylates and amines for metal-ion capture, and such metal-ion binding is
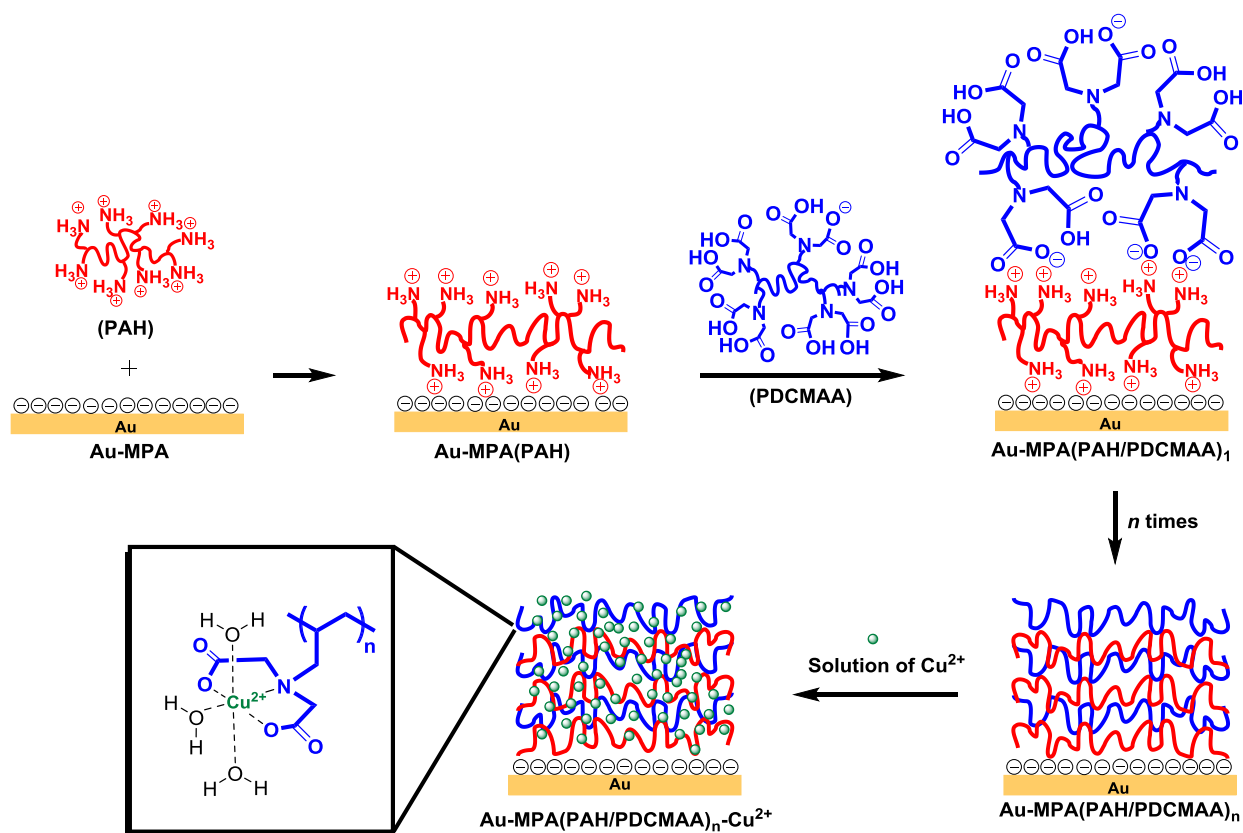
Figure 2.2. Schematic representation of the assembly of (PAH/PDCMAA)$_n$-Cu^{2+} films on Au-coated substrates modified with a monolayer of 3-mercaptopropionic acid (MPA). The layering of polymers represents the number of depositions steps, but is likely not present in the film structure.

relatively weak. Moreover, the film thickness per layer is relatively low. Strong binding is important to prevent metal-ion leaching in applications such as metal-affinity chromatography where proteins bind to immobilized metal ions.[2]

Several recent studies introduced polyanion/polycation complexes as building blocks for multilayer assembly, including the formation of films containing metal ions.[7,18] Compared to LBL assembly with conventional polyelectrolytes, deposition of polyanion/polycation complexes leads to thick films and high metal-ion loadings with only a few deposition steps. Nevertheless, metal-ion-binding is still relatively weak because the polyelectrolyte complexes typically contain conventional carboxylate- and amine-based polyelectrolytes.

Another approach to obtaining thick LBL films employs alternating assembly where one of the polyelectrolytes diffuses throughout the film, which leads to an exponential growth in film thickness with the number of deposited layers.[19] Typically, exponential growth occurs with polyelectrolytes that have a low charge density. In some cases such films undergo an exponential to linear growth transition because the depositing electrolyte cannot diffuse throughout the entire film, but the thickness per layer is still very high.[20,21]

This work first describes LBL adsorption (Figure 2.2) of PAH and poly[*N*,*N*-dicarboxymethyl(allylamine)] (PDCMAA) to give films with unusually high thicknesses, presumably because of an exponential growth mechanism. We chose to employ PDCMAA because its IDA-containing side chains form stable complexes with metal ions such as Cu^{2+}. IDA is also a well-known ligand for immobilized metal affinity chromatography.[22,23] Equally important, at low pH PDCMAA has a relatively low charge

density per number of atoms, which leads to rapid film growth. Controlling the deposition pH during assembly of (PAH/PDCMAA)$_n$ films affords tunable bilayer thicknesses up to 200 nm. Moreover, μm-thick films are stable over at least 4 cycles of Cu^{2+} binding and elution. The first part of this chapter will examine the growth of (PAH/PDCMAA)$_n$ films at several pH values and the thermodynamics and kinetics of Cu^{2+} binding to the thickest films.

However, binding of a metal ion such as Cu^{2+} or Zn^{2+} is a necessary but not sufficient condition for creating membranes that selectively capture large amounts of polyhistidine-tagged protein. The adsorbed polymer must also swell in water to provide enough space for protein-ligand interactions. Unfortunately, PAH/PDCMAA films do not swell sufficiently for extensive protein capture. The lack of PDCMAA swelling could stem from the hydrophobic backbone of this polymer, hence changing the backbone to the more hydrophilic polyethyleneimine may lead to increased swelling. Based on this assumption, I derivatized polyethyleneimine with chloro or bromoacetic acid to synthesize carboxymethylated polyethyleneimine (CMPEI) (Figure 2.1). Because at neutral pH CMPEI carries both positive (protonated amines) and negative (deprotonated carboxylic acids) charge, alternating adsorption of CMPEI and a polycation (PAH) leads to film growth. We showed that compared with the dry state, the thicknesses of CMPEI/PAH films increase ~6 fold after immersion in a pH 7 buffer. Thus, these coatings should have sufficient open space for binding proteins. Sequential adsorption of PAH and CMPEI leads to membranes that bind Ni^{2+} and capture ~60 mg of His-tagged ubiquitin per mL of membrane and this number is higher than the capacity of commercially available systems. To demonstrate these membranes can isolate His-

tagged protein directly from cell extracts, we purified His-tagged SUMO protein that was over-expressed in E. coli.

2.2. Experimental Section.

2.2.1.Materials.

Poly(allylamine hydrochloride) was purchased from Alfa Aesar (molecular weight 120,000 ~ 200,000 Da, used for LbL deposition) or from Aldrich (molecular weight ~58,000 Da, employed for PDCMAA synthesis). Poly(ethyleneimine) (PEI, 50 wt% solution in water, M_n~6.0 x10^4 Da, repeating unit M_W=473 gmol^{-1}) was also obtained from Aldrich. The appendix describes the synthesis of CMPEI and PDCMAA and provides NMR and IR spectra of the polymers (Figures A2.1, A2.2 and A2.5) along with a titration curve (Figure A2.3). (Figure numbers beginning with "A" refer are in the appendix.) Sodium chloroacetate (98%) and 3-mercaptopropionic acid (MPA, 99%) were received from Aldrich and used without further purification. Aqueous solutions of 0.02 M PAH and 0.01 M PDCMAA (polymer concentrations are given with respect to the repeating unit) were prepared in deionized water (18.2 MΩcm, Milli-Q). PDCMAA-containing solutions with various pH values (3.0, 5.0, 7.0 and 9.0) were obtained by first dissolving the polymer with the addition of 6 M NaOH to achieve a pH 9.0 solution and then adjusting the pH with 6 M HCl. Gold-coated wafers prepared by sputter coating of 200 nm of gold on 20 nm of Cr on Si(100) wafers (coating was performed by LGA Thin Films, Santa Clara, CA) were cleaned in a UV/O$_3$ chamber for 15 min just before use. A stock solution of Cu^{2+} was obtained by dissolving CuSO$_4$•5H$_2$O in 20 mM phosphate

solution. For binding studies, the stock solution was diluted with 20 mM phosphate solution to give the desired concentration of Cu^{2+} ions.

2.2.2. Preparation of (PAH/PDCMAA)$_n$ Films.

To immobilize a monolayer of –COOH groups on a substrate, Au-coated Si wafers (24 mm × 11 mm) were immersed in 5 mM MPA in ethanol for 12 h, rinsed with ethanol and dried with N_2. Subsequent adsorption of PAH occurred during substrate immersion for 5 min in a 0.02 M PAH solution adjusted to pH 3.0, 5.0, 7.0, or 9.0. After rinsing with flowing deionized water for 1 min and drying with N_2, the Au-MPA(PAH) substrates were immersed in a 0.01 M PDCMAA solution (adjusted to the desired pH of 3.0, 5.0, 7.0, or 9.0) for 5 min and again rinsed with deionized water and dried with N_2. This process was repeated to obtain the desired number of PAH/PDCMAA multilayers.

2.2.3. Quantitation of Cu^{2+} Binding to (PAH/PDCMAA)$_n$ Films.

Au-coated wafers modified with (PAH/PDCMAA)$_n$ films (n = 1 to 10) assembled at different pH values (pH 3.0, 5.0, 7.0 or 9.0) were separately immersed in vials containing 10 ml of 1.40 mM $CuSO_4$ (20 mM phosphate solution adjusted to pH 4.1 with HCl) and incubated for 15 h. Before the Cu^{2+}-sorption experiments but after film deposition, the back sides of the Au-coated wafers were covered with Scotch transparent duct tape to limit Cu^{2+} sorption to the front side of the film-coated wafer. (This reduced the Cu^{2+} sorption nearly 50%.)   After rinsing the wafers with deionized water from a squirt bottle for 1 min, the Cu^{2+} was eluted from the films by immersing the

substrates in 5.0 mL of 20 mM EDTA (adjusted to pH 7.4) for 12 h. Using atomic absorption spectroscopy (Varian Spectra AA-200 atomic absorption spectrophotometer), the amount of Cu^{2+} in the stripping solution was calculated from its absorbance using a calibration curve. Both the standard and sample solutions contained 20 mM EDTA (pH 7.4). To examine the effect of the Cu^{2+} solution pH on sorption, Au-coated wafers modified with $(PAH/PDCMAA)_{10}$ films (assembled at various pH values) were separately immersed in vials containing 10 ml of 1.40 mM $CuSO_4$ at pH 4.0, 5.0 and 6.0 (20 mM phosphate solutions adjusted to the desired pH), and incubated for 15 h. Elution of Cu^{2+} ions and sample analysis to determine the amount of Cu^{2+} bound to each film occurred as described above. When establishing the equilibration time for maximum Cu^{2+} sorption and evaluating the sorption kinetics of Cu^{2+} binding, $(PAH/PDCMAA)_{10}$-coated wafers were separately immersed in 10 mL of 1.40 mM Cu^{2+} (pH 4.0, 20 mM phosphate) for various times prior to determination of Cu^{2+} binding following the above procedure.

To obtain isotherms for Cu^{2+} sorption in $(PAH/PDCMAA)_{10}$ films deposited at pH 3.0, a series of Au-coated wafers modified with $(PAH/PDCMAA)_{10}$ films were immersed separately in 10 mL of 0.007-1.40 mM Cu^{2+} (pH 4.0, 20 mM phosphate) and incubated at five different temperatures (4, 16, 25, 31 or 37 ^{o}C) for 15 h. Then $(PAH/PDCMAA)_{10}$-Cu^{2+}-coated wafers were rinsed with deionized water for 1 min, and Cu^{2+} ions were eluted and analyzed as described above. For all ellipsometric thicknesses, refractive indices, and Cu^{2+} sorption data, uncertainties and error bars represent the standard deviations of measurements with at least 3 different films. In the case of isotherms,

59

each point represents sorption in a different film, but these data were not repeated due to the large number of measurements.

2.2.4. Characterization of Monomers, Polymers, and (PAH/PDCMAA)$_n$ Films.

A Varian UnityPlus-500 spectrometer was used to record ^{1}H and ^{13}C NMR spectra at room temperature for synthesized and purchased polymers. The chemical shifts are reported in ppm and referenced to residual signals from deuterated solvents. The "dry" thicknesses for multilayer polyelectrolyte films were determined with a rotating analyzer spectroscopic ellipsometer (model M-44, J. A. Woollam) using WVASE32 software. Both refractive index and thickness were fitting parameters. A Cauchy model was employed to fit the refractive index as a function of wavelength. In situ ellipsometry in aqueous solutions was performed using a home-built cell described previously.[24] After the dry layer thickness was determined in air, water was added to the cell, and the thickness of the swollen film was recorded after 10 min. Reflectance Fourier Transform Infrared (reflectance FTIR) spectra of films were obtained with a Thermo Nicolet 6700 FTIR spectrometer that contained a mercury-cadmium telluride detector and a PIKE grazing angle (80°) attachment. Typically, 128 scans were collected for each spectrum. The AFM morphology images (Cypher™ atomic force microscope) of (PAH/PDCMAA)$_{10}$ films on Au-coated wafers were recorded in tapping mode (amplitude ratio = 0.90-0.99) using a silicon nitride tip. AFM images are shown in height mode without any image processing except flattening. Scanning rates were between 1.0 and 2.0 Hz. SEM images were obtained with a Hitachi S-4700 II field-emission scanning electron microscope. The samples were coated with 5 nm of sputtered gold prior to imaging. For

cross sectional images, the samples were soaked in liquid nitrogen before fracturing to expose the cross section.

2.3. Results and Discussion.

2.3.1. Adsorption of μm-thick (PAH/PDCMAA)$_n$ Films.

Alternating adsorption of PAH and PDCMAA on Au-coated substrates modified with MPA provides a simple method for preparing films with metal-ion-binding groups. Remarkably the ellipsometric thicknesses of (PAH/PDCMAA)$_n$ films reach values as high as 1 μm after adsorption of only 10 bilayers (Figure 2.3b and d), creating films with high metal-binding capacities (see below). However, film thickness is a complicated function of the number of adsorbed layers and deposition pH.

For weak polyelectrolytes the pH of adsorption solutions controls the degree of ionization and hence the charge density along the polymer chain. This in turn greatly affects both the polymer conformation and the amount of polyelectrolyte that adsorbs on a surface.[25] In aqueous solutions the pK_a values of free IDA, the metal-binding group in PDCMAA repeating units, are pK_{a1} = 1.8, pK_{a2} = 2.5 and pK_{a3} = 9.1 (Scheme 2.1).[26,27] Titration of PDCMAA with HCl (Figure A2.3) suggests fully protonated amine groups in the polymer below pH 8.0, whereas protonation of carboxylic acid groups occurs primarily below pH 4.0. Moreover, on going from pH 4.0 to 10.0, the fraction of protonated amines in PAH decreases from 96 to 30%.[28] Therefore, solution pH controls the charge densities on both PAH and PDCMAA.
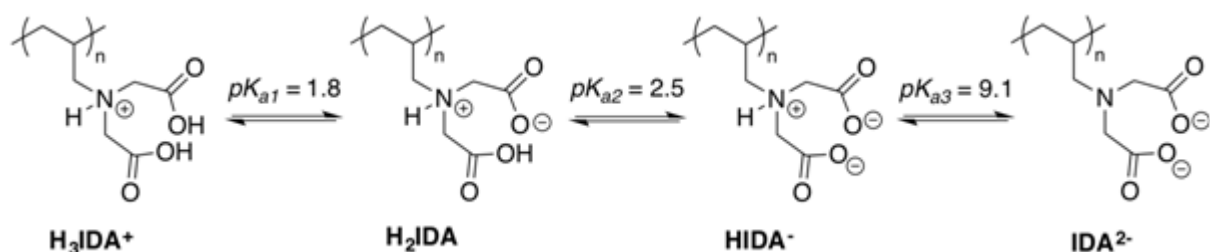
Scheme 2.1. Protonation states of the IDA groups of PDCMAA. The pK_a values are those of IDA that is not attached to a polymer.[27]
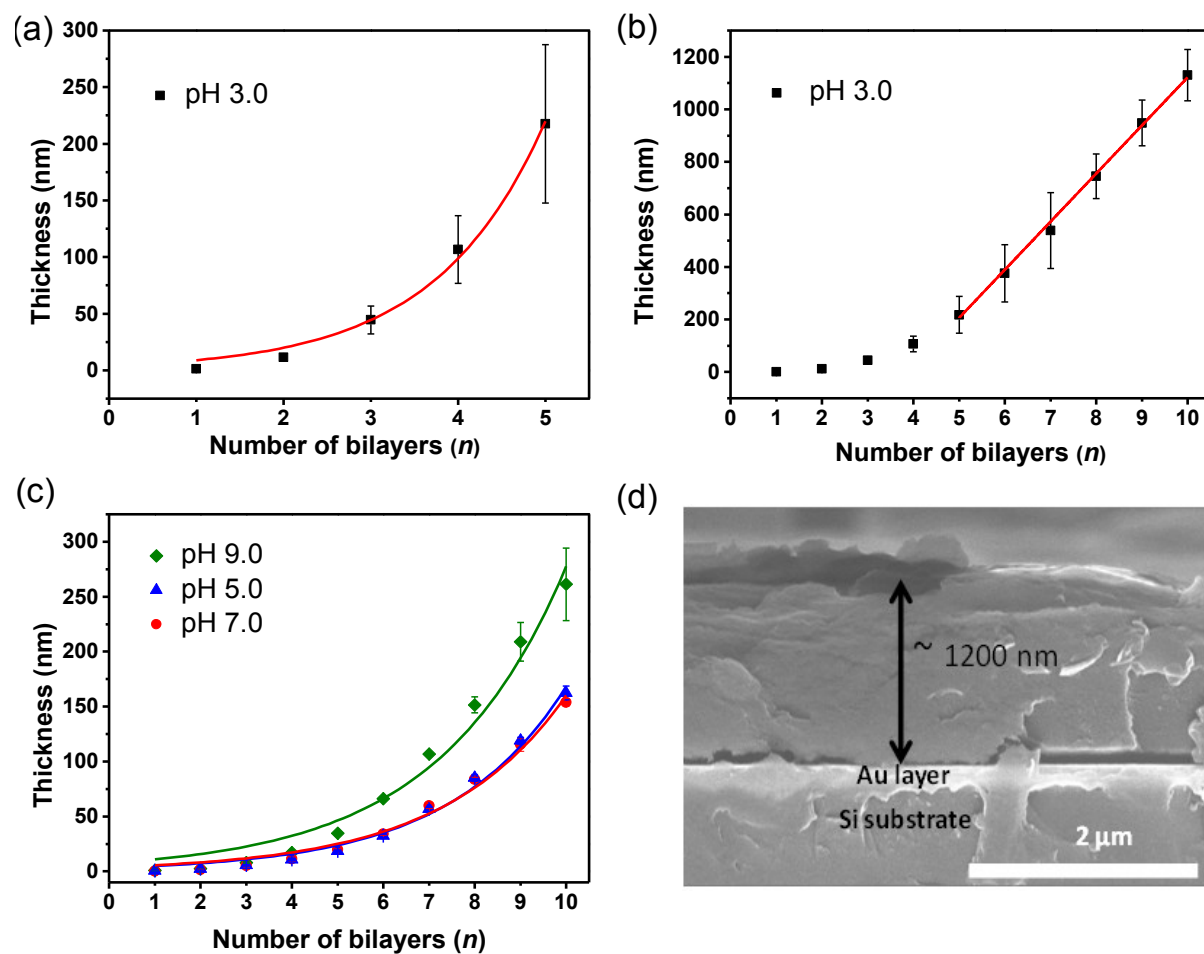
Figure 2.3. Thicknesses of (PAH/PDCMAA)$_n$ films adsorbed from solutions with different pH values. (a,b) Adsorption at pH 3.0 leads to an exponential increase in ellipsometric film thickness with the number of adsorbed layers for n=1 to 5 and a linear increase in film thickness for n = 5 to 10. (c) Adsorption at pH 5.0, 7.0 or 9.0 gives an exponential increase in ellipsometric film thicknesses for n=1 to 10. Curves show exponential or linear fits to the data. (d) Cross-sectional SEM image of a (PAH/PDCMAA)$_{10}$ film deposited at pH 3.0.

With respect to the adsorption solution pH, the thicknesses of (PAH/PDCMAA)$_n$ films increase in the order pH 5.0, 7.0< pH 9.0 < pH 3.0, and films deposited at pH 3.0 are especially thick (Figure 2.3). At adsorption pH values of 5.0 and 7.0 PAH is more than 80% protonated,[28] and PDCMAA should carry a net charge of ~-1 per repeating unit (Figure A2.3). These relatively high charge states likely lead to the most extended polymers and the thinnest films. When the deposition pH increases to 9.0, PAH becomes less protonated whereas PDCMAA should carry a net charge <-1 (Figure A2.3). The decreased ionization of PAH at pH 9.0 likely yields a less extended polymer that leads to a small (<2-fold) increase in thickness with respect to films formed at pH 5.0 or 7.0. In contrast, at pH 3.0 the net charge per repeat unit of PDCMAA is >-1 (Figure A2.3), and film thickness increases dramatically compared to assembly at other pH values, probably because of increased loops in the polymer and more penetration of PDCMAA into the film. Prior studies show that the rate of polyelectrolyte diffusion into multilayer films increases with decreasing charge density and affects the film growth mechanism.[29]

With adsorption at pH 3.0, film thickness initially increases exponentially with the number of bilayers (Figure 2.3a) and then becomes linear (Figure 2.3b). Models for such growth suggest that at first one of the polyelectrolytes deposits throughout the film, but subsequent changes in films structure restrict penetration of the polyelectrolyte to only an outer region of the film, albeit a large outer region.[21,30] For the linear region in Figure 2.3b, the growth rate is about 200 nm per bilayer. Although this rate is much larger than that for polyelectrolyte films prepared with strong electrolytes,[31,32] there are a

few examples of films with μm thicknesses prepared from weak polyelectrolytes via exponential growth.[33,34]

Deposition pH also affects film structure. The AFM images in Figure 2.4 show clear variations in surface morphologies of (PAH/PDCMAA)$_{10}$ films as a function of adsorption pH. Films deposited at pH 5.0 and 7.0 (Figure 2.4b and c) have surface roughnesses of 7 and 4 nm, respectively. In these coatings extended polyelectrolytes give rise to a relatively smooth surface. In contrast, PAH/PDCMAA deposition at pH 3.0 and 9.0 yields coatings with surface roughnesses of 74 and 24 nm, respectively (Figure 2.4a and 3d). Loops and tails in these films likely lead to the high roughness.[35] Such high roughnesses may cause errors in ellipsometric determinations of film thickness, because the models for ellipsometric data typically assume flat surfaces. However, even for the very rough films deposited at pH 3.0, thicknesses determined from SEM images are consistent with those from ellipsometry (see Figure 2.3d). Moreover, the surface roughness of 74 nm is only ~6% of the total film thickness.
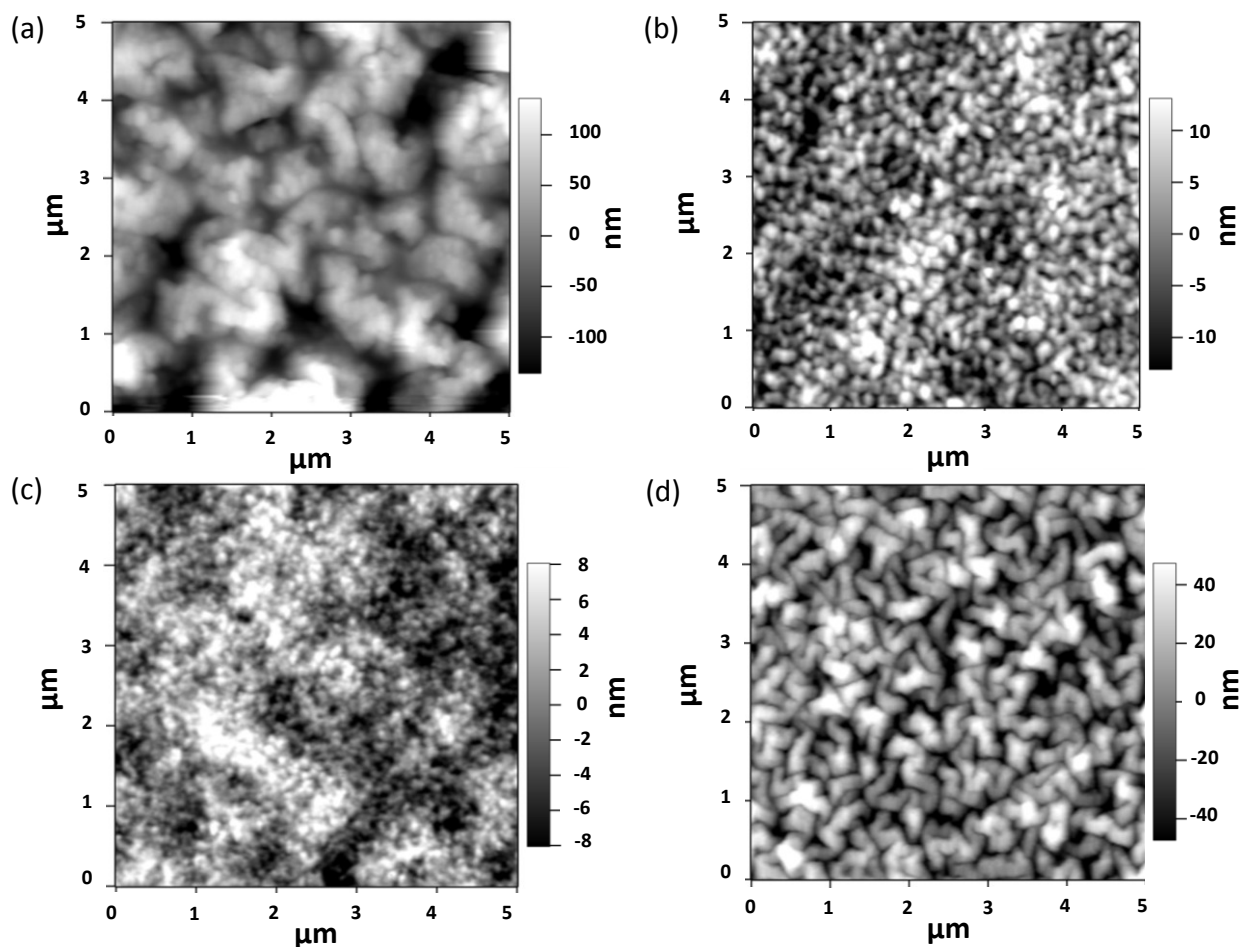
Figure 2.4. AFM topography images of (PAH/PDCMAA)$_{10}$ films adsorbed at (a) pH 3.0, (b) pH 5.0, (c) pH 7.0 and (d) pH 9.0.

Water contact angles on (PAH/PDCMAA)$_{10}$ films increase dramatically from 5° to 80° when the assembly pH increases from 3.0 to 9.0. Films deposited at pH 5.0 and 7.0 show intermediate water contact angles of 50° and 58°, respectively. Deposition of PDCMAA at pH 3.0 results in many –COOH groups, and subsequent deprotonation of these groups in water (see Figure A2.6a) probably leads to the very hydrophilic surface. Moreover, the high surface roughness and sorbed water in films deposited at pH 3.0 (see the appendix) should contribute to the low contact angles. In contrast, the high water contact angles on coatings formed at pH 9.0 indicate a surface dominated by

polymer backbones[36] or perhaps lightly protonated PAH. In films adsorbed at pH 9.0,

either most –COO[-] groups form ion pairs with ammonium groups of PAH, or PDCMAA

is buried within the film even though PDCMAA adsorption is the last step in film

formation. This is consistent with an exponential growth mechanism where PDCMAA

either diffuses into the film or PAH diffuses out of the film to form PDCMAA/PAH

complexes. Similar phenomena may occur at deposition pH values of 5.0 and 7.0 to

give the intermediate contact angles, but a more protonated PAH could lead to higher

surface energies. The appendix discusses measurements of ethylene glycol contact

angles to examine polar and nonpolar surface tensions (see Figure A2.7).

2.3.2. Sorption of Cu^{2+} Ions in $(PAH/PDCMAA)_n$ Films.

After immersion in a 1.40 mM $CuSO_4$ solution for 15 h and rinsing with deionized water,

changes in the reflectance IR spectra of a $(PAH/PDCMAA)_n$ film provide evidence for

Cu^{2+} coordination to carboxylate groups. Upon Cu^{2+} binding, the spectrum shows a –

COO[-] asymmetric stretching peak at 1641 cm^{-1} (see Figure A2.2a), presumably due to

the formation of a Cu^{2+}-iminodiacetate complex. Prior to complexation the spectrum of

the films contain an asymmetric –COO[-] stretching peak at 1652 cm^{-1} and a shoulder

due to the acid carbonyl stretch (1724 cm^{-1}). Spectral interpretation is difficult, however,

because the degree of ionization depends on pH, and in a resin containing IDA

functionalities, the Cu^{2+}-carboxylate stretch appeared around 1620 cm^{-1}.[37]

To quantify the amount of Cu^{2+} strongly sorbed in $(PAH/PDCMAA)_{10}$ films, we

immersed film-coated substrates in 1.40 mM $CuSO_4$ (pH 4.1), rinsed the films with

water, eluted the bound Cu^{2+} with 20 mM EDTA (pH 7.4) and determined the amount of

Cu^{2+} in the eluate using atomic absorption spectrophotometry. The excess EDTA relative to the amount of immobilized IDA should ensure elution of essentially all of the Cu^{2+} ions from the film. Moreover, EDTA has a higher binding constant for Cu^{2+} than IDA.[38] Figure 2.5a shows the Cu^{2+} binding capacities per unit area for coatings deposited at different pH values. For all films, the Cu^{2+} binding capacity increases with the number of bilayers, and the trends in Cu^{2+}-binding capacities as a function of film deposition pH are similar to trends in film thickness (compare Figure 2.5a and Figure 2.3).

Using the ellipsometric thicknesses of "dry" films, we estimated the concentrations of Cu^{2+} inside the different coatings (Figure 2.5b). For films with more than 4 or 5 bilayers, the concentrations of Cu^{2+} in the films do not change with the number of bilayers, showing that the Cu^{2+} binds throughout the film. Figure 2.5b suggests that for films with more than one bilayer, coatings deposited at pH 3.0 contain the lowest concentrations of Cu^{2+}. However, as discussed in the appendix (see Figures A2.10 and A2.11) "dry" $(PAH/PDCMAA)_n$ films deposited at pH 3.0 have a lower refractive index than films deposited at other pH values, probably because of some water sorption at ambient conditions. Thus the "dry" ellipsometric thicknesses of coatings adsorbed at pH 3.0 likely overestimate the true thickness of a dehydrated film, which will lead to an underestimation of the Cu^{2+} concentration in the film.

For films with 5 or more bilayers, the Cu^{2+} concentrations vary between 2.4 and 4.6 $mmol/cm^3$ (Figure 2.5b). If a film contains pure PDCMAA with a density of 1 g/cm^3, the Cu^{2+} binding capacity should be 5.8 $mmol/cm^3$. Given that the coatings also contain PAH and some water, the binding capacities between 2.4 and 4.6 $mmol/cm^3$ are

reasonable. Measurements of film thicknesses after deposition of each PDCMAA and PAH layer (see Figure A2.12 and A2.13) suggest that coatings deposited at pH 5.0, 7.0, and 9.0 are predominantly PDCMAA. (Swelling after deposition of PDCMAA prevents estimation of the contributions of PDCMAA and PAH to the thicknesses of films deposited at pH 3.0.)
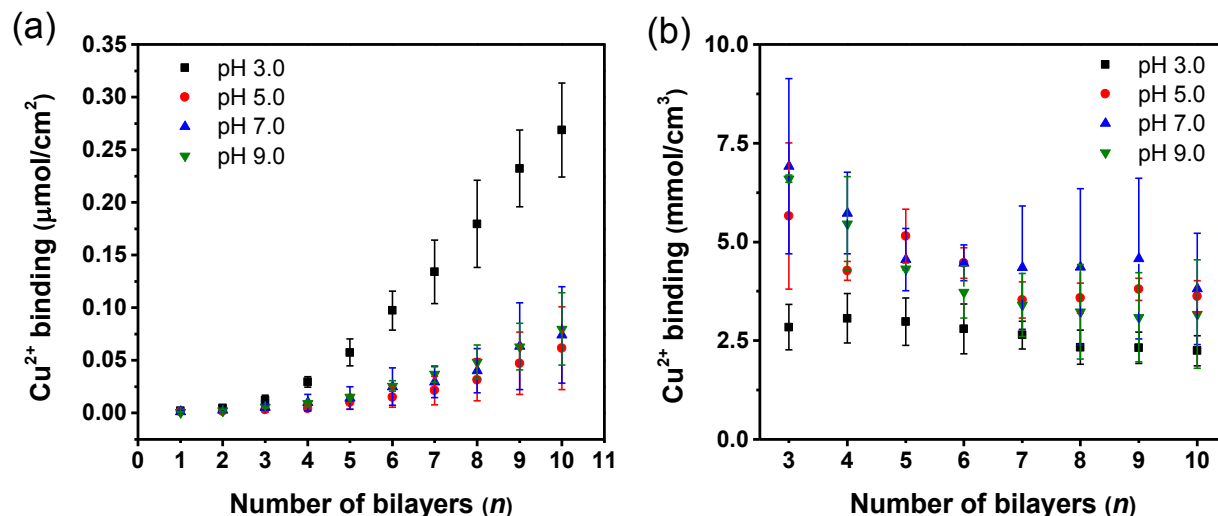
Figure 2.5. Cu^{2+}-binding capacities (a) per unit area and (b) per unit volume of $(PAH/PDCMAA)_n$ films deposited at various pH values. During Cu^{2+} sorption $C_{Cu^{2+}}$ = 1.40 mM, pH =4.1, and T = 25 °C. Film volumes were calculated using ellipsometric thicknesses of "dry" films without sorbed Cu^{2+}.

2.3.3. Effect of Solution pH on Cu^{2+} Sorption.

Decreased competition between protons and Cu^{2+} for IDA binding sites may lead to increased Cu^{2+} binding at high pH.[39] Figure 2.6 shows how Cu^{2+} sorption in $(PAH/PDCMAA)_{10}$ films varies with the pH of both the film deposition and the Cu^{2+} solutions. The concentrations of Cu^{2+} sorbed from the pH 4.0 solutions range from 2.1 ± 0.1 to 3.0 ± 0.2 mmol per cm^3 of film, consistent with saturation of the IDA binding groups. (The isotherms below show that the Cu^{2+} concentration in solution is sufficient

to essentially saturate binding sites.) After increasing the Cu^{2+} solution pH from 4 to 5, the Cu^{2+} sorption capacities increase 5- to 7-fold for (PAH/PDCMAA)$_{10}$ films prepared at pH 5.0, 7.0, and 9.0 (Figure 2.6). The increase in binding capacity suggests that at pH 5.0, amine groups of PAH may coordinate with Cu^{2+}.[40] Previous studies of Cu^{2+} binding to amine-containing polymers also show large increases in binding at solution pH values ranging from 4.0 to 6.0.[6,41] With PAH at pH 5.0, Cu^{2+} can likely effectively compete with protons for binding sites. However, the binding capacities at pH 5.0 are sometimes higher than we would expect. For a film containing 50 wt% PAH and 50 wt% PDCMAA with a composite density of 1 g/cm^3, the binding capacity would be 10 mmol Cu^{2+}/cm^3 if each amine and IDA functional group bound one Cu^{2+} ion. The even higher binding capacities for films deposited at pH 5.0 and 7.0 might suggest binding multiple Cu^{2+} ions per IDA group, where each carboxylate group binds to a different Cu^{2+} ion. Based on electron spin resonance data, Kinast et al. suggest that in some cases IDA-like ligands may bind to Cu^{2+} via only one carboxylate group.[42] Water or hydroxide should fill additional coordination sites.

In contrast, the films deposited at pH 3.0 show only a moderate Cu^{2+} sorption increase from 2.4 ± 0.0 mmol/cm^3 to 3.0 ± 0.4 mmol/cm^3 on going from a pH-4.0 to a pH-5.0 binding solution. This might indicate a higher pK_a of ammonium groups in these films compared to films deposited at other pH values and hence minimal binding of Cu^{2+} to PAH. The higher ammonium pK_a could stem from a high negative charge in these films, as –COOH groups present during deposition will deprotonate as the pH increases to add negative charge to the film and stabilize ammonium groups. We also attempted to examine binding at pH 6.0, but $Cu(OH)_2$ precipitates were clearly visible.
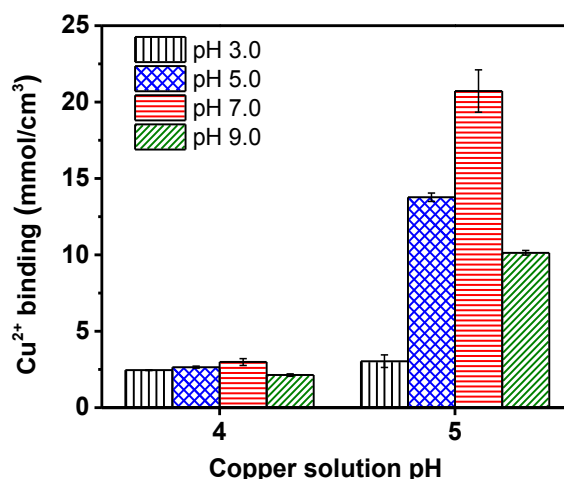
Figure 2.6. Cu^{2+}-binding capacities of $(PAH/PDCMAA)_{10}$ films in 1.40 mM $CuSO_4$ solutions adjusted to pH 4.0 and 5.0. Film assembly occurred at pH 3.0, 5.0, 7.0 or 9.0, and the legend refers to assembly pH.

The following sections examine kinetics and sorption isotherms for Cu^{2+} binding to $(PAH/PDCMAA)_{10}$ films deposited at pH 3.0. We decided to investigate films formed at this deposition pH because they have the highest thickness and Cu^{2+} sorption for a 10-bilayer film. Moreover most of the binding likely occurs through IDA units in these films.

2.3.4. Kinetics of Cu^{2+} Sorption.

To establish the equilibration time needed for maximum Cu^{2+} sorption and evaluate the binding kinetics in $(PAH/PDCMAA)_{10}$ films, we measured Cu^{2+} binding as a function of time. As Figure 2.7a shows, sorption approaches a maximum value after about 4 h of exposure to the 1.40 mM Cu^{2+} solution. When diffusion limits the sorption rate, at least initially the amount of sorption should be proportional to the square root of time with an intercept at the origin.[43] Figure 2.7b shows that this is the case, so

diffusion into the film must be slow compared to the rate of Cu^{2+} binding to ligands. In fact, diffusion may involve hopping between Cu^{2+} binding sites.[44]

If Fickian diffusion controls the rate of Cu^{2+} entry into a coating, equation (1) will describe the total amount of Cu^{2+}, M(t), in the film at a given time t, where M(∞) is the amount of Cu^{2+} in the film at equilibrium, I is the film thickness, and D is the diffusion coefficient.[45]

$$\frac{M(t)}{M(\infty)} = 1 - \sum_{n=0}^{\infty} \frac{8}{(2n+1)^2 \pi^2} \exp\left(-\frac{D(2n+1)^2 \pi^2 t}{4 l^2}\right) \tag{1}$$
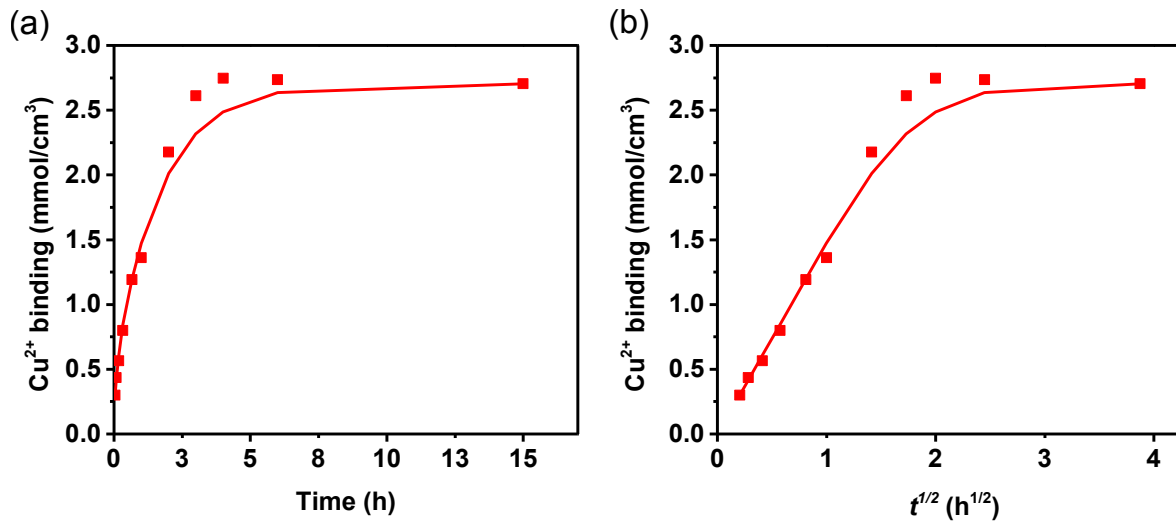
Figure 2.7. Cu^{2+} sorption in (PAH/PDCMAA)$_{10}$ films as a function of time (a) and the square root of time (b). Films were assembled at pH 3.0, and during Cu^{2+} adsorption $C_{Cu^{2+}}$ = 1.40 mM, pH =4.0, and T = 25 °C. The curves show fits to the data using equation (1) with D = 2.6 x 10^{-12} cm^2/sec and I = 2.0 μm.

Figure 2.7a and 6b show fits to the experimental data with equation (1) when using a swollen film thickness of 2 μm and a diffusion coefficient of 2.6 × 10^{-12} cm^2/s. This diffusion coefficient is 6-7 orders of magnitude lower than the diffusion coefficient in aqueous solution,[46] implying that the film greatly hinders ion movement. This low

diffusion coefficient is consistent with slow transport of divalent ions through some polyelectrolyte multilayer membranes.[47]

2.3.5. Sorption Isotherms.

After demonstrating that 4 h of exposure to a Cu^{2+} solution is sufficient to achieve equilibrium binding, we determined the equilibrium Cu^{2+} sorption capacity in (PAH/PDCMAA)$_{10}$ films as a function of the solution Cu^{2+} concentration. Figure 2.8 and Figure A2.18 and A2.19 show the sorption isotherms that result from these data, and at 25 °C binding reaches ~90% of saturation at solution Cu^{2+} concentrations <0.3 mM. Using a non-linear fitting method, we examined whether the data correspond well with Langmuir[48] or Sips[49] isotherms. Equation (2) describes the Langmuir isotherm

$$q_e = \frac{q_m K_L C_e}{1 + (K_L C_e)} \qquad (2)$$

where q_m is the maximum adsorption capacity; K_L is the Langmuir constant, which is a measure of the binding free energy; q_e is the amount of Cu^{2+} sorbed at equilibrium, and C_e is the concentration of Cu^{2+} in solution. Importantly, this model implies a fixed number of sorption sites with similar affinities for Cu^{2+}. In contrast, the Sips isotherm (the Freundlich[50] isotherm is a special case of the Sips model) described in equation (3) allows for a distribution of binding energies or accessibilities for the sorption sites.[51]

$$q_e = \frac{q_m (K_s C_e)^n}{1 + (K_s C_e)^n} \qquad (3)$$

In equation (3) K_s is the median association constant and n is the exponent of the Sips model. If the value of n is one, the Sips isotherm reverts to the Langmuir isotherm. In the case of Cu^{2+} sorption to (PAH/PDCMAA)$_{10}$ films at 4 °C, the Sips and Langmuir

models give essentially the same fit to the data, and the value for n in the Sips isotherm is 1.02. Thus, these films most likely have homogeneous binding sites.[52] However, at 25 and 37 °C, the values of n increase to 1.4 and 1.7, respectively. At the higher binding temperatures, the Langmuir model overpredicts the amount of sorption at low Cu^{2+} concentrations. Such an effect might stem from changes in the accessibility of binding sites with the amount of binding, or a distribution of binding site energies at the higher temperatures. All the temperatures give similar values of q_m, consistent with well-defined binding sites, presumably the IDA functionalities.
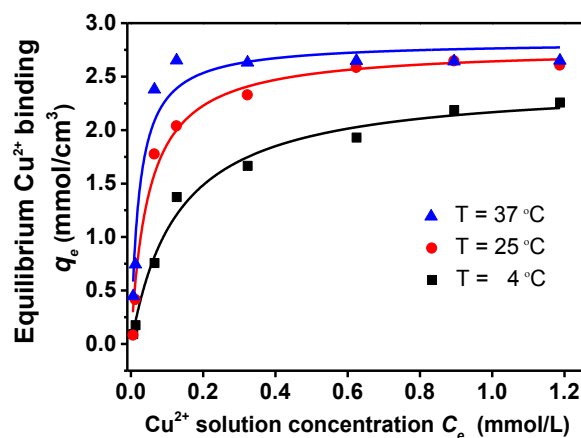
Figure 2.8. Sorption isotherms for Cu^{2+} binding to $(PAH/PDCMAA)_{10}$ films at different temperatures. Fits to the data (curves) result from Langmuir isotherms. Films were assembled at pH 3.0, and binding was allowed to occur for 15 h in pH 4.0 solution (20 mM phosphate). In the appendix Figure A2.17 shows fits of the data to the Sips isotherm, and Figure A2.18 and Figure A2.19 shows sorption isotherms at 16 and 31 °C.

Table 1 presents the values of free energy of association, ΔG_a^o, and binding constants at different temperatures. Both K_L and K_s increase by a factor of ~6 on going from 4 to 37 °C, and at 37 °C binding approaches saturation at Cu^{2+} concentrations of only 0.1 mM. Increased binding at higher temperatures indicates that entropic factors affect the spontaneity of the Cu^{2+} sorption.

Table 2.1. Fitting parameters from Langmuir and Sips isotherm models of Cu^{2+} sorption in (PAH/PDCMAA)$_{10}$ films.

Langmuir isotherm				
Temperature (^{o}C)	ΔG_a^o (kJ/mol)	q_m (mmol/cm^3)	K_L (L/mmol)	R^2
4	-20.7	2.44 ± 0.09	7.75 ± 1.15	0.987
16	-23.3	2.60 ± 0.02	15.9 ± 0.7	0.999
25	-24.7	2.77 ± 0.09	20.4 ± 3.7	0.980
31	-26.9	2.50 ± 0.11	41.0 ± 9.5	0.944
37	-27.6	2.83 ± 0.12	43.2 ± 10.9	0.948
Sips isotherm				
Temperature (^{o}C)	n	q_m (mmol/cm^3)	K_s (L/mmol)	R^2
4	1.02 ± 0.18	2.42 ± 0.19	7.96 ± 1.84	0.985
16	0.98 ± 0.04	2.62 ± 0.04	15.6 ± 0.9	0.998
25	1.36 ± 0.15	2.62 ± 0.07	23.3 ± 2.5	0.990
31	1.41 ± 0.10	2.43 ± 0.08	24.6 ± 10.5	0.967
37	1.71 ± 0.19	2.67 ± 0.05	49.5 ± 4.6	0.991

We determined ΔG_a^o for Cu^{2+} sorption, along with the enthalpy (ΔH_a^o) and the entropy (ΔS_a^o) of sorption using equations (4) and (5) and the plot of $ln\ K_L$ vs $1/T$ in Figure 2.9.

$$\Delta G_a^o = -RT \ln K_L \qquad\qquad (4)$$

$$\ln K_L = \frac{\Delta S_a^o}{R} - \frac{\Delta H_a^o}{RT} \qquad\qquad (5)$$

In these equations R is the gas constant (8.314 J/mol K) and T is temperature (K).[53,54]
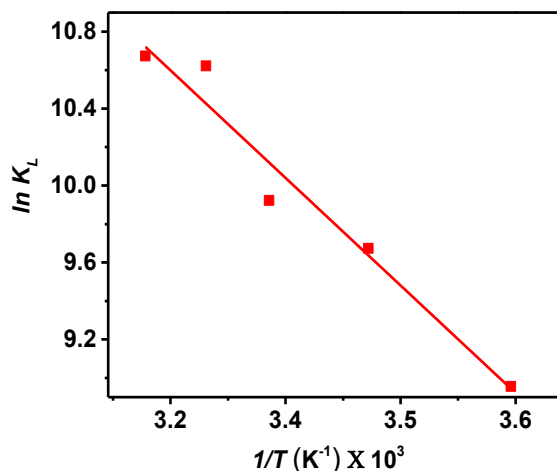
Figure 2.9. Plot of *ln K_L* versus *1/T* for equilibrium Cu^{2+} sorption in $(PAH/PDCMAA)_{10}$ films. Films were assembled at pH 3.0, and sorption occurred at pH =4.0 for 15 h.

The ΔH_a^o and ΔS_a^o values for the Cu^{2+} sorption were 39 ± 5 kJ/mol and 213 ± 15 J/mol K, respectively, similar to values obtained for Cu^{2+} binding (pH 5.0) to IDA ligands immobilized on polystyrene beads.[55] The positive enthalpy change indicates an endothermic reaction, which likely results from exchange of a proton for a Cu^{2+} ion (Scheme 2.2). Binding constants and pK_a values for the free IDA ligand (not immobilized to a polymer) also show a positive enthalpy and negative entropy for the exchange of a proton for Cu^{2+}.[56] The positive ΔS_a^o value probably results from liberation of water molecules in the metal-ion absorption process,[55] and the relatively large magnitude of ΔS_a^0 leads to negative ΔG_a^0 values and spontaneous metal chelation, especially at higher temperatures.[57]
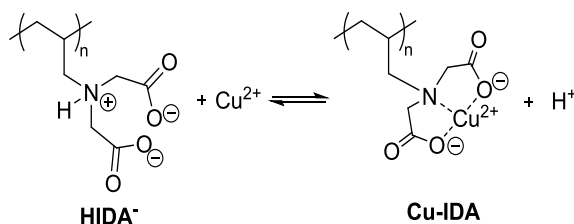
Scheme 2.2. Cu^{2+} chelation to IDA functional groups via exchange with a proton.

2.3.6. Repetitive Cu^{2+} Binding and Elution in $(PAH/PDCMAA)_{10}$ Films.

Figure 2.10 illustrates the sorption capacities of $(PAH/PDCMAA)_{10}$ films during four cycles of Cu^{2+} binding followed by elution with EDTA. For this set of films, which were all prepared from the same polyelectrolyte adsorption solutions, the Cu^{2+} sorption capacity increases from 2.46 ± 0.02 mmol/cm^3 to 2.64 ± 0.12 mmol/cm^3 after the first cycle and then remains constant. The 7% increase in binding capacity after the first cycle may stem from film rearrangement in the pH 7.4 EDTA solution. Despite the possible rearrangement, $(PAH/PDCMAA)_{10}$ films are clearly stable over several absorption/elution cycles, and presumably many more cycles of binding and elution are possible. This stability should allow reuse of the films in applications such as metal scavenging or protein binding.
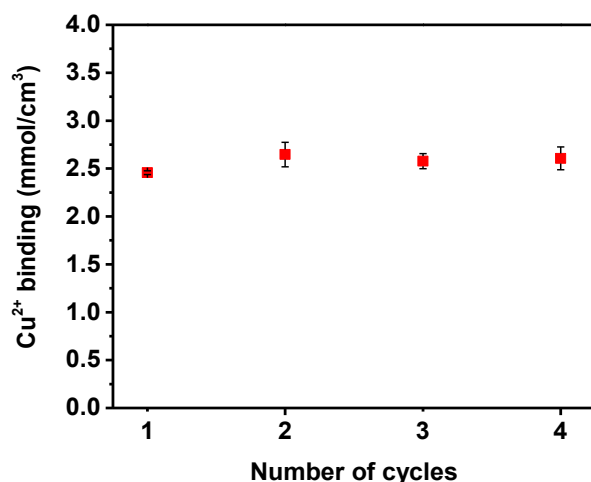
Figure 2.10. Cu^{2+} Sorption capacities of $(PAH/PDCMAA)_{10}$ coatings (formed at pH 3.0) over four cycles of binding and elution on the same films. Sorption occurred from 1.40 mM $CuSO_4$ solutions (pH 4.0, 20 mM phosphate solution) for 15 h, and Cu^{2+} was eluted with 20 mM EDTA (pH 7.4).

2.3.7. Film Swelling and Protein Binding in PDCMAA- and CMPEI-Containing Films.

This work aims to create thin films that selectively bind proteins in platforms such as porous membranes, and film swelling in aqueous solution is vital to enable extensive protein capture. To examine swelling, we initially performed in situ ellipsometry with (PAH/CMPEI)$_5$ films (deposited at pH 3 with 0.5 M NaCl) immersed in deionized water or 20 mM phosphate buffer (pH 7.4). After a 20-minute immersion, film thickness increased 160±30% in deionized water and 680±260% in buffer. Deprotonation of –COOH groups in pH 7.4 buffer likely enhances swelling, which should provide space for binding multilayers of protein in the film. As a comparison, the swelling of (PAH/PDCMAA)$_5$ films (deposited at pH 3 with 0.5 M NaCl) was 52±16% in deionized water and 220±20% in 20 mM phosphate buffer (pH 7.4). The high swelling of (PAH/CMPEI)$_5$ relative to (PAH/PDCMAA)$_5$ suggests that the ammonium-containing backbone and branched structure of CMPEI facilitate swelling. (PAH/CMPEI)$_5$ and (PAH/PDCMAA)$_5$ films have similar dry thicknesses of 40 and 60 nm, respectively.)

Modification of porous membranes to bind proteins will most likely involve adsorption of only a few polyelectrolyte bilayers to simplify the process and avoid plugging of pores. Moreover the films should contain metal-ion complexes for capture of proteins through metal-ion affinity interactions (Figure 2.11).
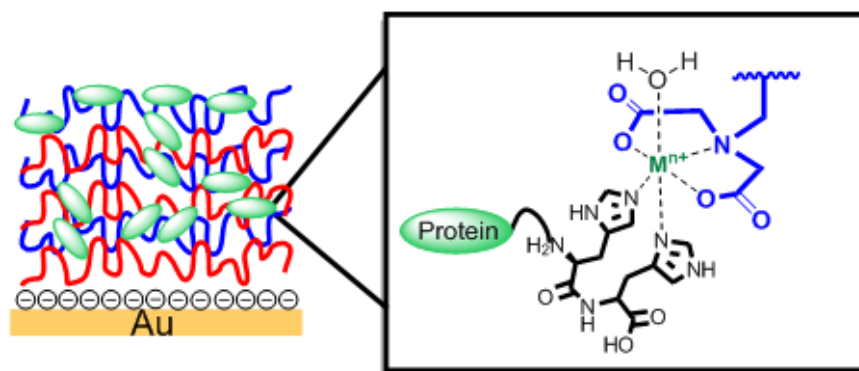
Au-(PAH/PDCMAA or CMPEI)$_n$-M^{n+}-Protein

Figure 2.11. His-tag protein binding to (PAH/PDCMAA or PAH/CMPEI)$_n$ films containing imminodiacetic acid-metal (IDA-M^{n+}) complexes.

Thus, we also examined swelling of (PAH/CMPEI)$_2$ and (PAH/PDCMAA)$_2$ films containing Cu^{2+} complexes. These studies employed binding 20 mM phosphate buffer at pH 6.0 to match subsequent Con A-binding studies, as Con A solutions are not stable at pH 7.4. For all film-adsorption pH values (pH 2 to 9), the (PAH/CMPEI)$_2$-Cu^{2+} swelling in pH 6.0 buffer is around 200%. In pH 7.4 buffer the swelling of a (PAH/CMPEI)$_2$-Cu^{2+} film (deposited at pH 3 with 0.5 M NaCl) is still only 220%. Thus, formation of the metal-ion complexes decreases film swelling, probably because Cu^{2+}-iminodiacetate complexes have no net charge. When immersed in pH 6.0 buffer, the (PAH/PDCMAA)$_2$-Cu^{2+} films show average swellings of only 100% for deposition pH vales of 3, 5, or 7. Although both CMPEI and PDCMAA contain iminodiacetate moieties, the amine or ammonium groups in the backbone of CMPEI films likely increase swelling compared to films with PDCMAA, which contains a hydrocarbon backbone (Figure 2.12).
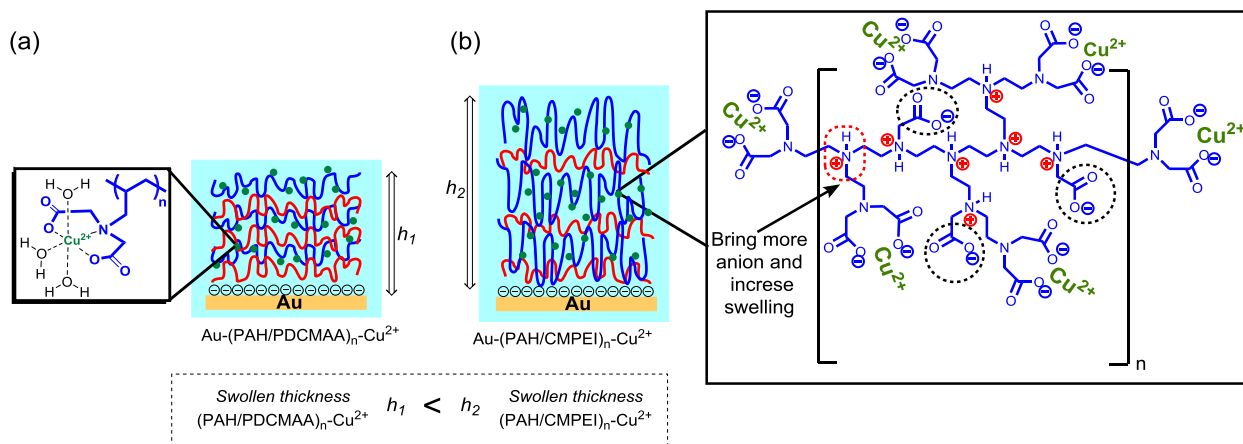
Figure 2.12. Graphical representation of swelling of (a) (PAH/PDCMAA)$_n$-Cu^{2+} and (b) (PAH/CMPEI)$_n$-Cu^{2+} films.

Initial studies of protein binding examined capture of Con A in (PAH/CMPEI)$_2$-Cu^{2+} and (PAH/PDCMAA)$_2$-Cu^{2+} films adsorbed on Au-coated Si wafers modified with MPA. Binding presumably occurs when histidine groups on the protein coordinate with immobilized Cu^{2+}. Using reflectance FTIR spectroscopy, we determine the amount of protein binding based on the amide absorbance, which we compare to the absorbance in spin-coated films with different thicknesses.[58] (PAH/PDCMAA)$_2$-Cu^{2+} films have average thicknesses ranging from 7-25 nm, depending on the deposition pH (see Figure 2.13), but these coatings bind the equivalent of <3 nm of protein, or less than a monolayer. (The dimensions of a Con A protomer, M_w=25,500 Da, are 4.2×4.0 ×3.9 nm.[59]) Even with an extra bilayer, (PAH/PDCMAA)$_3$-Cu^{2+} films with a thickness of ~60 nm (deposited at pH 2) bind only 8 nm of Con A. Such limited binding will lead to low capacities in membranes modified with these films. In contrast, (PAH/CMPEI)$_2$-Cu^{2+} films adsorbed at pH 2 have an average thickness of 48 nm and capture 18 nm of protein (Figure 2.13). Adsorption of (PAH/CMPEI)$_2$ at deposition pH values from 3-7 leads to thinner films than adsorption at pH 2 and binding of ≤5 nm of protein (Figure

2.13). Thus, polyelectrolyte adsorption at low pH to obtain relatively thick CMPEI films and high swelling is likely vital to achieving high binding capacities.
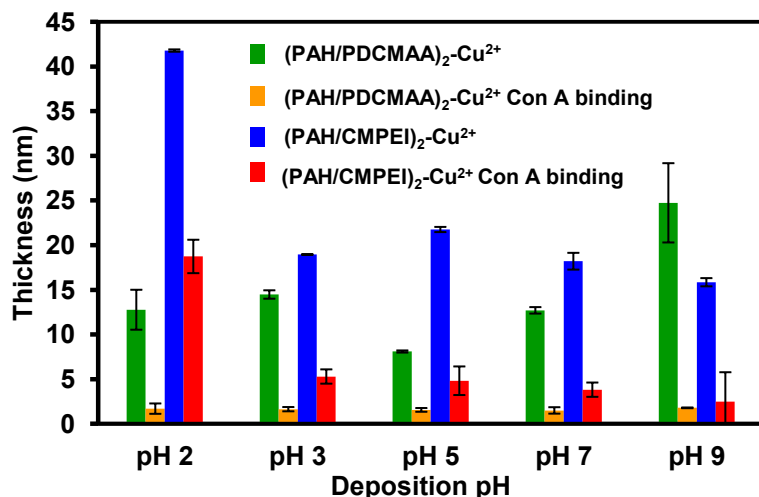
Figure 2.13. Thicknesses of (PAH/PDCMAA)$_2$ and (PAH/CMPEI)$_2$ multilayers after complexation of Cu^{2+}, and the equivalent thicknesses of Con A subsequently adsorbed in these films. PEMs were deposited from polyelectrolyte solutions containing 0.5 M NaCl at various pH values.

2.3.8. Capture of His-tagged Protein Using Membranes Containing PAH/CMPEI-Ni^{2+} Films.

Because PAH/CMPEI films show the highest Con A capture, Weijing Ning in the Bruening group determined the His-tagged ubiquitin binding capacity of nylon membranes modified with these films.[60] However, in this case we employed the CMPEI-Ni^{2+} complex, which is necessary for selective capture of His-tagged proteins. Based on breakthrough curves, the binding capacity is ~60 mg/mL, and protein elution gave a capacity of ~70 mg/mL. This His-U binding is about 2/3 of what we previously obtained using polymer brush- or (PAA/PEI/PAA)-NTA-Ni^{2+}-modified membranes (~90 mg/mL membrane).[1,3] However, this new strategy avoids the challenges of growing

80

polymer brushes or the expensive reaction of PAA/PEI/PAA with aminobutyl NTA. The dynamic binding capacity, i.e. the amount of protein bound when the effluent concentration is 10% of the loading concentration, is around 30 mg/mL.

To demonstrate that membranes can isolate His-tagged protein directly from cell extracts, we purified His-tagged SUMO protein that was over-expressed in *E. coli*. Figure 2.14 shows the SDS-PAGE analysis of a cell extract that contained His-tagged SUMO (lane 2), the same cell extract after passing through a (PAH/CMPEI)-modified membrane (lane 3), and the eluate (lane 4) from the membrane loaded with the cell extract. Notably, the effluent of the loading solution contains minimal His-tagged SUMO protein, and the only detectable band from the eluate stems from the His-tagged SUMO protein. Thus the membranes selectively capture His-tagged protein.
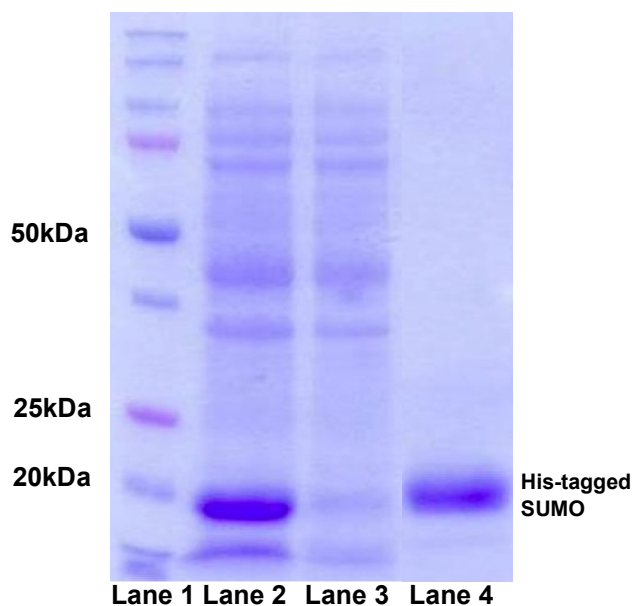
Figure 2.14. SDS-PAGE analysis of purification of overexpressed His-tagged SUMO protein from an *E. coli*. lysate. Lane 1: molecular marker; Lane 2: cell lysate containing His-tagged SUMO protein; Lane 3: the cell lysate after passing through a (PAH/CMPEI)-Ni^{2+}-modified CM membrane; Lane 4: the eluate of the loaded membrane. If complete protein recovery occurred, Lanes 2 and 4 should contain the same amount of His-tagged SUMO.

2.4. Conclusions.

This study describes fabrication of polyelectrolyte multilayer films with remarkably high thicknesses and Cu^{2+} binding capacities. When assembled at pH 3.0, (PAH/PDCMAA)$_{10}$ films have "dry" thicknesses of ~1.2 μm and Cu^{2+} binding capacities of 2-3 mmol/cm^3. The low deposition pH decreases the charge on PDCMAA during adsorption and increases film thicknesses 8-fold compared to assembly at pH 5.0 or 7.0. For μm-thick films, saturation of binding sites requires ~4 h, and the Cu^{2+} diffusion coefficient in these coatings is 6-7 orders of magnitude lower than that in aqueous solutions. Sorption is endothermic with a positive entropy, presumably because of an endothermic exchange between Cu^{2+} and H^+ with release of waters of hydration to increase entropy. Sorption capacities are stable over at least four cycles of Cu^{2+} binding and elution, suggesting possible applications in metal ion scavenging or protein binding.

Unfortunately, (PAH/PDCMAA)$_n$ films do not swell greatly in water so their metal-ion complexes do not bind large amounts of protein. (PAH/CMPEI)$_n$ films swell more extensively, presumably because of a more hydrophilic backbone. Thus, (PAH/CMPEI)$_n$ films deposited at low pH binding multilayers of protein. Moreover, PAH/CMPEI adsorption in a nylon membrane followed by formation of Ni^{2+} complexes leads to a His-tagged ubiquitin binding capacity of ~60 mg/mL, which is equal to the capacity of high-binding commercial beads. Such membranes can purify His-tagged protein directly from a cell extract.

APPENDIX

A2.1. Synthesis and Characterization of Polymers.

A2.1.1.Synthesis and characterization of poly[(*N,N*-dicarboxymethyl) allylamine].

Synthesis of poly[(*N,N*-dicarboxymethyl)allylamine] (PDCMAA) was carried out according to a literature procedure[1] with slight modifications. Under a N_2 atmosphere, chloroacetic acid (6.69 g, 0.07 mol), NaOH (2.80 g, 0.07 mol) and 25 ml of water were added to a two-neck round-bottomed flask, and the mixture was stirred at 30 °C for 10 min. This solution was added dropwise with stirring to an aqueous solution (100 mL) containing poly(allyamine hydrochloride) (PAH, M_n~5.8 $x10^4$ Da, 1.0 g, 0.011 mol) at 50 °C. The reaction mixture was kept at 50 °C for 1 h and then held at 90 °C for 2 h with occasional addition of 30% NaOH to maintain the pH at 10.0. The reaction mixture was stirred at room temperature for 12 h, and then the pH was adjusted to 1 by adding concentrated HCl. The supernatent was decanted, the remaining precipitate was dissolved by addition of 30% NaOH, and the solution was again adjusted to pH 1.0 with concentrated HCl. This process was repeated 2 times, and the precipitate was filtered and dried *in vacuo* for 12 h. The resulting white poly[(*N,N*-dicarboxymethyl)allylamine] (PDCMAA) solid (70% yield) was characterized by ^{1}H-NMR (Figure A2.1b) and FTIR (Figure A2.2c) spectroscopy. IR (KBr): 1631, 1735 and 1400 cm^{-1}; ^{1}H- NMR δ (ppm): 0.50-2.00 (br, s, 3H), 2.00-2.75 (br s, 2H), 2.80-3.50 and (br s, 4H).
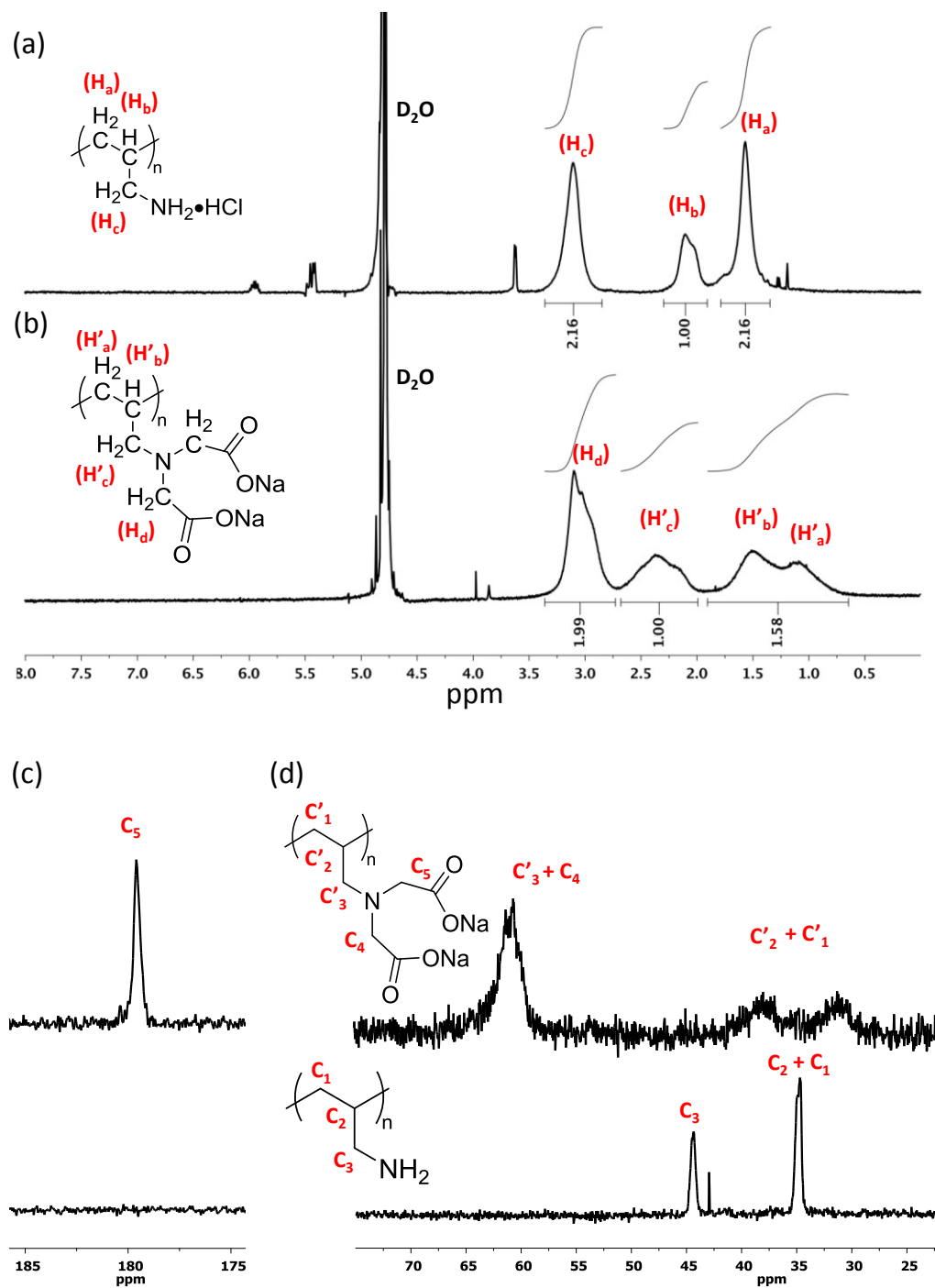
Figure A2.1. ^{1}H NMR spectra of (a) poly(allylamine hydrochloride) (PAH) in D$_2$O and (b) poly[(*N*,*N*-dicarboxymethyl)allylamine] in D$_2$O adjusted to pH >10 by addition of NaOD. (c) ^{13}C NMR spectra of PAH (bottom) and PDCMAA (top). Both spectra were acquired in D$_2$O adjusted to pH 10 by addition of NaOD. In the ^{13}C NMR spectrum of PDCMAA, the signals due to the carbons in the polymer backbone are likely low due to restricted relaxation.

85

The IR spectrum (Figure A2.2c) of the acidified PDCMAA shows the disappearance of bands that correspond to N-H deformation vibrations of PAH (1510 cm^{-1} and 1599 cm^{-1}) and the appearance of stretches from carboxylic acid groups. The absorption centered at 1731 cm^{-1} arises from the C=O stretching in the HN^+-CH_2COOH group, and the band at 1630 cm^{-1} is due to the assymetric stretching in the HN^+-CH_2COO^- group. The ^1H-NMR spectrum of PDCMAA shows a signal at δ 2.80-3.50 corresponding to the -NCH_2COO^- protons. Comparison of the signal integrations for the -CH_2N protons (H_c') at δ ~ 2.00-2.75 ppm and the carboxymethylene protons (H_d) at δ ~2.80-3.50 ppm suggests that the iminodiacetic moiety is introduced essentially quantitatively into the amino groups of PAH, consistent with previous work.[1]
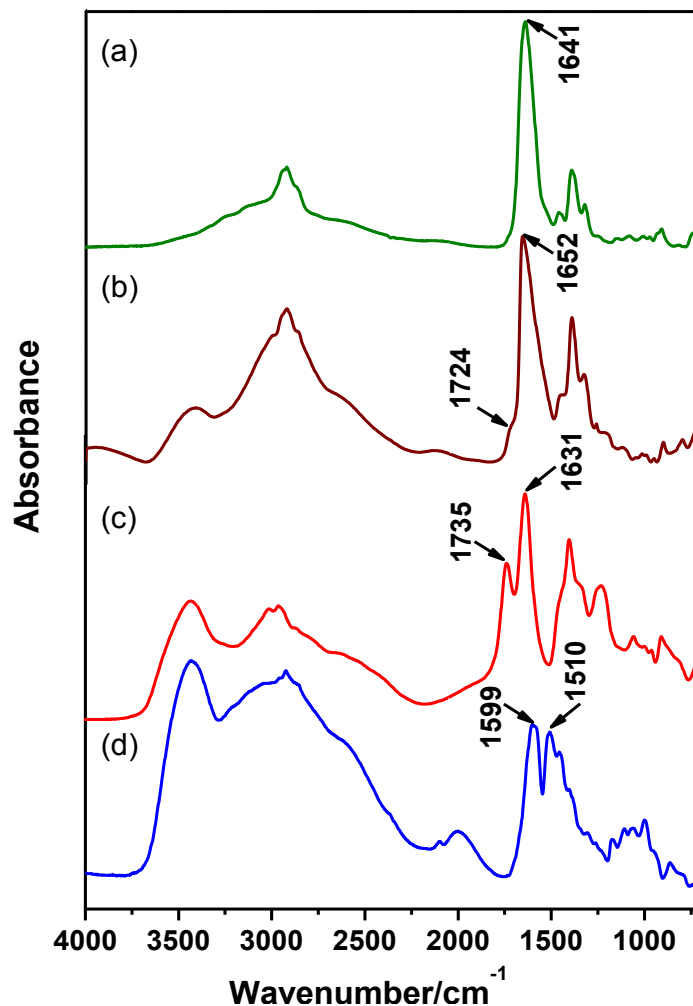
Figure A2.2. IR spectra of (a) a (PAH/PDCMAA)$_{10}$-Cu^{2+} film on Au (reflectance spectrum), (b) a (PAH/PDCMAA)$_{10}$ film on Au (reflectance spectrum), (c) PDCMAA (in KBr) and (d) PAH (in KBr). Absorbance scales are not the same for all spectra.

A2.1.2. Potentiometric Titration of PDCMAA.

A potentiometric titration of PDCMAA was performed according to a literature procedure with slight modifications.[1,2] The pH was monitored using a microprocessor-controlled pH-meter (ORION-420A) with a combined glass/reference electrode calibrated with standard pH 4.0, 7.0, and 10.0 buffers. (Uncertainties in pH values will increase outside of this calibration range.) PDCMAA and PAH were separately dissolved in 0.05 M

NaOH, and 1.0 M HCl served as the titrant for 200 mL of ~22 mM PDCMAA or PAH repeating units. Polymer concentrations are likely overestimated because of adsorbed water and Na$^+$ ions in the PDCMAA. Using a micropipette, the 1.0 M HCl was added in 100-200 μL aliquots, except for close to the equivalent point, where 20 μL aliquots were added. pH values were recorded after establishing equilibrium, which typically required 1-2 min. Figure A2.3 shows the resulting acid-base titration curves. For PDCMAA, the first equivalence point occurs around pH 6 after complete protonation of amine groups. Protonation of the two –COOH groups occurs primarily below pH 4. The titration curves agree with literature data.[1-3]
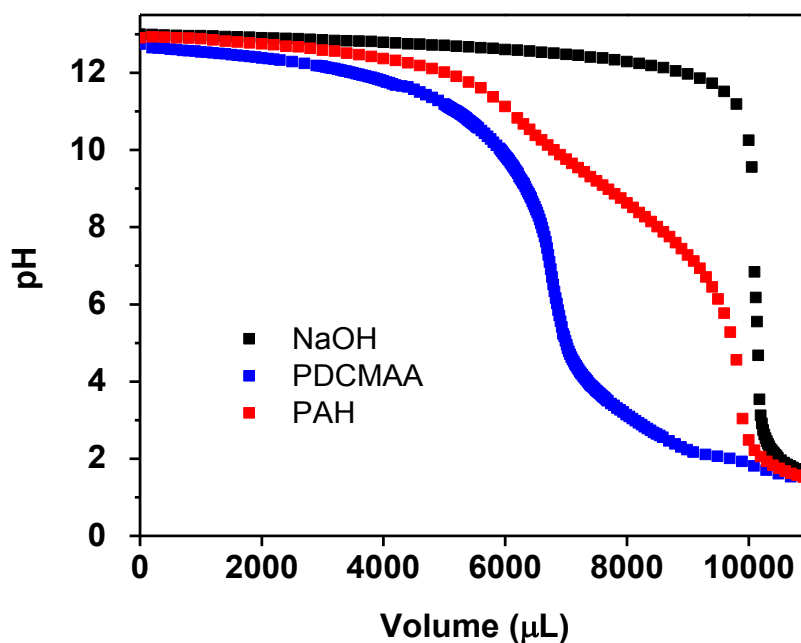
Figure A2.3. Acid-base titration curves for 0.05 M NaOH (black-squares), ~0.022 M PAH in 0.05 M NaOH (red-squares) and ~0.022 M PDCMAA in 0.05 M NaOH (blue-squares). The titrant contained 1.0 M HCl and the initial solution volume was 200 mL.

A2.1.3. Synthesis and Characterization of Carboxymethylated Polyethyleneimine (CMPEI).

Synthesis of CMPEI was carried out following the procedure for synthesis of PDCMAA, with slight modifications (Scheme A 2.1).[1,4] Under a N_2 atmosphere, sodium chloroacetate (20.0 g, 0.25 mol) and 25 mL of water were added to a two-neck round-bottomed flask, and the mixture was stirred at 30 °C for 10 min. This solution was added dropwise with stirring to an aqueous solution (100 mL) containing branched poly(ethyleneimine) (PEI, 50 wt% solution in water, $M_n \sim 6.0 \times 10^4$ Da, 10.0 g, 10.6 mmol assuming a repeating unit $M_W = 473$ gmol^{-1}) at 50 °C. The reaction mixture was kept at 50 °C for 1 h and then held at 90 °C for 2 h with occasional addition of 30% NaOH to maintain the pH at 10.0. The mixture was stirred at room temperature for 12 h, and then the pH was adjusted to 1 by adding concentrated HCl. The supernatant was decanted, the remaining precipitate was dissolved by addition of 30% NaOH, and the solution was again adjusted to pH 1.0 with concentrated HCl. This process was repeated 3 times, and the precipitate was filtered and dried in vacuo for 12 h. The resulting white carboxymethylated polyethyleneimine (CMPEI, solid, 3.2 g, 63% yield) was characterized by FTIR spectroscopy (KBr) and elemental analysis.

Scheme A 2.1. Synthesis of CMPEI.

A2.1.4.FTIR Characterization of CMPEI.

Comparison of the IR spectra (Figure A2.4) of acidified branched PEI and branched CMPEI shows the disappearance of bands that correspond to N-H deformation vibrations of PEI (1584 cm^{-1} and 1454 cm^{-1}) and the appearance of stretches from carboxylic acid groups. The absorption at 1733 cm^{-1} arises from the C=O stretching in the HN$^+$-CH$_2$COOH group, and the band at 1655 cm^{-1} is due to the asymmetric stretching in the HN$^+$-CH$_2$COO$^-$ groups. This confirms the presence of the iminodiacetic acid moiety in CMPEI.

Figure A2.4. FTIR spectra of branched PEI (red) and CMPEI (black). Both polymers were acidified prior to obtaining the spectra in KBr.

A2.1.5. Elemental Analysis of CMPEI.

We also performed elemental analysis to evaluate the synthesis of CMPEI. Table A2.1 provides possible structures for PEI and CMPEI along with elemental compositions. In its fully deprotonated state, the PEI starting material has the following percent composition: C, 55.78; H, 11.70; N, 32.52. Double carboxymethylation of each primary amine plus single carboxymethylation of each secondary amine leads to entry 2 (Table A2.1) with a percent composition of C, 47.52; H, 6.98; N, 13.85; O, 31.65. However, these values differ significantly from the elemental analysis data: C, 40.26; H,

6.65; N, 11.93. This difference likely stems from formation of hydrochloride salts. Without accounting for chloride, all other atom percentages will be artificially high. Formation of HCl salts only along the polymer backbone (addition of 5 Cl⁻) gives an elemental composition: C, 40.83; H, 6.39; Cl, 13.69; N, 11.90; O, 27.19 (Table A2.1, entry 3), which is reasonably close to the experimental values. Formation of HCl salts at all amine sites (Table A2.1, entry 4) leads to atomic percentages that are significantly lower than the experimental values. Unfortunately, we cannot specify the protonation state of CMPEI because of the low –COOH pKa values, and –COO⁻ groups, rather than Cl⁻, probably provide charge compensation for some of the ammonium groups. Thus, 5 Cl⁻ ions per repeating unit, as shown in entry 3 of Table A2.1, is possible. Most important, in entries 2-4 the carbon to nitrogen ratio, which does not depend on the number of Cl⁻ ions or the presence of residual water, is 3.43 close to the experimental value of 3.37. This confirms addition of acetate groups to the polymer in approximately the amount shown in entry 2. (The theoretical C to N ratio in the PEI starting material is only 1.72.)

Table A2.1. Possible elemental compositions of PEI and CMPEI with different numbers of HCl salts.

	Chemical Formula	Molecular Weight (g/mol)	Elemental Analysis
Poly(ethylenimine)	$C_{22}H_{55}N_{11}$	473.8	C, 55.78; H, 11.70; N, 32.52
	$C_{44}H_{77}N_{11}O_{22}$	1112.1	C, 47.52; H, 6.98; N, 13.85; O, 31.65
	$C_{44}H_{82}Cl_5N_{11}O_{22}$	1294.5	C, 40.83; H, 6.39; Cl, 13.69; N, 11.90; O, 27.19
	$C_{44}H_{88}Cl_{11}N_{11}O_{22}$	1513.2	C, 34.93; H, 5.86; Cl, 25.77; N, 10.18; O, 23.26

A2.2. Determination of Surface Energies.

Static contact angles were measured with a FirstTenAngstroms (FTA) goniometer. Droplets (30-40 µL) of deionized water or ethylene glycol were placed on the surfaces of $(PAH/PDCMAA)_{10}$ and $(PAH/PDCMAA)_{10}/PAH$ films assembled from solutions with various pH values. After a few seconds, droplet images were recorded and subsequently analyzed to determine the contact angle. To minimize variations due to humidity fluctuations, all the measurements were recorded on the same day. Furthermore, another set of films were tested after vacuum drying for 24 h to examine the effect of humidity. Contact angles were determined within 2 min of removing the film from vacuum.
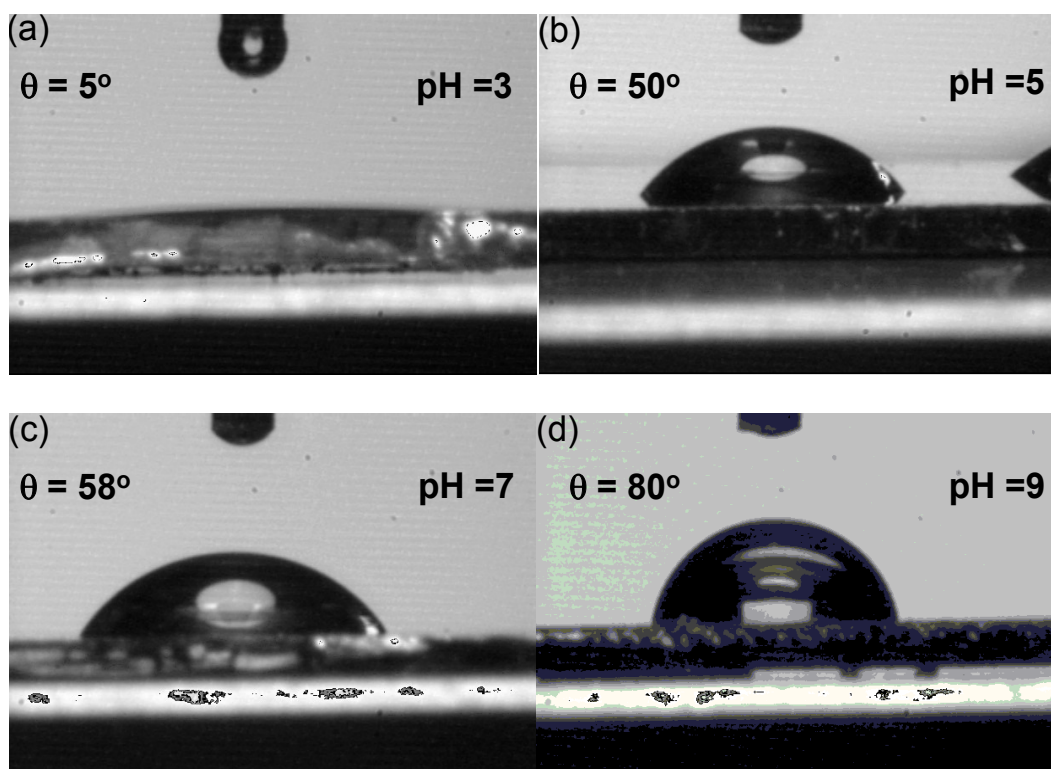
Figure A2.5. Images of water droplets on the surfaces of $(PAH/PDCMAA)_{10}$ films assembled at pH (a) 3.0, (b) 5.0, (c) 7.0 and (d) 9.0. Values of Ɵ represent the average contact angle determined from the image.

Table A2.2. Contact angles on (PAH/PDCMAA)$_{10}$ films deposited at different pH values.

Film deposition pH	Water Contact angles ($\circ$)		Ethylene glycol contact angles ($\circ$)[a]
	[a]Films in "ambient air"	[b]Vacuum dried films	
pH 3.0	5.5 ± 0.2	39.2 ± 2.6	15.8 ± 2.7
pH 5.0	50.3 ± 0.4	77.4 ± 4.0	27.2 ± 0.3
pH 7.0	58.4 ± 0.5	76.9 ± 5.5	30.4 ± 2.3
pH 9.0	80.3 ± 0.8	84.9 ± 3.3	43.7 ± 0.7

[a]Films were dried with a stream of N_2 and stored in ambient conditions prior to measurements. [b]Contact angles were determined after vacuum drying of the film for 24 h.

Table A2.3. Contact angles on (PAH/PDCMAA)$_{10}$/PAH films deposited at different pH values.

Film deposition pH	Water Contact angles ($\circ$)	
	[a]Films in "ambient air"	[b]Vacuum dried films
pH 3.0	67.7 ± 15.4	82.6 ± 7.1
pH 5.0	71.1 ± 9.5	78.4 ± 4.1
pH 7.0	73.5 ± 13.1	82.4 ± 3.2
pH 9.0	76.2 ± 3.6	85.7 ± 2.7

[a]Films were dried with a stream of N_2 and stored in ambient conditions prior to measurements. [b]Contact angles were determined after vacuum drying of the film for 24 h.
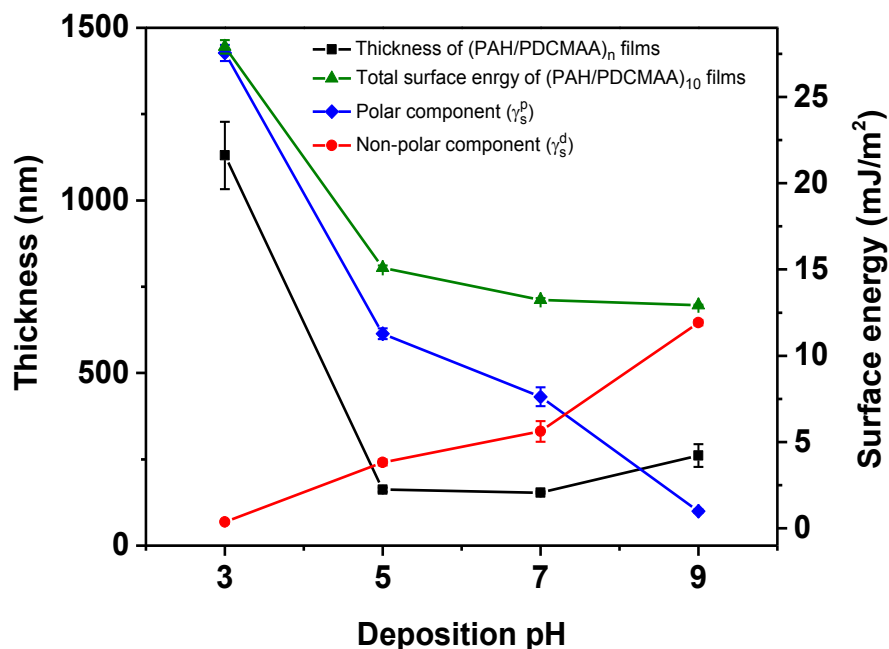
Figure A2.6. Total surface energies, polar (γ_s^p) and non-polar (γ_s^d) components of surface energies, and thicknesses of (PAH/PDCMAA)$_{10}$ films assembled at different pH values.

Figure A2.5 shows water contact angles on (PAH/PDCMAA)$_{10}$ films deposited at pH 3.0, 5.0, 7.0, and 9.0. The contact angles increase dramatically from a wetted surface for films deposited at pH 3.0 to 80° for films deposited at pH 9.0. To further interrogate surface energies, we employed water and ethylene glycol as reference liquids to determine the polar (γ_s^p) and the non-polar (γ_s^d) dispersive components of the surface energy. Table A2.2 shows the contact angle values on the different films. The observed contact angles were converted to surface energies using Fowkes' equation[5]:

$$\gamma_L(1+\cos\theta)=2\left[\sqrt{\gamma_L^d\gamma_s^d}+\sqrt{\gamma_L^p\gamma_s^p}\right]$$
Equation A 2.1

where γ_L is the total surface energy between the droplet and air (for water- 72.8 mJ/m^2 and for ethylene glycol- 48.0 mJ/m^2), γ_L^d is the dispersive component (for water- 21.8 mJ/m^2 and for ethylene glycol- 29.0 mJ/m^2), and γ_L^p is the polar component (for water- 51.0 mJ/m^2 and for ethylene glycol- 19.0 mJ/m^2) of the liquid-vapor surface energies. Application of Equation A3.1 to each of the probe liquids yields two equation with two unknowns, γ_s^p and γ_s^d, which we obtain from the solution of the two equations. The total energy of the film-air interface, γ_s, is a sum of polar (γ_s^p) and dispersive (γ_s^d) surface tensions.

Figure A2.6 shows γ_s, γ_s^p and γ_s^d as a function of assembly pH. The PEM deposited at pH 3.0 has the highest total surface energy, and the biggest change in surface energy occurs on increasing the deposition pH from 3.0 to 5.0. Moreover, γ_s^p decreases with the assembly pH, whereas γ_s^d increases. For films deposited at low pH, excess –COOH groups are likely exposed near the interface, and deprotonation of these groups at neutral pH should create a charged, hydrated polar surface. As the deposition pH increases, the films likely expose more and more polymer backbone to decrease γ_s^p and increase γ_s^d.[6] Capping of films by adsorption of a PAH layer gives rise to increased water contact angles when film deposition occurs at pH 3.0, 5.0, and 7.0 (Table A2.3), confirming the importance of –COO⁻ groups in creating a hydrophilic surface. Contact angles increase after vacuum drying of films (Table A2.2 and Table A2.3) indicating that sorbed water increases hydrophilicity, particularly for films adsorbed at low pH.

A2.3. Film Swelling and Refractive Indices.

The film refractive index is a function of both the constituent polymers and the amount
of sorbed water and thus allows estimation of water sorption at ambient conditions.[7,8]
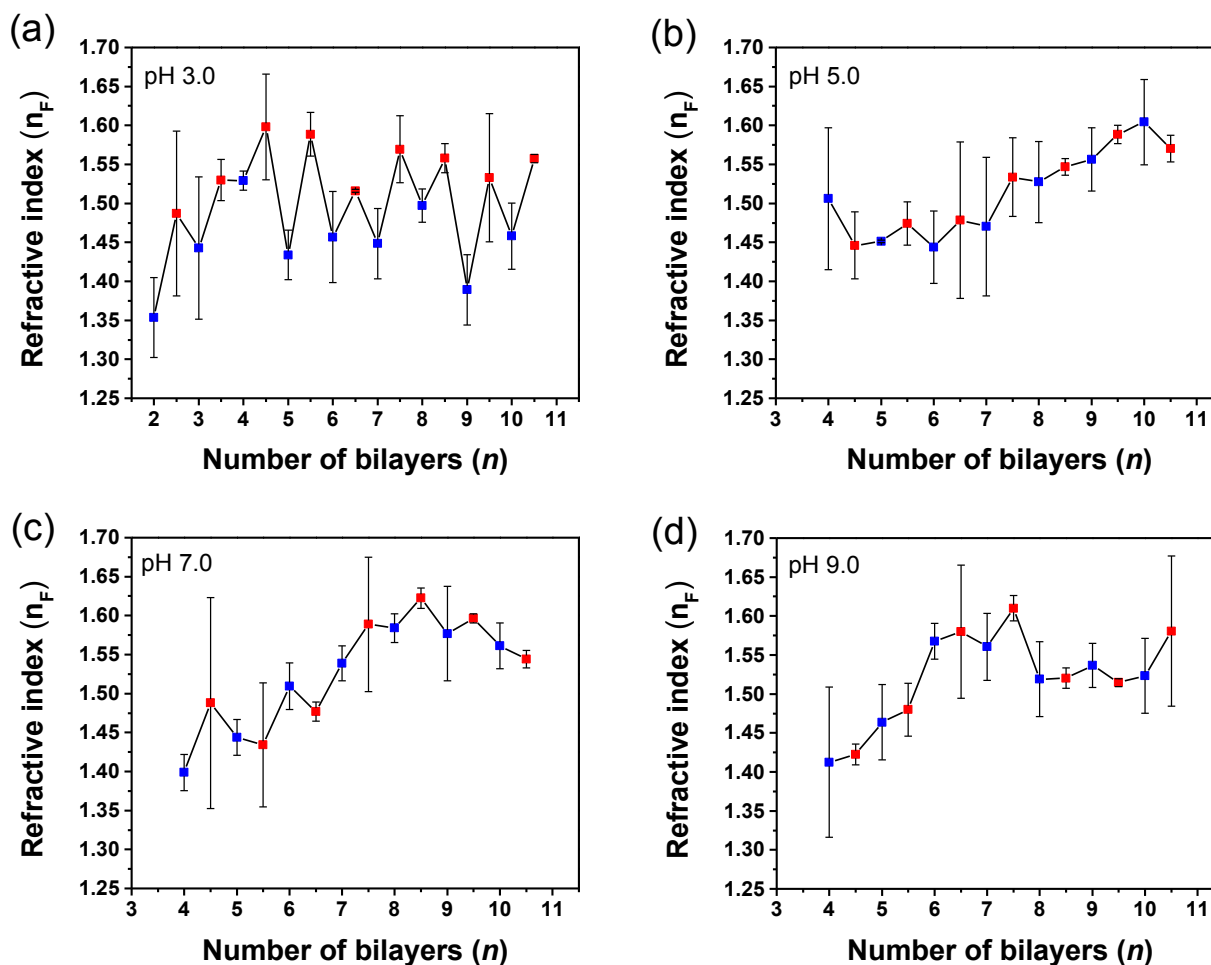
Figure A2.7. Ellipsometrically determined refractive indices (548.8 nm) for
(PAH/PDCMAA)n films deposited at pH 3.0, 5.0, 7.0 and 9.0. Integer numbers of
bilayers indicate films terminated with PDCMAA deposition (blue squares) and fractional
numbers represent terminal PAH deposition (red squares). Films with fewer layers did
not give reliable values for refractive indices because of their low thickness.

Figure A2.7. Ellipsometrically determined refractive indices (548.8 nm) for (PAH/PDCMAA)n films deposited at pH 3.0, 5.0, 7.0 and 9.0. Integer numbers of bilayers indicate films terminated with PDCMAA deposition (blue squares) and fractional numbers represent terminal PAH deposition (red squares). Films with fewer layers did not give reliable values for refractive indices because of their low thickness. Figure A2.8 shows how the refractive indices of PAH/PDCMAA films deposited at pH 3.0 vary with the number of adsorbed layers. Despite the uncertainty in the data, in general the refractive index increases after adsorption of PAH and decreases after adsorption of PDCMAA. The multilayers with PDCMAA as the last deposited layer show refractive indices of 1.35-1.53, whereas films ending in PAH deposition exhibit refractive indices from 1.49-1.59. These results suggest that PDCMAA deposited at pH 3.0 is more hydrophilic than PAH. During rinsing with water, hydrophilic free –COO$^-$ groups form (Figure A2.13a provides evidence for –COO$^-$ groups in films deposited at pH 3.0 and rinsed with water). Adsorption of PAH should lead to complexes of these groups and decrease swelling.

In contrast, the refractive indices of films deposited at pH 5.0, 7.0 and 9.0 show no detectable difference for films terminated with PDCMAA and PAH adsorption. Refractive index values are lower for films with 4-~7 bilayers, which may indicate more water in thinner films,[9,10] perhaps because of heterogeneous surface coverage.[8,11] However, the fitted values of refractive indices are less accurate in relatively thin films (Figure A2.11 gives values of film thicknesses). After adsorption of 10 bilayers, the refractive indices for films deposited at pH 5.0, 7.0, and 9.0 range from 1.52 to 1.59

(Figure A2.8b, c & d and Figure A2.8), which is consistent with values for other polyelectrolyte films.[6]
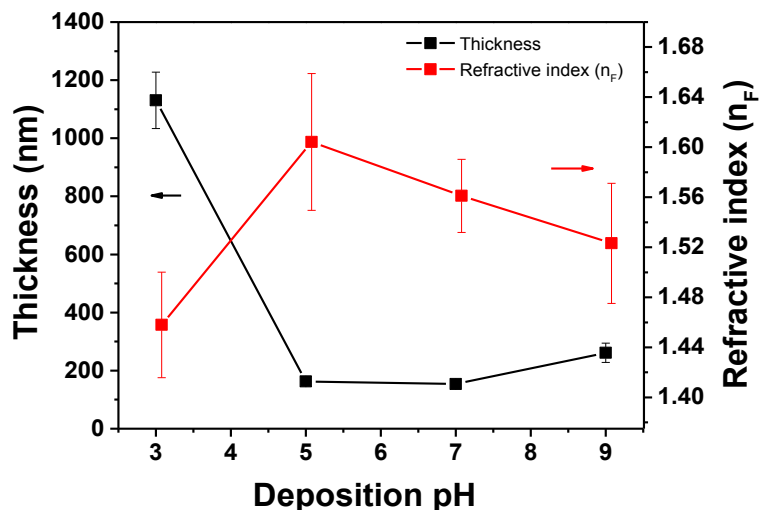
Figure A2.8. Ellipsometric thicknesses and refractive indices (548.8 nm) of (PAH/PDCMAA)$_{10}$ films assembled at different pH values.

Figure A2.8 shows the thicknesses and refractive indices of (PAH/PDCMAA)$_{10}$ films as a function of the pH of polyelectrolyte deposition solutions. We employed the refractive index values to estimate the water content of the film deposited at pH 3.0.[8,12] Equation A2.2 describes the film refractive index, n_f, as a linear combination of the refractive indices of the polymers, n_p, and water, n_w, where ϕ is the volume fraction of polymer in the film. Assuming that the film with the highest refractive index (1.59) contains no water (such a high refractive index is consistent with a non-hydrated polymer),[10]

$$n_f = \phi n_p + (1 - \phi)n_w \qquad \text{Equation A2.2}$$

this equation suggests that films deposited at pH 3.0 contains about 37% water (the refractive index of water is 1.33). However, even excluding the amount of water absorbed in the film, (PAH/PDCMAA)$_{10}$ films deposited at pH 3.0 would still be at least ~3-fold thicker than films deposited at any other pH value (See Figure A2.8 and Figure A2.9). Under ambient conditions, the estimated water content for the films deposited at other pH values was <15%.

To further confirm the presence of water in films formed at pH 3.0, we examined their thicknesses and refractive indices after drying in vacuo for 24 h. For films with 4 or more bilayers, the refractive indices of the dried films ranged from 1.52 to 1.62 (Figure A2.9). Moreover, the thicknesses of films with 6-10 bilayers were 14-40% lower than for films dried briefly with flowing N$_2$ and stored in ambient conditions.
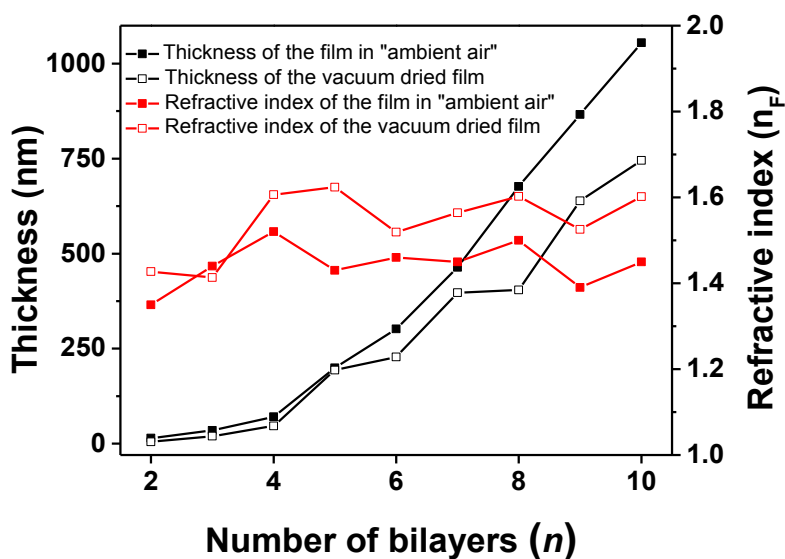
Figure A2.9. Ellipsometric thicknesses and refractive indices of PAH/PDCMAA films deposited at pH 3.0 and stored in ambient air or dried in vacuo for 24 h. (Thicknesses were measured within 2 min after removing the substrate from the vacuum chamber.)

We also examined film thickness during immersion in a pH 4.0 solution (20 mM phosphate) in an in situ ellipsometry cell. After 10 min of immersion, we determined the swollen thickness, and the swelling percentages using the following equation, where the "dry" thickness refers to the thickness in ambient air.

$$\% \text{ swelling} = \left[\frac{\text{swollen thickness-dry thickness}}{\text{dry thickness}} \right] \times 100 \qquad \text{Equation A2.3}$$

(a)

(b)
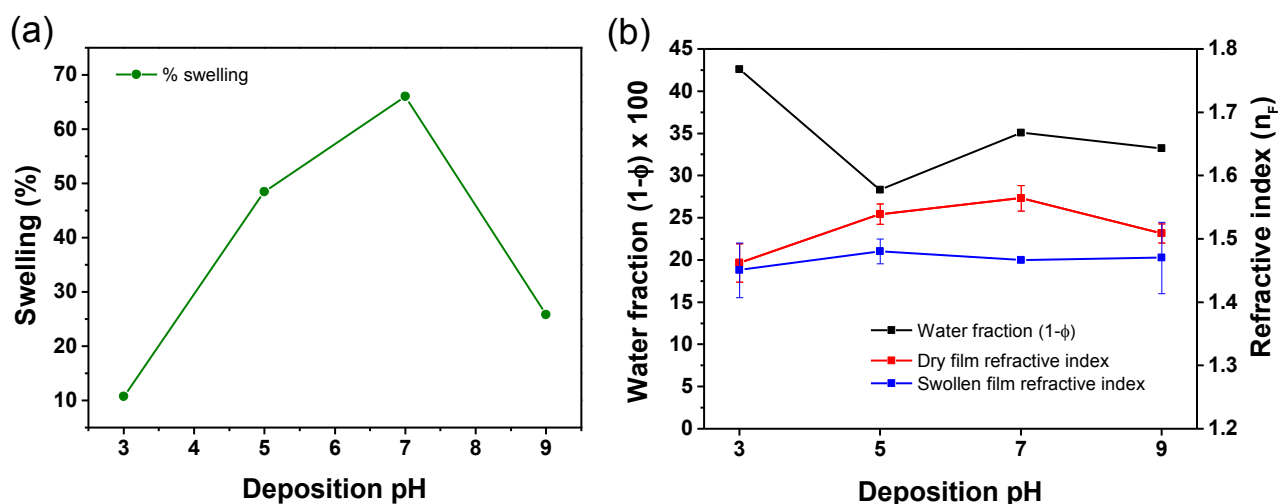
Figure A2.10. (a) Swelling percentages and (b) water volume fractions and refractive indices for (PAH/PDCMAA)$_{10}$ films assembled at different pH values and immersed in pH 4.0 water. Figure (b) gives the refractive indices of "dry" films (ambient conditions) for comparison.

Swelling of PAH/PDCMAA films in aqueous solutions will likely affect the rate of Cu^{2+} binding. Films assembled at pH 3.0 only swell 10% upon immersion in water, presumably because the "dry" films already contains ~40% water. However, after immersion in water, films deposited at pH 5.0, 7.0 and 9.0 increase in thickness by 48%, 66% and 26%, respectively. Taking into account swelling in the dry films calculated based on refractive indices, films assembled at pH 3.0, 5.0, 7.0, and 9.0 contain 42, 28,

35 and 33 vol% water when immersed in pH 4.0 phosphate solution. The similar refractive indices of all the films immersed in water also suggest similar swelling regardless of deposition pH (Figure A2.10b). Barrett et al. observed comparable swelling behaviors with PAH/PAA films.[7]

A2.4. Film Thickness Versus the Number of Adsorbed Layers.
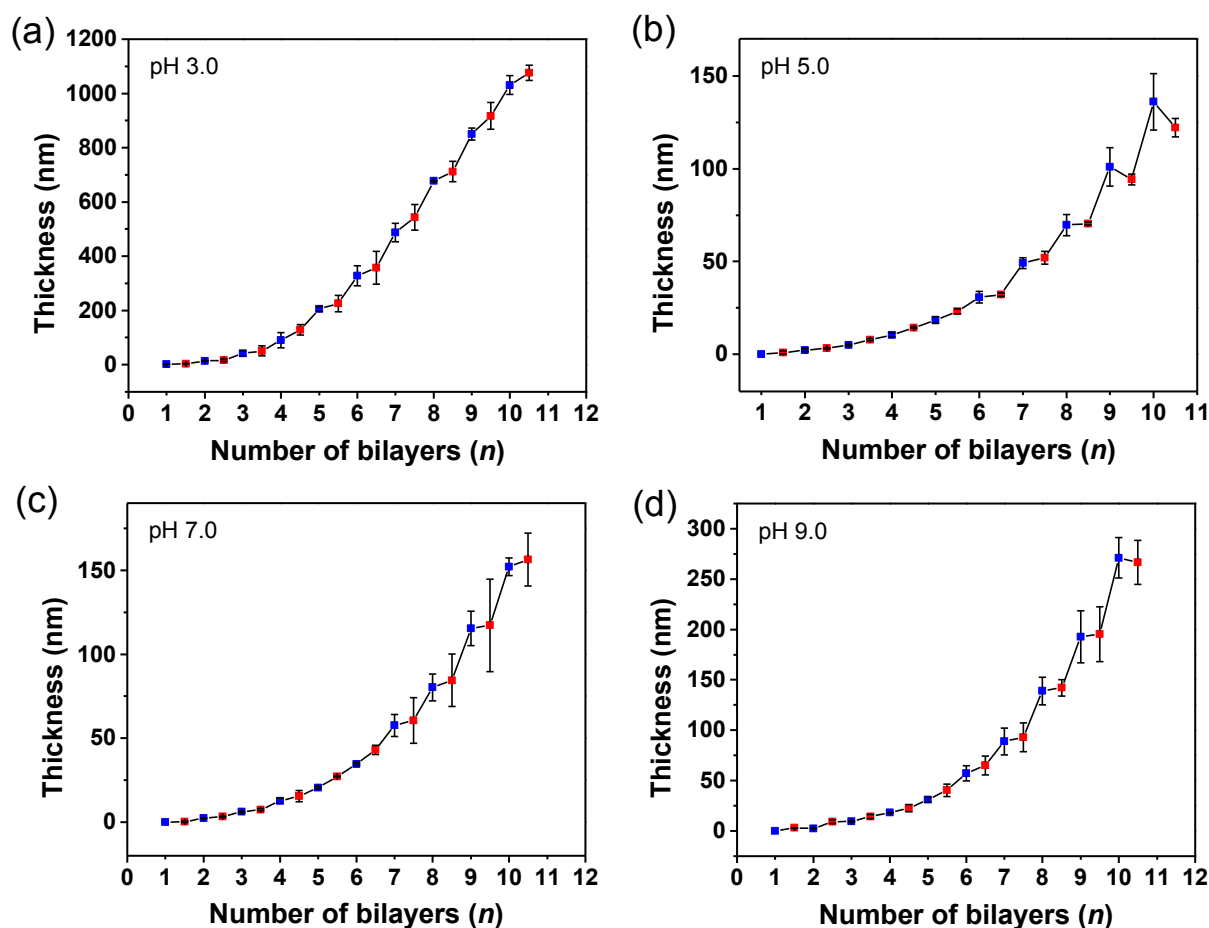
Figure A2.11. "Dry" (ambient conditions) thicknesses of $(PAH/PDCMAA)_n$ films adsorbed at (a) pH 3.0, (b) pH 5.0, (c) pH 7.0 and (d) pH 9.0. Fractional values of *n* (0.5, 1.5, 2.5, etc.) indicate terminal adsorption of PAH, whereas integers corresponds to terminal adsorption of PDCMAA.
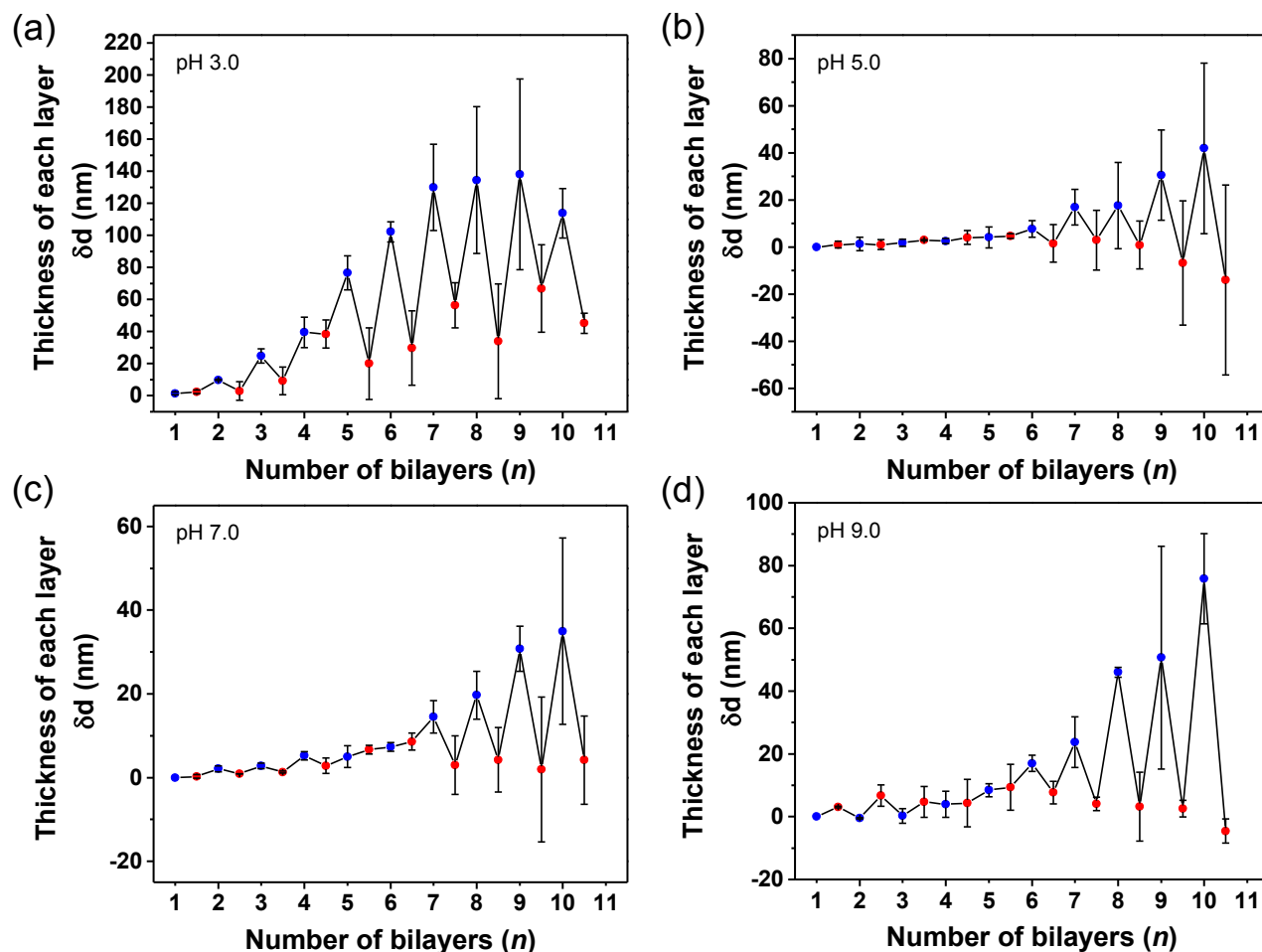
Figure A2.12. Changes in film thickness, δd, after the deposition of each layer in $(PAH/PDCMAA)_n$ films formed at (a) pH 3.0, (b) pH 5.0, (c) pH 7.0, and (d) pH 9.0. Blue and red circles show the increase in thickness after adsorption of PDCMAA and PAH, respectively.

Figure A2.11 shows film thickness after each adsorption step in LBL deposition. Reflectance FTIR spectra (Figure A2.13) show similar increases in absorbance as the number of deposited layers increases. Figure A2.12 presents the increase in film thickness after deposition of each layer, and Table A2.4 also provides values of thickness increases after each adsorption step. For deposition at pH 3.0, in the linear range of thickness versus layer number (n=5 to 10), the increases in film thickness after

PDCMAA and PAH adsorption range from 77-138 nm and 20-67 nm, respectively. The greater thickness increase after the PDCMAA deposition step could result from more sorption of PDCMAA than PAH. However, higher swelling of films after PDCMAA sorption also contributes to this thickness increase (see Figure A2.8a and the discussion of refractive indices).

Table A2.4. Changes in thickness after adsorption of each polyelectrolyte layer during deposition of (PAH/PDCMAA)$_n$ films at different pH values.*

Bilayer number (n)	Change in thickness (nm) after deposition of each layer			
	pH 3.0	pH 5.0	pH 7.0	pH 9.0
1.5	2.5	1.0	0.3	3.1
2.0	9.8	1.3	2.1	-0.5
2.5	3.0	0.9	0.9	6.7
3	25	1.8	2.8	0.2
3.5	9.3	2.9	1.3	4.7
4	40	2.5	5.2	4.0
4.5	38	4.0	2.8	4.3
5	77	4.0	5.0	8.4
5.5	20	4.7	6.7	9.4
6	102	7.6	7.3	17
6.5	30	1.5	8.6	7.7
7	130	17	14	24
7.5	56	2.9	3.0	4.1
8	134	18	20	46
8.5	34	0.8	4.2	3.2
9	138	31	31	51
9.5	67	-6.8	1.9	2.6
10	114	42	35	76
10.5	45	-14	4.2	-4.6

*Film thicknesses for 0.5- and 1.0-bilayer films were below detection.

At deposition pH values of 5.0, 7.0, and 9.0, thickness increases are also greater for PDCMAA than PAH, at least for layers 7-10, and refractive indices are similar for films terminating with PDCMAA and PAH. With deposition at pH 5.0, film thickness even appears to decrease in some case after the PAH deposition step. Holm et al.[13] suggested that such "odd-even effects" occur because the positively charged polyelectrolyte adsorbs to the surface in a relatively flat conformation. The subsequent PDCMAA deposition may yield complexes with the previously adsorbed PAH layer via coiling of both polymers to give a larger increase in thickness. The relatively low charge density on PDCMAA compared to PAH (at least at pH 5.0) should lead to a more coiled conformation of this polymer and more deposition of PDCMAA than PAH.

A2.5. Reflectance IR Spectra of (PAH/PDCMAA)$_{10}$ Films.
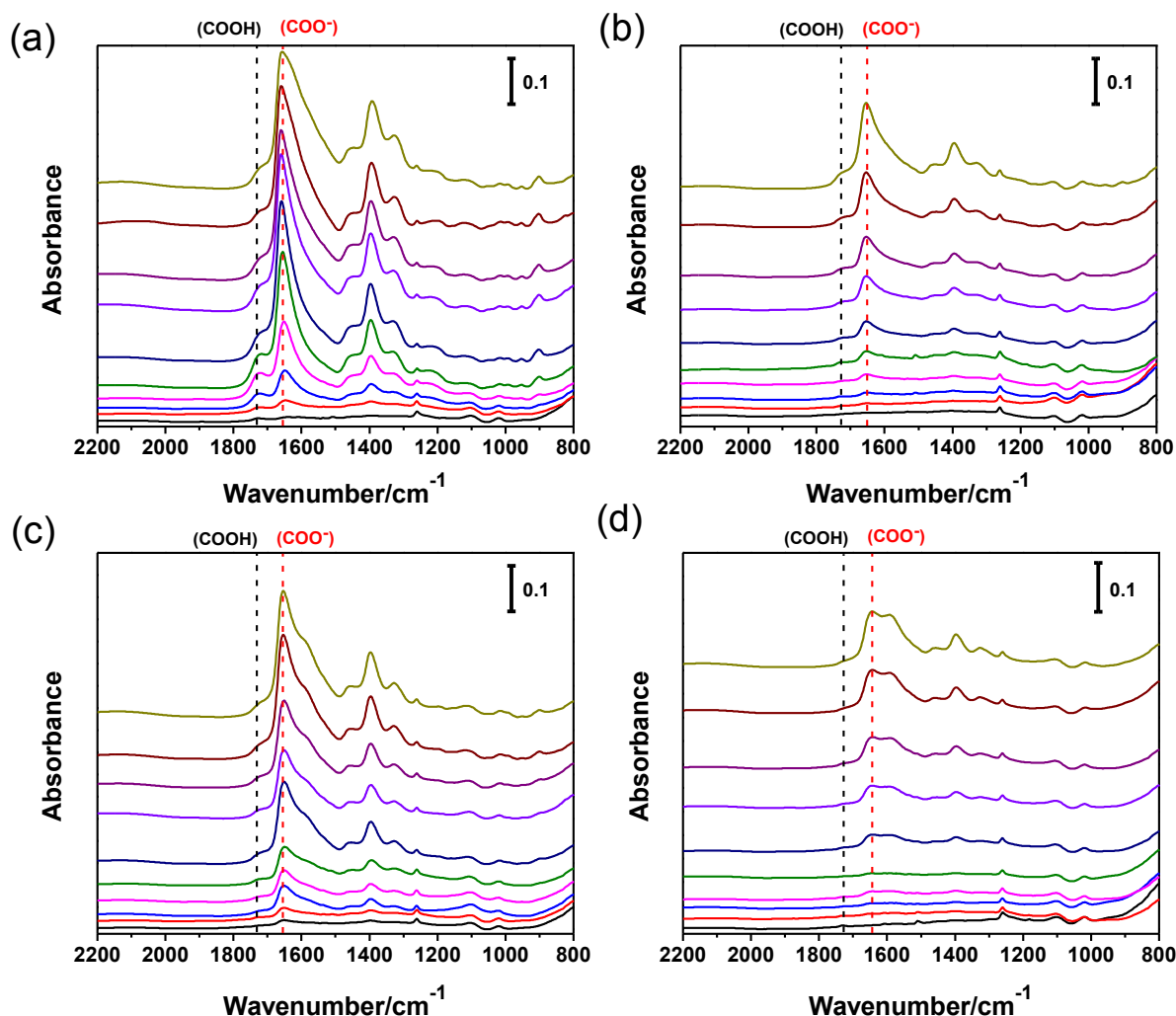
Figure A2.13. Reflectance IR spectra (2200-800 cm^{-1}) of (PAH/PDCMAA)$_n$ films deposited on MPA-modified Au at (a) pH 3.0 (b) pH 5.0, (c) pH 7.0 and (d) pH 9.0 Films were rinsed with deionized water and dried with N$_2$ prior to obtaining the spectra. In each graph, the number of bilayers in the film increases from n=1 (bottom, black line) to 10 (top, olive green). The large –COO$^-$ stretch (relative to the acid carbonyl stretch) shows that after rinsing with water most –COOH groups are deprotonated.

A2.6. AFM Images of (PAH/PDCMAA)$_{10}$ Films.
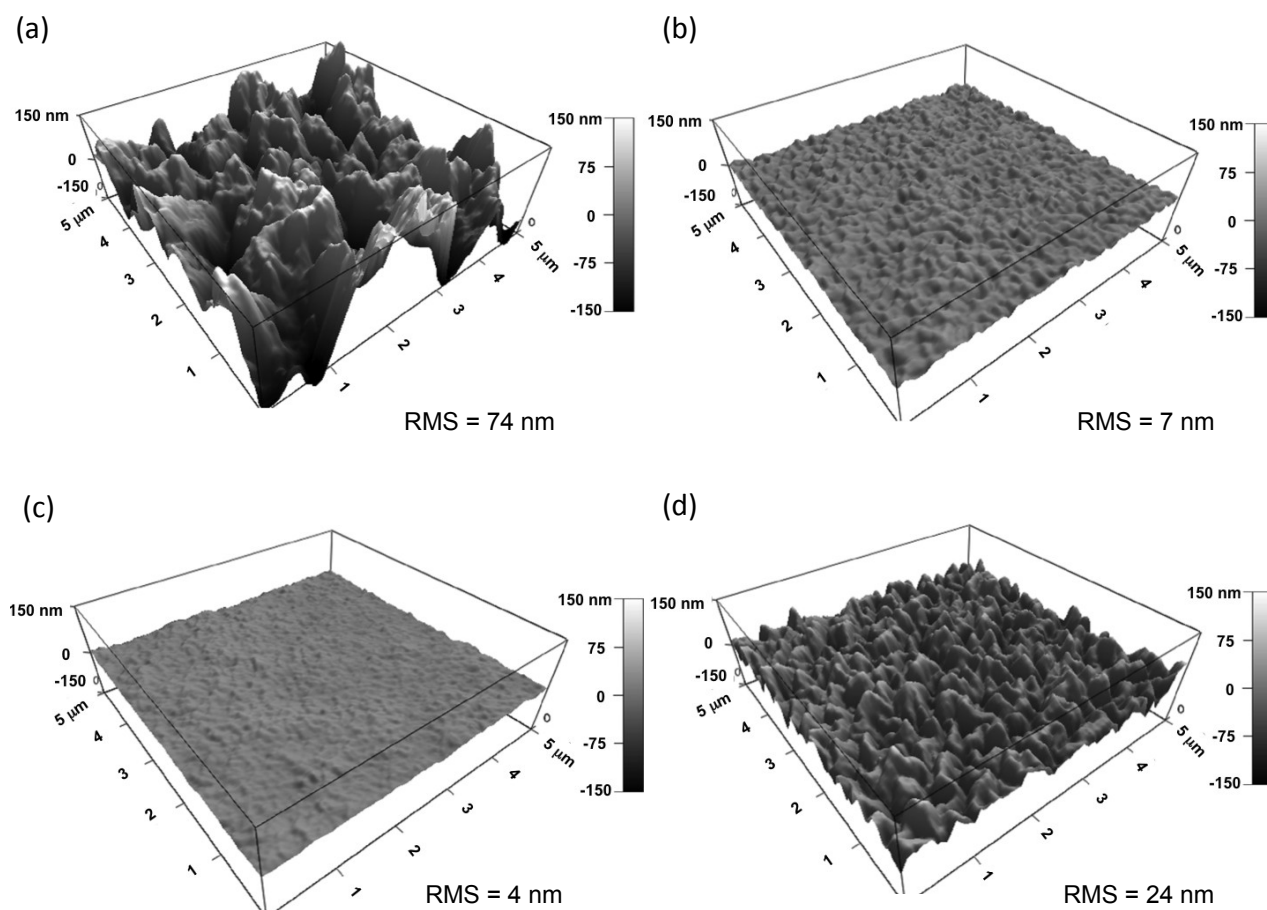
Figure A2.14. AFM 3D images of (PAH/PDCMAA)$_{10}$ films adsorbed at (a) pH 3.0, (b) pH 5.0, (c) pH 7.0 and (d) pH 9.0. (The Z scale is the same in all figures to facilitate comparison.) RMS values show the root mean square roughnesses.
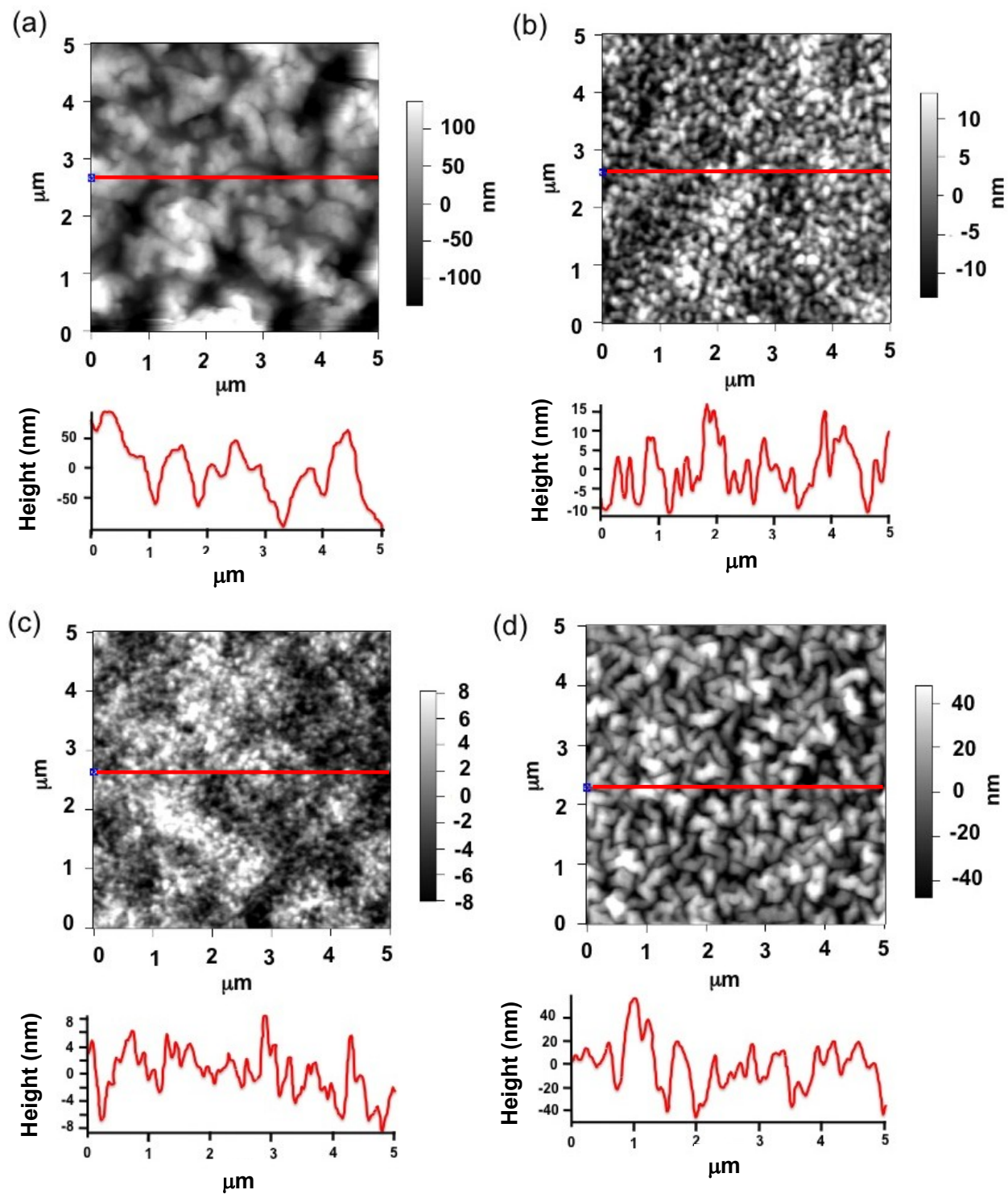
Figure A2.15. AFM line scans and corresponding images of (PAH/PDCMAA)$_{10}$ films adsorbed at (a) pH 3.0, (b) pH 5.0, (c) pH 7.0 and (d) pH 9.0.

A2.7. Sips Isotherms for Cu^{2+} Sorption in (PAH/PDCMAA)$_{10}$ Films at 4, 25 and 37 °C.
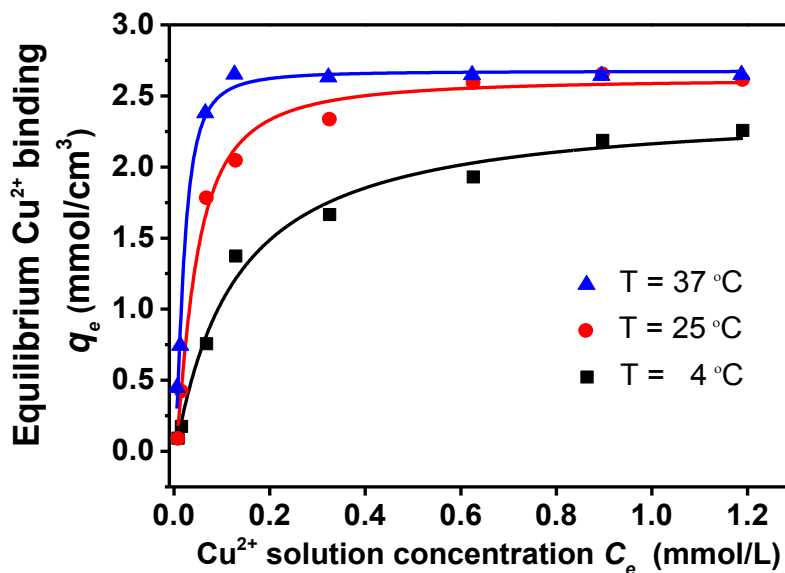
Figure A2.16. Sorption isotherms for Cu^{2+} binding to (PAH/PDCMAA)$_{10}$ at 4, 25 and 37 °C. Films were assembled at pH 3.0, and binding was allowed to occur for 15 h in a pH 4.0 solution (20 mM phosphate). The line shows a fit to the data using the Sips isotherm.

A2.8. Isotherms for Cu^{2+} Sorption in (PAH/PDCMAA)$_{10}$ Films at 16 and 31 ^{o}C.
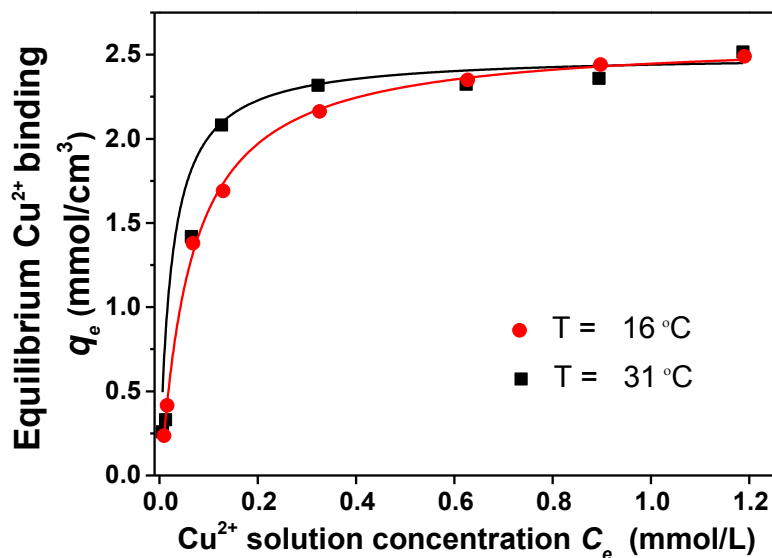
Figure A2.17. Sorption isotherms for Cu^{2+} binding to (PAH/PDCMAA)$_{10}$ at 16 and 31 ^{o}C. Films were assembled at pH 3.0, and binding was allowed to occur for 15 h in pH 4.0 solution (20 mM phosphate). The line shows a fit to the data using the Langmuir isotherm.
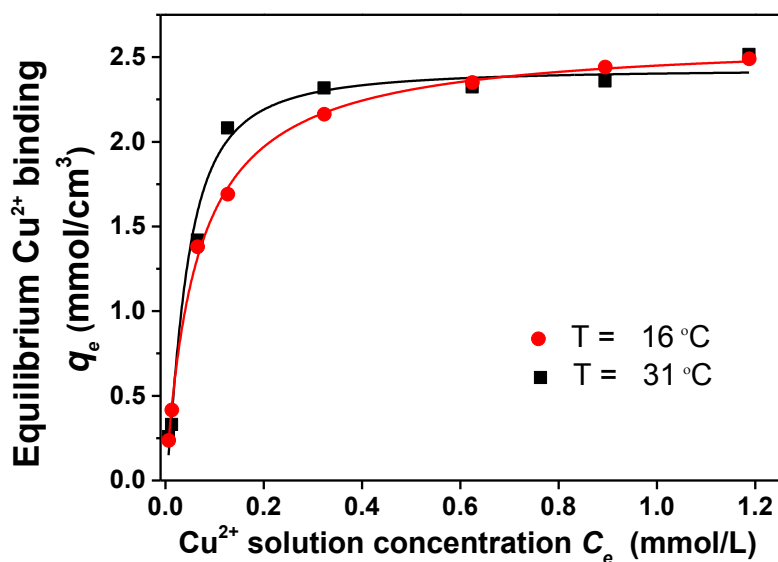
Figure A2.18. Sorption isotherms for Cu^{2+} binding to (PAH/PDCMAA)$_{10}$ at 16 and 31 ^{o}C. Films were assembled at pH 3.0, and binding was allowed to occur for 15 h in pH 4.0 solution (20 mM phosphate). The line shows a fit to the data using the Sips isotherm.

REFERENCES

REFERENCES

(1)   Naka, K.; Tachiyama, Y.; Hagihara, K.; Tanaka, Y.; Yoshimoto, M.; Ohki, A.; Maeda, S. *Polym. Bull.* **1995**, *35*, 659-663.

(2)   Petrov, A. I.; Antipov, A. A.; Sukhorukov, G. B. *Macromolecules* **2003**, *36*, 10079-10086.

(3)   Choi, J.; Rubner, M. F. *Macromolecules* **2005**, *38*, 116-124.

(4)   Wijeratne, S.; Bruening, M. L.; Baker, G. L. *Langmuir* **2013**, *29*, 12720-12729.

(5)   Fowkes, F. M. *Ind. Eng. Chem.* **1964**, *56*, 40-52.

(6)   Sailer, M.; Barrett, C. J. *Macromolecules* **2012**, *45*, 5704-5711.

(7)   Tanchak, O. M.; Barrett, C. J. *Chem. Mater.* **2004**, *16*, 2734-2739.

(8)   Halthur, T. J.; Elofsson, U. M. *Langmuir* **2004**, *20*, 1739-1745.

(9)   Tanchak, O. M.; Yager, K. G.; Fritzsche, H.; Harroun, T.; Katsaras, J.; Barrett, C. J. *Langmuir* **2006**, *22*, 5137-5143.

(10)   Wong, J. E.; Rehfeldt, F.; Hanni, P.; Tanaka, M.; Klitzing, R. V. *Macromolecules* **2004**, *37*, 7285-7289.

(11)   Schönhoff, M.; Ball, V.; Bausch, A. R.; Dejugnat, C.; Delorme, N.; Glinel, K.; Klitzing, R. V.; Steitz, R. *Colloid. Surface. A* **2007**, *303*, 14-29.

(12)   Ball, V.; Ramsden, J. J. *Biopolymers* **1998**, *46*, 489-492.

(13)   Messina, R.; Holm, C.; Kremer, K. *Langmuir* **2003**, *19*, 4473-4482

REFERENCES

REFERENCES

(1)   Bhattacharjee, S.; Dong, J. L.; Ma, Y. D.; Hovde, S.; Geiger, J. H.; Baker, G. L.; Bruening, M. L. *Langmuir* **2012**, *28*, 6885-6892.

(2)   Bhattacharjee, S.; Dong, J.; Ma, Y.; Hovde, S.; Geiger, J. H.; Baker, G. L.; Bruening, M. L. *Langmuir* **2012**, *28*, 6885-6892.

(3)   Anuraj, N.; Bhattacharjee, S.; Geiger, J. H.; Baker, G. L.; Bruening, M. L. *J. Membr. Sci.* **2012**, *389*, 117-125.

(4)   Zhang, G.; Ruan, Z.; Ji, S.; Liu, Z. *Langmuir* **2010**, *26*, 4782-4789

(5)   Stanton, B. W.; Harris, J. J.; Miller, M. D.; Bruening, M. L. *Langmuir* **2003**, *19*, 7038-7042.

(6)   Li, T.; Chen, S.; Li, H.; Li, Q.; Wu, L. *Langmuir* **2011**, *27*, 6753-6758.

(7)   Rahim, M. A.; Islam, M. S.; Bae, T. S.; Choi, W. S.; Noh, Y.-Y.; Lee, H.-J. *Langmuir* **2012**, *28*, 8486-8495.

(8)   Mentbayeva, A.; Ospanova, A.; Tashmuhambetova, Z.; Sokolova, V.; Sukhishvili, S. *Langmuir* **2012**, *28*, 11957-11964.

(9)   Welterlich, I.; Tieke, B. *Macromolecules* **2011**, *44*, 4194-4203.

(10)   de Paiva, R. G.; de Moraes, M. A.; de Godoi, F. C.; Beppu, M. M. *J. Appl. Polym.Sci.* **2012**, *126*, E17-E24.

(11)   Piñón, V., III; Weck, M. *Langmuir* **2012**, *28*, 3279-3284

(12)   Schuetz, P.; Caruso, F. *Adv. Funct. Mater* **2003**, *13*, 929-937.

(13)   Liu, J.; Chen, M.; Qian, D.-J. *Langmuir* **2012**, *28*, 9496-9505.

(14)   Kurth, D. G.; Higuchi, M. *Soft Matter* **2006**, *2*, 915-927.

(15)   Cao, M.; Wang, J.; Wang, Y. *Langmuir* **2007**, *23*, 3142-3149.

(16)   Kim, Y. G.; Yang, S. Y. *J Nanosci. Nanotechno.* **2010**, *10*, 6892-6895.

(17)   Dai, J. H.; Bruening, M. L. *Nano Letters* **2002**, *2*, 497-501.

(18)   Zhang, L.; Li, Y.; Sun, J.; Shen, J. *Langmuir* **2008**, *24*, 10851-10857.

(19)   Picart, C.; Mutterer, J.; Richert, L.; Luo, Y.; Prestwich, G. D.; Schaaf, P.; Voegel, J. C.; Lavalle, P. *Proc. Natl. Acad. Sci.* **2002**, *99*, 12531-12535.

(20)   Ghostine, R. A.; Markarian, M. Z.; Schlenoff, J. B. *J. Am. Chem. Soc.* **2013**, *135*, 7636-7646.

(21)   Porcel, C.; Lavalle, P.; Ball, V.; Decher, G.; Senger, B.; Voegel, J. C.; Schaaf, P. *Langmuir* **2006**, *22*, 4376-4383.

(22)   Hemdan, E. S.; Zhao, Y. J.; Sulkowski, E.; Porath, J. *Proc. Natl. Acad. Sci.* **1989**, *86*, 1811-1815.

(23)   Gaberc-Porekar, V.; Menart, V. *J. Biochem. Biophy. Meth.* **2001**, *49*, 335-360.

(24)   Harris, J. J.; Bruening, M. L. *Langmuir* **2000**, *16*, 2006-2013.

(25)   Shiratori, S. S.; Rubner, M. F. *Macromolecules* **2000**, *33*, 4213-4219.

(26)   Nakamoto, K.; Morimoto, Y.; Martell, A. E. *J. Am. Chem. Soc.* **1962**, *84*, 2081–2084.

(27)   Pack, D. W.; Arnold, F. H. *Chem. Phys. Lipids* **1997**, *86*, 135-152.

(28)   Choi, J.; Rubner, M. F. *Macromolecules* **2005**, *38*, 116-124.

(29)   Zacharia, N. S.; Modestino, M.; Hammond, P. T. *Macromolecules* **2007**, *40*, 9523-9528.

(30)   Hubsch, E.; Ball, V.; Senger, B.; Decher, G.; Voegel, J. C.; Schaaf, P. *Langmuir* **2004**, *20*, 1980-1985.

(31)   Sui, Z. J.; Salloum, D.; Schlenoff, J. B. *Langmuir* **2003**, *19*, 2491-2495.

(32)   Ladam, G.; Schaad, P.; Voegel, J. C.; Schaaf, P.; Decher, G.; Cuisinier, F. *Langmuir* **2000**, *16*, 1249-1255.

(33)   Yuan, W. Y.; Lu, Z. S.; Li, C. M. *J. Mater. Chem.* **2012**, *22*, 9351-9357.

(34)   Yuan, W. Y.; Lu, Z. S.; Wang, H. L.; Li, C. M. *Adv. Funct. Mater.* **2012**, *22*, 1932-1939.

(35)   Mendelsohn, J. D.; Barrett, C. J.; Chan, V. V.; Pal, A. J.; Mayes, A. M.; Rubner, M. F. *Langmuir* **2000**, *16*, 5017-5023.

(36)   Sailer, M.; Barrett, C. J. *Macromolecules* **2012**, *45*, 5704-5711.

(37) Yuchi, A.; Sato, T.; Morimoto, Y.; Mizuno, H.; Wada, H. *Anal. Chem.* **1997**, *69*, 2941-2944.

(38) Tseng, J. Y.; Chang, C. Y.; Chang, C. F.; Chen, Y. H.; Chang, C. C.; Ji, D. R.; Chiu, C. Y.; Chiang, P. C. *J Hazard Mater.* **2009**, *171*, 370-377.

(39) Ling, P.; Liu, F.; Li, L.; Jing, X.; Yin, B.; Chen, K.; Li, A. *Talanta* **2010**, *81*, 424-432.

(40) Rivas, B. L.; Pereira, E. D. *Bol. Soc. Chil. Quim.* **2000**, *45*, 165-171.

(41) Liu, C.; Bai, R.; Hong, L. *J. Colloid Interf. Sci.* **2006**, *303*, 99-108.

(42) Vasiliev, A. N.; Golovko, L. V.; Trachevsky, V. V.; Hall, G. S.; Khinast, J. G. *Micropor Mesopor Mat.* **2009**, *118*, 251-257.

(43) Srivastava, V. C.; Swamy, M. M.; Mall, I. D.; Prasad, B.; Mishra, I. M. *Colloid Surface A* **2006**, *272*, 89-104.

(44) Ghostine, R. A.; Schlenoff, J. B. *Langmuir* **2011**, *27*, 8241-8247.

(45) Crank, J. *The Mathematics of Diffusion*; Oxford University Press: Bristol, England, 1979.

(46) Hinatsu, J. T.; Foulkes, F. R. *J. Electrochem. Soc.* **1989**, *136*, 125-132.

(47) Cheng, C.; Yaroshchuk, A.; Bruening, M. L. *Langmuir* **2013**, *29*, 1885-1892.

(48) Langmuir, I. *J. Am. Chem. Soc.* **1918**, *40*, 1361-1403.

(49) Sips, R. *J.Chemi. Phy.* **1948**, *16*, 490-495.

(50) Freundlich, H. *Zeitschrift Fur Phy. Chemi. Stochiomet. Verwandt.* **1906**, *57*, 385-470.

(51) Ho, Y. S.; Porter, J. F.; McKay, G. *Water Air Soil Poll.* **2002**, *141*, 1-33.

(52) Ngah, W. S. W.; Fatinathan, S. *Chem. Eng. J.* **2008**, *143*, 62-72.

(53) Kamari, A.; Ngah, W. S. W. *Colloids Surfaces B* **2009**, *73*, 257-266.

(54) Panahi, H. A.; Mehmandost, N.; Moniri, E.; Galaev, I. Y. *J. Appl. Polym. Sci.* **2012**, *126*, 480-489.

(55) Liu, F.; Li, L.; Ling, P.; Jing, X.; Li, C.; Li, A.; You, X. *Chem. Eng. J.* **2011**, *173*, 106-114.

(56)   Martell, A. E.; Smith, R. M. *Critical stability constants*; Plenum Press: New York, 1975; Vol. 1.

(57)   Donia, A. M.; Atia, A. A.; El-Boraey, H.; Mabrouk, D. H. *Sep. Purif. Technol.* **2006**, *49*, 64-70.

(58)   Dai, J. H.; Bao, Z. Y.; Sun, L.; Hong, S. U.; Baker, G. L.; Bruening, M. L. *Langmuir* **2006**, *22*, 4274-4281.

(59)   Becker, J. W.; Reeke, G. N.; Wang, J. L.; Cunningham, B. A.; Edelman, G. M. *J. Biol. Chem.* **1975**, *250*, 1513-1524.

(60)   Ning, W.; Wijeratne, S.; Dong, J.; Bruening, M. L. *ACS appl. mater. interfaces* **2015**, *7*, 2575-2584.

This chapter is adapted from a recently submitted manuscript (Salinda Wijeratne, Jinlan Dong, Wenjing Ning, Wejing Liu, Gregory L. Baker and Merlin L. Bruening). Dr. Jinlan Dong initiated the protein binding in membranes modified with new polymers, and Wenjing Ning and Wejing Liu carried on the work upon Dr. Dong' s graduation. Professor Kevin D Walker at Michigan State University provided the Phenylalanine Amminomutase (*Pa*PAM) and L-Aldolase, and Dr. Dilini Ratnayake purified and characterized these proteins.

CHAPTER 3. LAYER-BY-LAYER DEPOSITION WITH POLYMERS CONTAINING NITRILOTRIACETATE, A CONVENIENT ROUTE TO FABRICATE METAL- AND PROTEIN-BINDING FILMS.

3.1. Introduction.

Films that bind metal ions are attractive for applications ranging from water remediation[1-3] to metal-affinity chromatography of peptides[4] and proteins.[5,6] Deposition of such coatings on beads or in the pores of membranes can enable high-capacity capture of metal ions and biomolecules, and film formation in membranes is particularly attractive for rapid analyte capture because of low radial diffusion distances and convective flow in membrane pores.[7-11] Anchored metal-ion complexes are also important for binding proteins in microarrays and sensors.[12-16] In most cases, increased binding will lower detection limits in protein microarrays and increase output in affinity-based purifications. Thus, these applications will benefit from high-capacity coatings.

Traditional methods for covalently immobilizing metal-ion-binding ligands yield only a monolayer of ligand,[12-18] which limits capacity. In contrast, polymer coatings may contain many multilayers of ligands and potentially capture multilayers of protein.[4] Common approaches to formation of polymer films on flat surfaces, beads and in membrane pores include synthesis of polymer brushes[19,20] and layer-by-layer (LBL) polyelectrolyte adsorption,[6] and the latter technique is attractive for its simplicity. Several groups examined metal-ion binding in LBL polyelectrolyte films,[6,21,22] but most studies employed weak-binding ligands such as the carboxylic acid groups of poly(acrylic acid) (PAA). Multilayer films containing PAA and branched polyethyleneimine (BPEI) or quaternized poly-4-vinylpyridine bind Co^{2+} and/or Cu^{2+} ions through coordination to amine or acid groups.[23,24] Additionally, post-deposition functionalization of PAA/protonated poly(allylamine) (PAH) or PAA/BPEI films with nitrilotriacetate (NTA) yields coatings with a high affinity for a number of metal ions,[5] but the derivatization process is expensive and inefficient.

To simplify the immobilization of metal-ion-binding ligands in thin films, we began developing relatively inexpensive ligand-containing polymers for LBL adsorption.[25,26] Thus far, these polymers contained iminodiacetic acid (IDA) ligands, and multilayer polyelectrolyte films formed using these polymers bind large amounts of metal ions (Cu^{2+} binding capacity of ~2.5 mmol per cm^3 of film)[25] and proteins (60±6 mg of His-tagged ubiquitin per mL of membrane).[26] However, IDA binds metal ions less strongly than NTA, which contains an extra carboxylate group for metal-ion complexation. As an example the Cu^{2+}-ligand formation constant is 3 orders of magnitude less for IDA than

for NTA.[27] Thus, in metal affinity chromatography IDA will allow significantly more metal-ion leaching than NTA.

This study reports a convenient synthesis of poly(2,2-(5-acrylamido-1-carboxypentylazanediyl) diacetic acid) [PNTA-100], an NTA-containing polymer, and incorporation of this polymer into polyelectrolyte multilayers to capture metal ions and proteins that bind to these immobilized ions (Figure 3.1).
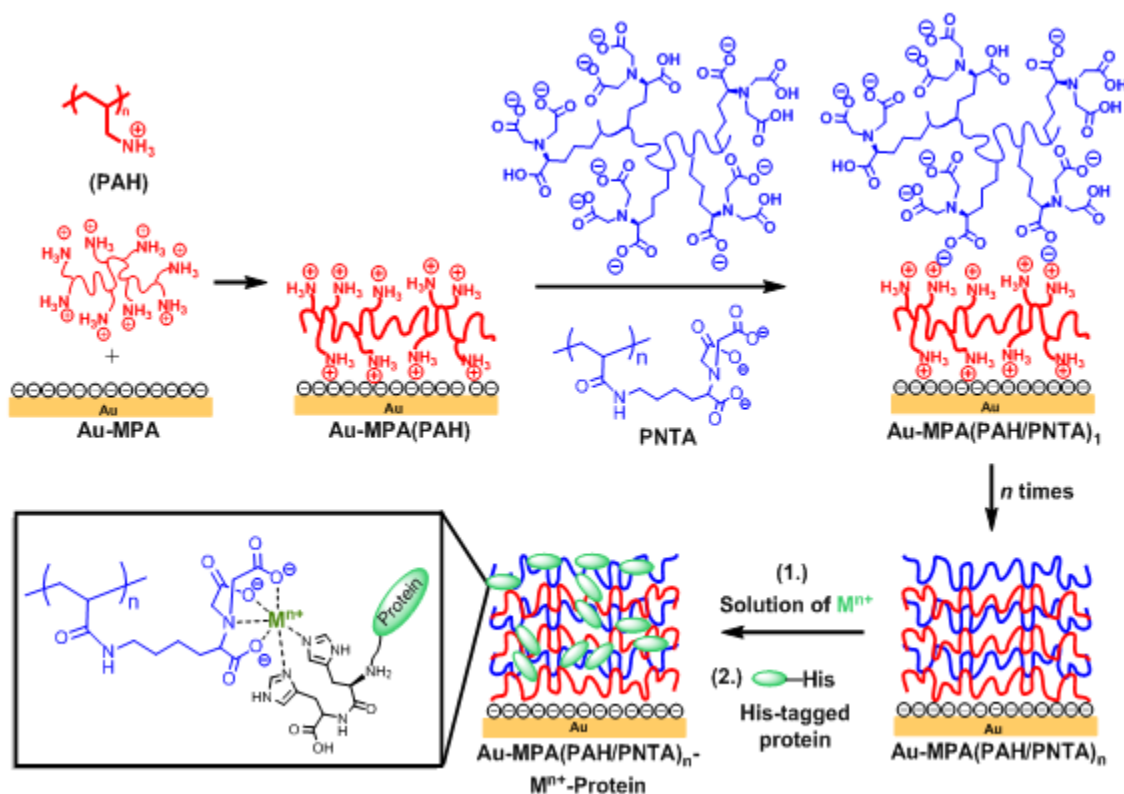
Figure 3.1. Schematic representation of the assembly of (PAH/PNTA-100)$_n$ films on Au-coated substrates modified with a monolayer of 3-mercaptopropionic acid (MPA). Polymers are likely much more intermingled in the true film structure.

We also examine whether copolymers with both NTA ligands and acrylic acid promote polymer swelling to increase protein binding to immobilized metal-ion complexes. Direct adsorption of metal-binding polymers to construct protein-binding films is more

convenient and should be less expensive than post-deposition functionalization of coating by reaction with an NTA derivative. Membranes modified with LBL films containing PNTA-100 capture as much as 48 mg of His-tagged protein per mL of membrane. Moreover, copolymers with acrylic acid capture similar amounts of proteins with fewer NTA-containing units.

3.2. Experimental.

3.2.1. Materials.

Poly(allylamine hydrochloride) (PAH, M_w=120,000–210,000, Alfa-Aesar), branched polyethyleneimine (BPEI, M_w = 25,000, Sigma-Aldrich), poly(acrylic acid) (PAA, M_w = 90,000, 25% aqueous solution, Polysciences), *N*-(3-dimethylaminopropyl)-*N'*-ethylcarbodiimide hydrochloride (EDC), *N*-hydroxysuccinimide (NHS), and N_α, N_α-bis(carboxymethyl)-L-lysine hydrate (aminobutyl NTA), and 3-Mercaptopropionic acid (MPA, 99%) were purchased from Sigma-Aldrich and used without further purification. L-lysine monohydrochloride (98%), acryloyl chloride (97%, contains <210 ppm MEHQ as stabilizer), copper(II) carbonate basic (≥95%), 8-hydroxyquinoline and bromoacetic acid (≥97%) were purchased from Aldrich. The appendix describes the synthesis of NTA-containing copolymers and provides NMR and IR spectra of the monomers and polymers (Figures A3.1 to A4.10) along with a titration curve (Figure A3.11). (Figure numbers beginning with "A" refer to the appendix). Aqueous solutions containing 1 mg/ml PAH or 1 mg/mL PNTA-X were prepared in deionized water (18.2 MΩcm, Milli-Q). PNTA-containing solutions with pH values of 3.0 or 9.0 were obtained by first

dissolving the polymer with the addition of 6 M NaOH to achieve a pH 9.0 solution and then adjusting the pH with 6 M HCl. Gold-coated wafers (200 nm of gold and 20 nm of Cr sputtered on Si(100) wafers at LGA Thin Films, Santa Clara, CA) were cleaned in a UV/O$_3$ chamber for 15 min just before use.

Hydroxylated nylon (LoProdyne® LP, Pall, 1.2 μm pore size, 110 μm thick), nylon (GE, non-hydroxylated, 1.2 μm pore size, average thickness of 95 μm), and polyethersulfone (GE, 1.2 μm pore size, average thickness of 130 μm) membranes were cut into 25 mm-diameter discs prior to use. Coomassie protein assay reagent (Thermo Scientific), Histidine$_6$-tagged Ubiquitin (HisU, human recombinant, Enzo Life Sciences), and conconavalin A (Con A) from *Canavaliaensiformis* (Jack bean) were used as received. His-tagged COP9 signalosome complex subunit 8 (CSN 8) was overexpressed in BL21DE3 cells as described previously.[28] Professor Kevin D Walker at Michigan State University provided the Phenylalanine Amminomutase (*Pa*PAM) and L-threonine aldolase.[29,30]

3.2.2. Synthesis of Poly(2,2-(5-acrylamido-1-carboxypentylazanediyl) diacetic acid), [PNTA-100].

Poly(ε-acryloyl L-lysine) was synthesized using a literature procedure with some modifications.[31] Initiator, 4,4-azobis-4-cyanovaleric acid (12.5 mg, 0.045 mmol = 0.36 mol % with respect to monomer), was dissolved in water (40 mL), and the monomer ε-acryloyl L-lysine (2.5 g, 0.0125 mol) was added to the solution while stirring. The pH was adjusted to between 6 and 7 using 0.1 M NaOH. Subsequently the mixture was

degassed by five freeze−pump-thaw cycles, and polymerization was carried out at 75 °C for 24 h. The reaction was monitored using ^{1}H NMR spectroscopy and stopped by exposing the mixture to air. For characterization only, the polymer was precipitated using tetrahydrofuran and acetone. After vacuum drying, 2.2 g of a colorless solid was obtained (~80%). ^{1}H NMR (D$_2$O, δ ppm): 1.26-1.30 (br, 2H, CH$_2$), 1.35-139 (br, 2H, CH$_2$), 1.54 (br, 2H, CH$_2$), 1.76 (br, 2H, CH$_2$), 1.99 (br, 1H, CH), 2.99 (br, 2H, CH$_2$), 3.71 (bm, 1H, CH), 7.88 (br, 1H, CONH).

Under a N$_2$ atmosphere, bromoacetic acid (12.5 g, 0.09 mol), NaOH (3.5 g, 0.09 mol) and 50 mL of water were added to a two-neck round-bottomed flask, and the mixture was stirred at room temperature for 10 min. This solution was added dropwise with stirring to an aqueous solution (100 mL) containing poly(ε-acryloyl-L-lysine) (2.5 g, 0.0125 mol) at 50 °C. The reaction mixture was kept at 50 °C for 24 h with occasional addition of 3% NaOH to maintain the pH at 10.0. At the end of the reaction, polymer was precipitated by adjusting the solution pH to 1 by adding 5 M HCl. The supernatant was decanted, the remaining precipitate was dissolved by addition of 3% NaOH, and the solution was again adjusted to pH 1.0 with 5 M HCl. This process was repeated 2 times, and the precipitate was filtered and dried in vacuum for 12 h to give poly(2,2-(5-acrylamido-1-carboxypentylazanediyl) diacetic acid) as a white solid, 2.8 g (yield of 70%, the number of carboxymethylene groups added per ε-acryloyl-L-lysine repeating unit is 1.62). ^{1}HNMR (D$_2$O, δ ppm): 1.33 (bm, 2H, CH$_2$), 1.43 (br, 2H, CH$_2$), 1.53 (br, 2H, CH$_2$), 1.78 (br, 2H, CH$_2$), 2.0 (br, 1H, CH), 3.0 (br, 2H, CH$_2$), 3.49 (br, 1H, CH), 3.59 (br, 4H, 2×CH$_2$), 7.86 (br, 1H, CONH). Elemental analysis (%) calcd. for C$_{13}$H$_{20}$N$_2$O$_7$: C, 49.36; H, 6.37; N, 8.86. Found: C, 43.63; H, 6.57; N, 8.13. (The supporting information

describes the NMR characterization and elemental analysis in detail and explains the discrepancy betwee the calculated and experimental elemental analyses.)

3.2.3. Synthesis of Poly(2,2-(5-acrylamido-1-carboxypentylazanediyl) diacetic acid-*co*-acrylic acid) [PNTA-50 or 25].

Poly(ε-acryloyl L-lysine)-*co*-(acrylic acid) was prepared and allowed to react with bromoacetic acid. Copolymers were synthesized with 2 different NTA repeat unit to acrylic acid compositions. In the nomenclature PNTA-X, the value of X is the percentage of polymer repeat units that contain NTA. The supporting information in the appendix gives details on synthesis and characterization.

3.2.4. Film Formation on Gold-coated Wafers.

A monolayer of -COOH groups was formed on Au-coated Si wafers (24 mm × 11 mm) by immersing the substrate in 5 mM MPA in ethanol for 12 h, rinsing with ethanol, and drying with N_2. A subsequent PAH or BPEI layer was deposited by immersing the MPA-coated substrates for 5 min in a 1 mg/ml PAH or BPEI solution adjusted to pH 3.0 or 9.0 (in some case these polyelectrolyte solutions also contained 0.5 M NaCl). After polyelectrolyte adsorption, the substrate was washed with deionized water for ~1 min and dried with N_2. The Au-MPA(PAH) or Au-MPA(BPEI) substrates were then immersed in a 1mg/ml PNTA-X or PAA solution (pH of 3.0 or 9.0, with or without 0.5 M

NaCl) for 5 min and again rinsed with deionized water and dried with N_2. This process was repeated to obtain the desired number of (PAH or BPEI/PNTA-X or PAA)$_n$ multilayers. Figure 3.1 illustrates the process.

3.2.5. Preparation of BPEI/PAA-NTA Films on Gold Coated Wafers.

To incorporate NTA ligands into (BPEI/PAA)$_n$ films, coated wafers were first immersed in 10 ml of aqueous 0.1 M NHS/EDC for 4 h. The wafers were then sequentially washed with distilled water and ethanol and dried with N_2 prior to immersion in a 0.1 M aminobutyl NTA solution for 12 h. The resulting NTA-containing films were thoroughly washed with water and dried with N_2.

3.2.6. Characterization of Films on Gold Coated Wafers.

Spectroscopic ellipsometry (J. A. Woollam M-44 instrument) was used to determine film thickness. Both refractive index and thickness were fitting parameters, and a Cauchy model, $n(\lambda) = A_n + \dfrac{B_n}{\lambda^2} + \dfrac{C_n}{\lambda^4}$ was employed to fit the refractive index, n, as a function of wavelength, λ. In situ ellipsometry in aqueous solution was carried out in a home-built cell as described previously.[32] After measuring the dry film thickness in air, 20 mM phosphate buffer (pH 7.4) was added to the cell, and the swollen film thickness was determined after 10 min. Swelling of PEMs was carried out before and after formation of metal-ion complexes (see below).

3.2.7. Metal-ion Binding to (PAH/PNTA-X)$_n$ Films on Gold-coated Wafers.

(PAH/PNTA-X)$_n$ (n = 1 to 5)-coated Au wafers assembled at different pH values and ionic strengths (with and without 0.5 M NaCl) were separately immersed in vials containing 10 mL of 0.5 M CuSO$_4$ or NiSO$_4$ and incubated for 15 h. The back side of the gold-coated wafers was covered with Scotch^{TM} transparent duct tape to prevent metal-ion sorption on this face of the substrate. (Control experiments showed minimal metal-ion binding to tape-covered wafers.) After rinsing the wafers with deionized water from a squirt bottle for 1 min, adsorbed metal ions were eluted from the films by immersing the substrates in 5.0 mL of 20 mM EDTA (adjusted to pH 7.4) for 12 h. Using atomic absorption spectroscopy (Varian Spectra AA-200 atomic absorption spectrophotometer), the amount of metal ion in the stripping solution was calculated from its absorbance using appropriate calibration curves. Both the standard and sample solutions contained 20 mM EDTA (pH 7.4).

3.2.8. Protein Binding in (PAH/PNTA-X)$_n$ and (BPEI/PAA)$_n$-NTA PEM Films.

In investigations of protein binding in these films, His U, conconavalin A (Con A), L-Aldolase and His-tagged phenylalanine aminomutase (*Pa*PAM) served as model proteins. The substrates coated with (BPEI/PAA)$_n$-NTA-Ni^{2+}/Cu^{2+} or (PAH/PNTA-X)$_n$-Ni^{2+}/Cu^{2+} (Ni^{2+} for his tagged proteins and Cu^{2+} for Con A) were immersed in 0.1 mg/mL protein solutions in 20 mM phosphate buffer (pH 7.4 or 6.0) for 20 h at room temperature. (Con A is unstable at pH 7.4 so we examined binding of this protein at pH 6.0.) Subsequently, using a Pasteur pipette these substrates were rinsed with 10 mL of

washing buffer (20 mM phosphate buffer containing 0.1% Tween-20 surfactant) and 10 mL of water for ~1 min each and dried with N_2. The amount of protein binding was determined by reflectance FTIR spectroscopy and expressed as the equivalent thickness of a spin-coated protein that would give the same absorbance.[33] The equivalent thickness d is calculated from the difference of absorbance (ΔA) at 1680 cm^{-1} (amide I band) before and after binding protein, using the equation $d(nm) = \Delta A / 0.0017$. Some of these thicknesses were confirmed using ellipsometry. Assuming a protein density of ~1 g/cm^3, each nm of equivalent thickness corresponds to approximately 1 mg/m^2 of surface coverage.

3.2.9. Membranes.

3.2.9.1. Membrane Modification with (PAH/PNTA-X)$_n$ PEM Films.

Hydroxylated nylon 6,6 membrane discs were cleaned for 10 min with UV/ozone and placed in a homemade Teflon holder (similar to an Amicon cell) connected to a peristaltic pump. The membrane holder exposes 3.1 cm^2 of external membrane surface area. Subsequently, a 5-mL solution containing 0.5 M NaCl and 20 mM PSS or PAA was circulated through the membrane for 20 min at a flow rate of 1 mL/min. Additional polycation (PAH) and polyanion (PNTA-X) layers were deposited similarly using 1 mg/mL solutions containing 0.5 M NaCl. After deposition of each polyelectrolyte, 20 mL of water was passed through the membrane at the same flow rate. The pH of PAA, and PNTA solutions was 3, while the pH of the PAH solutions was adjusted to pH 3 or pH 9 with 1 M NaOH or 1M HCl.
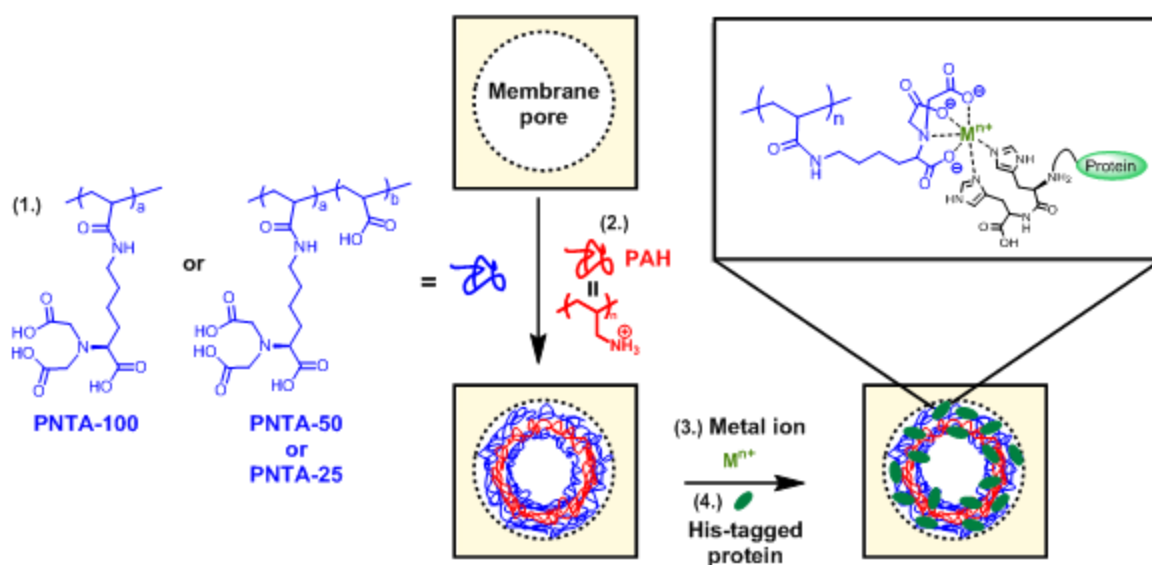
Figure 3.2. Schematic representation of direct assembly of metal-ion-binding PNTA-X, X=100, 50 or 25, in a nylon membrane.

To improve film stability during protein binding to PNTA-25 modified membranes, films were crosslinked using a modified literature procedure.[28] First we added 0.007 mol of Ni^{2+} (to protect NTA groups on the polymer chain) to 5-mL solutions of 1 mg/mL PNTA-25 in 0.5 M NaCl. Subsequently, membrane modification was carried out according to the protocol above, and aqueous 0.1 M EDC/NHS was circulated through the PAA/PAH/PNTA-25-Ni^{2+}-modified membrane for 2 h to form crosslinks between amines and carboxylic acids. Subsequent washing with ~pH 9 buffer solution was performed to hydrolyze unreacted NHS esters. The films were loaded with 0.1 M $NiSO_4$ as described below and used for protein binding. Cross-linked membranes were used only for comparing protein binding to PAA/PAH/PNTA-25-Ni^{2+}- and PAA/BPEI/PAA-NTA-Ni^{2+}-modified membranes.

3.2.9.2. Metal-ion Binding and Leaching in (PAH/PNTA-X)$_n$-modified Membranes.

After membrane modification with polyelectrolyte multilayers, 0.1 M CuSO$_4$ or NiSO$_4$ solutions were circulated through the membrane for 1 h, followed by a 20-mL water wash. The bound metal ions were eluted with two 5-mL aliquots of 0.1 M EDTA (pH 7.6) or 2% HNO$_3$. The concentrations of metal ions were determined using atomic absorption spectroscopy with calibration curves.   Standard solutions contained 0 to 10 ppm metal ions in 0.1 M EDTA or in 2% HNO$_3$. The metal-ion binding capacity was calculated by dividing the mass of eluted metal ion by the volume of membrane, which is about 0.035 cm^3 (the membranes are 110 µm thick). A GE Healthcare HiTrap^{TM} IMAC FF column was used as a comparison and loaded with Ni^{2+} by passing 2 mL of 0.1 M NiSO$_4$ through the syringe column (flow rate of 1 mL/min) followed by 75 mL of deionized water.   To study metal-ion leaching, first we compared Cu^{2+} leaching in membranes modified with (PAH/PNTA-100)$_2$ and PAA/BPEI/PAA-NTA..   After Cu^{2+} loading and rinsing with water, the membranes were washed sequentially with 2.5 mL (75 membrane bed volumes) of four different buffers (pH 7.4) and then 0.1 M EDTA. This protocol was also followed to determine the amount of Ni^{2+} binding/leaching in (PAH/PNTA-100)$_2$- or PAA/BPEI/PAA-NTA-modified membranes. For comparison a GE Healthcare HiTrap^{TM} IMAC FF column (1 mL) was washed with 75 bed volumes (75 mL) of the same buffers: binding buffer1- 20 mM phosphate buffer with 0.3 M NaCl and 10 mM imidazole; washing buffer 1- 20 mM phosphate buffer with 0.15 M NaCl and 0.1% Tween-20; washing buffer 2- 20 mM phosphate buffer with 0.15 M NaCl and 45 mM imidazole; and elution buffer 1- 20 mM phosphate buffer with 0.5 M NaCl and 0.3 M

imidazole. Also we compared the metal-ion leaching of membranes modified with different PAA(PAH/PNTA-X) films. The PAA(PAH/PNTA-X)-modified nylon membranes were loaded with Ni^{2+} using the above procedure (including rinsing with 20 mL of water) and washed consecutively with 160 bed volumes (5 mL) of binding buffer 2, washing buffer 3, washing buffer 4, elution buffer 2 and 2% HNO_3. The buffer compositions were: binding buffer 2- 20 mM phosphate; washing buffer 3- 20 mM phosphate with 0.15 M NaCl and 0.1% Tween-20; washing buffer 4- 20 mM phosphate with 0.15 M NaCl and 45 mM imidazole; and elution buffer 2- 20 mM phosphate with 0.5 M NaCl and 0.5 M imidazole. All buffers had a pH of 7.4.

3.2.9.3. His-tagged Protein Binding in Nylon Membranes.

Membranes with an exposed diameter of 1 cm were used for all protein-binding studies. Solutions for His-tagged protein binding to Ni^{2+}-containing membranes contained 0.3 mg of protein per mL in 20 mM phosphate buffer at pH 7.4. After the membranes were loaded with buffered protein solution and rinsed with 5 mL of washing buffer 3 followed by 5 mL of phosphate buffer at 7.4, bound protein was eluted in two 4-mL aliquots of of elution buffer 2. The concentrations of protein in the feed, permeate and eluate solutions were determined using a Bradford assay (the protein of interest was used to determine the calibration curve). The binding capacity was calculated from the amount of bound protein divided by the volume of the membrane.

3.2.9.4.Purification of His-tagged Protein from Cell Lysate.

His-tagged COP9 signalosome complex subunit 7 (His-CSN7) overexpressed in BL21DE3 cells was used to examine isolation of His-tagged protein from cell lysate. Three mL of lysate supernatant diluted 1:2 using binding buffer 1 containing 6 M urea was passed through a PAA/PAH/PNTA-Ni^{2+}-modified membrane that was previously equilibrated with binding buffer. Since His-CSN7 has low solubility without urea, all the buffers used for its purification were supplemented with 6 M urea. After washing with 3 mL of washing buffer 1, 3 mL of washing buffer 2, and 3 mL of phosphate buffer at a flow rate of 1mL/min, His-CSN7 was eluted with elution buffer. A 30 μL sample from all loading, washing, and elution solutions was collected and analyzed using gel electrophoresis.

3.3. Results and Discussion.

3.3.1.Synthesis of Poly(2,2-(5-acrylamido-1-carboxypentylazanediyl) diacetic acid) [PNTA-100] and *Co*-polymers PNTA-50 and PNTA-25.

This work first presents a convenient synthesis of a polymer that contains metal-ion-binding NTA groups. Although two studies describe syntheses of NTA-containing polymers, both methods derivatize a polymer with aminobutyl NTA, which is expensive

to purchase or prepare due to protection and deprotection steps.[34-36]
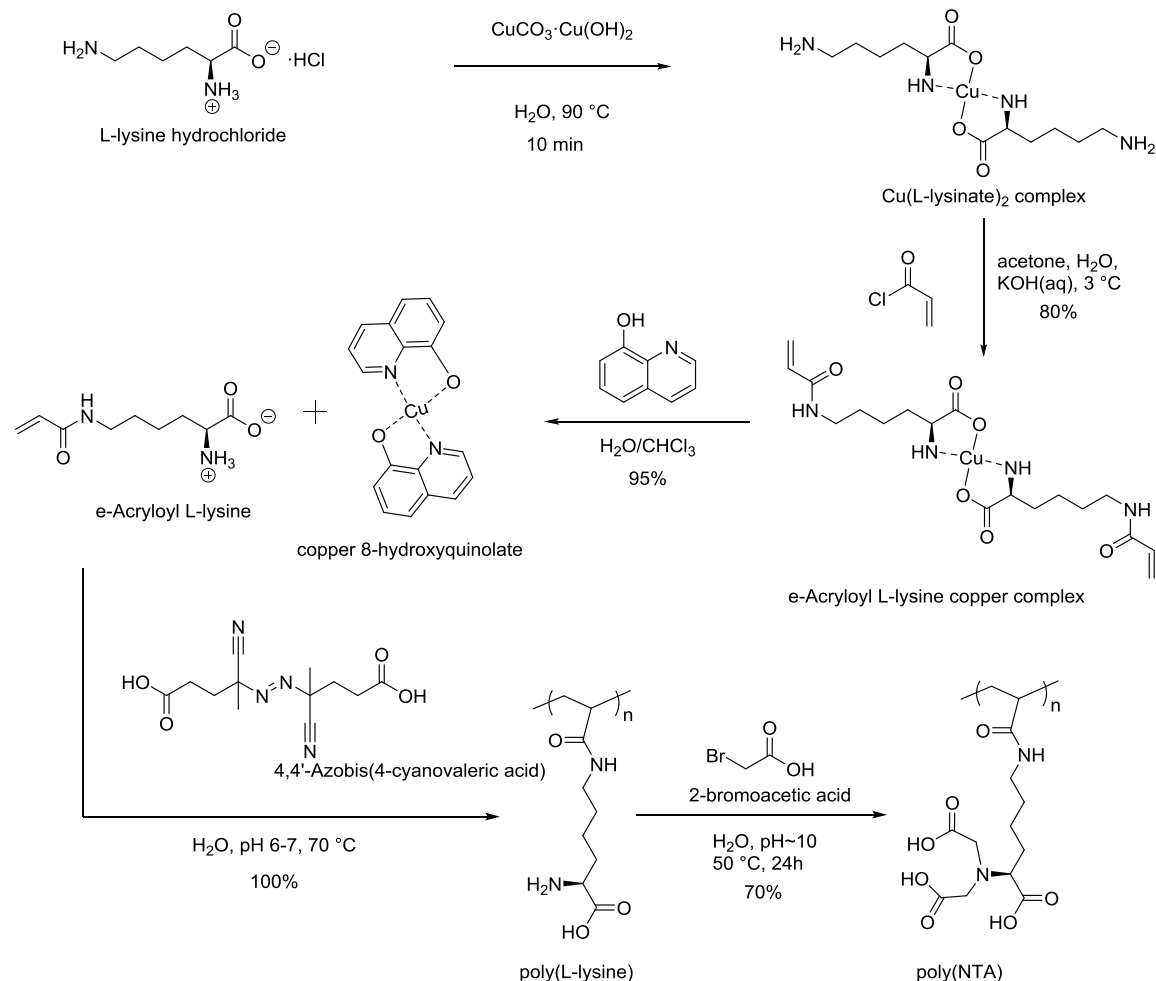
Scheme 3.1. Synthesis of poly(2,2-(5-acrylamido-1-carboxypentylazanediyl) diacetic acid) [PNTA-100] based upon ε-acryloyl L lysine and poly(ε-acryloyl L lysine).

Scheme 3.1 shows our synthesis of poly(2,2-(5-acrylamido-1-carboxypentylazanediyl) diacetic acid) [PNTA-100], which includes a modified literature procedure to prepare the monomer ε-acryloyl-L-lysine.[37] The Cu^{2+} protection strategy in this monomer synthesis bypasses the cumbersome protection-de-protection steps in other protocols. Also, the highly pure final product avoids lengthy column purification. Subsequent initiation of free radical polymerization with 4,4′-azobis(4-cyanovaleric acid) yields the intermediate

polymer, poly(ε-acryloyl L lysine) [PLys-100], with 90% yield, and the product ^{1}H NMR spectrum is consistent with polymerization (Figure A3.3). Based on ^{1}H NMR end-group analysis, the PLys-100 has an average degree of polymerization (DP$_n$) of 233, which corresponds to a molecular weight of 46,879 g/mol ($M_{n,theoretical}$ = 49,726 g mol^{-1}).

Finally, carboxymethylation of PLys-100 using bromoacetic acid leads to PNTA-100 with 70% yield, and the ^{1}H NMR spectrum confirms (Figure A3.4) the formation of the desired polymer. Integration of the spectrum suggests the addition of 1.62 carboxymethyl groups per repeat unit of PLys-100 (see the appendix).

Relatively low swelling of (PAH/PNTA-100) films containing metal-ion complexes may limit protein access to metal-ion complexes. Thus, to increase swelling, we incorporated acrylic acid monomers into the PNTA. The synthesis included copolymerization of acrylic acid (AA) and ε-acryloyl L lysine (Figure A3.5) and subsequent derivatization of these polymers through reaction with 2-bromoacetic acid (Figure A3.7). Deprotonation of the AA repeat units after film formation should increase film swelling to facilitate protein capture.[26] Specifically, we prepared poly(NTA-co-AA) aiming to achieve polymers with 25% [PNTA-25] or 50% [PNTA-50] of the repeating units containing NTA ligands along with the corresponding 75% or 50% AA units, respectively. (See the supporting information in the appendix for details on the polymer synthesis. NMR analysis suggest the PNTA-25 contains only 12% NTA-containing units and PNTA-50 contains only 40% NTA-containing units). Table 1 shows the properties of the different polymers.

Table 3.1. Characteristics of Synthesized Polymers

Polymer sample	Conversion (%)	[M]/[I][a]	DP_n[b]	M_n (g mol^{-1})[c]	NTA unit (per repeating unit)
PLys-100	84	278	233	46,879	-
PNTA-100	70		233	68,538	1.6
PLys-50	78	278	220	25,631	-
PNTA-50			220	34,062	1.8
PLys-25	85	278	240	21,233	-
PNTA-25	60		240	24,142	1.6

[a]Ratio of the monomer concentration [M] to the initiator concentration [I]. [b]From DP_n = [M]/[I]×conversion. [c]See supporting information for details of this calculation based on NMR analysis.

3.3.2. LBL Deposition of (PAH/PNTA-X)$_n$ Films.

This work aims to create and tune the performance of thin films that selectively bind metal ions and proteins, and alternating adsorption of PAH and PNTA-X provides a simple technique for preparing films with metal-ion-binding groups. Moreover, because PAH and PNTA-X are weak polyelectrolytes, the deposition pH will affect the film thickness and structure.[38] The pH of the polyelectrolyte solution controls the degree of ionization and hence the charge density of the polymer, which influences both the polymer conformation and the degree of ionic cross-linking in layer-by-layer films. In aqueous solutions, the pK_a values of free NTA (analog of the metal-binding group in PNTA-100 repeating units) are pK_{a1} = 1.89, pK_{a2} = 2.49, and pK_{a3} = 9.73 (Scheme 3.2).[39,40] Titration of PNTA-100 with 0.1 M HCl shows the presence of fully protonated tertiary amines in the polymer below pH 9, whereas the three carboxylic acid groups

protonate below pH 3 (See Figure A3.11). In addition, on going from pH 3.0 to 9.0, the fraction of protonated amines in PAH decreases from 96 to 30%.[41]
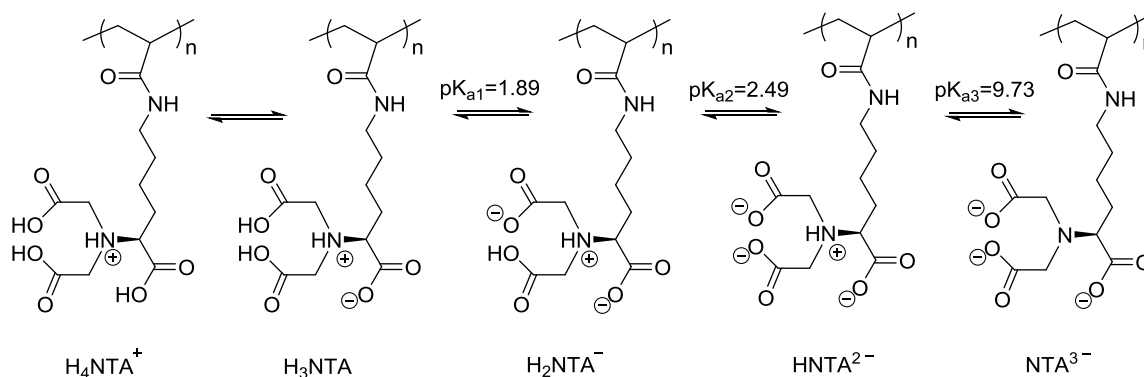
Scheme 3.2. Protonation states of the NTA groups of PNTA-100. The pK_a values are those of NTA that is not attached to a polymer.

Adsorption of (PAH/PNTA-100)$_5$ films at pH 3 yields a thickness of ~20 nm (Figure A3.12 shows film thickness as a function of the number of layers). Deposition at pH 9 also gives a thickness of 20 nm for these films. In contrast, adsorption of PNTA-100 at pH 3 and PAH at pH 9 leads to much greater film thicknesses. Ellipsometry and AFM data indicate that such (PAH/PNTA-100)$_5$ films are 400-500 nm thick (Figure 3.3). At pH 9, PAH likely adsorbs with a significant degree of deprotonation, and subsequent protonation of adsorbed PAH at pH 3 during PNTA-100 deposition leads to excess positive surface charge that enhances PNTA-100 adsorption. Subsequent deprotonation of the adsorbed PNTA-100 likely increases the net negative charge density in the film and augments PAH deposition at pH 9. Surprisingly, addition of NaCl to deposition solutions decreases film thickness significantly (see Figure 3.3a) when

depositing PNTA-100 at pH 3 and PAH at pH 9. In this case, the NaCl may screen

excess surface charge to limit adsorption.
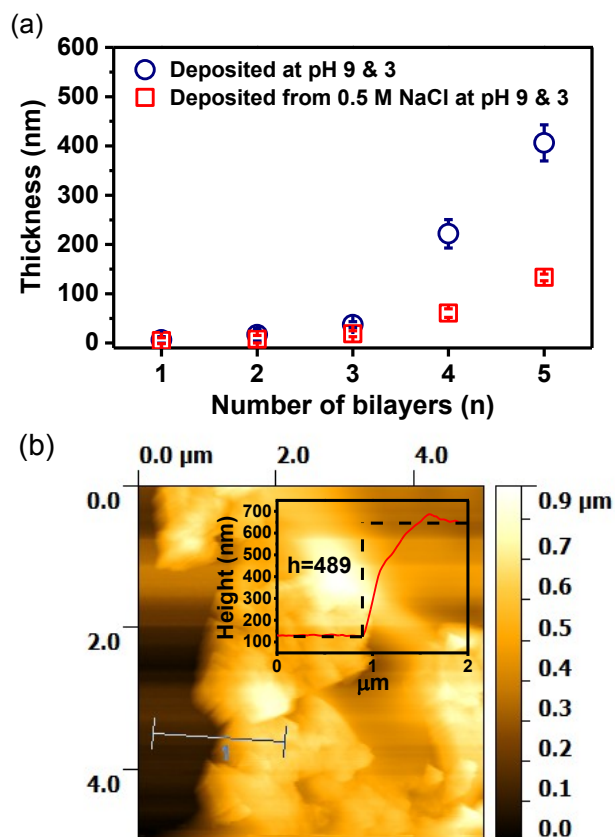
Figure 3.3. (a) Ellipsometric thicknesses of (PAH/PNTA-100)$_n$ films adsorbed from solutions of PAH at pH 9 and PNTA-100 at pH 3.0. Squares correspond to deposition solutions with no added salt, and circles represent deposition from solutions containing 0.5 M NaCl. (b) AFM image of a scratched (PAH/PNTA-100)$_5$ film adsorbed under the conditions in (a) without salt. The inset shows the height profile along the line at the lower left.

Even though adsorption without added supporting electrolyte leads to thick films,

preliminary studies show low protein binding to these films, which may suggest

significant electrostatic crosslinking. In contrast films prepared from solutions containing

0.5 M NaCl show multilayer protein binding (See Figure A3.16 and the discussion

below). Thus, in layer-by-layer adsorption of (PAH/PNTA-X)$_n$ films, we focus on deposition from polymer solutions containing 0.5 M NaCl.
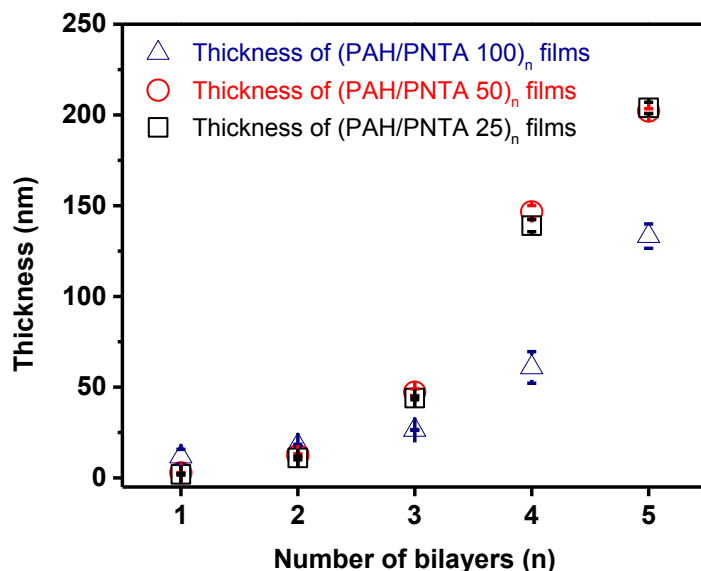
Figure 3.4. Thicknesses of (PAH/PNTA-X)$_n$ films adsorbed at pH 9.0 for PAH and pH 3.0 for PNTA-X from solutions that contain 0.5 M NaCl. Blue triangles, Red circles and black squares represent (PAH/PNTA-100)$_n$, (PAH/PNTA-50)$_n$ and (PAH/PNTA-25)$_n$ films, respectively. Here n=1 to 5.

Adsorption of (PAH/copolymer)$_n$ coatings yields thicker films than the corresponding adsorption with the homopolymer when both films are deposited from solutions containing 0.5 M NaCl (adsorption of pH 9 for PAH and pH 3 for PNTA-100 or copolymers). As Figure 3.4 shows, thicknesses of films containing either PNTA-50 or PNTA-25 reach 200 nm after adsorption of five PAH/PNTA-X bilayers. Since PNTA-50-containing polymer films are not significantly different in protein binding from PNTA-100 films (Figure A3.17), hereafter we compare only films containing PNTA-100 and PNTA-25 .

3.3.3. Metal Sorption in (PAH/PNTA-X)$_3$ Films.

Modification of porous materials with (PAH/PNTA-X)$_n$ will likely employ films with only a few bilayers to avoid plugging of pores. We examined metal-ion binding in (PAH/PNTA-X)$_3$ and (BPEI/PAA)$_3$-NTA films to achieve readily detectable amounts of bound metal in a relatively thin film. We chose to compare with (BPEI/PAA)$_3$-NTA coatings because they bind large amounts of metal ions.[6] After immersion of a (PAH/PNTA-100)$_3$ film in a 0.1 M NiSO$_4$ (or CuSO$_4$) solution for 15 h and rinsing with deionized water, changes in the IR spectrum of the film give evidence for Ni^{2+} (or Cu^{2+}) coordination to carboxylic groups of the NTA ligand (not shown). Prior to complexation the spectrum of the film contains an asymmetric −COO$^-$ stretching peak at 1652 cm^{-1} and a shoulder due to the acid carbonyl stretch (1724 cm^{-1}). After coordination with Ni^{2+}, the acid carbonyl stretch disappears and the −COO$^-$ asymmetric stretching peak shifts to 1641 cm^{-1}, presumably because of the NTA-Ni^{2+} complexation.[42] We subsequently eluted the bound metal ions with 20 mM EDTA (pH 7.4) and quantified their concentration in the eluate with atomic absorption spectroscopy. Using the ellipsometric thicknesses of "dry" films along with the amount of eluted Ni^{2+}, the concentration of Ni^{2+} inside the film is 1.8 mmol/cm^3 (Figure 3.5).
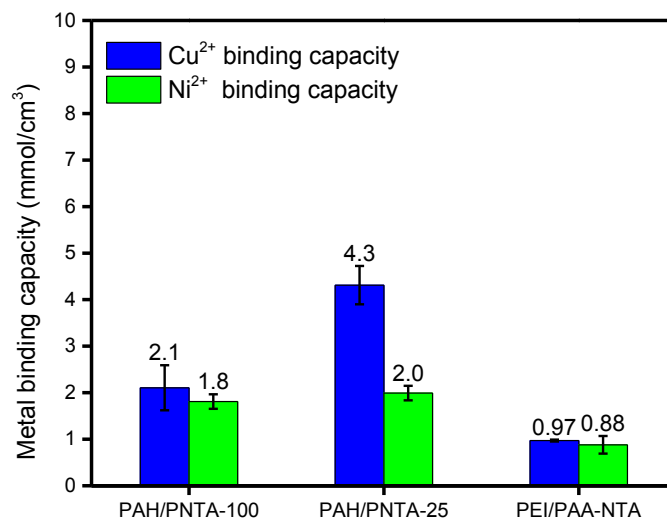
Figure 3.5. Cu^{2+} and Ni^{2+} binding capacities in $(PAH/PNTA-X)_3$ and $(PEI/PAA)_3$-NTA films. Films were deposited at pH 9.0 for PAH and pH 3.0 for PNTA-X using solutions containing 0.5 M NaCl. The experimental section gives PEI and PAA deposition conditions. During metal sorption, $C_{M^{2+}}$ = 0.1 M and pH ≈ 4.1. Film volumes were calculated using ellipsometric thicknesses of "dry" films without sorbed metal ions.

If a film contained pure PNTA-100 with a density of 1 g/cm^3, the Ni^{2+} binding capacity should be 3.2 $mmol/cm^3$. However, coatings contain PAH and some water, so 1.8 $mmol/cm^3$ is a reasonable capacity, and binding of Cu^{2+} gives a similar result (Figure 3.4). Moreover, $(PAH/PNTA-25)_3$ films show a similar Ni^{2+} binding capacity of 2.0 $mmol/cm^3$. This number may indicate that compared to $(PAH/PNTA-25)_3$, more NTA ligands in $(PAH/PNTA-100)_3$ coatings are ionically linked to ammonium groups and not available for metal binding. Perhaps more likely, some Ni^{2+} may bind to acrylates. The Cu^{2+} binding capacity for $(PAH/PNTA-25)_3$ films is 4.3 $mmol/cm^3$, strongly suggesting binding of Cu^{2+} to acrylic acid in these films. On the other hand the metal-ion binding capacity in $(BPEI/PAA)_3$-NTA films is around 1 $mmol/cm^3$. The low binding capacity compared to PNTA-X systems may stem from the low amount of NTA in these films.

3.3.4.Swelling of (PAH/PNTA-X)$_3$ and (BPEI/PAA)$_3$-NTA Films.

Film swelling in aqueous buffers is vital to enable extensive protein binding to metal-ion complexes in (PAH/PNTA-X)$_n$ films, so we performed in situ ellipsometry to assess the swelling of these films before and after metal-ion complexation. After a 10-min immersion of (PAH/PNTA-100)$_3$ films in pH 7.4 buffer, the film thickness increases 450% compared to a "dry" film rinsed only with water (Figure 3.6). Deprotonation of the –COOH groups in the pH 7.4 buffer induces cations and water to enter the film. Similar swelling (450%) occurs with (PAH/PNTA-25)$_3$ films. (Note that the final deposition step for these films occurs at pH 3, and a 1-min rinse with deionized water prior to drying is insufficient to substantially deprotonate the film.) The reflectance IR spectra of (PAH/PNTA-100)$_3$ films confirm the deprotonation –COOH after immersing in buffer.

For comparison, we also examined the swelling of (BPEI/PAA)$_3$-NTA films, where film derivatization with aminobutyl NTA introduces the chelating functionality. Previous studies showed that (BPEI-PAA)$_x$-NTA films are attractive for binding metal ions and proteins on surfaces and in membrane pores.[28] Interestingly, (BPEI/PAA)$_3$-NTA films swell only ~170%, which is much lower than the swelling of the (PAH/PNTA-X)$_3$ coatings. Prior to attachment of aminobutyl NTA, the EDC/NHS activation may lead to crosslinking reactions between amine groups of PEI and activated carboxylic acid units,[43] and such crosslinking might reduce the swelling of these films. Prior to EDC/NHS activation and NTA attachment, (BPEI/PAA) films (deposited at pH 3) swell around 360%.
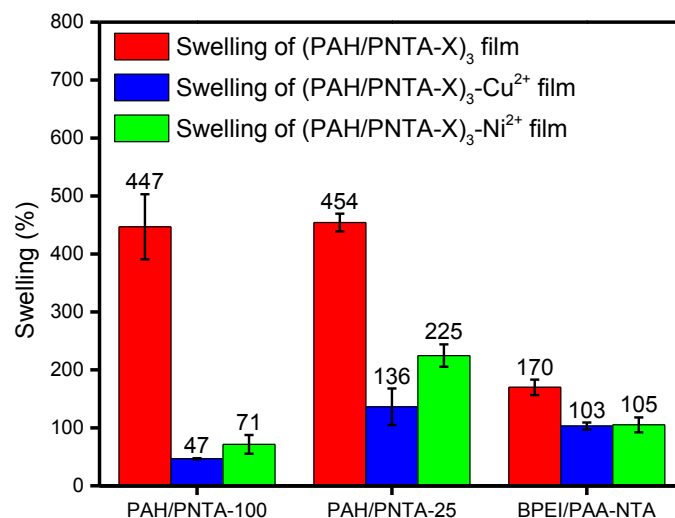
Figure 3.6. Swelling percentages for $(PAH/PNTA-X)_3$ and $(BPEI/PAA)_3$-NTA films before and after binding Cu^{2+} and Ni^{2+}. The swelling compares the ellipsometric thickness immediately after film formation, rinsing, and drying with the thickness in 20 mM phosphate buffer at pH 7.4 after 10 min of immersion. Films were deposited at pH 9.0 for PAH and pH 3.0 for PNTA-X from solutions containing 0.5 M NaCl. The last deposition step prior to rinsing occurred at pH 3.0. Data for swelling of films with metal-ion complexes use the thickness of the dry film without the metal ion to calculate swelling.

To extensively capture His-tagged protein from buffered solutions, $(PAH/PNTA-X)_n$ films must swell even after binding metal ions, but $(PAH/PNTA-100)_3$-Cu^{2+} and $(PAH/PNTA-100)_3$-Ni^{2+} films swell only 47% and 71%, respectively in pH 7.4 buffer (Figure 3.6). Formation of the metal-ligand complex reduces the overall charge density inside the film and decreases swelling. In contrast, $(PAH/PNTA-25)_3$-Cu^{2+} and $(PAH/PNTA-25)_3$-Ni^{2+} films swell 136% and 225%, respectively, at pH 7.4. The acrylate groups in the polymers do not saturate with metal ions and, thus, provide charged groups that increase swelling. More extensive binding of Cu^{2+} than Ni^{2+} (see the previous section) leads to less swelling of the $(PAH/PNTA-25)_3$ films with Cu^{2+} complexes. $(BPEI/PAA)_3$-NTA films with Cu^{2+} and Ni^{2+} swell around 105%, which is

significantly less than the 170% without metal-ion complexation, but still higher than the swelling of the $(PAH/PNTA-100)_3$ films with metal ions.

3.3.5.Binding of Proteins to $(PAH/PNTA-X)_n$- and $(PAH/PNTA-X)_3$-Ni^{2+}/Cu^{2+} Films.

Based on the amide absorbance of adsorbed protein, reflectance infrared spectroscopy provides an estimate of the protein binding to polyelectrolyte coatings. Specifically, these experiments compare the amide I band IR absorbance at 1680 cm^{-1} for protein adsorbed in polyelectrolyte films and spin-coated protein films with different thicknesses. Thus, the method yields an "equivalent thickness" of protein bound to the film.

Binding of His-tagged PaPAM to $(PAH/PNTA-100)_3$-Ni^{2+} is very different for films prepared in the presence and absence of NaCl (for all films PAH was deposited at pH 9 and PNTA-100 at pH 3). Although $(PAH/PNTA-100)_3$ films deposited in the absence of NaCl have a thickness of 38 ± 6.0 nm, after Ni^{2+} complexation, such films bind <1 nm of His-tagged *Pa*Pam. In contrast, $(PAH/PNTA-100)_3$-Ni^{2+} films prepared with polyelectrolyte adsorption from 0.5 M NaCl are 19±5 nm thick and bind the equivalent of 10±1.0 nm of protein, or 1.6-2.5 monolayer layers of *Pa*PAM. (The dimensions of a *Pa*PAM molecule, M_w = 59000 Da, are 8.4×3.1×2.9 nm.)[29] Among the tested deposition conditions, films deposited at pH 9 for PAH and pH 3 for PNTA-100 with salt has the highest film growth and significant protein binding on the surface (See Figure A3.16). Therefore these conditions were used for subsequent protein binding experiments.

To examine the kinetics of protein binding in (PAH/PNTA-100)$_3$-Ni^{2+} and (PAH/PNTA-25)$_3$-Ni^{2+} films, we determined the His-tagged *Pa*PAM binding to these films after immersion in protein solutions in pH 7.4 phosphate buffer for various times. As Figure 3.7a shows, the (PAH/PNTA-25)$_3$-Ni^{2+} film binds 2.5 times as much protein as the (PAH/PNTA-100)$_3$-Ni^{2+} coating, and the binding approaches saturation after 20 h. However, a significant fraction (80%) of binding also occurs within 15 min.
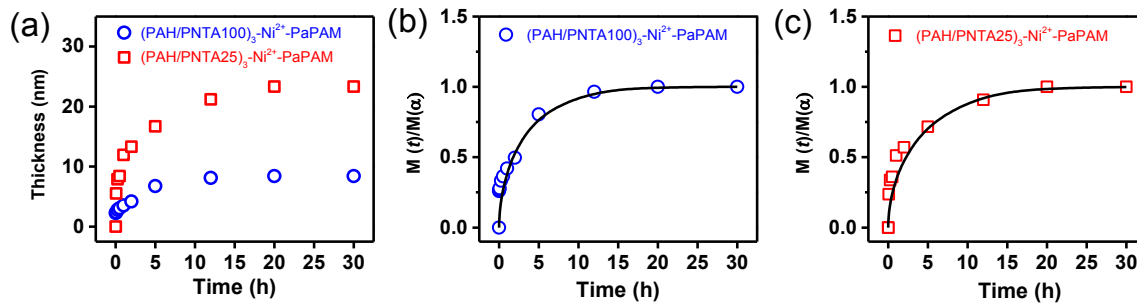
Figure 3.7. (a) *Pa*PAM binding in (PAH/PNTA-100)$_3$-Ni^{2+} (blue circles) and (PAH/PNTA-25)$_3$-Ni^{2+} (red squares) films as a function of time. The curves in (b) and (c) show fits to the data using equation 4.1 and (b) $D = 8.0 \times 10^{-16}$ cm^2/sec and l = 49 nm or (c) $D = 1.3 \times 10^{-14}$ cm^2/sec and l = 225 nm. Films were deposited from pH 9.0 PAH solutions and pH 3.0 PNTA-X solutions containing 0.5 M NaCl. *Pa*PAM binding occurred from a 0.1 mg/ml solution in pH 7.4 buffer at room temperature.

The binding kinetics in Figure 3.7 fit well to a Fickian diffusion model, particularly at long times. If diffusion controls the rate of protein capture in a coating, equation 4.1 should describe the total amount of protein, *M(t)*, in the film at a given time *t*, where *M(∞)* is the amount of protein in the film at equilibrium, *l* is the film thickness, and *D* is the diffusion coefficient.[44]

$$\frac{M(t)}{M(\infty)} = 1 - \sum_{n=0}^{\infty} \frac{8}{(2n+1)^2 \pi^2} \exp\left(-\frac{D(2n+1)^2 \pi^2 t}{4l^2}\right) \quad \text{(Equation 4.1)}$$

Figure 3.7b & c, show modeling of the experimental data with equation (4.1) when using swollen film thicknesses of 49 nm and 225 nm for (PAH/PNTA-100)$_3$-Ni^{2+} and (PAH/PNTA-25)$_3$-Ni^{2+} films, respectively. The fits yield relatively low diffusion coefficients of 8.0×10^{-16} and 1.3×10^{-14} cm^2/s for (PAH/PNTA-100)$_3$-Ni^{2+} and (PAH/PNTA-25)$_3$-Ni^{2+} films, respectively. These low diffusion coefficients are consistent with previously reported protein diffusion coefficients through polyelectrolyte multilayers and polymer brush systems (2.2×10^{-14} cm^2/s).[33] Nevertheless, the larger diffusion coefficient for (PAH/PNTA-25)$_3$-Ni^{2+} is consistent with the higher swelling of these films. Smaller proteins would presumably give larger diffusion coefficients.
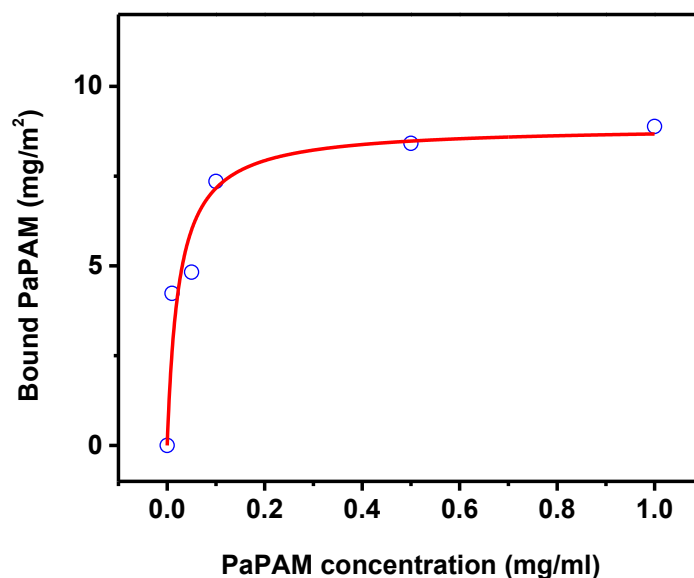
Figure 3.8. Amount of *Pa*PAM bound to PAH/PNTA-100-Ni^{2+} films as a function of protein concentration. Data are the average of two batches of experiments on 6 different samples prepared from PAH/PNTA-100-Ni^{2+} films with similar thicknesses (~28 nm). The experiment employed 20-h equilibration times. Solid lines represent simulations based on the Langmuir isotherm (Equation 3.2).

Thermodynamics of *Pa*PAM sorption to PAH/PNTA-100-Ni^{2+} films follow a Langmuir isotherm, equation 3.2,

$$\Gamma = \frac{\Gamma_m C}{K_d + C}$$ (Equation 3.2)

where Γ is protein coverage (mg/m^2), Γ_m is the maximum coverage, C is the His-tagged *Pa*PAM concentration in solution (mg/mL) and K_d is the dissociation constant (mg/mL). According to the fit in the Figure 3.8, Γ_m=8.9 ± 0.7 mg/m^2 and K_d is 0.024 ± 0.008 mg/mL. This value of K_d is equivalent to 4.1×10^{-7} M, which is consistent with literature values of ~10^{-6} M for binding of His-tagged protein to Ni^{2+}-NTA groups on surfaces.[45] The small dissociation constants indicates the strong affinity between His tags and the (PAH/PNTA-100)$_3$-Ni^{2+} films.

We also determined binding capacities for four different proteins, His-tagged Ubiquitin (9.6 kDa), Con A (25 kDa), His-tagged threonine aldolase (36.5 kDa), and His-tagged PaPAM (59 kDa). Figure 3.9 shows the amounts of these proteins captured in (PAH/PNTA-100)$_3$, (BPEI/PAA)$_3$-NTA, and (PAH/PNTA-25)$_3$ coatings. Capture of the His-tagged proteins in these films employed Ni^{2+} complexes, whereas Con A binding utilized Cu^{2+} complexes. With the exception of (PAH/PNTA-25)$_3$, the films do not show a clear trend of increased protein binding with decreasing protein molecular mass. Notably, (PAH/PNTA-25)$_3$ also shows the most swelling in buffer, suggesting that even for small proteins extensive binding throughout the film requires high swelling. These films also show the highest capture of the largest protein, His-tagged *Pa*PAM.

(PAH/PNTA-100)$_3$ is the least swollen of the three films examined and shows the least capture of His-tagged PaPAM and His-tagged ubiquitin. However, for reasons we

do not understand, this protein binds the equivalent of 5-6 multilayers of His-tagged threonine aldolase and Con A.
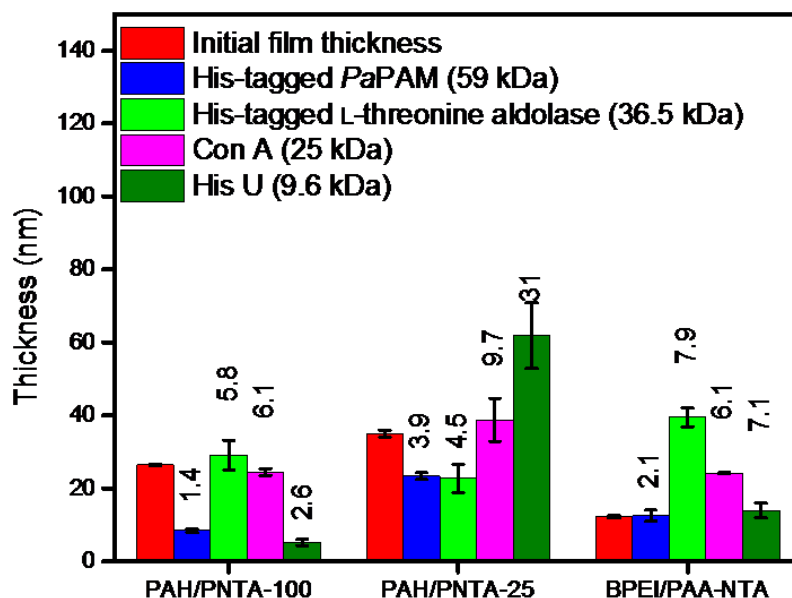
Figure 3.9. Thicknesses of (PAH/PNTA-X)$_3$ and (BPEI/PAA)$_3$-NTA multilayers after complexation of Cu^{2+} or Ni^{2+} (red bars) and the equivalent thicknesses of protein adsorbed in these films. (The equivalent thickness is the thickness of a spin-coated protein film that would give the same amide absorbance in reflectance FTIR spectroscopy.) The numbers above the bars are the approximate number of multilayers the protein binding represents (see the supporting information for protein dimensions.) Films were adsorbed at pH 9.0 for PAH and pH 3.0 for PNTA-X, and the polymer solutions contained 0.5 M NaCl. Protein adsorption occurred for 20 h from a pH 7.4 phosphate buffer.

The (BPEI/PAA)$_3$-NTA films also binds threonine aldolase and Con A at a higher capacity than HisU and *Pa*PAM. Clearly, protein binding is not a simple function of molecular mass and may depend on the affinity of binding interactions or protein conformations in the film. Uhlig et al. showed that protein binding to PEMs is independent of the size or the charge of the protein.[46] However, membranes (see

below) show a much clearer trend of protein binding as a function of molecular mass. Importantly, all the films in Figure 3.9 show multilayer protein binding, and for these films (PAH/PNTA-25)$_3$ has the highest protein-binding capacity for all proteins except His-tagged threonine aldolase.

3.3.6. Protein Binding to Membranes Modified with NTA-Containing Films.

Figure 3.2 shows the strategy for membrane modification with PNTA-X/PAH/PNTA-X films containing metal-ion complexes. The composition of the initial layer in the membrane is important to create a charged surface for further film growth, and our previous work suggests that PSS and PAA adsorb strongly to nylon membranes.[6] Thus, we also examined membrane modification with PAA/PAH/PNTA-X films.
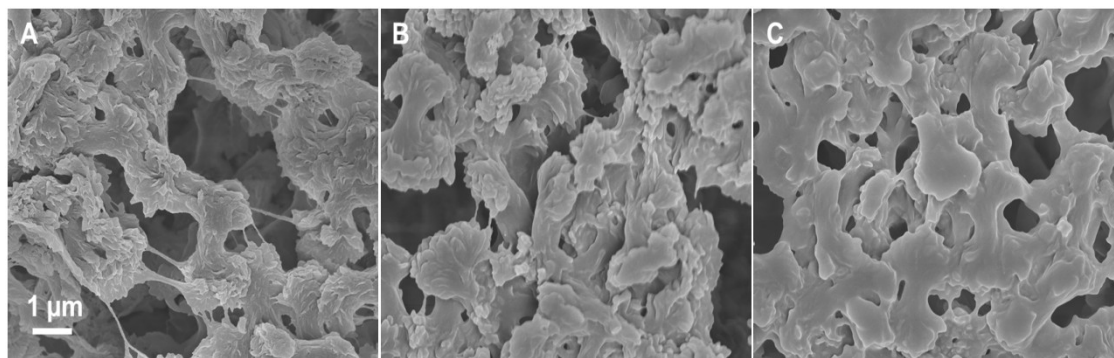
Figure 3.11. SEM images of nylon membranes before (A) and after modification with (B) PAA/PAH/PNTA and (c) PAA(PAH/PNTA)$_2$ coatings. The films were deposited from 0.5 M NaCl solutions containing 20 mM PAA (pH 3), 1 mg/mL PNTA-100 (pH 3) or 1 mg/mL PAH (pH 9).

Figure 3.11 shows the SEM images of PEM-modified membranes. Adsorption of PAA/PAH/PNTA-100 does not cause major changes to the membrane morphology, whereas deposition of the PAA(PAH/PNTA-100)$_2$ films begins to decrease the porosity of the membrane. Swelling in buffer will further decrease porosity and limit flow.

Table 3.2 show the metal-ion-binding capacities for several modified membranes. For both Cu^{2+} and Ni^{2+}, the binding capacities more than double on going from PAA/PAH/PNTA-100 to PAA/(PAH/PNTA-100)$_2$ films. Notably, the Cu^{2+} binding capacity is 60-80% higher than that for Ni^{2+}. Because free –COOH groups in PAA likely bind some Cu^{2+}, we also determined the Cu^{2+} capture by membranes modified with a PAA/PAH film. Such membranes bind only 1.7 mg Cu^{2+}/cm^3 of membrane, which is not sufficient to account for the difference in Cu^{2+} and Ni^{2+} binding. Thus the higher Cu^{2+} binding likely reflects stronger affinity for NTA sites in the film. Because of electrostatic interactions between NTA and protonated amines, the NTA ligands may exhibit a range of affinities for metal ions, and low affinity sites may not capture Ni^{2+} under the loading conditions.

Table 3.2. Cu^{2+} and Ni^{2+} binding capacities in membranes modified with PAA/PAH/PNTA-100, PAA(PAH/PNTA-100)$_2$, and PAA/PAH/PNTA-25 films. The films were deposited from 0.5 M NaCl solutions containing 20 mM PAA (pH 3), 1 mg/mL PNTA-100 (pH 3) or 1 mg/mL PAH (pH 9).

Films	Cu^{2+} binding capacity (mg/mL)	Ni^{2+} binding capacity (mg/mL)
PAA/PAH/PNTA-100	6.8±0.2	3.7±0.2
PAA(PAH/PNTA-100)$_2$	14.6±0.4	8.9±0.2
PAA/PAH/PNTA25	-	3.4±0.6

In addition to metal-ion binding capacity, leaching of bound metal ions may also affect protein purification. Initially, we compare Cu^{2+} leaching from membranes modified with modified with $PAA(PAH/PNTA-100)_2$ and PAA/PEI/PAA-NTA films. After adsorption of Cu^{2+}, these membranes were washed sequentially with 2 mL of four different buffers (pH 7.4) and 0.1 M EDTA.
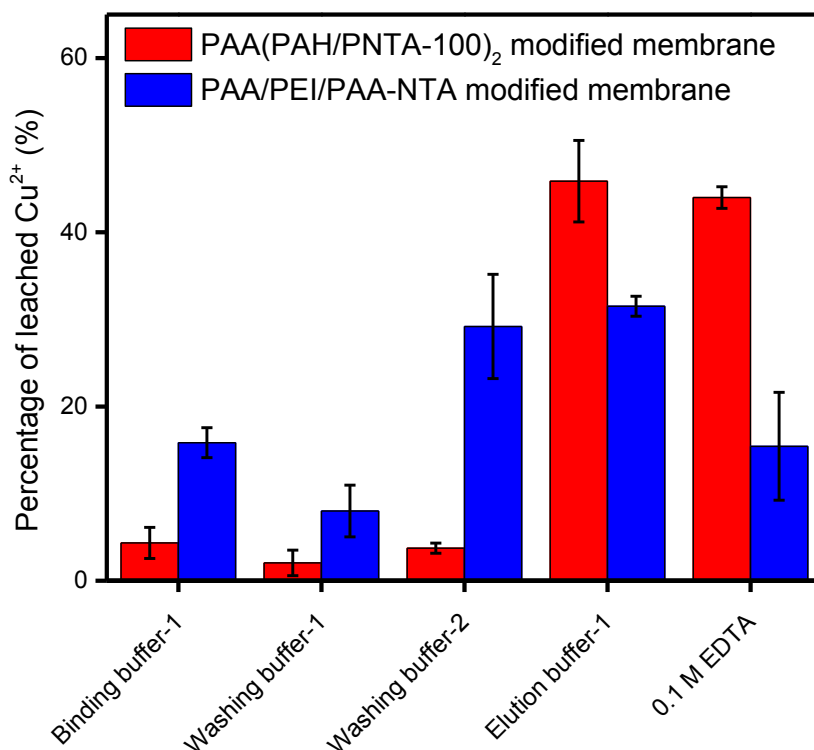
Figure 3.12. Percentage of the bound Cu^{2+} leached from PAA/PEI/PAA-NTA- and $PAA(PAH/PNTA)_2$-modified membranes when passing buffers (5 mL) sequentially through the membranes. The buffer compositions were: binding buffer 1- 20 mM phosphate buffer with 0.3 M NaCl and 10 mM imidazole; washing buffer 1- 20 mM phosphate buffer with 0.15 M NaCl and 0.1% Tween-20; washing buffer 2- 20 mM phosphate buffer with 0.15 M NaCl and 45 mM imidazole; and elution buffer-1- 20 mM phosphate buffer with 0.5 M NaCl and 0.3 M imidazole.

Figure 3.12 compares Cu^{2+} leaching from membranes modified with complexes of PAA(PAH/PNTA)$_2$ and PAA/BPEI/PAA-NTA films. For the latter coating, about 50% of the Cu^{2+} leaches from the membrane in binding and washing buffers, whereas the corresponding leaching is only ~10% for membranes with PAA(PAH/PNTA)$_2$. This suggests substantial weak Cu^{2+} binding to residual acrylic acid sites in PAA/BPEI/PAA-NTA films. (Derivatization with NTA does not occur at all acrylic acid sites.) The PAA(PAH/PNTA)$_2$ shows more leaching in the 0.5 M imidazole elution buffer because the film still contains most of its Cu^{2+} prior to this step, and imidazole strongly binds Cu^{2+}. The EDTA step elutes the remaining Cu^{2+} from the membranes, and shows that the PAA(PAH/PNTA)$_2$ film retains around 45% of its Cu^{2+} through binding, washing, and imidazole elution. In contrast, the PAA(PEI/PAA)-NTA film retains only 15% of its Cu^{2+} through these steps.

The leaching of Ni^{2+} shows even more obvious differences between the PAA/BPEI/PAA-NTA- and PAA(PAH/PNTA-100)$_2$-modified membranes. In the PAA/BPEI/PAA-NTA-modified membrane, the binding buffer which contains only 10 mM imidazole, elutes about 50% of the bound Ni^{2+} (Figure 3.13). Again, some metal ions likely bind to free PAA –COOH groups, which have a lower affinity for Cu^{2+} and Ni^{2+} than NTA groups.
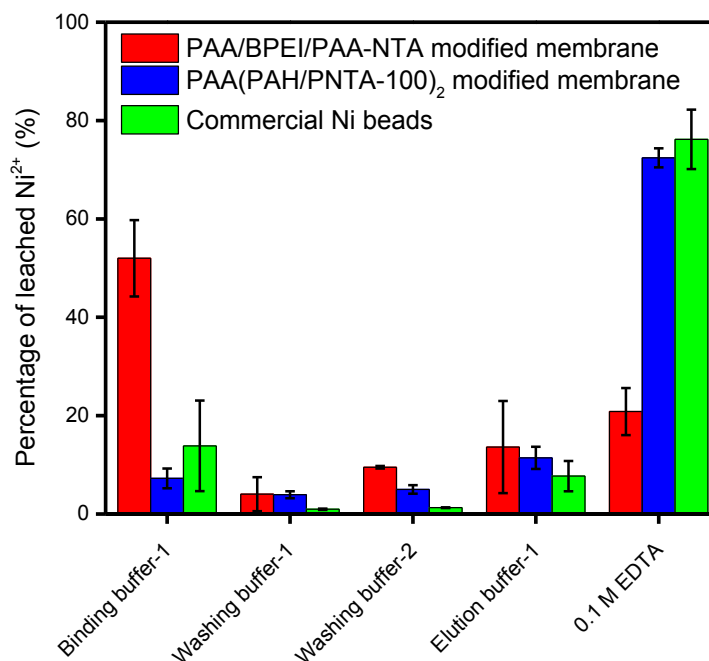
Figure 3.13. Percentage of the bound Ni^{2+} leached from PAA/BPEI/PAA-NTA- and PAA(PAH/PNTA-100)$_2$-modified membranes and commercial Ni beads when passing buffers sequentially through the membranes. The buffer compositions were: binding buffer 1- 20 mM phosphate buffer with 0.3 M NaCl and 10 mM imidazole; washing buffer 1- 20 mM phosphate buffer with 0.15 M NaCl and 0.1% Tween-20; washing buffer 2- 20 mM phosphate buffer with 0.15 M NaCl and 45 mM imidazole; and elution buffer-1- 20 mM phosphate buffer with 0.5 M NaCl and 0.3 M imidazole. Buffer volumes were 2.5 mL for membranes and 75 mL for beads.

The PNTA-100-containing films show much less leaching than membranes with PAA/BPEI/PAA-NTA. Even after the membrane was washed with the elution buffer containing 0.5 M imidazole, >70% of the Ni^{2+} remained on the membrane as shown in the subsequent elution with 0.1 M EDTA. Leaching from the membrane with PAA(PAH/PNTA-100)$_2$ is similar to that from commercial beads with NTA. Furthermore, we compared leaching from different PNTA-X systems. Figure 3.14 examines leaching from membranes containing either PAA/PAH/PNTA-100- or PAA/PAH/PNTA-25 films.

Again leaching is low in binding buffer-2 and washing buffers (3 & 4), even lower than for films containing two PTNA layers. Comparing PNTA-25 and PNTA-100, the film with PNTA-25 shows about double the leaching in the 0.5 M imidazole buffer. Nevertheless, the elution with 2% HNO_3 shows that both films retain more than 70% of their Ni^{2+} through the binding and imidazole elution. Even with 0.5 M imidazole, the Ni^{2+} concentration is less than 10 ppm in the 5 mL of elution buffer passed through the PAA/PAH/PNTA-100-modified membrane.
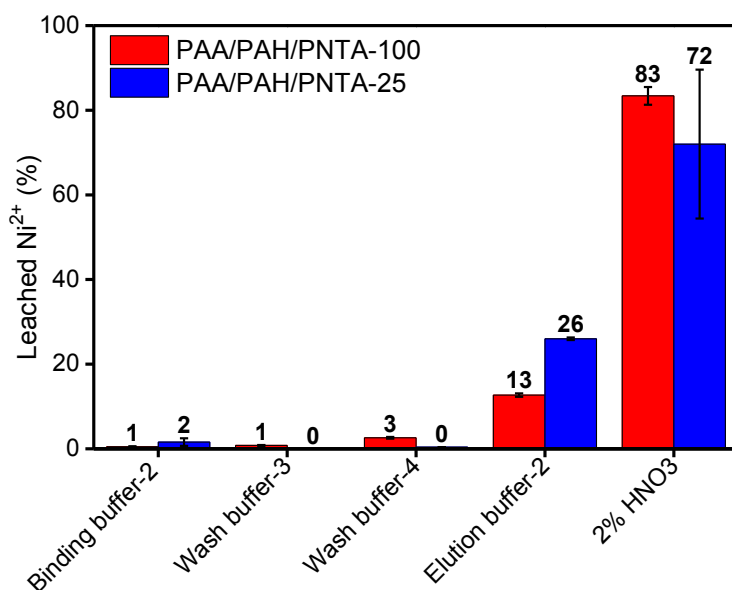
Figure 3.14. Ni^{2+} leaching from nylon membranes modified with PAA/PAH/PNTA-100 and PAA/PAH/PNTA-25 coatings. The numbers represent the percentage of initially adsorbed Ni^{2+} ions leached in 160 bed volumes (5 mL) of each solution passed through the membrane at a flow rate of 1 mg/ml. The buffer compositions were: binding buffer 2- 20 mM phosphate; washing buffer 3- 20 mM phosphate with 0.15 M NaCl and 0.1% Tween-20; washing buffer 4- 20 mM phosphate with 0.15 M NaCl and 45 mM imidazole; and elution buffer 2- 20 mM phosphate with 0.5 M NaCl and 0.5 M imidazole. All buffers had a pH of 7.4.The experiment was repeated twice for all substrates, and errors are differences between two trials. Numbers above the bars show the average value.

3.3.7. Protein Binding to Cu^{2+}/Ni^{2+}-containing Membranes.

Based on experiments with polyelectrolyte multilayers PEMs on Au-coated wafers, $(PAH/PNTA-25)_n$ binds more protein than $(PAH/PNTA-100)_n$ (see binding capacities in Figure 3.9). However, passage of a 0.3 mg/ml ConA solution through membranes modified with $PAA/PAH/PNTA-X-Cu^{2+}$ films showed that films with both PNTA-25 and PNTA-100 bind only 20-25 mg of ConA per cm^3 of membrane. Thus the acrylic acid groups in PNTA-25 did not increase protein binding in membranes containing only one $PAH/PNTA-X-Cu^{2+}$ bilayer. The effect of the additional acrylic acid groups on protein binding may prove more important in $PAA(PAH/PNTA-25)_n-Cu^{2+}$ films, but adsorption of a second PAH/PNTA-25 bilayer plugged the membrane pores.

Because $PAA(PAH/PNTA-100)_2$ films do not plug membrane pores, we initially studied the binding of HisU to membranes modified with $PAA(PAH/PNTA)_2-Ni^{2+}$ films. Unfortunately the binding capacity of these membranes is only 18±1 mg/ml, which is much less than that of $(PAA/PEI/PAA)-NTA-Ni^{2+}$-modified membranes (~90 mg/ml of membrane). Interestingly, for a $PAA/PAH/PNTA-100-Ni^{2+}$-modified membrane, the His-U binding capacity is 47±5 mg/ml based on breakthrough curves, and elution gives a binding capacity of 40±3 mg/ml. Adsorption of a second PAH/PNTA-100 leads to less protein capture. Plugging of pores may block some binding sites, and the SEM image in Figure 3.11 suggests that a highly swollen $(PAA/PAH/PNTA-100)_2-Ni^{2+}$ films could block some pores.

Furthermore we compared protein-binding capacities of membrane modified with PAA/PAH/PNTA-100, PAA/PAH/PNTA-25 and PAA/PEI/PAA-NTA films using His U as a model protein. Membranes containing PAA/PAH/PNTA-25 bind the same amount of

protein (46 mg of His U per mL) as membranes with PAA/PAH/PNTA-100. As Table 3.3 shows, membranes modified with PAA/PEI/PAA-NTA films bind 89 mg His U/ml of membrane, or approximately twice the amount of His U captured in membranes countaining PAA/PAH/PNTA-25-Ni^{2+}. Membranes with PAA/BPEI/PAA-NTA apparently present more protein-accessible Ni^{2+} binding sites than membranes containing PAA/PAH/PNTA-25.

Table 3.3. Protein binding capacities of PAA/PEI/PAA-NTA and PAA/PAH/PNTA-X membranes.

Membrane modification conditions	His U binding capacity (mg/mL)		Con A bindinga capacity (mg/mL)		Aldolase binding capacity (mg/mL)		*Pa*PAM binding capacity (mg/mL)	
	From break through curve	From elution	From break through curve	From elution	From break through curve	From elution	From break through curve	From elution
PAA/PAH/PNTA-100	47	40	25	28	-	-	-	-
PAA(PAH/PNTA-100)$_2$	-	-	33	43	-	-	-	-
PAA/PAH/PNTA-50	-	-	20	25				
PAA/PAH/PNTA-25	46	34	25	30	22	18	7.8	-
PAA/BPEI/PAA-NTA	89	85	73	70	55	56	11	14

[a]The concentration of Con A in the loading solution was 0.3 mg/mL in 20 mM phosphate buffer at pH 6.0. The flow rate was 10 cm/h through a membrane with a diameter of 1.0 cm. The deposition conditions are the same as described in the experimental section except the membranes modified with PAA/BPEI/PAA-NTA and PAA/PAH/PNTA25. PAA/PAH/PNTA25 films were cross-linked as described in the experimental section, Membrane modification with PAA/BPEI/PAA-NTA was given in a previous publication.[28]

Finally, we used proteins with four different molecular masses (Table 4.3, bottom two rows) to study the effect of the protein size on the binding capacity of these

membranes. PAA/BPEI/PAA-NTA- and PAA/PAH/PNTA-25-modified membranes reach their highest binding capacities of 89 and 46 mg/ml respectively, when using the smallest protein, His U. Unfortunately, the binding capacity decreases with the molecular mass of the protein for both PAA/BPEI/PAA-NTA and PAA/PAH/PNTA-25, declining to around 10 mg/mL for His-tagged *Pa*PAM which has a molecular weight of 59 kDa. Nevertheless, we do not know if this trend is protein-dependent. In most cases membranes with PAA/PAH/PNTA-25 bind around 1/3 to 1/2 of the protein captured in membranes with PAA/BPEI/PAA-NTA. However, even the capacity of PAA/PAH/PNTA-modified membranes is comparable to that of commercial beads.[47] Moreover, this new modification strategy is easy to apply and minimizes metal-ion leaching compared to membranes with PAA/BPEI/PAA-NTA.

3.3.8. His-tagged Protein Purification from Cell Lysate.

To demonstrate that membranes can capture His-tagged protein selectively from protein mixtures, we purified His-CSN 7 protein from a whole-cell extract using a PAA/PAH/PNTA-Ni^{2+}-modified membrane. Figure 3.15 shows the SDS-PAGE analysis of the purification process. Elution of the captured protein from the membrane (Lane 4) yields highly purified His-CSN7, demonstrating the high selectivity of this system.
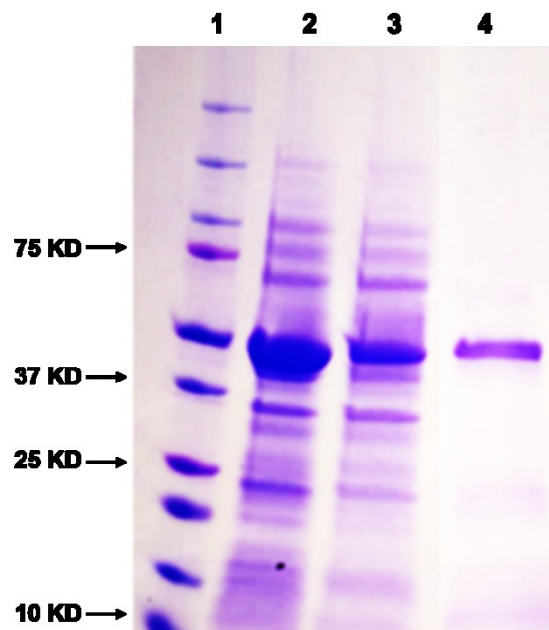
Figure 3.15. SDS-PAGE demonstrating purification of overexpressed His-CSN7 protein from cell lysate. Lane 1: molecular ladder; Lane 2: cell lysate containing His-CSN7 protein; Lane 3: the cell lysate after passing through a PAA/PAH/PNTA-100-Ni^{2+}-containing membrane; Lane 4: the eluate from the membrane.

3.4. Conclusion.

This study shows a simple approach, LBL adsorption with polymers containing NTA groups, to create films for selective capture of His-tagged proteins. Reaction of poly(ε-acryloyl L-lysine) with chloroacetic acid provides a convenient route to NTA-containing polymers, and adsorption of a PAA/PAH/PNTA-100-Ni^{2+} film in a porous membrane yields a His-tagged ubiquitin binding capacity of 47±5 mg/mL, which is comparable to that of commercial beads. The NTA functionality in the polymer decreases metal-ion leaching compared to films containing PAA derivatized with aminobutyl NTA. Wafers modified with (PAH/PNTA-25)$_3$-Ni^{2+} show ~3 times the protein binding of corresponding substrates modified with (PAH/PNTA-100)$_3$-Ni^{2+}, presumably

because of more swelling with $(PAH/PNTA-25)_3$. These high $(PAH/PNTA-25)_3-Ni^{2+}$ binding capacities are also 2-5 time higher than for $(BPEI/PAA)_3-NTA-Ni^{2+}$ films and might be useful for sensing applications. The His-tagged protein-binding capacity of the $(PAH/PNTA-X)-Ni^{2+}$-modified membranes is 1/2 of that for membranes modified through adsorption of PAA/BPEI/PAA followed by aminobutyl NTA derivatization. However, direct adsorption of PAH and PNTA-X in membranes is much simpler and less expensive than previous membrane modification methods and may lead to inexpensive, disposable membranes for rapid purification of His-tagged protein.

APPENDIX

APPENDIX 3 . LAYER-BY-LAYER DEPOSITION WITH POLYMERS CONTAINING NITRILOTRIACETATE, A CONVENIENT ROUTE TO FABRICATE METAL- AND PROTEIN-BINDING FILMS.

A3.1. Synthesis of ε-Acryloyl L Lysine Monomer.

ε-Acryloyl L lysine was synthesized according to the procedure described by Nagaoka et al.[1] L-Lysine hydrochloride (20 g, 109.5 mmol) was added to water (250 mL) and heated at 90 °C for 5-10 min until it completely dissolved. Cupric carbonate (13.3 g, 60.2 mmol) was added slowly to the mixture, which was stirred for 10 min and cooled to room temperature prior to addition of 120 mL of acetone. The solution was filtered to remove insoluble residues, and a small portion of this solution was evaporated to obtain pure Cu(L-lysinate)$_2$. Complex formation was confirmed by FTIR spectroscopy and elemental analysis. IR (cm^{-1}): 3143-3444, ν-NH2 str; 2935, ν-CH2 str.; 1660, ν–COO$^-$ assym str; 1400, ν-CH2 scissor deformation; 1328, ν-CH2 wagging; 590, v-Cu-N assym. Elemental analysis (%) calcd. for C$_{12}$H$_{32}$N$_4$O$_6$Cu: C, 31.13; H, 6.98; N, 12.10. Found: C, 30.67; H, 6.90; N, 11.80.

Next, 55 mL of 2.0 M KOH was added to the solution of the L-lysine copper complex. An aqueous solution containing acryloyl chloride (1.38 mL, 17.1 mmol) and 7.7 mL of aqueous 2.0 M KOH was cooled to 0 °C and added to the solution of the L-lysine complex every 5 min at 0 °C. This procedure was repeated eight times. After stirring for 12 h at room temperature, the precipitated ε-acryloyl L-lysine Cu^{2+} complex was collected by filtration and washed successively with water, methanol, and ether. The yield was 18 g (71%). The structure was confirmed by IR spectroscopy and

elemental analysis. IR (cm^{-1} ε-Acryloyl L-lysine): 3100–3400, ν N-H (amide, amine); 2880–2960, ν C-H; 1660, ν C-O (amide I); 1620, ν N-H (amide II); 670, ν N-H (amide V). Elemental analysis (%) calcd. for $C_{18}H_{30}N_4O_6Cu$: C, 46.80; H, 6.55; N, 12.13. Found: C, 46.00; H, 6.52; N, 11.81.

ε-Acryloyl L-lysine copper complex (5.0 g, 11 mmol) was added to an Erlenmeyer flask and dispersed in 100 mL of water. Next, 8-hydroxyquinolinol (2.0 g, 13.6 mmol) dissolved in chloroform (100 mL) was added slowly while stirring at room temperature. The solution was continuously stirred for 12 h, and a green precipitate in the chloroform layer was removed by filtration. Three washing cycles with chloroform (50 mL × 3) were performed to remove traces of 8-hydroxyquinoline. The water layer was evaporated to 50 mL, and white ε-acryloyl L-lysine precipitated upon addition of tetrahydrofuran. The yield was 4.1 g (93%). ^{1}H NMR (D$_2$O, δ ppm): 1.43 (m, 2H, CH$_2$), 1.61 (m, 2H, CH$_2$), 1.84 (m, 2H, CH$_2$), 3.25 (t, 2H, CH$_2$), 3.75 (t, 2H, CH$_2$), 5.70 (d, 1H, CH$_2$=CH[trans]), 6.19 (d, 1H, CH$_2$=CH[cis]), 6.21 (dd, 1H, CH$_2$=CH). Elemental analysis (%) calcd. for $C_9H_{16}N_2O_3$: C, 53.99; H, 8.05; N, 13.99. Found: C, 53.73; H, 7.97; N, 13.84.
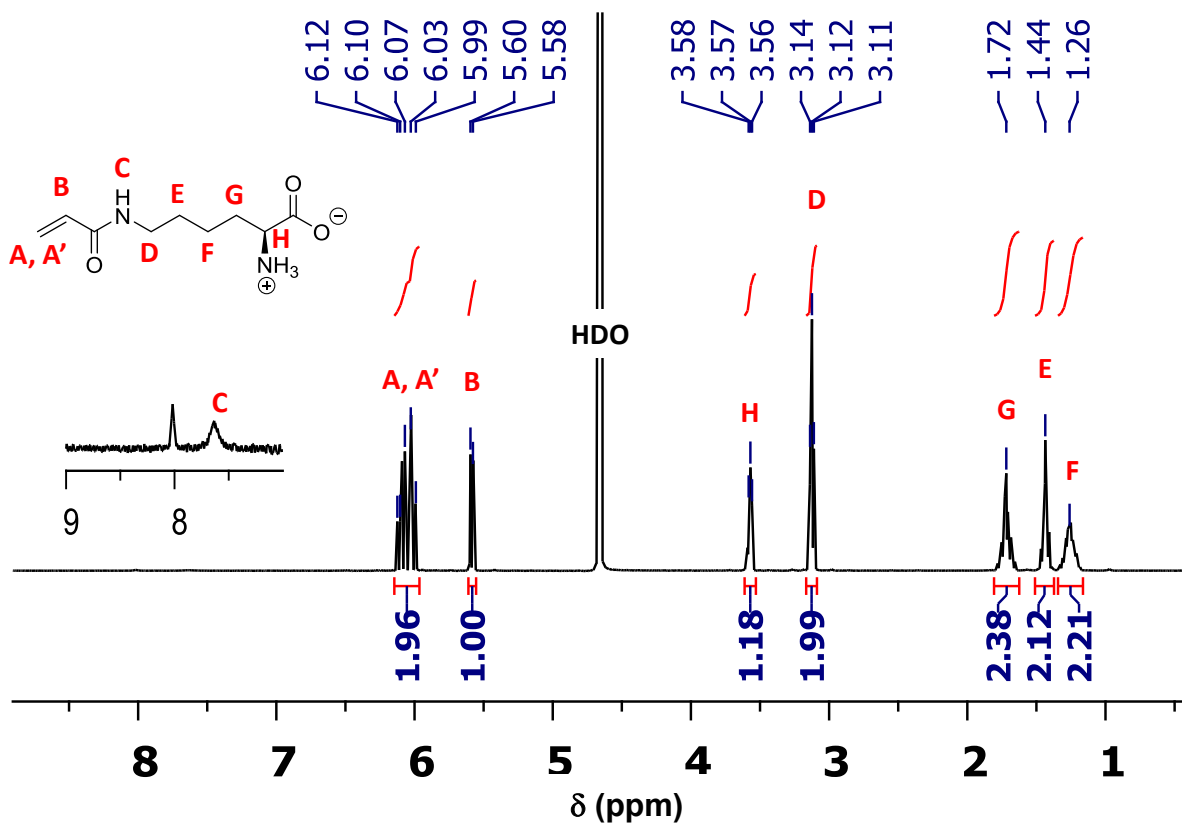
Figure A3.1. ^{1}H NMR spectrum of ε-acryloyl L lysine in D_2O.
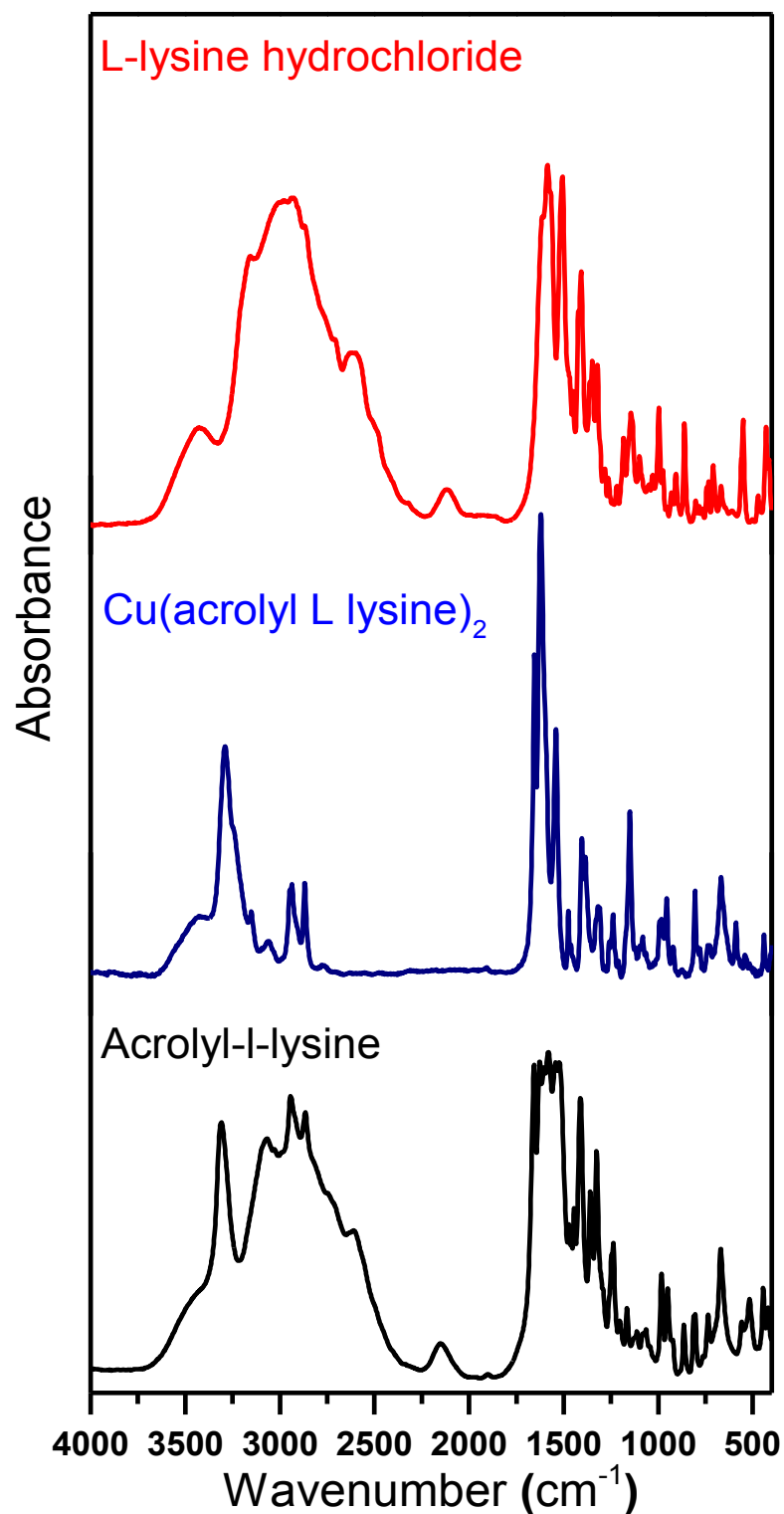
Figure A3.2. IR spectra of L-lysine hydrochloride (starting material, top spectrum), the Cu(acrolyl L lysine)$_2$ complex (middle spectrum) and the final product, acryloyl-L-lysine (bottom spectrum) (in KBr). Absorbance scales are not the same for all spectra.

A3.2. Characterization of Poly(2,2-(5-acrylamido-1-carboxypentylazanediyl) diacetic acid) [PNTA-100].

A3.2.1.Calculation of Conversion of poly(ε-Acryloyl L lysine) [PLys-100].

After polymerization of ε-Acryloyl L-lysine, vinyl proton signals (representing the C=CH$_2$ groups) at 5.8-6.0 ppm in the ^{1}H NMR spectrum of the reaction mixture show unreacted ε-acryloyl lysine. The integral for these two protons is 0.29. On the other hand, CO-NH-C**H$_2$**-methylene protons for unreacted and reacted acryloyl lysine appear at 3.0 ppm with a total integration of 1.10. To determine the unreacted acryloyl lysine, we performed the following calculation.

$$\text{Unreacted acrolyl lysine} = \frac{\dfrac{\text{Vinyl proton integral}}{\text{Number of protons in C=CH}_2\text{ group}}}{\dfrac{\text{Sum of methylene CO-NH-CH}_2\text{ integrals}}{\text{Number of protons in CO-NH-CH}_2\text{ groups}}}\% \quad \text{Equation A 3.1}$$

$$\text{Unreacted acrolyl lysine} = \frac{\dfrac{0.22}{2}}{\dfrac{2.71}{4}} \times 100\% = 16\%$$

Therefore, conversion is 84%.
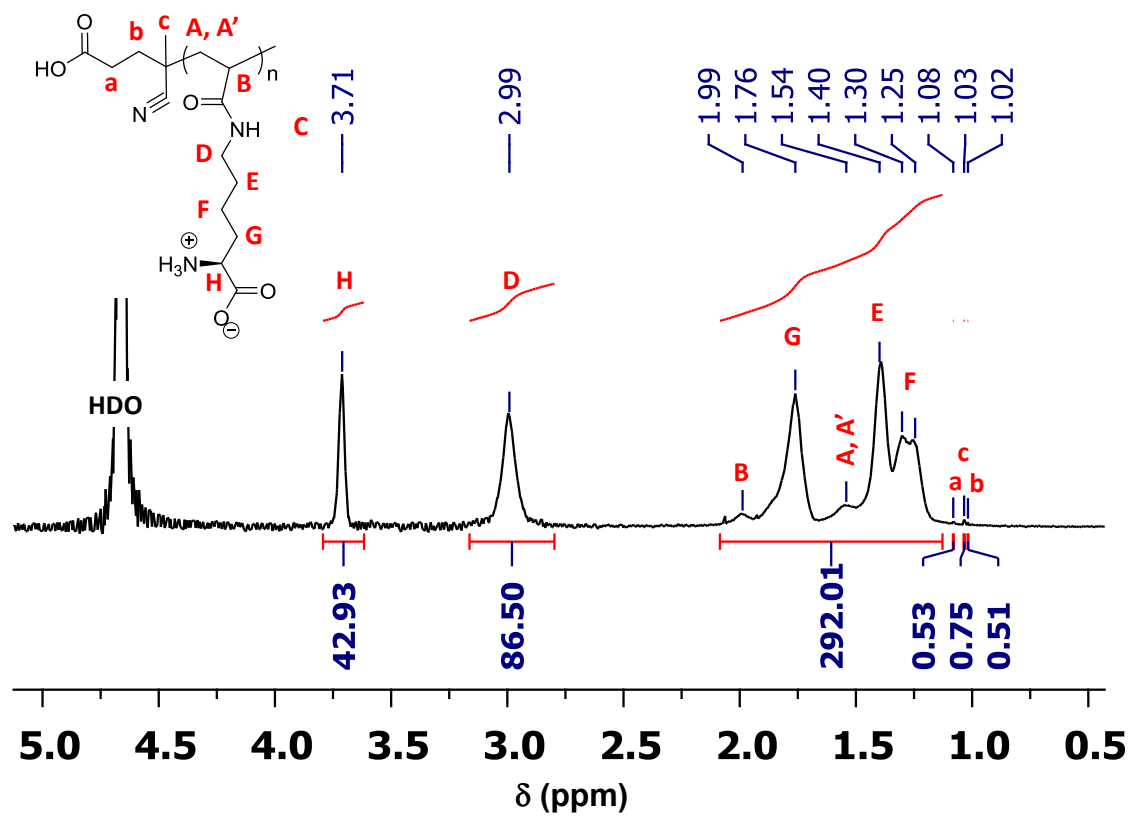
Figure A3.3. ^{1}H NMR spectrum of poly(ε-acryloyl-L-lysine) in D$_2$O adjusted to pH 7 by addition of NaOD.

A3.2.2.Calculation of the Degree of Polymerization (DP) and Molecular Weight (M_n) of (PLys-100).

End group FW = 126.14   Repeating unit $(200.12)_n$ End group FW = 126.14
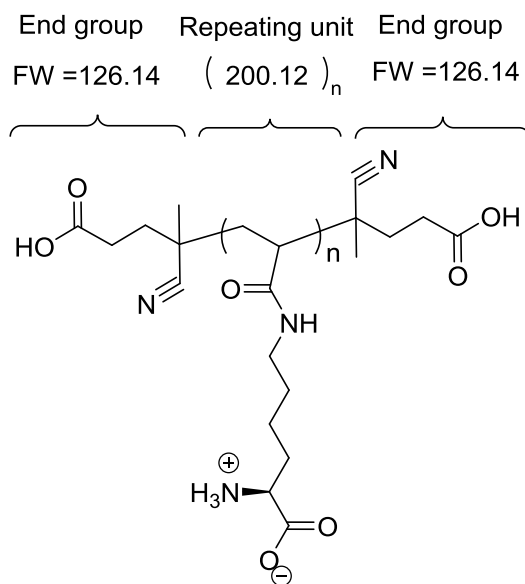
1) Calculation, integral per proton:

Use the end group proton signals (-C-CH$_2$-1.02 ppm, -C-CH$_3$ 1.03 ppm & -CO-CH$_2$-1.08 ppm)

$$\text{Integral per proton} = \frac{\text{sum of methyl \& methylene proton integrals}}{[\text{\# of protons in methyl \& methylene group}]\times 2}$$

$$\Downarrow$$

$$= \frac{0.51 + 0.75 + 0.53}{14}$$

$$\Downarrow$$

$$= 0.128 \text{ per proton}$$

2) Calculation, number of repeating monomer units, n:

Use the C-CH- (methylene) proton signal (H, Figure A3.3, 3.71 ppm)

$$n = \frac{\text{(methylene proton integral) / \# of methylene protons per unit}}{\text{previously calculated integral per end group proton}}$$

$$\Downarrow$$

$$= \frac{(42.93) / 1}{0.128}$$

$$\Downarrow$$

$$= 335 \text{ repeating monomer units, } n$$

Calculation of $DP_{,theo}$

$$DP,theo = \frac{[M]_0}{[I]_0} \times Conversion = \frac{12.5}{0.045} \times 0.84 = 233$$

3) Calculation of M_n:

M_n = (MW of end groups) + (MW of repeating unit)(n)

= (126.14)×2 + (200.12)(233) = 46,879 gmol^{-1}

Calculation of $M_{n, theo}$

$$M_{n, theo} = Conversion \times \frac{[M]_0}{[I]_0} \times MW_{monomer} + MW_{end\ groups}$$

$$M_{n, theo} = 0.84 \times \frac{12.5}{0.045} \times 200.12 + (126.14) \times 2 = 49,726 \text{ g mol}^{-1}$$
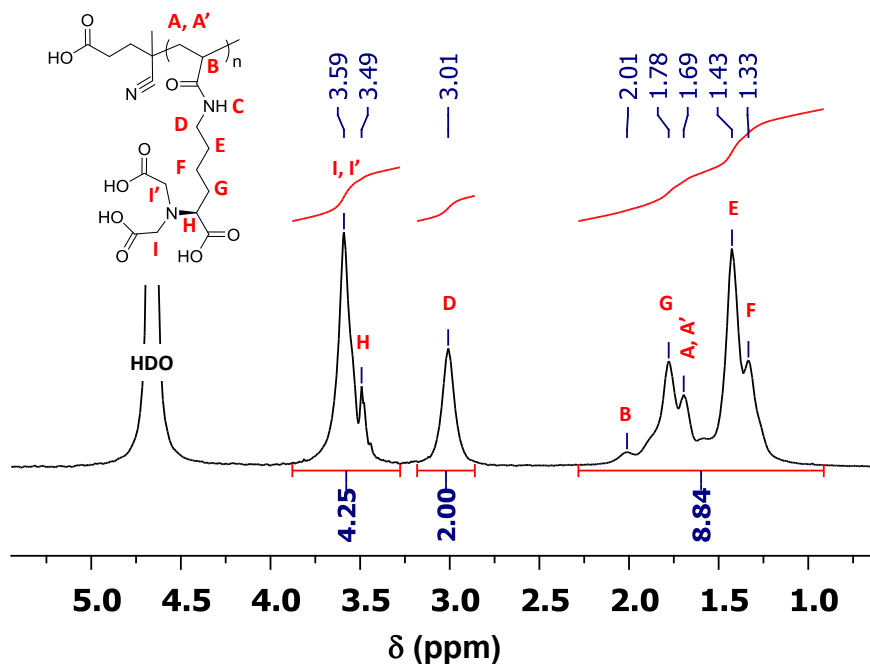
Figure A3.4. ^{1}H NMR spectrum of poly(2,2-(5-acrylamido-1-carboxypentylazanediyl) diacetic acid) [PNTA-100] in D_2O adjusted to pH 7 by addition of NaOD.

The number of carboyymethylene groups added per repeating unit (during reaction of poly(ε-acryloyl-L-lysine) with bromoacetic acid) was calculated with the following equation (All the letters and integrations in the equation referred to the signals in Figure A3.4).

Carboxymethylene groups added per repeating unit =

$$\frac{\text{Number of protons on carboxymethylene groups per repeating unit}}{\text{Number of D protons on polymer backbone per repeating unit}} \qquad \text{Equation A 0.2}$$

$$\text{NTA functionality per repeating unit} \ = \frac{[\text{Proton integrals I, I' and H}]-[\text{D proton integral/2}]}{\text{D proton integral}}$$

Here we assume integration of the H proton = D proton integral/2

$$\text{Carboxymethylene groups added per repeating unit} = \frac{[4.25]-[2.0/2]}{2.0} = 1.63$$

End group   Repeating unit Repeating unit   End group

FW =126.14 $\left(\ 316.31\ \right)_a$ $\left(\ 200.12\ \right)_b$ FW =126.14
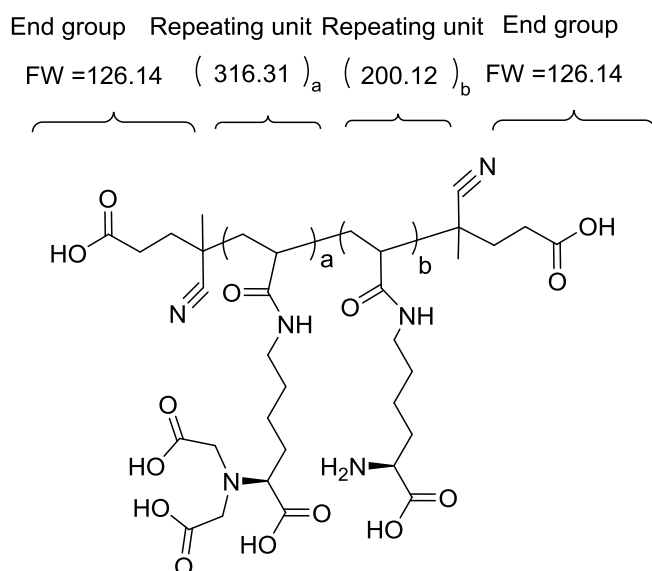
Calculation of the molecular weight assumes a polymer containing two end group functionalies and has underivatized lysine repeating units. Based on NMR analysis 80% of the lysines are derivatized with two bromoacetic acid and 20% remain completely unreacted (equivalently, we could have partial reaction of some repeat units).

Calculation of M_n:

$$M_n = \text{(FW end groups)} + \text{(FW repeating unit)}(n)$$

$$\Downarrow$$

$$= (126.14)\times 2 + (316.31\times 0.80 + 200.12\times 0.20)(233)$$

$$\Downarrow$$

$$= 68{,}538\ \text{gmol}^{-1}$$

A3.3. Synthesis and Characterization of Poly(2,2-(5-acrylamido-1-carboxypentylazanediyl) diacetic acid)-*co*-poly acrylic acid [PNTA-50].

A3.3.1.Synthesis of Poly(ε-acryloyl-L-lysine-*co*-acrylic acid), poly(Lys-50-*co*-AA-50).

The initiator 4,4-azobis-4-cyanovaleric acid (12.5 mg, 45×10^{-3} mmol = 0.4 mol % with respect to monomer) was dissolved in water (40 mL) and added to the monomers, ε-acryloyl L-Lysine (1.25 g, 0.00625 mol) and acrylic acid (0.44 g, 0.00625 mol). The solution was stirred at room temperature for 10 min, and the pH was adjusted to between 6 and 7. The mixture was then degassed with five freeze−pump-thaw cycles and subsequently polymerized at 75 °C for 24 h. The reaction was monitored using ^{1}H NMR spectroscopy. The polymer was precipitated using tetrahydrofuran and acetone, and vacuum drying gave 1.38 g of a colorless solid (conversion ~78%, M_n = 25,631 g mol^{-1}). ^{1}H NMR spectroscopy (D$_2$O, δ ppm): 1.28 (br, 2H, CH2), 1.40 (br, 2H, CH2), 1.47-1.71 (br, 4H, 2×CH2), 1.76 (br, 2H, CH2), 1.90 (br, 2H, 2×CH), 2.44 (NH2), 2.99 (br, 2H, CH2), 3.41-3.48 (m, 1H, C**H**-NH2), 3.59 (br, 1H, C**H**-NH3+), 7.82 (br, 1H, CONH).
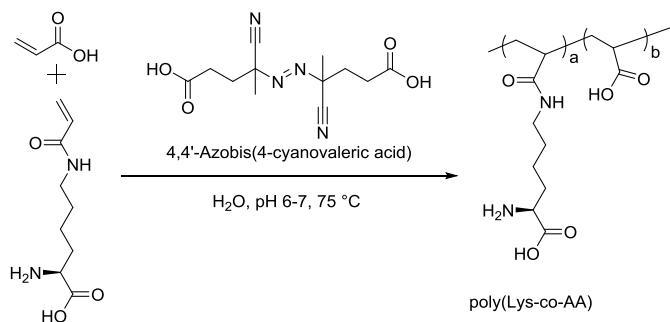
Figure A3.5. Synthesis of poly(ε-acryloyl-L-lysine-co-acrylic acid), poly(Lys-50-co-AA-50).
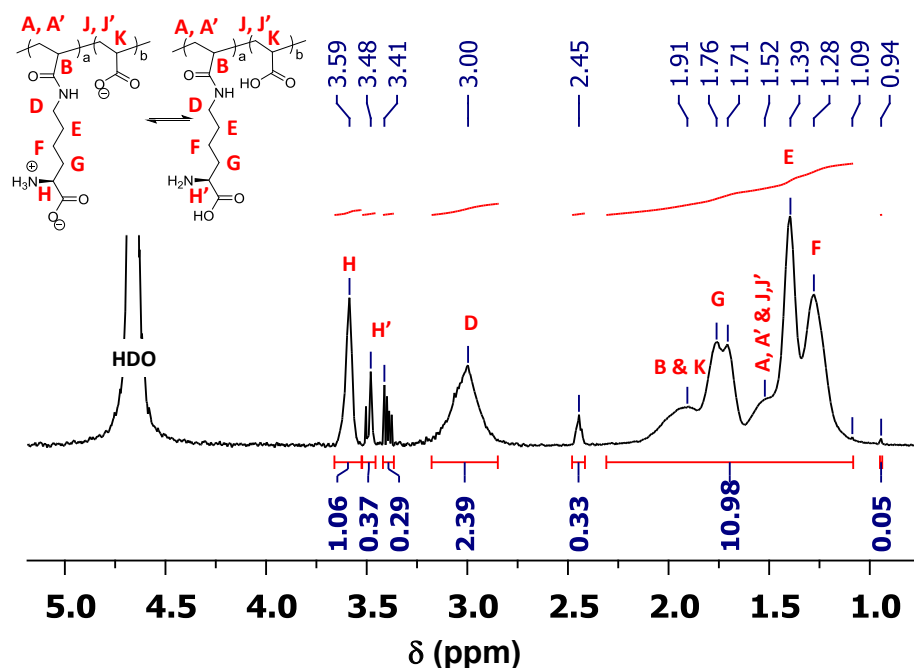
Figure A3.6. ^{1}H NMR spectrum of poly(ε-acryloyl-L-lysine-co-acrylic acid) poly(Lys-50-co-AA-50) in D$_2$O adjusted to pH 7 by addition of NaOD.

A3.3.2. Calculation of Conversion of Poly(Lys-50-*co*-AA-50).

Vinyl proton signals of the C=CH$_2$ groups of ε-acryloyl-L-lysine appear in the 5.8-6.0 ppm region of the 1H NMR spectrum of the copolymerization solution. These signals correspond to unreacted monomer, and their integral is 0.22 (Figure A3.6). NH-CH$_2$-methylene protons for unreacted and reacted ε-acryloyl-L-lysine appear around 3.0 ppm with a total integration of 1.06. We used the equation in A3.2 to calculate the fraction of unreacted acryloyl lysine, which is 44%. Therefore, 56% percent of the ε-acryloyl-L-lysine (0.0035 mol) polymerizes. In contrast, the crude NMR spectrum of PLys-50 shows complete incorporation of AA (0.00625 mol) into the polymer backbone. The total number of moles for both of the monomers in the polymer is 0.00975 mol, which

represents 78% conversion of both monomers. The fraction of acryloyl repeat units in the polymer is 36%.

A3.3.3.Calculation of the Theoretical Degree of Polymerization and M_n Values for Poly(Lys-50-*co*-AA-50).

End group   Repeating unit   Repeating unit   End group

FW =126.14 $\left(\; 200.12\; \right)_a$ $\left(\; 72.06\; \right)_b$ FW =126.14
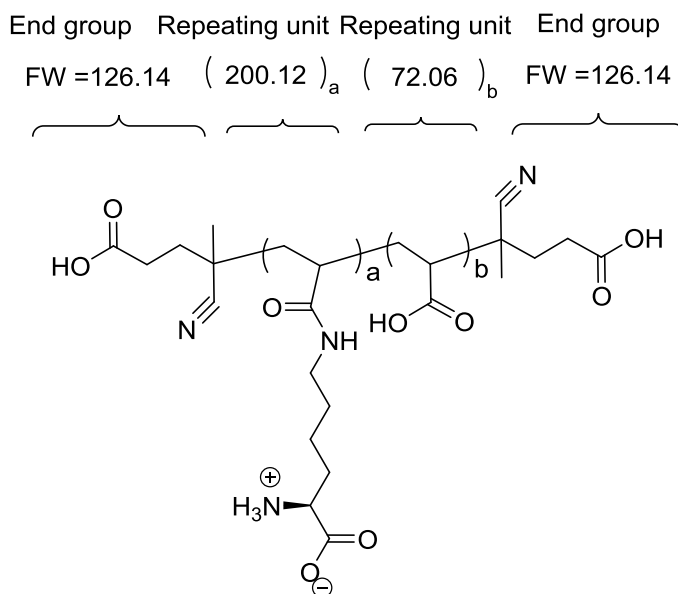
Calculation of DP$_{, theo}$

$$DP=\frac{[M]_0}{[I]_0} \times Conversion = \frac{12.5}{0.045} \times 0.78 = 217$$

Calculation, M_n:

M_n =   (FW end groups) + (FW repeating unit)(n=a+b)

⇓

=(126.14)×2 + (200.12*0.36 + 72.06x0.64)(217) = 25,631gmol^{-1}

A3.4. Synthesis of Poly(2,2-(5-acrylamido-1-carboxypentylazanediyl) diacetic acid-*co*-acrylic acid), [PNTA-50].

Under a N_2 atmosphere, bromoacetic acid (4.7 g, 0.034 mol), NaOH (1.35 g, 0.034 mol) and 50 mL of water were added to a two-neck round-bottomed flask, and the mixture was stirred at room temperature for 10 min. This solution was added dropwise with stirring to an aqueous solution (50 mL) containing poly(Lys-50-co-AA-50) (1.38 g, 0.0048 mol of lysine repeating units) at 50 °C. The reaction mixture was kept at 50 °C for 24 h with occasional addition of 30% NaOH to maintain the pH at 10.0. Subsequently, the pH was adjusted to 1 by addition of concentrated HCl. The supernatant was decanted, the remaining precipitate was dissolved by addition of 30% NaOH, and the solution was again adjusted to pH 1.0 with concentrated HCl. This process was repeated 2 times, and the precipitate was filtered and dried in vacuo for 12 h to give white, solid poly(2,2-(5-acrylamido-1-carboxypentylazanediyl) diacetic acid-co-acrylic acid) (PNTA-50), 0.80 g (degree of carboxymethylene functionalization per repeating unit is 1.83, M_n = 34,062 g mol^{-1}). This structure was confirmed by ^{1}H NMR spectroscopy (D_2O, δ ppm): 1.31 (br, 2H, CH2), 1.41 (br, 2H, CH2), 1.53 (br, 4H, 2×CH2), 1.67-1.75 (br, 2H, CH2), 1.87-1.96 (br, 2H, 2×CH), 2.99 (br, 2H, CH2), 3.58 (br, 5H, 2×CH2 and CH), 7.85 (br, 1H, CONH). Elemental analysis (%) calcd. for $C_{16}H_{24}N_2O_9$: C, 49.48; H, 6.23; N, 7.21. Found: C, 42.67; H, 6.13; N, 6.48. See section A3.5.3 for a discussion of discrepancies in elemental analysis.
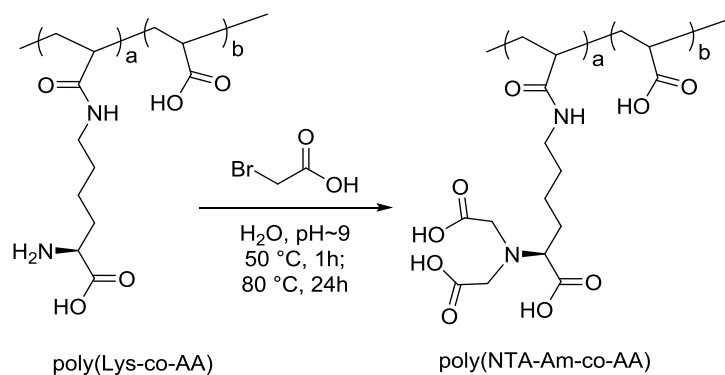
Figure A3.7. Synthesis of Poly(2,2-(5-acrylamido-1-carboxypentylazanediyl) diacetic acid-*co*-acrylic acid) [PNTA-50].
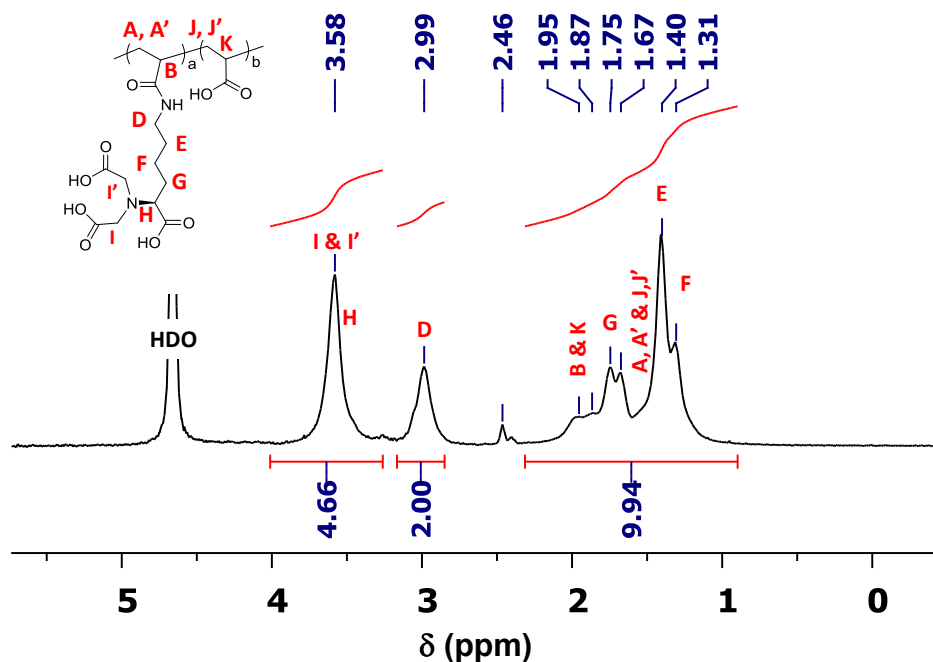
Figure A3.8. ^{1}H NMR spectrum of poly(2,2-(5-acrylamido-1-carboxypentylazanediyl) diacetic acid-*co*-acrylic acid) [PNTA-50] in D$_2$O adjusted to pH 7 by addition of NaOD.

174

The number of carboxymethylene groups added per ε-acryloyl-L-lysine repeating unit, 1.83, was calculated from the ^{1}H NMR spectrum in the same way as for PNTA-100 (see section A3.2.2).
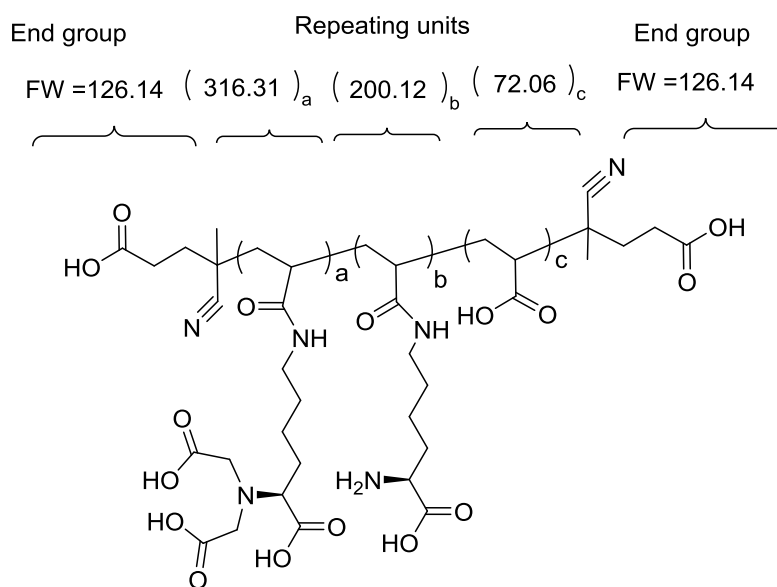
Calculation, M_n:

M_n = (FW end groups) + (FW repeating unit)(n=a+b+c)

$\Downarrow$

=(126.14)×2 +[(316.31×0.90 +200.12×0.10)×0.36+72.06×0.64)(217)

$\Downarrow$

= 34,062 gmol^{-1}

A3.5. Synthesis of Poly(ε-acryloyl-L-lysine-25-*co*-acrylic acid-75), poly(Lys-25-*co*-AA-75).

As in the synthesis of poly(ε-acryloyl-L-lysine-50-*co*-acrylic acid-50), the initiator 4,4-azobis-4-cyanovaleric acid (18.9 mg, 0.045 mmol = 0.4 mol % with respect to monomer) was dissolved in water (40 mL) and added to the monomers, ε-acryloyl-L-lysine (0.945

g, 0.0047 mol) and acrylic acid (1.0 g, 0.0142 mol). The reaction was stirred at room temperature for 10 min, and the pH was adjusted to 6-7. Then the mixture was degassed by five freeze−pump-thaw cycles and subsequently polymerized at 75 °C for 24 h. The reaction was monitored using ^{1}H NMR spectroscopy, and the polymer was precipitated using tetrahydrofuran and acetone. Vacuum drying gave 1.12 g of a colorless solid (Conversion ~85%, 53% of ε-acryloyl-L-lysine is incorporated into the polymer, M_n = 21,233 g mol^{-1}). ^{1}H NMR spectroscopy (D$_2$O, δ ppm): 1.29 (br, 2H, CH2), 1.40 (br, 2H, CH2), 1.47-1.70 (br, 4H, 2×CH2), 1.71-1.78 (br, 2H, CH2), 1.96 (br, 2H, 2×CH), 2.45 (NH2), 3.02 (br, 2H, CH2), 3.41-3.48 (m, 1H, C**H**-NH2), 3.60 (br, 1H, C**H**-NH3+), 7.81 (br, 1H, CONH).
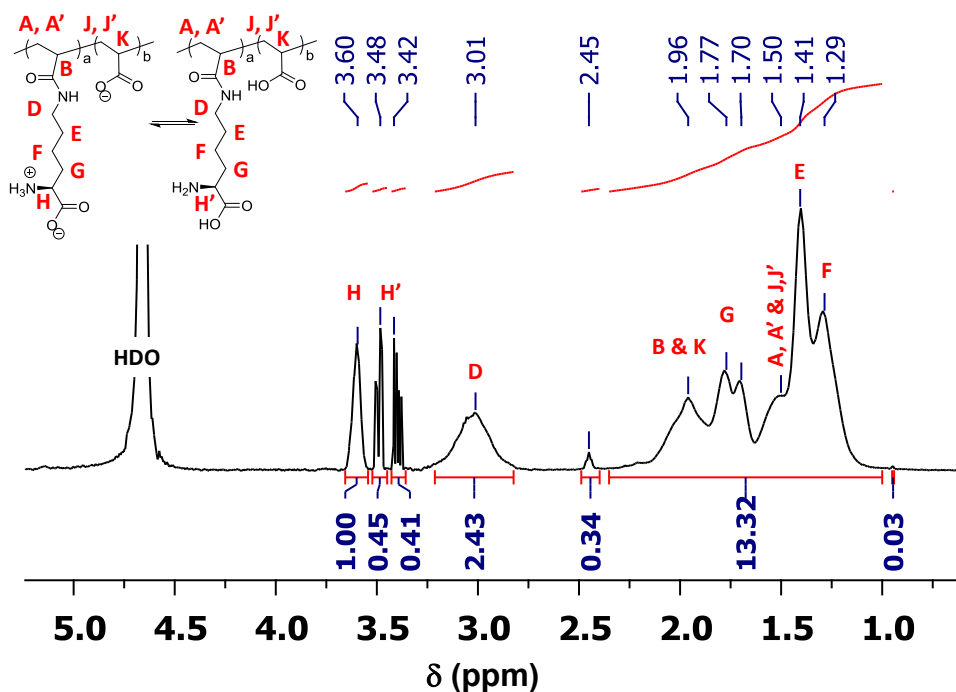
Figure A3.9. ^{1}H NMR spectrum of poly(ε-acryloyl-L-lysine-co-acrylic acid) poly(Lys-25-*co*-AA-75) in D$_2$O adjusted to pH 7 by addition of NaOD.

A3.5.1.Calculation of Conversion of Poly(Lys-25-co-AA-75).

The conversion was calculated using the method in section 3.3.2. The NMR spectrum of the reaction mixture shows 57% unreacted ε-acryloyl-L-lysine and complete incorporation of AA into the polymer. Thus, the polymer contains 0.0020 mol of reacted ε-acryloyl-L-lysine and 0.0142 mol of AA repeating units, which corresponds to a total conversion of 85%. The fraction of repeat units that result from ε-acryloyl-L-lysine is 12.3%.

A3.5.2.Synthesis of Poly(2,2-(5-acrylamido-1-carboxypentylazanediyl) diacetic acid-*co*-acrylic acid), [PNTA-25].

Under N_2, bromoacetic acid (4.7 g, 0.034 mol), NaOH (1.35 g, 0.034 mol) and 50 ml of water were added to a two-neck round-bottomed flask, and the mixture was stirred at room temperature for 10 min. This solution was added dropwise with stirring to an aqueous solution (50 mL) containing poly(Lys-25-*co*-AA-75) (1.12 g) at 50 °C. The reaction mixture was kept at 50 °C for 24 h with occasional addition of 30% NaOH to maintain the pH at 10.0. Then the pH was adjusted to 1 by adding concentrated HCl. The supernatant was decanted, the remaining precipitate was dissolved by addition of 30% NaOH, and the solution was again adjusted to pH 1.0 with concentrated HCl. This process was repeated 2 times, and the precipitate was filtered and dried in vacuo for 12 h to give white poly(2,2-(5-acrylamido-1-carbo xypentylazanediyl) diacetic acid-co-acrylic acid) as a solid [PNTA-25], 1.46 g (degree of functionalization is 1.6, M_n = 24,142 g mol^{-1}). This structure was confirmed by ^{1}HNMR (D$_2$O, δ ppm): 1.32 (br, 2H, CH2),

1.42 (br, 2H, CH2), 1.50-1.52 (br, 4H, 2×CH2), 1.67-1.73 (br, 2H, CH2), 1.90-1.97 (br, 2H, 2×CH), 3.0 (br, 2H, CH2), 3.55 (br, 5H, 2×CH2 and CH), 7.83 (br, 1H, CONH). Elemental analysis (%) calcd. for $C_{22}H_{32}N_2O_{13}$: C, 49.62; H, 6.06; N, 5.26. Found: C, 43.69; H, 5.03; N, 2.96.
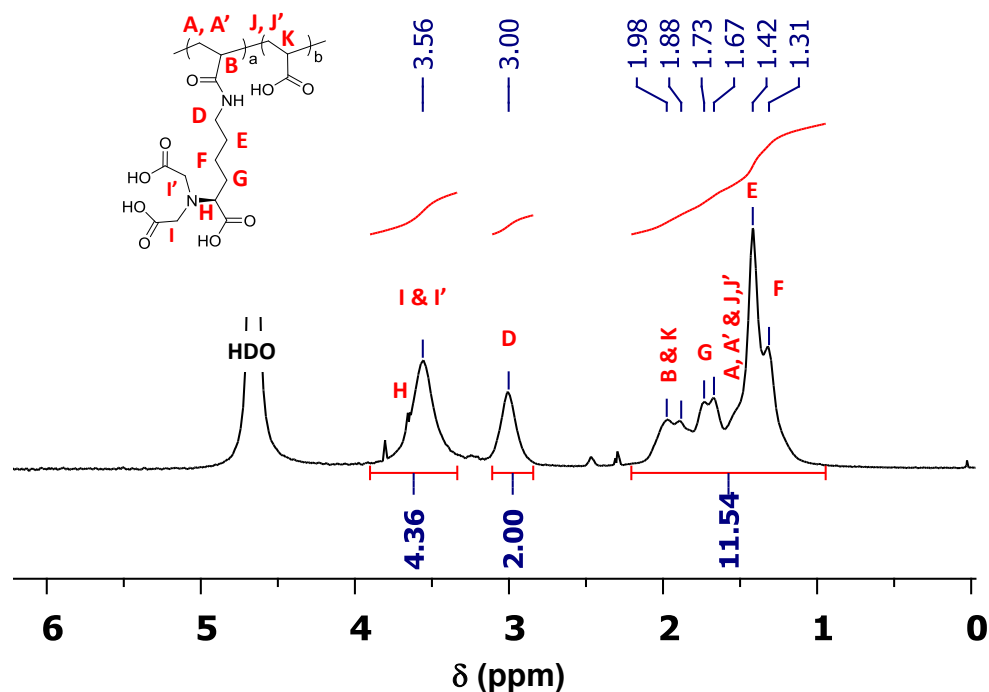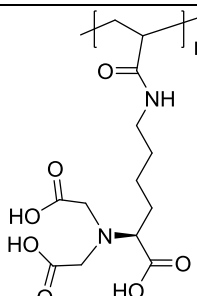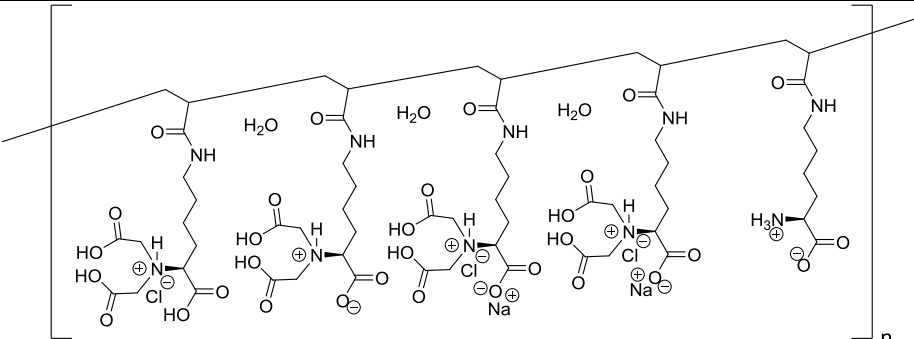
Figure A3.10. ^{1}H NMR spectrum of poly(2,2-(5-acrylamido-1-carboxypentylazanediyl) diacetic acid-*co*-acrylic acid) [PNTA-25] in D_2O adjusted to pH 7 by addition of NaOD.

The number of carboxymethylene groups added per ε-acryloyl-L-lysine repeating unit, 1.64, was calculated from the ^{1}H NMR spectrum in the same way as for PNTA-100 (see section A3.2.2).

A3.5.3.Elemental Analysis of PNTA-X.

The use of elemental analysis to evaluate the synthesis of PNTA-X is complicated by the different possible salt the polymer may form. Table A3.1 and Table A3.2 provides possible structures for PNTA-X along with elemental compositions.

Table A3.1. Possible elemental compositions of PNTA-100 with different numbers of salts and water content.
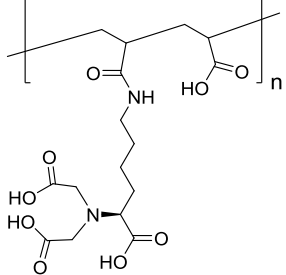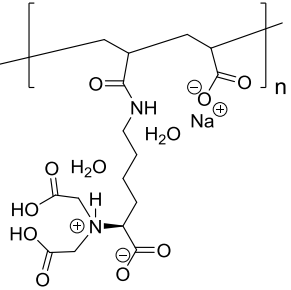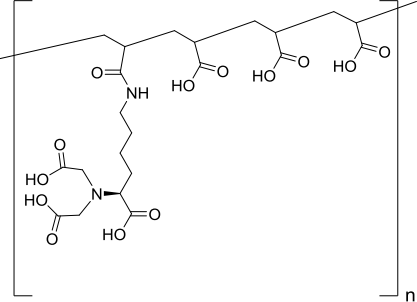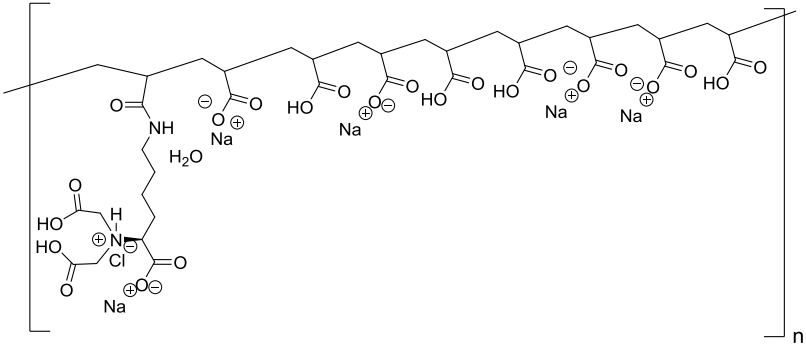
Entry	Potential structure, Chemical formula, Molecular weight and elemental composition
1	Chemical Formula: $C_{13}H_{20}N_2O_7$ Molecular Weight: 316.31 Elemental Analysis: C, 49.36; H, 6.37; N, 8.86; O, 35.41
2	Chemical Formula: $C_{61}H_{103}Cl_3N_{10}Na_2O_{34}$ Molecular Weight: 1672.86 Elemental Analysis: C, 43.80; H, 6.21; Cl, 6.36; N, 8.37; Na, 2.75; O, 32.52

The calculated composition for PNTA-100 as shown in entry 1 of Table A3.1 is C, 49.36; H, 6.37; N, 8.86. This structure assumes all the.Lysines are carboxymethylated with bromoacetic acid and the polymer has no counterions. However, these numbers are significantly different from the experimental elemental analysis data: Found: C,

43.63; H, 6.57; N, 8.13. This difference likely stems from Na$^+$, Cl$^-$, water and unreacted lysine units. The ^{1}H NMR spectrum of the polymer is consistent with 80% doubly carboxymethylated lysine units and 20% unreacted lysine units. Entry 2 in Table A3.1 reflect the partial derivatization along with the presence of charged polymer and counterions. This structure gives an elemental composition: C, 43.80; H, 6.21; N, 8.37, which is reasonably closer to the experimental values. The presence of salts and water will significantly lower the atomic percentages. Unfortunately, we cannot specifiy the exact protonation state of the PNTA-100, because of the low –COOH pKa values. Some –COO$^-$ groups, rather than Cl$^-$ probably provide charge compensation for some of the ammonium groups. However, protonation and water will not affect the C:N ratio, which is 5.6 for the calculated structure and 5.4 for the experimental data. Thus the elemental analysis and experimental data agree reasonable well.

Similarly, we rationalized the elemental compositions for PNTA-50 and 25. Based on monomer ratios in the synthesis of PLys-50, the polymer should have a 1:1 ratio of lysine to AA, and PNTA-50 should show 1:1 NTA and AA groups as shown inTable A3.2, entry 1. The calculated elemental analysis for this structure is C, 49.48; H, 6.23; N, 7.21. However, actual values are quite different (C, 42.67; H, 6.13; N, 6.48) because of the reasons mentioned above as well as the low conversion of ε-acryloyl-L-lysine during polymerization and only partial reaction of the polymer with bromoacetic acid. For the case of PNTA-50, the ratio between doubly carboxymethylated lysine and unreacted lysine is 9:1. But we couldn't draw a structure, which can show closer elemental composition to calculated values, if included 10% unreacted lysine to polymer chain.

Table A3.2 Possible elemental compositions of PNTA-50 and 25 with different numbers of salts and water content.

Entry	Potential structure, Chemical formula, Molecular weight and elemental composition
1	 Chemical Formula: $C_{16}H_{24}N_2O_9$ Molecular Weight: 388.37 Elemental Analysis: C, 49.48; H, 6.23; N, 7.21; O, 37.08
2	 Chemical Formula: $C_{16}H_{27}N_2NaO_{11}$ Molecular Weight: 446.38 Elemental Analysis: C, 43.05; H, 6.10; N, 6.28; Na, 5.15; O, 39.43
3	 Chemical Formula: $C_{22}H_{32}N_2O_{13}$ Molecular Weight: 532.50 Elemental Analysis: C, 49.62; H, 6.06; N, 5.26; O, 39.06
4	 Chemical Formula: $C_{39}H_{56}ClN_2Na_5O_{24}$ Molecular Weight: 1087.27 Elemental Analysis: C, 43.08; H, 5.19; Cl, 3.26; N, 2.58; Na, 10.57; O, 35.32

Nevertheless, if we assumed all the lysines are fully reacted with bromoacetic acids, also some salts and water presence, structure shown in Table A3.2, entry 2 gives the elemental composition: C, 43.05; H, 6.10; N, 6.28. This is much closer to the experimental value. For PNTA-25, theoretically ration between NTA:AA is 1:3. and figure shown in Table A3.2, entry 3 resemble the structure for the polymer. Elemental composition for that structure is C, 49.62; H, 6.06; N, 5.26. The experimental values are C, 43.69; H, 5.03; N, 2.96. However actual incorporation of NTA:AA is 1:9 and with presence of water and salts, figure shown in Table A3.2, represent the actual structure of the polymer. Elemental composition for this structure is C, 43.08; H, 5.19; N, 2.58 and much closer to the experimental values.

A3.6. Potentiometric Titration of PNTA-X.

A potentiometric titration of PNTA-X was performed according to a literature procedure with slight modifications.[2,3] The pH was monitored using a microprocessor-controlled pH-meter (ORION-420A) with a combined glass/reference electrode calibrated with standard pH 4.0, 7.0, and 10.0 buffers. (Uncertainties in pH values will increase outside of this calibration range.) PNTA-X and PAH were separately adjusted to pH ~12 by adding 5 M NaOH, and 1.0 M HCl served as the titrant for 200 mL of ~1.0 mg/ml PNTA-X. Polymer concentrations are likely overestimated because of adsorbed water and Na$^+$ ions in the PNTA-X. Using a micropipette, the 1.0 M HCl was added in 100-200 μL aliquots, except for close to the equivalent point, where 20 μL aliquots were added. pH values were recorded after establishing equilibrium, which typically required 1-2 min. Figure A4.1 shows the resulting acid-base titration curves. For PNTA-X, the first

equivalence point occurs around pH 6 after complete protonation of amine groups. Since PNTA-100 has a higher number of tertiary amine groups than PNTA-50 and PNTA-25, titration required additional H^+ to protonate these sites for PNTA-100. For all polymers, protonation of the the –COOH groups occurs primarily below pH 4 and is difficult to see.
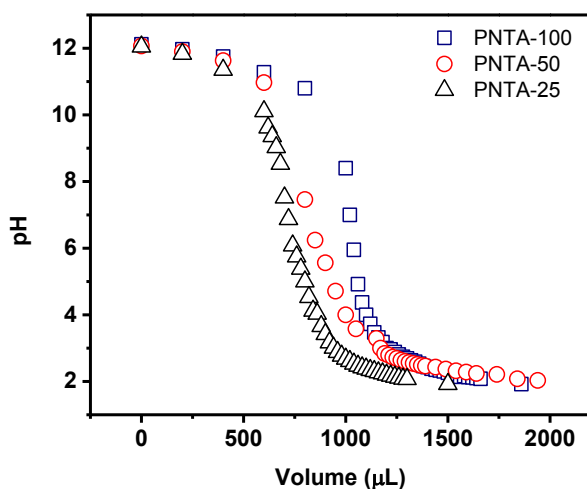
Figure A3.11. Acid-base titration curves for 1 mg/ml PNTA-25 (black triangles), PNTA-50 (red circles) and PNTA-100 (blue-squares). All polymers were initially dissolved in 5 M KOH. The titrant contained 1.0 M HCl and the initial solution volume was 100 mL.

A3.7. LBL Deposition of (PAH/PNTA-X)$_n$ Films.
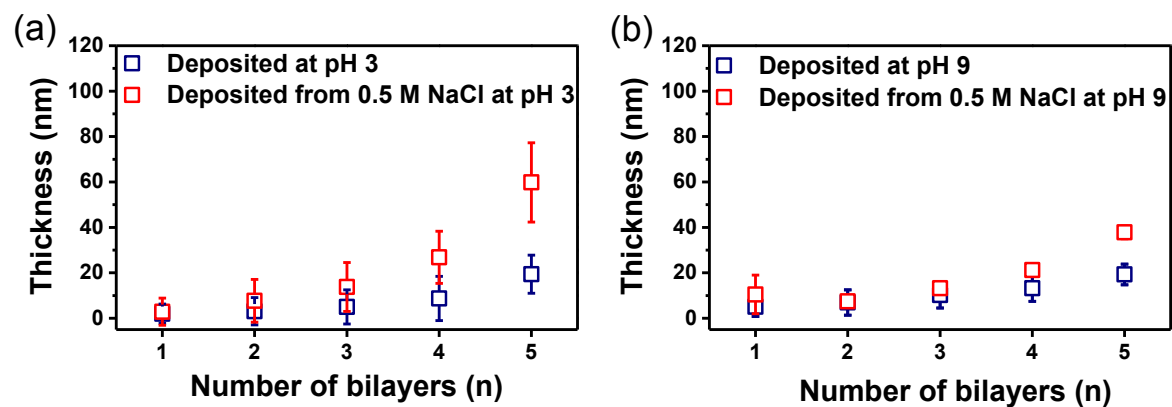
Figure A3.12. Thicknesses of (PAH/PNTA-100)$_n$ films adsorbed from polymer solutions adjusted to (a) pH 3.0 and (b) pH 9.0. Red squares correspond to deposition solutions with no added salt, and blue squares correspond to deposition from solutions containing 0.5 M NaCl.

A3.8. Reflectance IR Spectra of (PAH/PNTA-100)$_n$ Films.
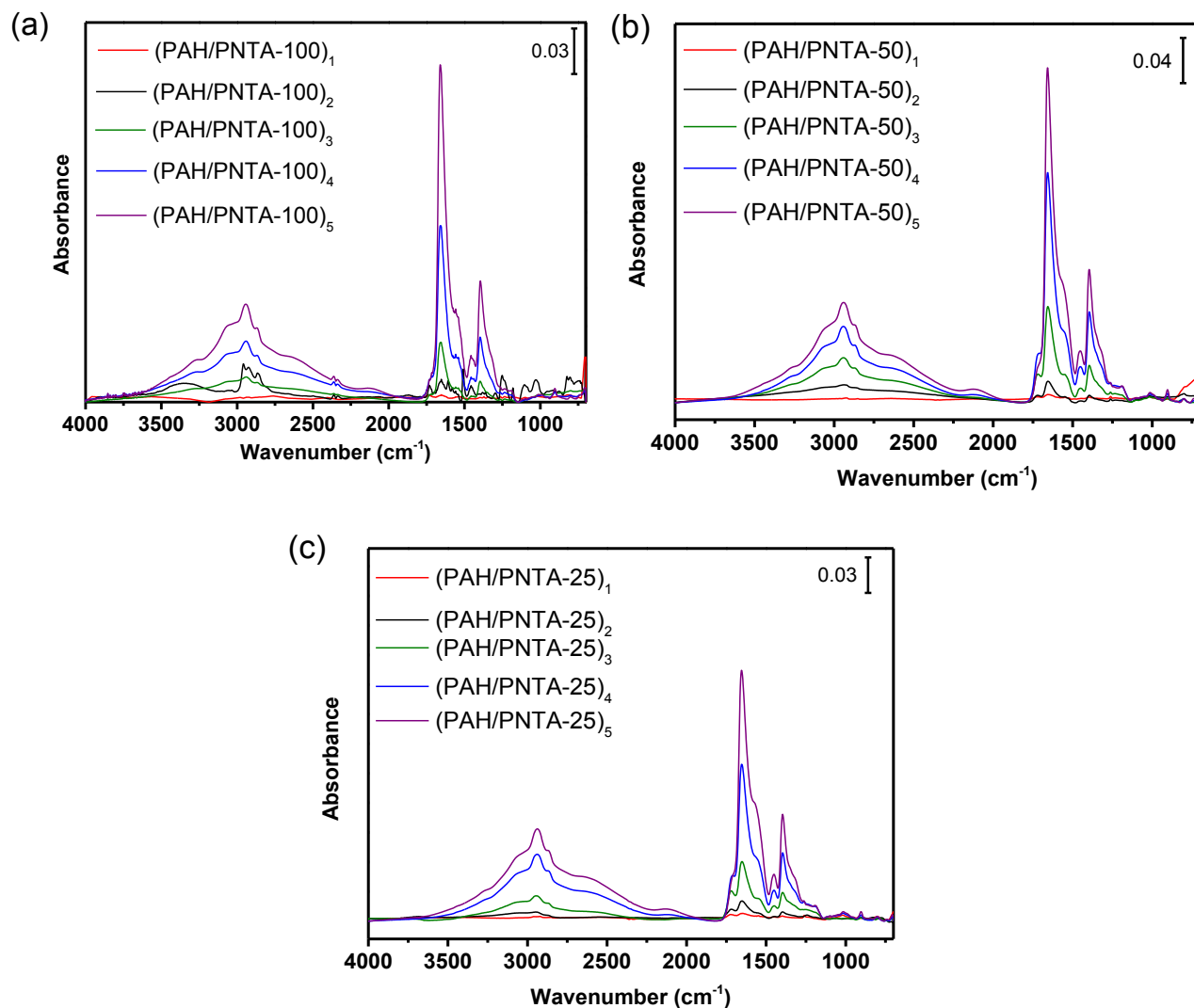
Figure A3.13. Reflectance IR spectra (4000-700 cm^{-1}) of (PAH/PNTA-X)$_n$ films deposited on MPA-modified Au at pH 9 for PAH and pH 3 for PNTA-X. Films were rinsed with deionized water and dried with N$_2$ prior to obtaining the spectra. In each graph, the number of bilayers in the film increase from n=1 (bottom red spectrum) to 5 (top purple spectrum). The large –COO$^-$ stretch at 1650 cm^{-1} relative to the acid carbonyl stretch at 1730 cm^{-1} shows that after rinsing with water most –COOH groups are deprotonated.

A3.9. Swelling of (PAH/PNTA-X)$_3$ Films.

Table A3.3. Swelling percentages for (PAH/PNTA-100)$_3$ and (PAH/PNTA-100)$_3$-Cu^{2+} films assembled at different pH values and immersed in pH 7.4 PBS.

Deposition Conditions	Film	Swelling %
PAH-pH 3, PNTA-pH 3 No salt	(PAH/PNTA-100)$_3$	380±166
	(PAH/PNTA-100)$_3$-Cu^{2+}	131±34
PAH-pH 3, PNTA-pH 3 0.5 M NaCl	(PAH/PNTA-100)$_3$	366±130
	(PAH/PNTA-100)$_3$-Cu^{2+}	30±14
PAH-pH 9, PNTA-pH 9 No salt	(PAH/PNTA-100)$_3$	175±73
	(PAH/PNTA-100)$_3$-Cu^{2+}	130±35
PAH-pH 9, PNTA-pH 9 0.5 M NaCl	(PAH/PNTA-100)$_3$	554±1.0
	(PAH/PNTA-100)$_3$-Cu^{2+}	104±58
PAH-pH 9, PNTA-pH 3 No salt	(PAH/PNTA-100)$_3$	432±178
	(PAH/PNTA-100)$_3$-Cu^{2+}	31±4.0
PAH-pH 9, PNTA-pH 3 0.5 M NaCl	(PAH/PNTA-100)$_3$	500±115
	(PAH/PNTA-100)$_3$-Cu^{2+}	47±1.0
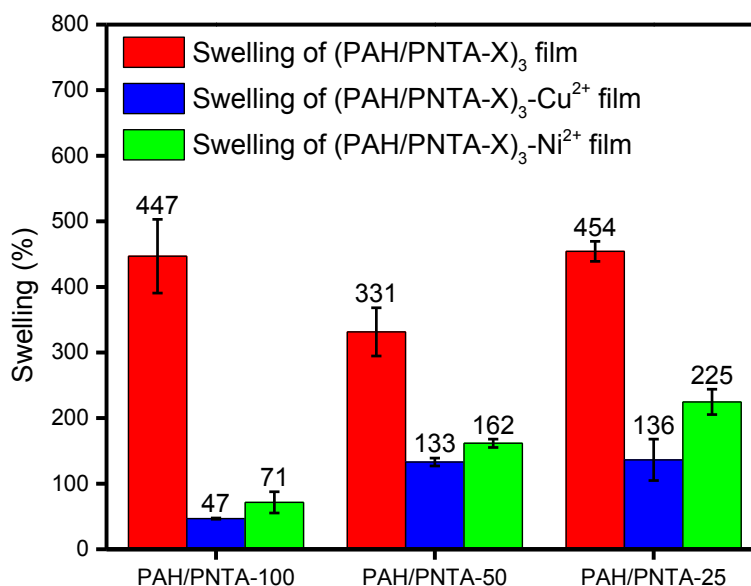
Figure A3.14. Swelling percentages of (PAH/PNTA-X)$_3$ and (PAH/PNTA-X)$_3$-metal ion films deposited at pH 9.0 (PAH) and pH 3.0 (PNTA-X) with 0.5 M NaCl in polyelectrolyte solutions. The swollen ellipsometric thickness of each film was measured after immersion in 20 mM phosphate buffer at pH 7.4 for 10 min.

A3.10. Metal-ion Binding to (PAH/PNTA-X)$_n$ Films Deposited at Different Solution pH Values (pH 3, 9 and pH 9/3) and Constant Ionic Strength.

A3.10.1. Copper Ion Sorption on PAH/PNTA-100 Films on Au Coated-wafers.

Table A3.4. Amounts of Cu^{2+} adsorbed in PAH/PNTA-100 films deposited at different conditions. During metal sorption $C_{Cu^{2+}}$ = 0.1 M and pH =~4.1. Film volumes were calculated using ellipsometric thicknesses of "dry" films without sorbed metal ions.

Deposition Conditions	Film	Cu^{2+}-binding capacity (mmol/cm^3)
PAH-pH 3 PNTA-pH 3 No salt	(PAH/PNTA-100)$_3$	1.6±0.2
PAH-pH 3 PNTA-pH 3 0.5 M NaCl	(PAH/PNTA-100)$_3$	1.2±0.0
PAH-pH 9 PNTA-pH 9 No salt	(PAH/PNTA-100)$_3$	1.6±0.1
PAH-pH 9 PNTA-pH 9 0.5 M NaCl	(PAH/PNTA-100)$_3$	1.5±0.0
PAH-pH 9 PNTA-pH 3 No salt	(PAH/PNTA-100)$_3$	1.9±0.5
PAH-pH 9 PNTA-pH 3 0.5 M NaCl	(PAH/PNTA-100)$_3$	2.1±0.5

A3.10.2. Copper and Nickel Ion Sorption on PAH/PNTA-X Films on Au Coated-Wafers.
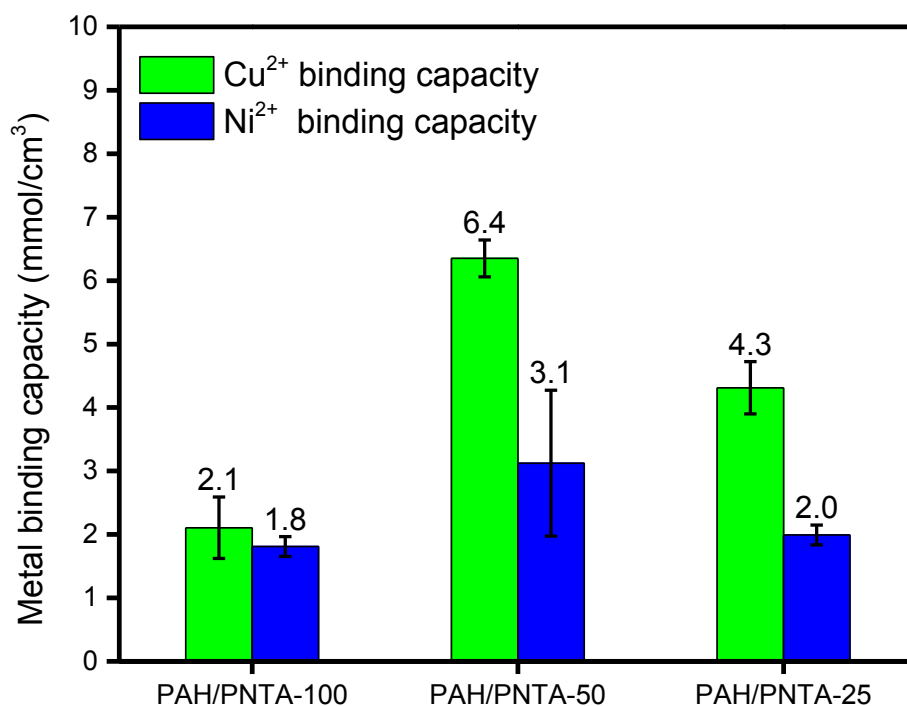
Figure A3.15. Cu^{2+} and Ni^{2+} binding capacities per unit volume of $(PAH/PNTA-X)_3$ films deposited at pH 9.0 for PAH and pH 3.0 for PNTA-X with 0.5 M NaCl in deposition solutions. During metal sorption $C_{M^{2+}}$ = 0.1 M and pH =~4.1. Film volumes were calculated using ellipsometric thicknesses of "dry" films without sorbed metal ions.

A3.11. Effect of Deposition pH on His-tagged Protein Absorption to (PAH/PNTA-100)$_3$-Ni^{2+} Films.
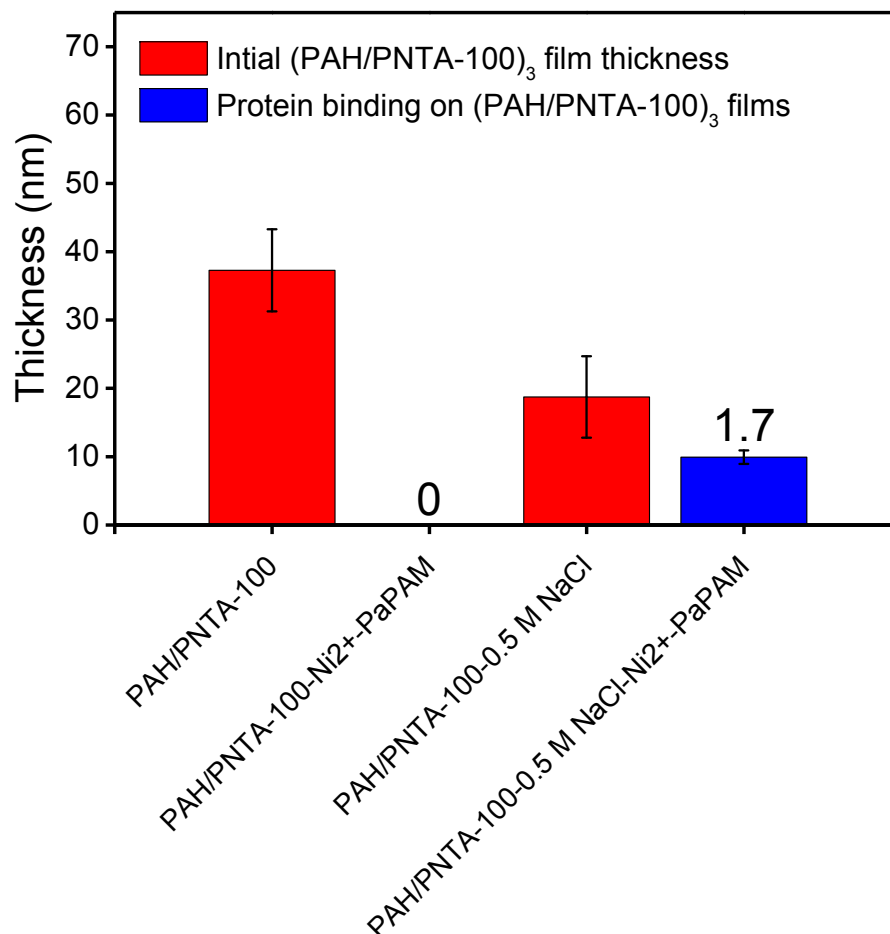
Figure A3.16. Film thicknesses and the equivalent thicknesses of PaPAM sorbed in (PAH/PNTA-100)$_3$ multilayers deposited from polyelectrolyte solutions with or without supporting electrolyte NaCl. Films were deposited at pH 9.0 for PAH and pH 3.0 for PNTA-100. The numbers above the bars represent the ratios of the PaPAM equivalent thickness to the film thickness. The equivalent thickness is the thickness of spin-coated protein that would give an FTIR absorbance equivalent to that of the sorbed PaPAM. Error bars show the standard deviations of measurements on at least three different films.

A3.12. Protein Sorption in (PAH/PNTA-X)$_3$-M^{2+} Films.
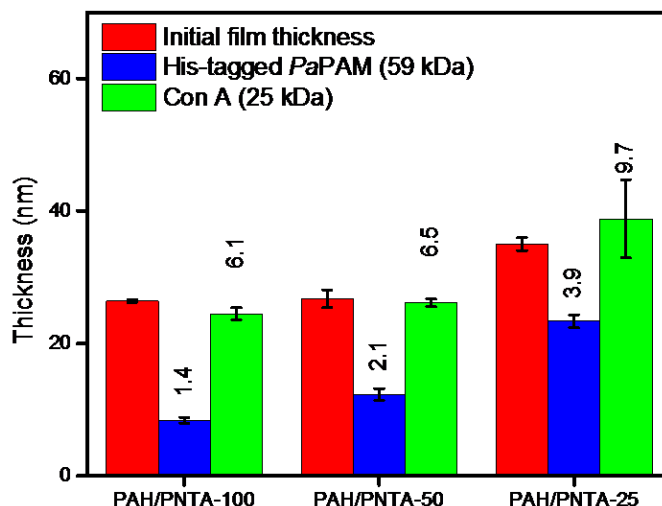
Figure A3.17. Film thicknesses and the equivalent thicknesses of *Pa*PAM and Con A sorbed in (PAH/PNTA-X)$_3$ multilayers deposited from polyelectrolyte solutions with 0.5 M NaCl. Films were deposited at pH 9.0 for PAH and pH 3.0 for PNTA-X. The numbers above the bars represent the ratios of the *Pa*PAM equivalent thickness to the film thickness. The equivalent thickness is the thickness of spin-coated protein that would give an FTIR absorbance equivalent to that of the sorbed *Pa*PAM. Error bars show the standard deviations of measurements on at least three different films.

A3.13. Characteristics of Different Proteins.

Protein	M$_w$ (kDa)	PI (Charge)[a]	Dimensions (nm)[b]
*Pa*PAM	59	5.64 (-)	8.4×3.1×2.9
L-thrionine aldolase[4]	36.5	5.81(-)	5.8×4.7×2.3
Con A[5]	25.5	5.27 (-)	4.2×4.0×3.9
His U	9.6	6.56 (-)	3.2×2.3×2.4

[a]Calculated from protein identification and analysis tools on the ExPASy server
[b]Measured from Pymol software

190

REFERENCES

REFERENCES

(1)   Nagaoka, S.; Shundo, A.; Satoh, T.; Nagira, K.; Kishi, R.; Ueno, K.; Iio, K.; Ihara, H. *Synth. Commun.* **2005**, *35*, 2529-2534.

(2)   Naka, K.; Tachiyama, Y.; Hagihara, K.; Tanaka, Y.; Yoshimoto, M.; Ohki, A.; Maeda, S. *Polym. Bull.* **1995**, *35*, 659-663.

(3)   Petrov, A. I.; Antipov, A. A.; Sukhorukov, G. B. *Macromolecules* **2003**, *36*, 10079-10086.

(4)   di Salvo, M. L.; Remesh, S. G.; Vivoli, M.; Ghatge, M. S.; Paiardini, A.; D'Aguanno, S.; Safo, M. K.; Contestabile, R. *Febs J* **2014**, *281*, 129-145.

(5)   Becker, J. W.; Reeke, G. N.; Wang, J. L.; Cunningham, B. A.; Edelman, G. M. *J. Biol. Chem.* **1975**, *250*, 1513-1524.

REFERENCES

REFERENCES

(1)   Zhang, G.; Ruan, Z.; Ji, S.; Liu, Z. *Langmuir* **2010**, *26*, 4782-4789

(2)   Stanton, B. W.; Harris, J. J.; Miller, M. D.; Bruening, M. L. *Langmuir* **2003**, *19*, 7038-7042.

(3)   Li, T.; Chen, S.; Li, H.; Li, Q.; Wu, L. *Langmuir* **2011**, *27*, 6753-6758.

(4)   Maruyama, T.; Tabayashi, S.; Honjo, T.; Hoe, K.; Tanaka, T.; Shimada, J.; Goto, M.; Matsuyama, H. *Rsc Advances* **2012**, *2*, 125-127.

(5)   Anuraj, N.; Bhattacharjee, S.; Geiger, J. H.; Baker, G. L.; Bruening, M. L. *J. Membr. Sci.* **2012**, *389*, 117-125.

(6)   Bhattacharjee, S.; Dong, J. L.; Ma, Y. D.; Hovde, S.; Geiger, J. H.; Baker, G. L.; Bruening, M. L. *Langmuir* **2012**, *28*, 6885-6892.

(7)   Saito, K.; Tsuneda, S.; Kim, M.; Kubota, N.; Sugita, K.; Sugo, T. *Radiat. Phys. Chem.* **1999**, *54*, 517-525.

(8)   Kawai, T.; Saito, K.; Lee, W. *J. chromatogr. B* **2003**, *790*, 131-142.

(9)   Bhut, B. V.; Husson, S. M. *J. Membr. Sci.* **2009**, *337*, 215-223.

(10)   Ghosh, R. *J. Chromatogr. A* **2002**, *952*, 13-27.

(11)   Datta, S.; Bhattacharyya, D.; Ray, P. D.; Nath, A.; Toborek, M. *Sep. Sci. Technol.* **2007**, *42*, 2451-2471.

(12)   Zhu, H.; Bilgin, M.; Bangham, R.; Hall, D.; Casamayor, A.; Bertone, P.; Lan, N.; Jansen, R.; Bidlingmaier, S.; Houfek, T.; Mitchell, T.; Miller, P.; Dean, R. A.; Gerstein, M.; Snyder, M. *Science* **2001**, *293*, 2101-2105.

(13)   Phizicky, E.; Bastiaens, P. I. H.; Zhu, H.; Snyder, M.; Fields, S. *Nature* **2003**, *422*, 208-215.

(14)   Bruening, M. L.; Zhou, Y. F.; Aguilar, G.; Agee, R.; Bergbreiter, D. E.; Crooks, R. M. *Langmuir* **1997**, *13*, 770-778.

(15)   Ng, K.; Pack, D. W.; Sasaki, D. Y.; Arnold, F. H. *Langmuir* **1995**, *11*, 4048-4055.

(16)   Sigal, G. B.; Bamdad, C.; Barberis, A.; Strominger, J.; Whitesides, G. M. *Anal. Chem.* **1996**, *68*, 490-497.

(17) Xu, F.; Geiger, J. H.; Baker, G. L.; Bruening, M. L. *Langmuir* **2011**, *27*, 3106-3112.

(18) Valiokas, R.; Klenkar, G.; Tinazli, A.; Reichel, A.; Tampé, R.; Piehler, J.; Liedberg, B. *Langmuir* **2008**, *24*, 4959-4967.

(19) Jain, P.; Sun, L.; Dai, J. H.; Baker, G. L.; Bruening, M. L. *Biomacromolecules* **2007**, *8*, 3102-3107.

(20) Jain, P.; Vyas, M. K.; Geiger, J. H.; Baker, G. L.; Bruening, M. L. *Biomacromolecules* **2010**, *11*, 1019-1026.

(21) Mentbayeva, A.; Ospanova, A.; Tashmuhambetova, Z.; Sokolova, V.; Sukhishvili, S. *Langmuir* **2012**, *28*, 11957-11964.

(22) Cao, M.; Wang, J.; Wang, Y. *Langmuir* **2007**, *23*, 3142-3149.

(23) Mentbayeva, A.; Ospanova, A.; Tashmuhambetova, Z.; Sokolova, V.; Sukhishvili, S. *Langmuir* **2012**, *28*, 11948-11955.

(24) Huang, X.; Schubert, A. B.; Chrisman, J. D.; Zacharia, N. S. *Langmuir* **2013**, *29*, 12959-12968.

(25) Wijeratne, S.; Bruening, M. L.; Baker, G. L. *Langmuir* **2013**, *29*, 12720-12729.

(26) Ning, W.; Wijeratne, S.; Dong, J.; Bruening, M. L. *ACS appl. mater. interfaces* **2015**, *7*, 2575-2584.

(27) Anderegg, G. A., F.; Delgado, R.; Felcman, J.; Popov, K. *Pure Appl. Chem.* **2005**, *77*, 1445–1495.

(28) Bhattacharjee, S.; Dong, J.; Ma, Y.; Hovde, S.; Geiger, J. H.; Baker, G. L.; Bruening, M. L. *Langmuir* **2012**, *28*, 6885-6892.

(29) Strom, S.; Wanninayake, U.; Ratnayake, N. D.; Walker, K. D.; Geiger, J. H. *Angew. Chem. Int. Edit.* **2012**, *51*, 2898-2902.

(30) Liu, J.-Q.; Dairi, T.; Itoh, N.; Kataoka, M.; Shimizu, S.; Yamada, H. *Eur. J. Biochem.* **1998**, *255*, 220-226.

(31) Weller, D.; Medina-Oliva, A.; Claus, H.; Gietzen, S.; Mohr, K.; Reuter, A.; Schaffel, D.; Schottler, S.; Koynov, K.; Bros, M.; Grabbe, S.; Fischer, K.; Schmidtt, M. *Macromolecules* **2013**, *46*, 8519-8527.

(32) Harris, J. J.; Bruening, M. L. *Langmuir* **2000**, *16*, 2006-2013.

(33)   Dai, J. H.; Bao, Z. Y.; Sun, L.; Hong, S. U.; Baker, G. L.; Bruening, M. L. *Langmuir* **2006**, *22*, 4274-4281.

(34)   Tahir, M. N.; Natalio, F.; Therese, H. A.; Yella, A.; Metz, N.; Shah, M. R.; Mugnaioli, E.; Berger, R.; Theato, P.; Schroder, H. C.; Muller, W. E. G.; Tremel, W. *Adv. Funct. Mater.* **2009**, *19*, 285-291.

(35)   Zhen, G.; Zurcher, S.; Falconnet, D.; Xu, F.; Kuennemann, E.; Textor, M. In *Conference proceedings, Annual International Conference of the IEEE Engineering in Medicine and Biology Society. IEEE Engineering in Medicine and Biology Society. Annual Conference*; 2007/02/07 ed. 2005; Vol. 1, p 1036-1038.

(36)   Ehrbar, M.; Schoenmakers, R.; Christen, E. H.; Fussenegger, M.; Weber, W. *Nature materials* **2008**, *7*, 800-804.

(37)   Nagaoka, S.; Shundo, A.; Satoh, T.; Nagira, K.; Kishi, R.; Ueno, K.; Iio, K.; Ihara, H. *Synthetic Commun.* **2005**, *35*, 2529-2534.

(38)   Shiratori, S. S.; Rubner, M. F. *Macromolecules* **2000**, *33*, 4213-4219.

(39)   Irving, H. M. N. H.; Miles, M. G. *Journal of the Chemical Society A: Inorganic, Physical, Theoretical* **1966**, 1268-1275.

(40)   Nakamoto, K.; Morimoto, Y.; Martell, A. E. *J. Am. Chem. Soc.* **1962**, *84*, 2081-2084.

(41)   Choi, J.; Rubner, M. F. *Macromolecules* **2005**, *38*, 116-124.

(42)   Sinitsyna, T. A.; Alekseeva, I. A.; Voronina, N. M. *J. Appl. Spectrosc.* **1980**, *32*, 362-364.

(43)   Picart, C.; Senger, B.; Sengupta, K.; Dubreuil, F.; Fery, A. *Colloid Surface A* **2007**, *303*, 30-36.

(44)   Crank, J. *The Mathematics of Diffusion*; Oxford University Press: Bristol, England, 1979.

(45)   Nieba, L.; Nieba-Axmann, S. E.; Persson, A.; Hämäläinen, M.; Edebratt, F.; Hansson, A.; Lidholm, J.; Magnusson, K.; Karlsson, Å. F.; Plückthun, A. *Anal. Biochem.* **1997**, *252*, 217-228.

(46)   Uhlig, K.; Madaboosi, N.; Schmidt, S.; Jager, M. S.; Rose, J.; Duschl, C.; Volodkin, D. V. *Soft Matter* **2012**, *8*, 11786-11789.

(47)   HisTrap FF crude for faster purification of histidine-tagged protein. http://www.gelifesciences.com/webapp/wcs/stores/servlet/ProductDisplay?catego ryId=11448&catalogId=10101&productId=19665&storeId=11787&langId=-1 (accessed July 16, 2015).

CHAPTER 4. POROUS STAR-STAR POLYELECTROLYTE MULTILAYERS FOR ENHANCED PROTEIN-BINDING KINETICS AND CAPTURE.

4.1. Introduction.

Layer-by-layer (LBL) assembly is a versatile method for fabrication of ultrathin[1,2] to µm-thick coatings[3,4] with a range of compositions. Tailoring of the composition and permeabilities of these films makes them attractive in antifogging coatings,[5] nanofiltration membranes,[6-8] drug delivery,[9,10] and protective clothing.[11] Although many of these functions of polyelectrolyte multilayers (PEMs) rely on limiting or controlling film permeability, for applications such as capture of proteins high swelling[12] and permeability[13] are essential. In the case of PEMs with weak polyelectrolytes, ionization by either protonation of deprotonation of polyelectrolytes after film formation may lead to chain rearrangement due to charge repulsion and uptake of water and ions into the film.[14] This and related strategies can increase swelling to enhance the rate or amount of adsorption in such films. Nevertheless, such swelling may not create sufficient space for rapid adsorption of large biomacromolecules throughout PEMs.

This work aims to create porous PEMs to facilitate protein diffusion and adsorption in these coatings. We focus on PEMs with star polyelectrolytes because compared to their linear counterparts, PEMs with star polymers should show less chain entanglement and facilitate protein permeation.[15] Previous efforts to create porous PEMs employed post-deposition solvent etching[16] and UV,[17] thermal,[18,19] acid,[16,20,21] or salt[22,23] treatments. Nanoporous films can also form through self-assembly of building

blocks such as charged silica particles,[24,25] block copolymers and micelles.[26-28] Of particular importance to this work, Hammond et al. showed that post-deposition acid treatment of star-poly[2-(dimethylamino)ethyl methacrylate] (star-PDMAEMA) and star-poly(acrylic acid) (star-PAA) LBL films leads to porous surfaces.[16] Guo et al. found that LBL films of star PDMAEMA/poly(sodium 4-styrenesulfonate) grow exponentially with the number of layers as a function of arm length and number of arms.[29] The number of star polymer arms also affects film morphological changes after acid treatment. Apart from these studies, several other groups performed LBL assembly with star polyelectroytes. Tsukruk et al.[15] used star-PDMAEMA and -PAA to construct LBL films and study pH-controlled film growth. Using hydrogen bonding, Yang et al. formed composite thin films composed of poly(vinylpyrrolidone) and star-shaped PAA with a poly(methylsilsesquioxane) core.[30] Moreover, Connal et al. showed that thin films assembled with star-PAA and linear poly(allylamine hydrochloride) (PAH) show pH-responsive reversible morphological transitions.[31] Although these studies discuss the surface morphologies of films containing star polymer, they did not demonstrate direct formation of porous films upon deposition of star polyelectrolytes.

This work aims to fabricate porous star-polymer multilayer coatings without post treatment, and to utilize these porous coatings for rapid protein capture on both flat substrates and in porous membranes. We report the preparation of porous star LBL films using anionic star-PAA and cationic star-PDMAEMA. Porosity and swelling vary with the number of arms on the star polymers and the number of layers in the film, and pore diameters reach 800 nm. Remarkably, highly swollen films bind 10-20 multilayers

of protein, and membranes capture as much as 120 mg of lysozyme per mL of membrane at pH 5.4.

4.2. Experimental.

4.2.1. Materials.

Triethylamine was distilled from calcium hydride under a nitrogen atmosphere and stored under nitrogen. Monomers, 2-(dimethylamino)ethyl methacrylate (DMAEMA, 98%) and *tert*-butyl acrylate (*t*BA, 98%), were passed through a column of activated basic alumina (length × diameter: 10 cm × 3 cm) to remove inhibitors before synthesis of star-DMAEMA or star *tert*-butyl acrylate (star-*t*BA). 1,3,5-trihydroxybenzene (Aldrich, ≥99.0% (HPLC)), pentaerythritol (Aldrich, 98%) and dipentaerythritol (Aldrich, technical grade) were dried in vacuo at room temperature before use. 2-Bromoisobutyryl bromide (Fluka, 97%) and 4-dimethyl-aminopyridine (DMAP) (Fluka, 99%) were used as received. *N,N,N',N",N"*-pentamethyldiethylenetriamine (PMDETA) (Aldrich, 99%), 1,1,4,7,10,10-hexamethyltriethylenetetramine (HMTETA), CuBr (Aldrich, 99.999%) and acetone (Aldrich, 99%) were used without further purification. Other solvents such as THF, DMF, dichloromethane, ethanol and methanol were reagent or HPLC grade. Trifluoroacetic acid (TFA) (Aldrich, 99%) was used for hydrolysis. The supporting information describes the synthesis of star polymers and also provides NMR spectra of the polymers (Figures A4.11 and A4.13) along with the hydrodynamic radii of polymers at different pH values (Figure A4.16) (Figure numbers beginning with "A" refer to the supporting information in appendix). Cationic and anionic star polymers are abbreviated

as follows, star-poly[2-(dimethylamino)ethyl methacrylate] (star-PDMAEMA-X) and star-poly(acrylic acid) (star-PAA-X). X, the number of arms in each star polymer, was 3, 4 or 6.

4.2.2. Synthesis of star-polyelectrolytes.

Star- PDMAEMA and -PAA were synthesized by ATRP in a core-first approach following a modified literature procedure.[32,33,34,35] The appendix described the polyelectrolyte synthesis in detail.

4.2.3. LBL assembly of star polymers at low pH and constant ionic strength.

Aqueous solutions of 0.01 M PDMAEMA-X or PAA-X (polymer concentrations are given with respect to the repeating unit assuming repeat unit molecular masses of PAA = 76.1 g mol^{-1} and PDMAEMA = 157 g mol^{-1}) were prepared in deionized water (18.2 MΩcm, Milli-Q) containing 0.5 M NaCl . Star-PAA-containing solutions with a pH of 3.0 were obtained by first dissolving the polymer with the addition of 6 M NaOH to achieve a pH 9.0 solution and then adjusting the pH with 6 M HCl. Gold-coated wafers prepared by sputter coating of 200 nm of gold on 20 nm of Cr on Si(100) wafers (coating was performed by LGA Thin Films, Santa Clara, CA) were cleaned in a UV/O$_3$ chamber for 30 min just before use. A monolayer with -COOH groups was adsorbed on Au-coated Si wafers (24 mm × 11 mm) by immersing the wafer in 5 mM MPA in ethanol for 12 h, rinsing with ethanol, and drying with N$_2$. A star-PDMAEMA-X layer was

deposited by immersion of an MPA-coated substrate in a 0.01 M solution of star-PDMAEMA-X for 5 min, where solution pH values were adjusted to pH 3.0 prior to adsorption (with 0.5 M NaCl in solutions). After washing with pH 3 water (~0.001 M HCl) for ~1 min and drying with N_2, the Au-MPA(star-PDMAEMA-X) substrates were immersed in a 0.01 M star-PAA solution (adjusted to the desired pH of 3.0 with 0.5 M NaCl in solutions) for 5 min and again rinsed with pH 3 water and dried with N_2. This polyelectrolyte adsorption process was repeated to obtain the desired number of Au-MPA(star-PDMAEMA-X /star-PAA-X)$_n$ multilayers.

4.2.4. Characterization of Initiators, Monomers, Polymers, and (PDMAEMA-X/PAA-X)$_n$ Films.

The appendix provides detailed characterization of initiators, monomers and polymers. The thicknesses of multilayer polyelectrolyte films were determined with a rotating analyzer spectroscopic ellipsometer (model M-44, J. A. Woollam) using WVASE32 software. Both refractive index and thickness were fitting parameters. A Cauchy model, $n(\lambda) = A_n + \dfrac{B_n}{\lambda^2} + \dfrac{C_n}{\lambda^4}$ was employed to fit the refractive index as a function of wavelength. In situ ellipsometry in aqueous solutions was performed using a home-built cell described previously.[36] After the dry layer thickness was determined in air, pH 5.4 phosphate buffer (20 mM) was added to the cell, and the thickness of the swollen film was recorded after 10 min. Reflectance Fourier Transform Infrared (reflectance FTIR) spectra of films were obtained with a Thermo Nicolet 6700 FTIR spectrometer

that contained a mercury-cadmium telluride detector and a PIKE grazing angle (80°) attachment. Typically, 128 scans were collected for each spectrum. The AFM morphology images (Cypher™ atomic force microscope) of (star-PDMAEMA-X/star-PAA-X)$_n$ films on Au-coated wafers were recorded in tapping mode (amplitude ratio = 0.90-0.99) using a silicon nitride tip. AFM images are shown in height mode without any image processing except flattening. Scanning rates were between 1.0 and 2.0 Hz.

4.2.5. Lysozyme Binding.

Substrates coated with (star-PDMAEMA-X/star-PAA-X)$_n$ were immersed in 1.0 mg/mL lysozyme (Sigma, lyophilized powder, >90%) in 20 mM phosphate buffer (pH 5.4) for 24 h. Because these films are not stable in pH 7.4 phosphate buffer, we choose pH 5.4 buffer for swelling and protein binding studies. After protein sorption, each substrate was separately rinsed with 5 mL of washing buffer (20 mM phosphate buffer at pH 5.4) and 10 mL of deionized water for ~1 min each and dried with N$_2$. The amount of lysozyme binding was determined by reflectance FTIR spectroscopy and reported with respect to the equivalent thickness of spin-coated lysozyme which would give a similar absorbance. The equivalent thickness d can be calculated from the difference of absorbance (ΔA) at 1680 cm^{-1} (amide band I of lysozyme) before and after binding lysozyme, using the equation d(nm) = $\Delta A/0.0017$.[37]

Lysozyme binding capacities of porous membranes were obtained using breakthrough curves obtained by passing protein solutions (in 20 mM phosphate buffer at pH 5.4) through membranes with 3.1 cm^2 of exposed external membrane surface

area. Bradford assays (using calibration with the protein of interest) were employed to quantify the concentrations of proteins in the membrane effluent or eluate. Prior to protein elution with 0.5 M NaCl, the protein-containing membrane was rinsed with 10 mL of 20 mM phosphate buffer (pH 5.4).

4.3. Results and Discussion.

4.3.1. LBL Assembly of Porous Star Polymer Films.

This work aims to create porous thin films to enhance the rate and amount of protein binding in platforms such as porous membranes. We hypothesized that at appropriate ratios of polyanion and polycation charge, aggregates of star-PDMAEMA and star-PAA would give porous surfaces. Prior work shows that post-deposition treatment of PEMs with salts creates some film porosity due to electrostatic screening.[38,39] Therefore, we added salts to each polyelectrolyte solution.

As Figure 4.1a shows, the first step in film formation, deposition of cationic star polymer, templates the surface coverage, which should depend on the number of arms (geometry) and charge density of the cationic star polymer. Hence we employed three different cationic star polymers in an effort to vary coverage. Washing (Figure 4.1b) should remove loosely bound polymers and eventually give islands of polyelectrolyte. Subsequent adsorption of star-polyanions (Figure 4.1c) may create cationic-anionic polymer aggregates on the surface. Similar to the cationic polymer, the arm number and charge density of these electrolytes should determine the amount and how strongly

these polymers adsorb to the surface. Repeating this procedure (Figure 4.1d) n times, will increase the layer thickness as well as the surface coverage (aggregates grow in the z-, x-, and y-direction). Eventually small aggregates will merge to form larger polyelectrolyte domains.   However washing should again remove loosely bound polyelectrolyte from the surface (Figure 4.1e), so only stable polyelectrolyte domains remain on the surface. With increasing numbers of bilayers, adjacent domains will grow and merge (Figure 4.1f). Drying may rearrange the polyelectrolyte domains to form macro pores (Figure 4.1g), but at large numbers of bilayers (Figure 4.1h) the film will eventually fully cover the surface.
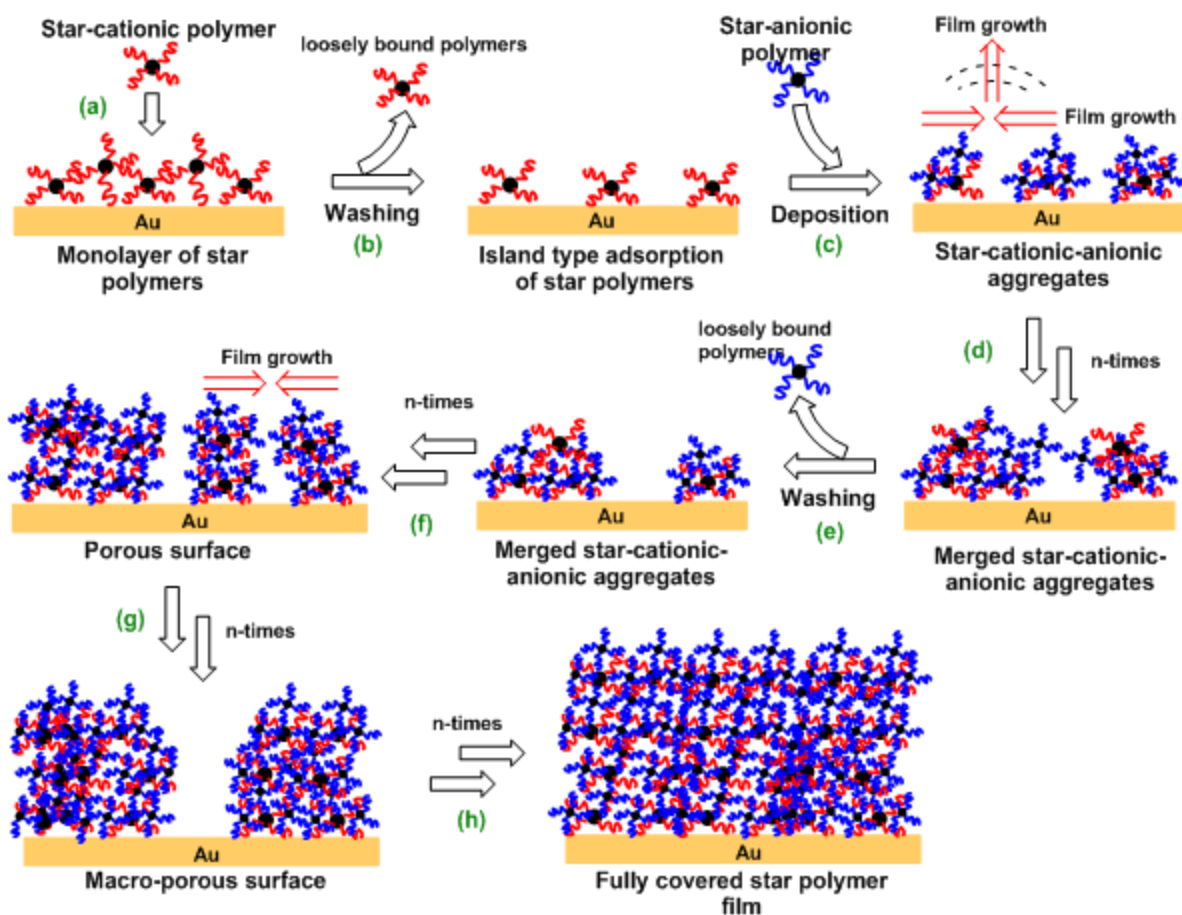
Figure 4.1. Schematic representation of porous film formation with star-cationic (PDMAEMA) and star-anionic (PAA) polymers.

To examine pore formation, we constructed PEMs with cationic star-PDMAEMA and anionic star-PAA having different numbers of arms (3 and 4) and similar molecular weights (see characteristics of all components in Tables A4.1, A4.2 and A4.3). The pH of polyelectrolyte deposition affects the charge density and hence the conformation of the polymers.
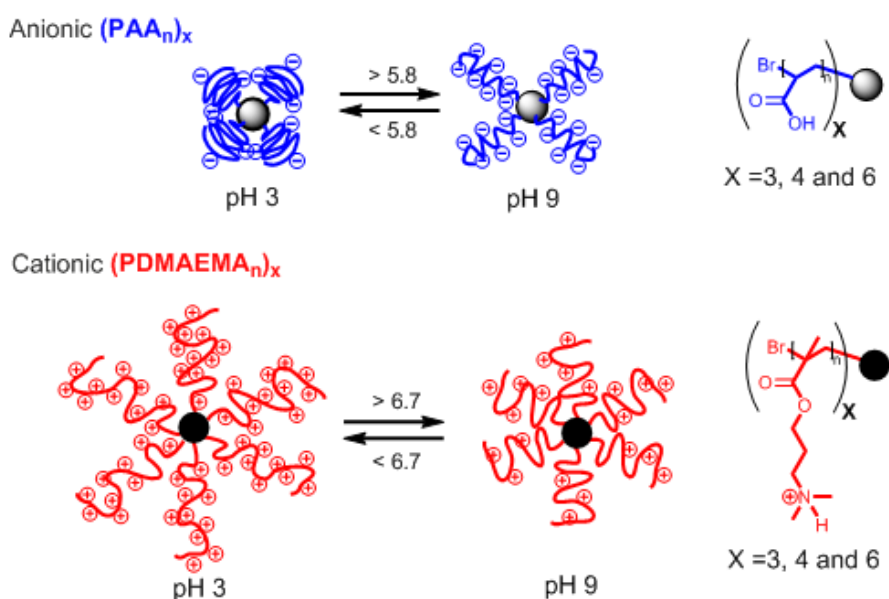
Scheme 4.1. pH-dependent molecular conformations of (a) PAA-X and (b) PDMAEMA-X star polyelectrolytes.

Typically, the average pK_a values of star polymers differ from those of their linear counterparts due to a more dense packing of charged groups in the star structures. As examples, the pKa of protonated PDMAEMA decreases from 7.0 (linear) to 6.8 (star) and that of PAA changes from 5.8 (linear) to 6.4 (star).[40] These numbers should vary slightly with number of arms in the star polymer. Based on these average pK_a values, we chose pH 3.0 as the deposition pH for PDMAEMA to achieve full protonation of this

polycation. At low pH values, the PDMAEMA arms will extend due to electrostatic repulsion between protonated side chains (Scheme 4.1, the appendix discusses hydrodynamic radii). On the other hand, star-PAA is mostly protonated at pH 3 and should exist in a compact form (Scheme 4.1) due to reduced electrostatic repulsion between acid side chains.

Figure 4.2 shows dry ellipsometric thicknesses of (star-PDMAEMA-X/star-PAA-X)$_n$ films adsorbed at pH 3. Film thickness increases nonlinearly with the number of layers, regardless of the number of arms in the polymer. However, comparison of polymers with different numbers of arms reveals a lower thickness for films when PAA contains 3 rather than 4 arms (Figure 4.2). In the case of PDAEMA, increasing the number of arms from 3 to 4 has little effect on the film thickness.
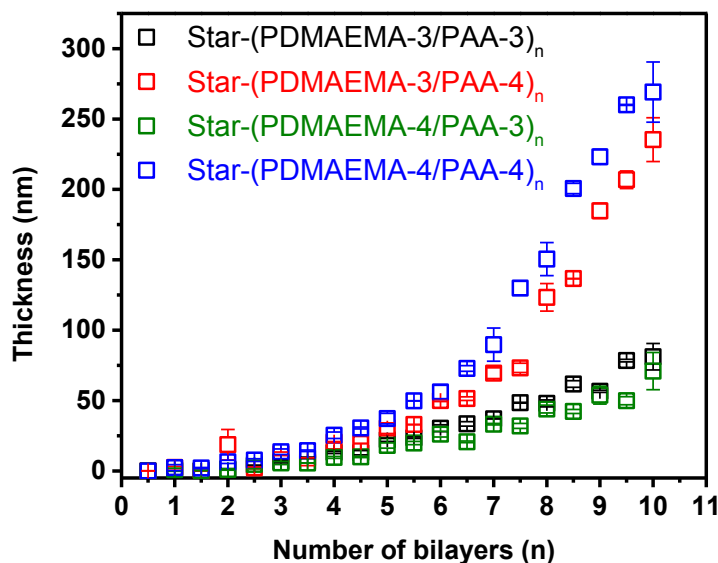
Figure 4.2. Evolution of the ellipsometric thicknesses of LBL multilayer films assembled with star polymers containing either 3 or 4 arms. Films with a non-integer number of bilayers terminate in PAA. All films were assembled at pH 3 from a solution containing 0.5 M NaCl.

4.3.2. Film Morphology.

The formation of a porous film is particularly evident for (star-PDMAEMA-4/star-PAA-4)$_n$ films. The diameters of the spherical features (70-150 nm diameter, Figure 4.3a) in the AFM image of a (star-PDMAEMA-4/star-PAA-4)$_2$ film indicate formation of polycation-polyanion aggregates. Moreover, the size of the features in the AFM image increases on going from 2 to 4 bilayers in the film suggestion coalescence of smaller aggregates. The width of features in the 4-bilayer film ranges from 300-420 nm (see Figure 4.3b).
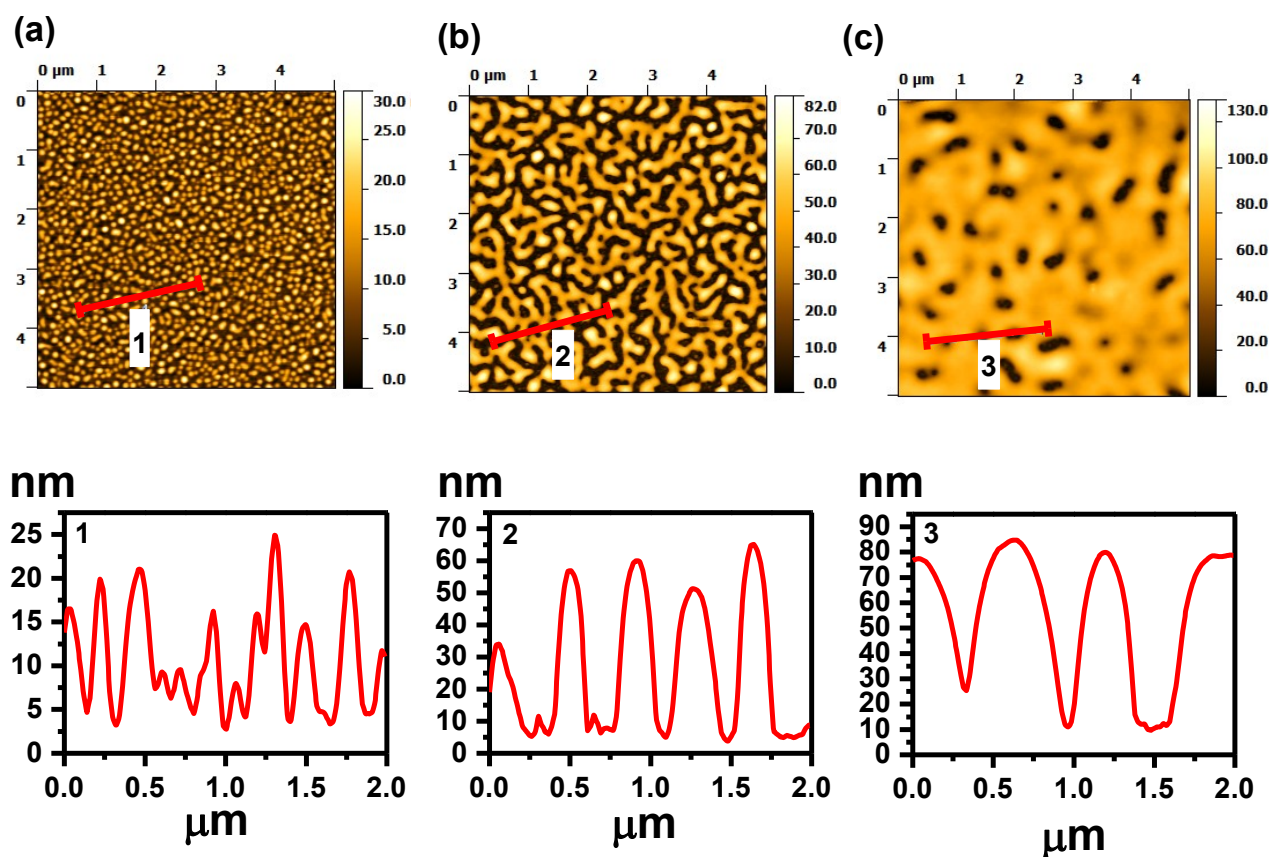
Figure 4.3. Top views and line-scan analyses from AFM images of (a) (star-PDMAEMA-4/star-PAA-4)$_2$, (b) (star-PDMAEMA-4/star-PAA-4)$_4$, and (c) (star-PDMAEMA-4/star-PAA-4)$_6$.

However, further increasing the bilayer number to 6 leads to an apparent increase in surface coverage and the formation of spherical features with diameters of 200-550 nm (Figure 4.3 c). Figure 4.4 schematically depicts (star-PDMAEMA-4/star-PAA-4)$_2$ and (star-PDMAEMA-4/star-PAA-4)$_6$ films.
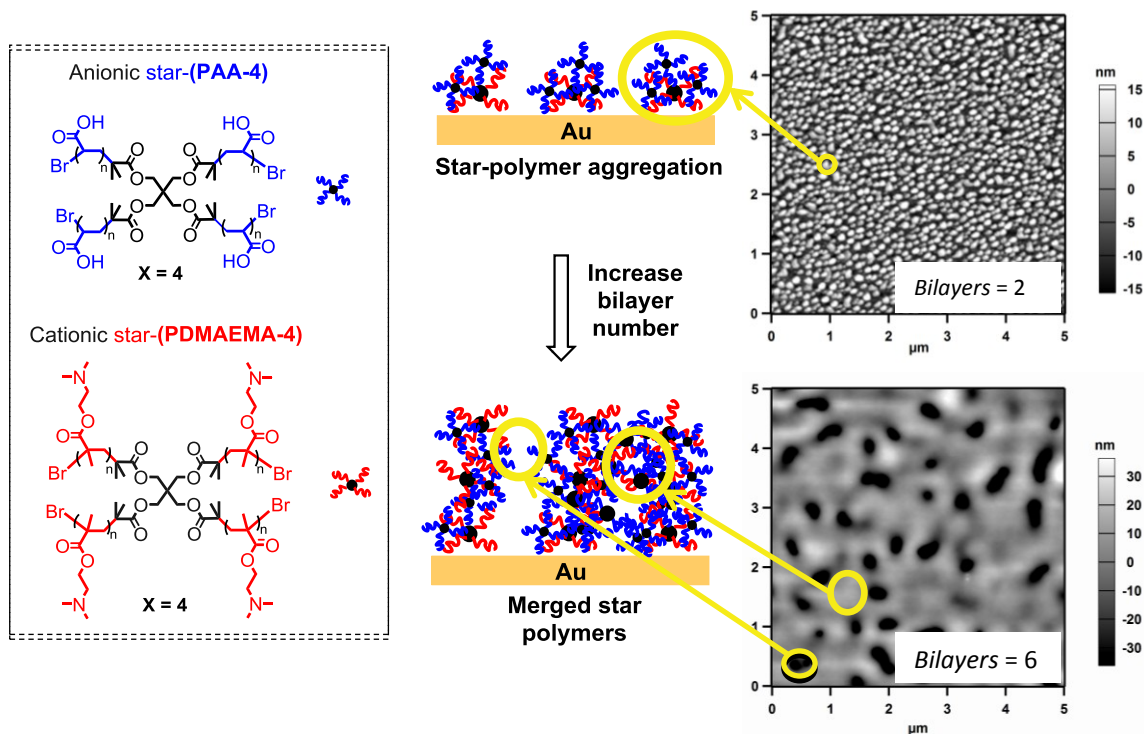
Figure 4.4. Schematic illustration of the structure of porous (star-PDMAEMA-4/star-PAA-4)$_2$ and (star-PDMAEMA-4/star-PAA-4)$_6$ films.

We also investigated the effect of the number of star polymer arms on film morphology. Figure 4.5 shows AFM images of (PDMAEMA-X/PAA-X)$_n$ films (X=3 and 4) with n=2,4, or 6. Due to the small size of star pAA-3 at this pH, films prepared with this polymer show no large features (Figure 4.5a-c and g-i).
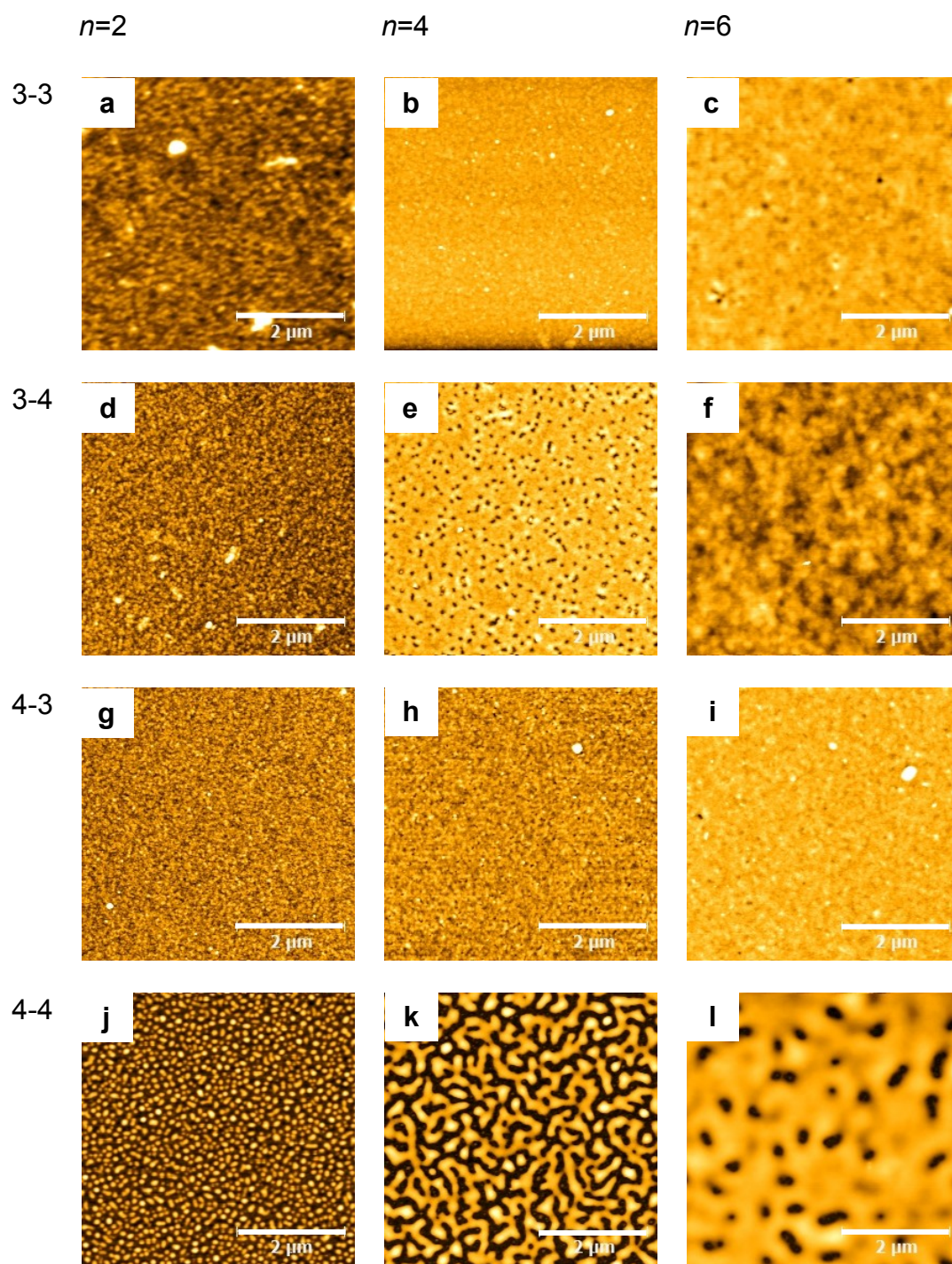
Figure 4.5. Representative AFM images of (star-PDMAEMA-X/star-PAA-X)$_n$ multilayer films with n = 2 to 6 (denoted at the top) and X = 3 and 4 (listed at the left for PDMAEMA follow by PAA). All images are in height mode with dimensions of 5 × 5 μm^2.

In contrast, (star-PDMAEMA-3/star-PAA-4)$_4$ films form well distributed pores diameters ranging from 190-250 nm (Figure 4.5g-i) after adsorption of 4 bilayers. Further increasing the bilayer number to 6 leads to some macropores (Figure 4.5f) but enhanced surface coverage. Films comprised of PAA-4 and PDMAEMA-4 show the largest and most distinct features in AFM images (Figure 4.5j-l). Thus, larger polymers appear to give the most aggregation and largest features. RMS roughnesses (Figure 4.3) are consistent with the larger features in (star-PDMAEMA-4/star-PAA-4)$_n$ films.
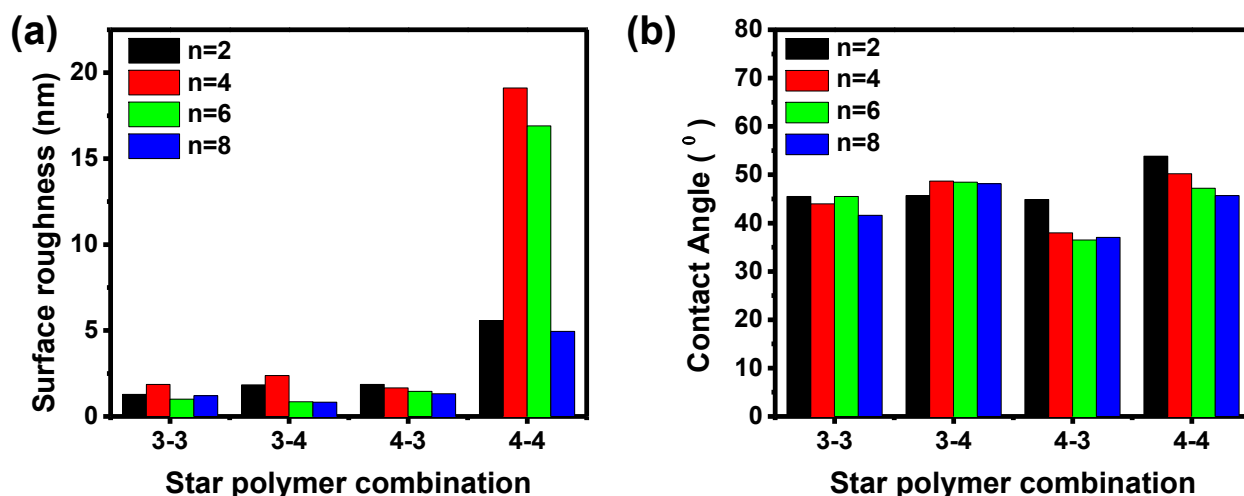
Figure 4.6.(a) rms roughness and (b) static contact angles for (star-PDMAEMA-X/star-PAA-X)$_n$ films with differn numbers of bilayers (n). The labels 3-3, 3-4, 4-3, and 4-4 refer to the number of arms on PEMAEMA (first number) and PAA (second number).

Surface wettability depends on both the surface chemical composition and roughness.[41] Figure 4.6b shows contact angles of a pH 3 water droplet on (star-PDMAEMA-X/star-PAA-X)$_n$ films. The static contact angles of the PEM surfaces are all fairly similar, ranging from 35-55º. For contact angles less than 90º, increased surface roughness should decrease the contact angle, although roughness at the nm scale

shown in these images should only have a small effect.[42] Essentially, all films show similar wetabilities, which is consistent with both comparable compositions for all the films and contact angles on other polyelectrolyte surfaces.[43,44]

4.3.3. Swelling and Variation of Lysozyme Sorption with the Number of Polyelectrolyte Bilayers.

This work aims to create thin coatings that selectively bind proteins in platforms such as porous membranes, and film swelling is vital to achieving high protein binding. Figure 4.7 shows the percent increase in film ellipsometric thickness (percent swelling) after immersion of (star-PDMAEMA-X/star-PAA-X)$_n$ films in a pH 5.4, 20 mM phosphate buffer. All star-PDMAEMA-X/star-PAA-X films with 4 bilayers show swelling of 180% or more, but (star-PDMAEMA-3/star-PAA-3)$_4$ films swell nearly 350%. Regardless of star polymer combination, with an increasing number of bilayers the swelling percentage decreases, suggesting decreasing porosity as well as increasing charge-charge cross linking between the film.[45]   While keeping the star-PDMAEMA arm number constant at 3 or 4, increasing the star-PAA arm number from 3 to 4 decreases the swelling percentage (see Figure 4.7a and b).
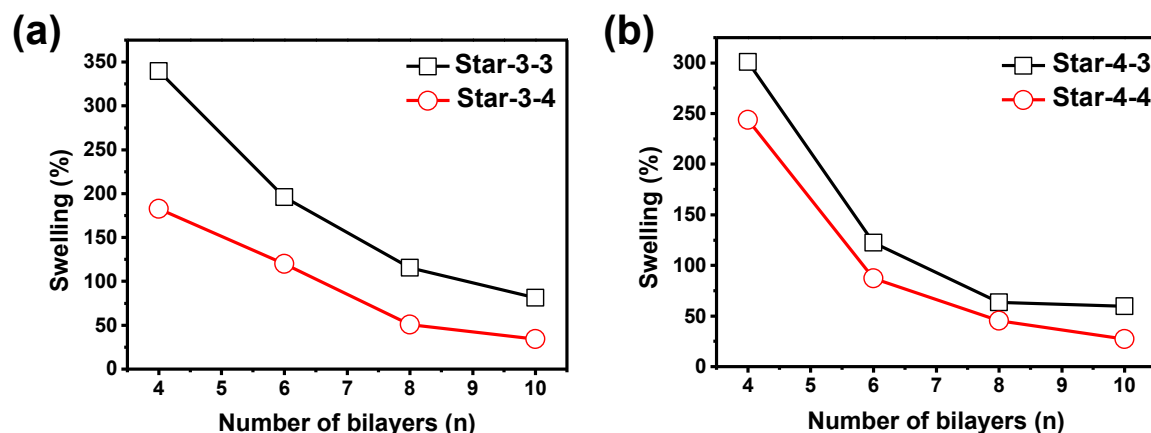
Figure 4.7. Swelling percentages star- (a) (star-PDMAEMA-3/star-PAA-3)$_n$ and (star-PDMAEMA-3/star-PAA-3)$_n$, and (b) (star-PDMAEMA-4/star-PAA-3)$_n$ and (star-PDMAEMA-4/star-PAA-4)$_n$ films.

Protein-binding studies first examined capture of lysozyme in (star-PDMAEMA-X/star-PAA-X)$_n$ films adsorbed on Au-coated Si wafers modified with MPA. Capture occurs when positively charge lysozyme binds to negatively charged star-PAA. Using reflectance FTIR spectroscopy, we determined the amount of protein binding based on the amide absorbance, which we compare to the absorbance in spin-coated films. To examine PEMs with similar dry thicknesses, we initially quantified binding to (star-PDMAEMA-3/star-PAA-3)$_7$, (star-PDMAEMA-4/star-PAA-3)$_7$, (star-PDMAEMA-3/star-PAA-4)$_5$ and (star-PDMAEMA-4/star-PAA-4)$_5$. These films have "dry" ellipsometric thickness of 37, 33, 30 and 37 nm, respectively. All of the films show similar lysozyme capture: (star-PDMAEMA-3/star-PAA-3)$_7$ and (star-PDMAEMA-4/star-PAA-3)$_7$ films bind ~4-5 fold of protein (138-144 nm) compare to initial thickness, whereas (star-PDMAEMA-3/star-PAA-4)$_5$ and (star-PDMAEMA-4/star-PAA-4)$_5$ films bind four fold (95-134 nm) of protein. This protein binding correlates well with the swelling of these films. The increase in thickness upon lysozyme binding is similar to the increase in thickness

due to swelling. Ma et al,[46] showed that under similar film deposition conditions (pH 3 and with 0.5 M NaCl) (PAH/PAA)$_5$ films prepared from linear polymers have a dry film thickness of 30 nm and bind the equivalent of 18.9 ± 0.2 nm of lysozyme in pH 5 phosphate buffer. This is significantly lower than the corresponding amount of protein binding to the star-polyelectrolyte films with similar thicknesses. However, for protein-binding in a pH 7.4 buffer, the equivalent thickness of protein bound to (PAH/PAA)$_5$ increases to 150 nm. Higher swelling at pH 7.4 as well as a greater negative charge likely leads to increased lysozyme sorption. The star-polymer films apparently have sufficient swelling and charge to binding such high protein amounts at a lower pH (5.4). Unfortunately, the star polymer films are not stable at pH 7.4.

Figure 4.8 shows the thicknesses of a range of star polymer films along with the equivalent thickness of lysozyme that they bind. Most notably, for (star-PDMAEMA-3/star-PAA-4)$_4$ and (star-PDMAEMA-4/ star-PAA-4)$_4$ films (Figure 4.8b and d) the protein binding capacity reaches a maximum for films with 7 bilayers. The rapid decline in protein binding after adsorption of additional bilayers is consistent with the AFM studies that show increased surface coverage for films with more than 8 bilayers. This suggests that film pores facilitate protein binding on (star-PDMAEMA-3/star-PAA-4)$_n$ and (star-PDMAEMA-4/star-PAA-4)$_n$ films with <8 bilayers. Once the pores coalesce steric effects dramatically limit protein binding. As Figure 4.9 shows, films with 8-bilayer show features with much less depth than films with 6 bilayers.
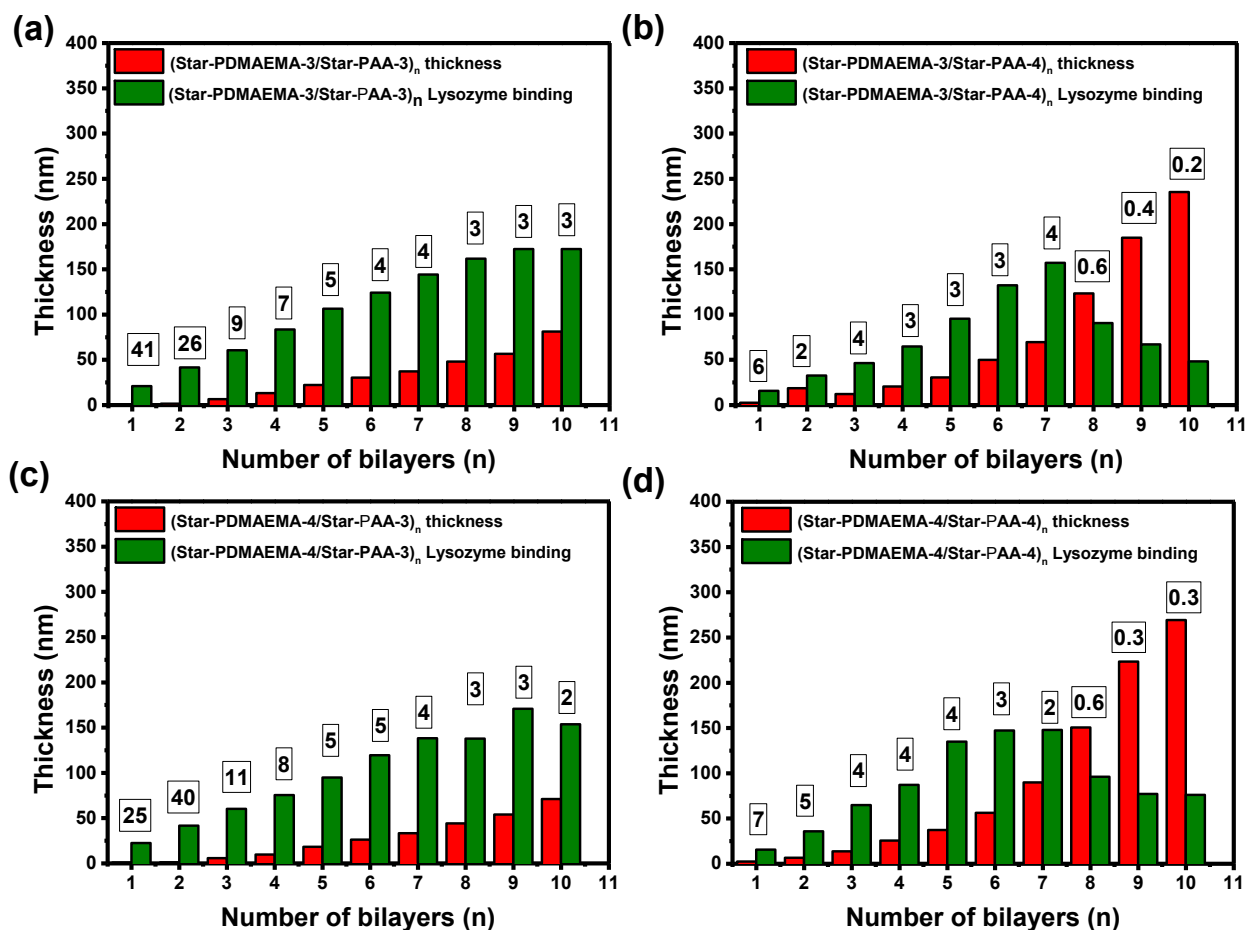
Figure 4.8. Lysozyme binding capacities of (star-PDMAEMA-X/star-PAA-X)$_n$ multilayers (n = 1–10 and X=3 and 4) deposited from polyelectrolyte solutions containing 0.5 M NaCl at pH 3. The numbers above the bars represent the ratios of the lysozyme equivalent thickness to the film thickness. The equivalent thickness is the thickness of spin-coated lysozyme that would give an FTIR absorbance equivalent to that of the sorbed lysozyme.

Interestingly, films prepared with star-PAA-3 (Figure 4.8a and c) show a plateau in lysozyme binding at high numbers of multilayers, but no rapid decline in protein capture with an increasing number of arms. This likely reflects the greater swelling of these films (Figure 4.7) due to the lower number of arms.
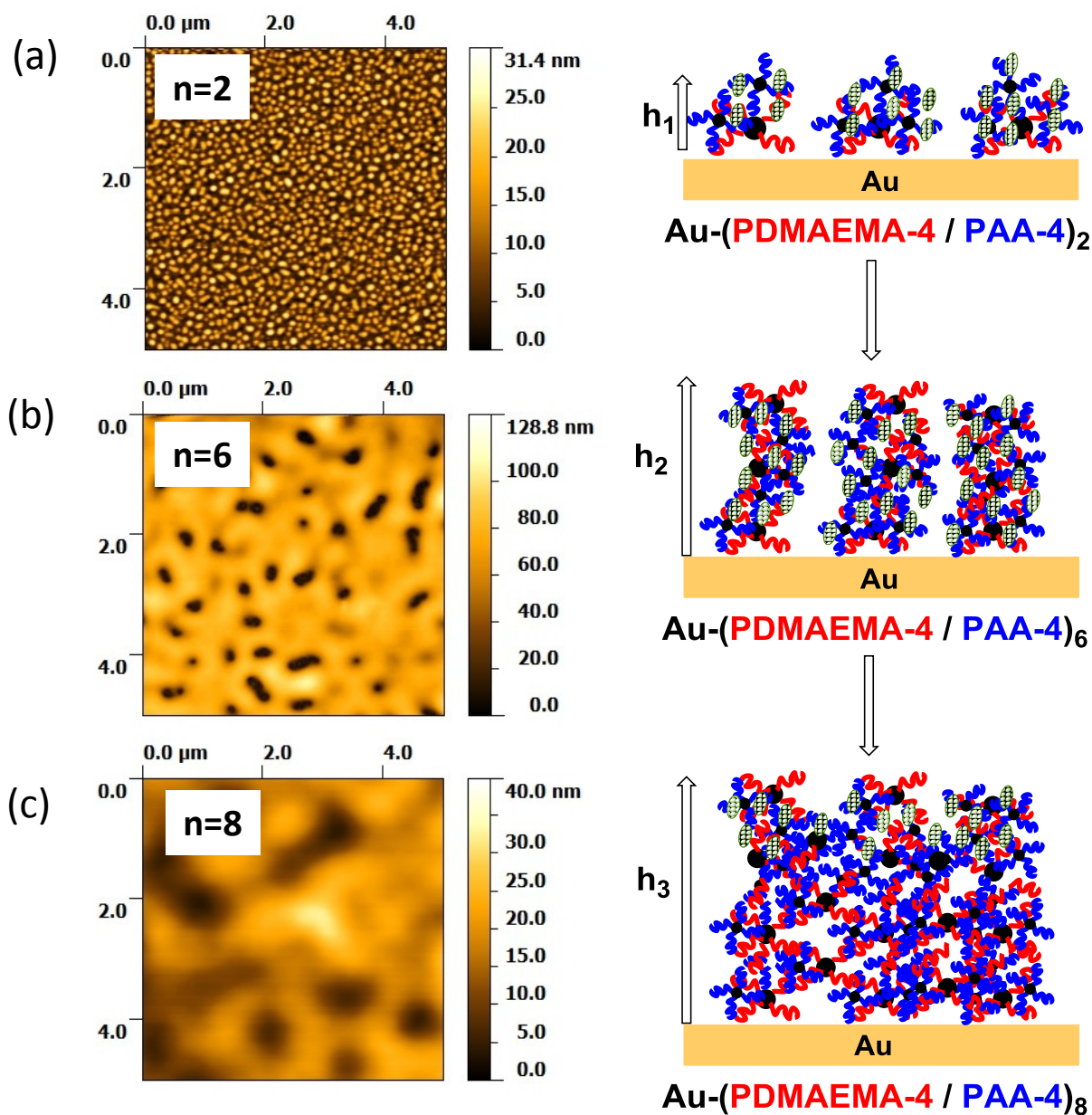
Figure 4.9. AFM images of (star-PDMAEMA-4/star-PAA-4)$_n$ films and a schematic illustration of protein binding to these porous films.

We also modified nylon membranes (nominal pore size of 1.2 μm) with these star-polymer PEMs to see if the high lysozyme-binding capacities of films on gold transfer to other substrates. Figure 4.10 shows the lysozyme breakthrough curves for nylon membranes modified with (star-PAA-X/star-PDMAEMA-X)$_n$. We employed films

with 2.5 bilayers to avoid plugging of membrane pores, and the extra ½ bilayer shows that the films terminate in PAA, which should enhance lysozyme capture. Regardless of the number of arms in the star polymers, the lysozyme capture is around ~120 mg/mL. The high binding capacity for all types of films likely reflects their high porosity. The dynamic binding capacity, (the amount of protein bound when the concentration in the feed is 10% of that in the permeate) is around 30 mg/mL for all the systems. These binding capacities are significantly higher than those of commercial ion-exchange membranes. Commercial Mustang S ion-exchange membranes show lysozyme binding capacities of only 45−50 mg/cm^3 even at high pH as 7.4.[47] Membranes modified with PAA/PEI/PAA films prepared using linear polymers have a lysozyme binding capacity of 105 mg/cm^3 at pH 7.4.[48]
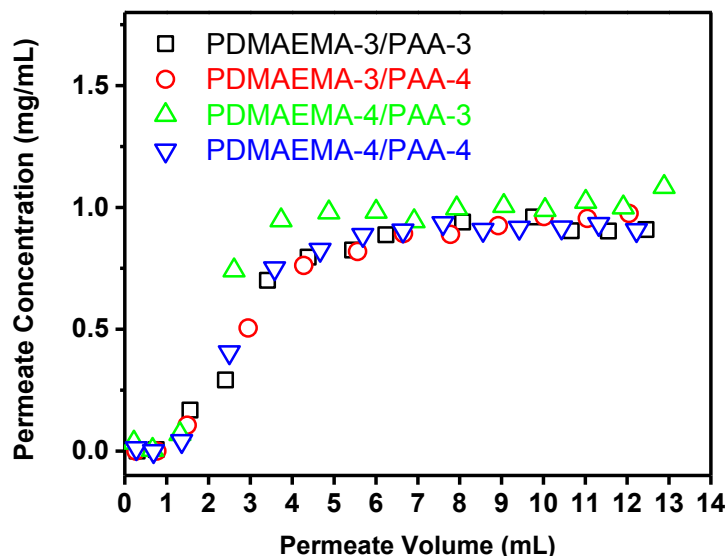
Figure 4.10. Breakthrough curves for adsorption of lysozyme in membranes modified with (□) star-(PAA-3/PDMAEMA-3)$_{2.5}$, (○) star-(PAA-3/PDMAEMA-4)$_{2.5}$, (△) star-(PAA-4/PDMAEMA-3)$_{2.5}$ and (△) star-(PAA-4/PDMAEMA-4)$_{2.5}$ multilayers. The feed solution contained 1.0 mg protein/mL in pH 5.4 buffer, and the solution flow rate was 1.0 mL/min. Films were deposited from polyelectrolyte solutions containing 0.5 M NaCl at pH 3.

4.4. Conclusions.

Under the appropriate deposition conditions, LBL adsorption of star-PDMAEMA and star-PAA leads to highly porous films. Porosity varies with the number of arms in the polycationic PDMAEMA. When changing the PDMAEMA arm number from 3 to 4 while keeping the PAA star arm number at 3, pore sizes changes dramatically from 150 to 400 nm. The size of surface pores regularly increases (from 200 to 550 nm) when increasing the number of bilayers from 2 to 6. Films with a few bilayers can swell more that 200-300% in water, but swelling decreases with additional bilayers or an increase in the number of arms on the polymers. At pH 5.4, star-polymer films with 5 bilayers bind as much as ~100-120 nm of lysozyme, which is ~5-fold greater than lysozyme binding to $(PAA/PAH)_n$ films (18 nm) at the same pH. Sequential adsorption of PDMAEMA-X and PAA-X leads to membranes that capture ~120 mg of lysozyme per mL of membrane, regardless of the number of arms on the polymer, presumably due to high swelling from films with only a few bilayers. This protein binding capacity is about twice that for commercial ion-exchange membranes, but similar to the capacity for membranes containing linear polyelectrolyte films.

APPENDIX

A4.1. Synthesis and Characterization of Initiators.

Synthesis of initiators for star polymerization was carried out using slightly modified literature procedures.[1]

A4.1.1. Synthesis of the Three-arm ATRP Initiator 1,3,5-(2-Bromo-2-methyl propionate) benzene.

Under a N_2 atmosphere, 1,3,5-trihydroxybenzene (2.0 g, 0.016 mol) and DMAP (dimethyl amino pyridine, 1.93 g, 0.016 mol) were dissolved in 150 mL of anhydrous THF, and the solution was stirred for 10 min at room temperature. Subsequently TEA (8 mL, 0.11 mol) was added to the mixture, the temperature was adjusted to 0 °C using an ice bath, and 2-BIB (6.2 mL, 0.050 mol) was added drop wise to the reaction mixture, while maintaining the temperature at 0 °C. After, addition of reactants, the reaction mixture was stirred overnight at room temperature. The reaction progress was monitored using ^{1}H NMR spectroscopy. The THF was evaporated, and the resulting powder was dissolved in CH_2Cl_2, washed with water twice and washed with 5% aqueous sodium bicarbonate to remove unreacted 2-bromoisobutyryl bromide. The organic phase was collected, dried over $MgSO_4$, and finally vacuum dried. For further purification, the solid was dissolved in diethyl acetate and recrystallized in 20% ethyl acetate-80% hexane solution. Drying in vacuo afforded the 1,3,5-(2-bromo-2-methyl propionate) benzene as a white solid with 53% yield (4.87 g, 0.0085 mol); IR (KBr): 2980, 2927, 1756, 1608, 1141, 678 cm^{-1}; ^{1}H NMR (500 MHz, CDCl$_3$): δ (ppm) 2.05 (s, 18H), 6.97 (s, 3H), ^{13}C NMR (125 MHz, CDCl$_3$): 30.52, 54.86, 112.51, 151.29, 169.38.

A4.1.2. Synthesis of the Four-arm ATRP Initiator Pentaerythritol Tetrakis(2-bromoisobutyrate) initiator.

Similar to a previous procedure,[1] the reaction of pentaerythritol (2.2 g, 0.016 mol) with 2-BIB (8 ml, 0.098 mol) in the presence of DMAP (1.93 g, 0.016 mol) and TEA (8.0 mL, 0.11 mol) afforded pentaerythritol tetrakis(2-bromoisobutyrate) in 34% yield (after recrystallization in diethyl ether, 4.0 g, 0.0055 mol); IR (KBr): 2983, 2929, 1739, 646 cm^{-1}; ^{1}H NMR (500 MHz, CDCl$_3$): δ 1.93 (s, 24H), 4.32 (s, 8H), ^{13}C NMR (125 MHz, CDCl$_3$): 30.62, 43.65, 55.17, 62.87, 170.84.

A4.1.3. Synthesis of the Six-arm ATRP Initiator Di-pentaerythritol hexakis(2-bromoisobutyrate).

In a similar manner,[1] the reaction of di-pentaerythritol (4.0 g, 0.016 mol) with 2-BIB (8 ml, 0.098 mol) in the presence of DMAP (1.93 g, 0.016 mol) and TEA (8.0 ml, 0.11 mol) afforded di-pentaerythritol hexakis(2-bromoisobutyrate) in 47% yield (after recrystallizationin diethyl ether, 8.7 g, 0.0075 mol); IR (KBr): 2978, 2921, 1736, 1468, 646 cm^{-1}; ^{1}H NMR (500 MHz, CDCl$_3$): δ 1.94 (s, 36H), 3.60 (s, 4H), 4.30 (s, 12H), ^{13}C NMR (125 MHz, CDCl$_3$): 30.53, 44.11, 55.59, 63.32, 64.38, 170.86.

A4.2. Synthesis and Characterization of Star Polymers.

Cationic and anionic star polymers with different numbers of arms were synthesized according to literature procedures with some modifications.[2-4]

A4.2.1.Synthesis of Four-arm Star-poly(*tert*-butyl acrylate)[2] [Star-P*t*BA-4].

Tert-butyl acrylate (*t*BA) (29 mL, 0.2 mol) and *N,N,N',N',N''*-pentamethyldiethylenetriamine (PMDETA) (0.05 mL, 0.25 mmol) were dissolved in acetone (10% v/v) in a 100-mL Schlenk flask. After three freeze-pump-thaw cycles, CuBr (36 mg, 0.25 mmol) and tetra(2-bromoisobutyryl) pentaerythritol (0.4 g, 0.5 mmol) were added to a frozen mixture under N_2, which was then thawed and degassed with another two freeze-pump-thaw cycles. ATRP was carried out at 60 ^{0}C, and monomer conversion was monitored periodically using ^{1}H NMR analysis. After completion, the reaction mixture was exposed to air and passed through a basic-alumina column to remove copper ions. Then polymer was precipitated using a distilled water-methanol (1:1) solution. The resulting white star-P*t*BA-4 was dried in vacuo and characterized by ^{1}H NMR spectroscopy and gel permeation chromatography (GPC) with refractive index detection. ^{1}H NMR (500 MHz, CDCl$_3$): δ 4.0-4.2 (bm, 4H, CH$_2$CH-Br and 8H, C[CH**$_2$**-O]4), 2.17 (bm, 14H, CH$_2$CHCO), 1.48, 1.17 (m, 26H, CH$_2$CHCO), 1.46 (s, 133H, C(CH$_3$)$_3$). GPC: M$_n$ = 38400 g mol^{-1}, PDI = 1.27. Similar procedures with different initiators gave polymers with 3 and 6 arms (see below).

A4.2.2. Synthesis of Four-arm Star-poly(acrylic acid) [Star-PAA-4].[5]

Star-P*t*BA-4 (2.3 g) was dissolved in 20 mL of dichloromethane, and trifluoroacetic acid (10 g) was added to this mixture. After, 24 h, precipitated star poly(acrylic acid) was recovered (2.0 g) through filtration and freeze dried. ^{1}H NMR (500 MHz, CDCl$_3$): δ 3.91 (bm, 4C(CH**$_2$**-O), 1.92 (bm, CH$_2$CHCO), 1.38 (bm, CH$_2$CHCO).

A4.2.3. Synthesis of Three-arm Star-poly(acrylic acid) [Star-PAA-3].

Similar to the procedure in A4.2.1, ATRP of *tert*-butyl acrylate (29 ml, 0.2 mol) from 1,3,5-(2-bromo-2-methyl propionate) benzene initiator (0.6 g, 0.5 mmol) in the presence of CuBr (36 mg, 0.25 mmol)/ (PMDETA) (0.05 ml, 0.25 mmol) catalyst afforded Star-PtBA-3 with 85% conversion. ^{1}H NMR (500 MHz, CDCl$_3$): δ 6.81 (s, 3H, benzene-H), 4.06-4.18 (bm, 3H, CH$_2$CH-Br), 2.12-2.35 (bm, 35H, CH$_2$CHCO), 1.84, 1.53 (m, 60H, CH$_2$CHCO), 1.44 (s, 276H, C(CH$_3$)$_3$). GPC: M$_n$ = 30 700 g mol^{-1}, PDI = 1.21. Acid hydrolysis gave the three-arm star-acrylate. ^{1}H NMR (500 MHz, CDCl$_3$): 1.80-2.10 (bm, CH$_2$CHCO), 1.70-1.10 (bm, CH$_2$CHCO).

A4.2.4. Synthesis of Six-arm Star-poly(acrylic acid) [Star-PAA-6].

Similar to the procedure in A42.1, ATRP of *tert*-butyl acrylate (29 ml, 0.2 mol) from di-pentaerythritol hexakis (2-bromoisobutyrate) initiator (0.3 g, 0.5 mmol) in the presence of CuBr (36 mg, 0.25 mmol)/ (PMDETA) (0.05 ml, 0.25 mmol) catalyst afforded Star-PtBA-6 with 73% conversion. ^{1}H NMR (500 MHz, CDCl$_3$): δ 3.90-4.20 (bm, 6H, CH$_2$CH-Br and 12H, C[CH$_2$-O]$_6$), 3.35 (bm, 4H, [C-CH$_2$-O]$_2$), 2.10-2.40 (bm, 40H, CH$_2$CHCO), 1.82, 1.51 (m, 75H, CH$_2$CHCO), 1.42 (s, 308H, C(CH$_3$)$_3$). GPC: M$_n$ = 32 910 g mol^{-1}, PDI = 1.079. Acid hydrolysis affored Star-PAA-6. ^{1}H NMR (500 MHz, CDCl$_3$): 3.90-4.20 (bm, CH$_2$CH-Br and C[CH$_2$-O]$_6$), 1.80-2.28 (bm, CH$_2$CHCO), 1.72-1.12 (bm, CH$_2$CHCO).
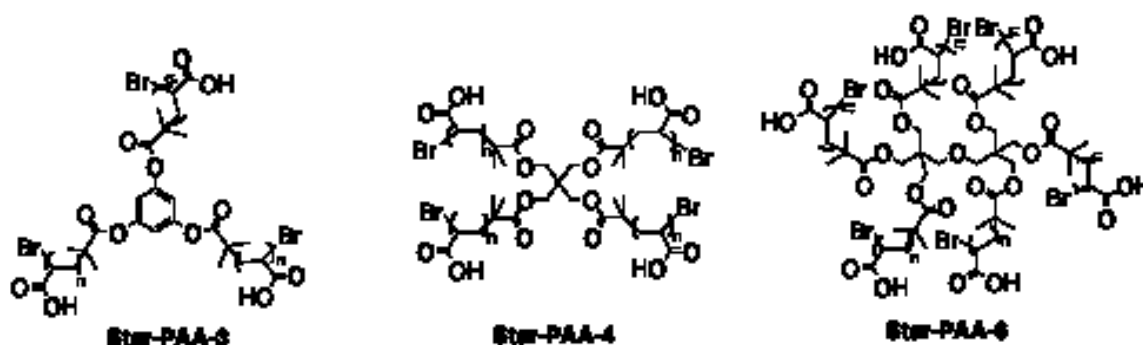
Figure A4.1. Different star poly(acrylic acid) polymers.

A4.2.5. Synthesis of Four-arm Star-poly(2-(dimethylamino)ethyl methacrylate) [Star-PDMAEMA-4].[3]

N,N-dimethylaminoethyl methacrylate (DMAEMA) (25 mL, 0.15 mol) and *N,N,N',N'',N''',N'''*-hexamethyltriethylenetetraamine (HMTETA) (0.27 mL, 1.0 mmol) were dissolved in THF (10 ml) in a 100-mL Schlenk flask. After three freeze-pump-thaw cycles, CuBr (72 mg, 0.5 mmol) and tetra(2-bromoisobutyryl)pentaerythritol (0.4 g, 0.5 mmol) were added to the frozen mixture under a N_2 atmosphere, which was then thawed and degassed by two freeze-pump-thaw cycles. The mixture was stirred at room temperature, and monomer conversion was measured by ^{1}H NMR analysis. After completion (~76% conversion), the reaction mixture was exposed to air and passed through a basic-alumina column to remove copper ions. The polymer was precipitated using a heptane-ethylacetate mixture, and the white star-PDMAEMA-4 was dried in vacuo. ^{1}H NMR (500 MHz, CDCl$_3$): δ 3.99 (bm, 2H, -O-CH$_2$C-), 2.49 (bm, 2H, -C-CH$_2$-N), 2.22 (s, 6H, -N(CH$_3$)$_2$), 1.85, 1.76 (bm, 2H, -C-CH$_2$-C-), 0.99, 0.84 (m, 3H, -C(CH$_3$)-

C-). GPC : M_n = 36 600 g mol^{-1}, PDI = 1.15.   Star polymers with 3 and 6 arms were synthesized similarly (see below).

A4.2.6. Synthesis of Three-arm Star-poly(2-(dimethylamino)ethyl methacrylate) [Star-PDMAEMA-3].

Similar to the procedure in A4.2.5, ATRP of DMAEMA (25 mL, 0.15 mol) from 1,3,5-(2-bromo-2-methyl propionate) benzene initiator (0.6 g, 0.5 mmol) in the presence of CuBr (72 mg, 0.50 mmol)/ (HMTETA) (0.27 mL, 1.0 mmol) catalyst afforded star-PDMAEMA-3 with 73% conversion. ^{1}H NMR (500 MHz, CDCl$_3$): δ 4.00 (bm, 2H, -O-CH$_2$C-), 2.51 (bm, 2H, -C-CH$_2$-N), 2.22 (s, 6H, -N(CH3)2), 1.86, 1.77 (bm, 2H, -C-CH$_2$-C-), 1.01, 0.86 (m, 3H, -C(CH$_3$)-C-). GPC : M_n = 37 400 g mol^{-1}, PDI = 1.13.

A4.2.7. Synthesis of Six-arm Star-poly(2-(dimethylamino)ethyl methacrylate) [Star-PDMAEMA-6].

Similar to the procedure in A5.2.5, ATRP reaction of DMAEMA (25 ml, 0.15 mol) from di-pentaerythritol hexakis (2-bromoisobutyrate) initiator (0.3 g, 0.5 mmol) in the presence of CuBr (72 mg, 0.50 mmol)/ (HMTETA) (0.27 ml, 1.0 mmol) catalyst afforded star-PDMAEMA-6 with 75% conversion. ^{1}H NMR (500 MHz, CDCl$_3$): δ 4.03 (bm, 2H, -O-CH$_2$C-), 2.54 (bm, 2H, -C-CH$_2$-N), 2.26-2.22 (s, 6H, -N(CH$_3$)$_2$), 1.89, 1.80 (bm, 2H, -C-CH$_2$-C-), 1.03, 0.84 (m, 3H, -C(CH$_3$)-C-). GPC : M_n = 37 000 g mol^{-1}, PDI = 1.13.
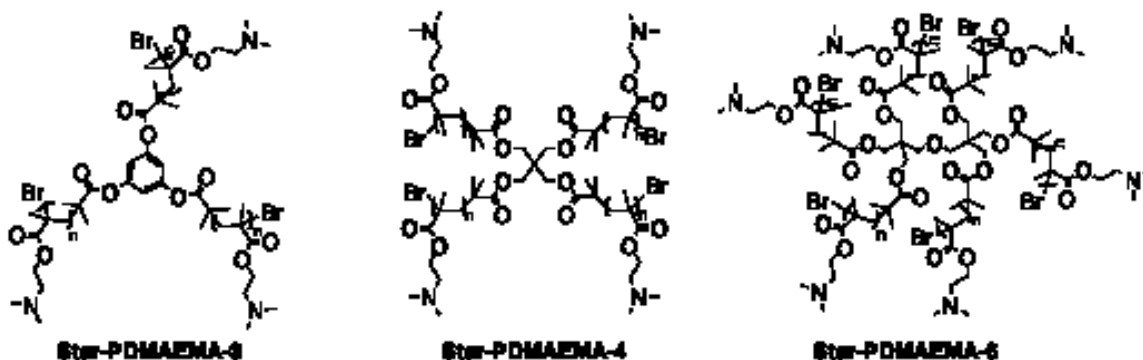
Figure A4.2. Star-poly(2-(dimethylamino)ethyl methacrylate)-X structures.

A4.3. Results and Discussion.

A4.3.1. Synthesis and Characterization of Star-PAA Polymers.

Synthesis of star-PAA-X in included formation of star-PtBA-X followed by hydrolysis (Figure A4.3). For this ATRP reaction, CuBr served as the catalyst and PMDETA as the ligand to increase the solubility of the catalyst to provide a persistent radical effect. Also the monomer, tBA, was diluted with 10% acetone to keep the concentration of the monomer as high as possible throughout the reaction, which will minimize the termination reactions via coupling of active species. A second advantage of addition of a strong solvent is increased catalyst stability. We kept our M/I_0 ratio as high as 400 and conducted the ATRP reaction at 60 °C to give 4-arm star tBA polymer with molecular weight M_n 38400 g/mol^{-1} after 24 h of polymerization.
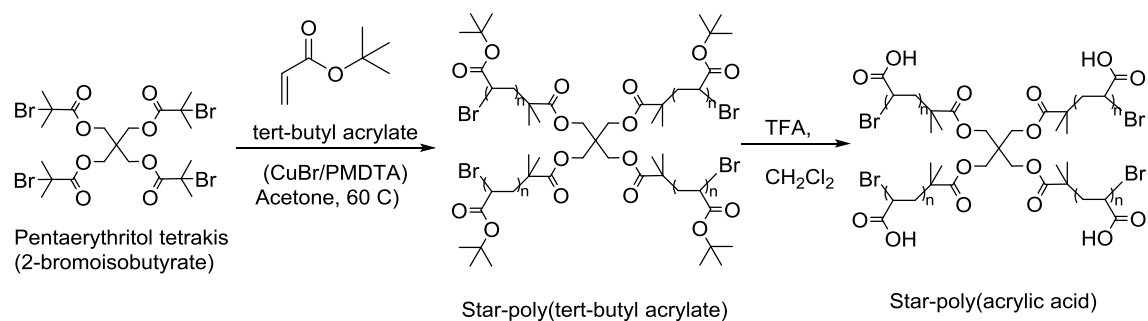
Figure A4.3. Synthesis of four arm star-poly(acrylic acid).
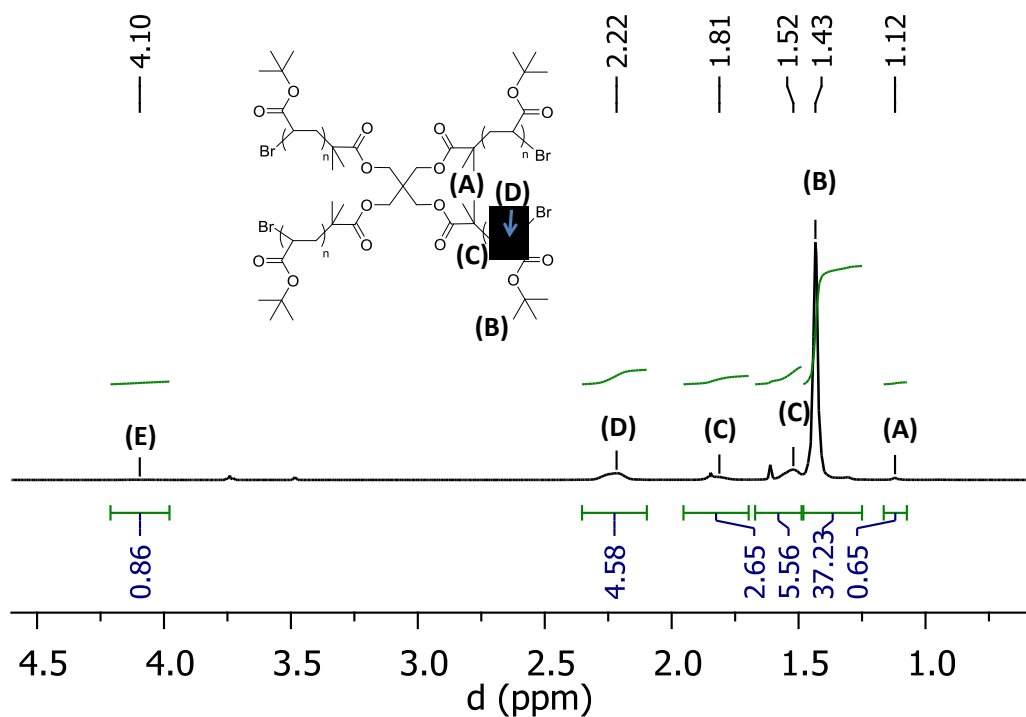
Figure A4.4. ^{1}H NMR spectrum of star-P*t*BA-4 in CDCl$_3$.

The monomer conversion was monitored using ^{1}H NMR analysis of the crude reaction mixture (Figure A4.5). Signals corresponding to the *tert*-butyl groups of the monomer and polymer appear in two distinct regions, around 1.46 and 1.40 ppm, respectively. The total integration of these two peaks is proportional to the total amount

of monomers present at the beginning of the reaction. Thus the integral of the *tert*-butyl

signal of the polymer divided by total *tert*-butyl integral gives the conversion. After 24 h

this reactions goes to completion (Table A4.1).
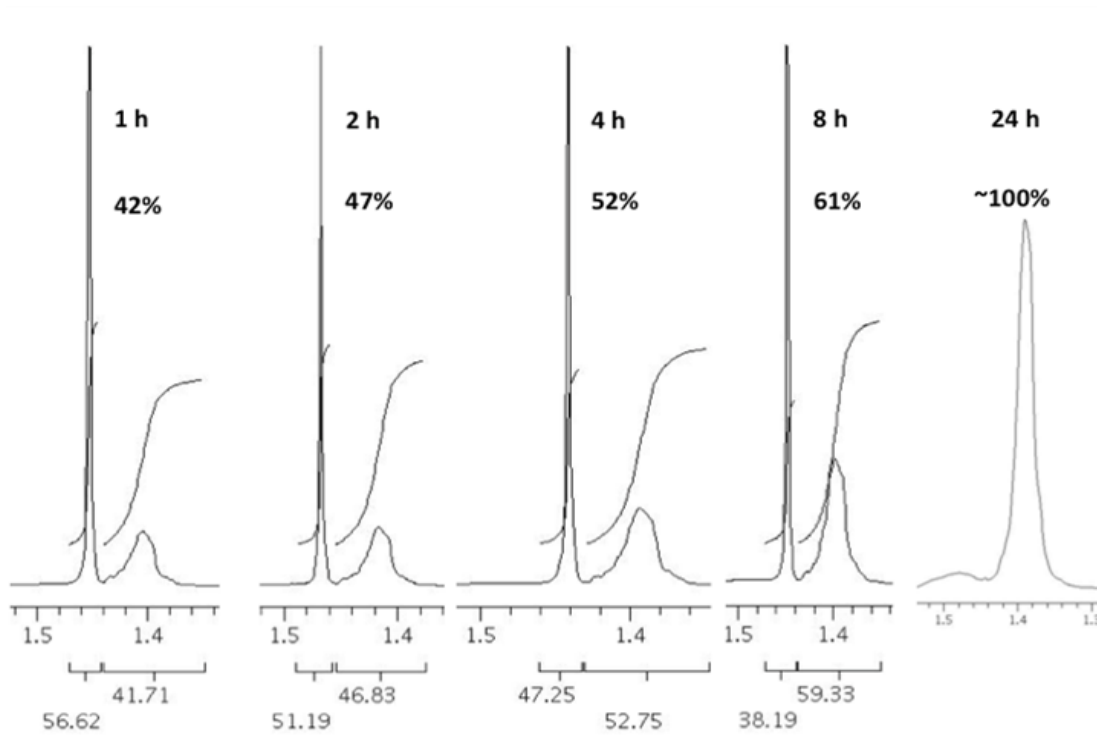
Figure A4.5. ^{1}H NMR spectra (in CDCl$_3$) showing the kinetics of ATRP of *tert*-butyl acrylate using a 4-arm initiator. The figure shows the region between 1.35 and 1.5 ppm in the crude reaction mixture at several times. The bands centered at ~1.46 ppm and 1.40 ppm correspond to *tert*-butyl protons in monomers and polymers, respectively.

In addition to relatively rapid polymerization, this reaction provided a low

polydispersity of ~1.26 (Table A4.1). This indicates well-defined sizes of the 4-arm star

polymers. The high monomer to initiator ratio (about 400) helps to avoid star-star

coupling reactions.   Figure A4.7 shows that the plot of log([M]$_0$/[M]$_t$) vs time is nearly

linear for star-P*t*BA-4, indicating an essentially constant number of propagating species throughout the polymerization.
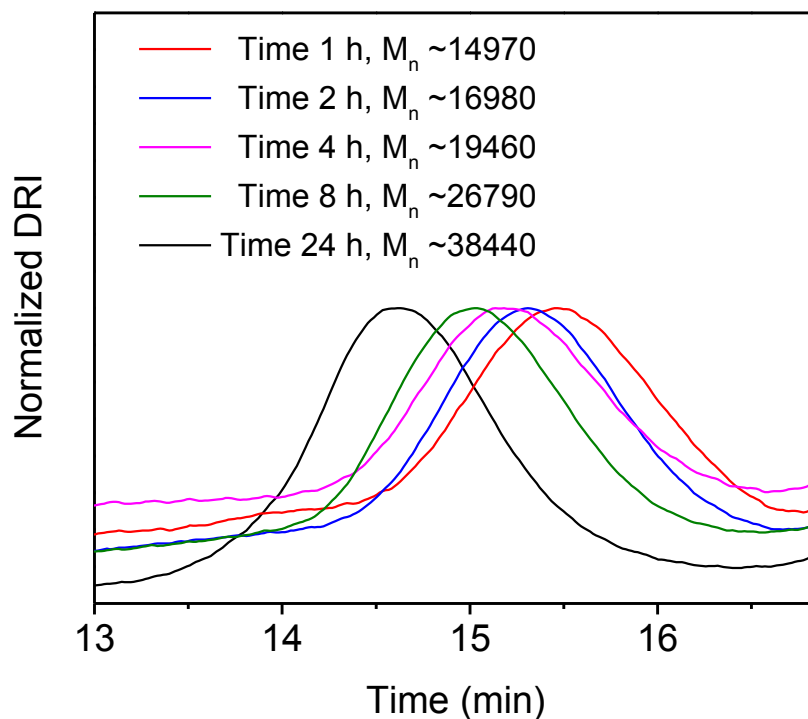
Figure A4.6. GPC profiles of star-P*t*BA-4 formed during 1, 2, 4, 8 and 24 h of ATRP. The Y-axis is the normalized differential refractive index values of polymers.

Furthermore, GPC was used to follow the increase of polymer molar mass during polymerization (Figure A4.6). The symmetry of the chromatograms suggests that no star-star coupling occurs. Moreover, the molecular weight increases approximately linearly with the polymer conversion, implying a controlled polymerization (Figure A4.8). The agreement between the theoretical and GPC M_n values (Figure A4.8) is reasonable considering that the GPC values employ linear polystyrene standards.
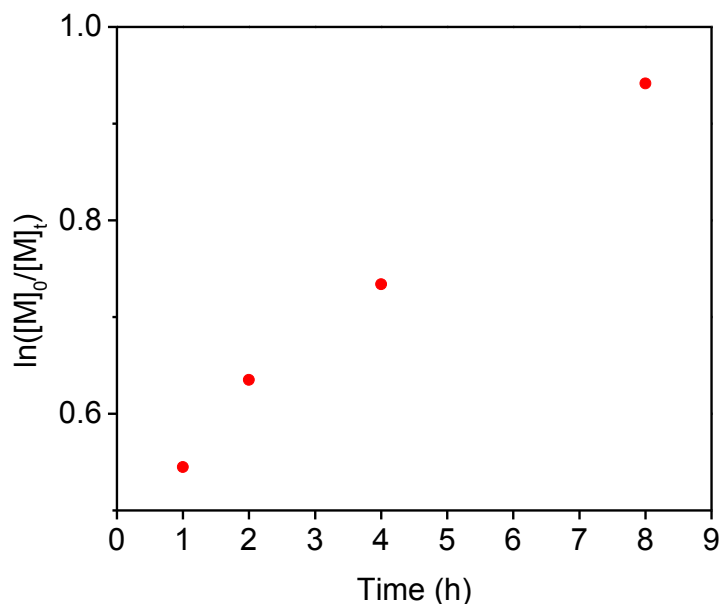
Figure A4.7. First-order kinetic plot for ATRP of (*tert*-butyl acrylate) from a 4-arm initiator; pentaerythritol tetrakis(2-bromoisobutyrate).

Similar to star-P*t*BA-4, polymers with 3 and 6 arms show low polydispersity and M_n values between 30 and 40 kDa (Figure A4.9).
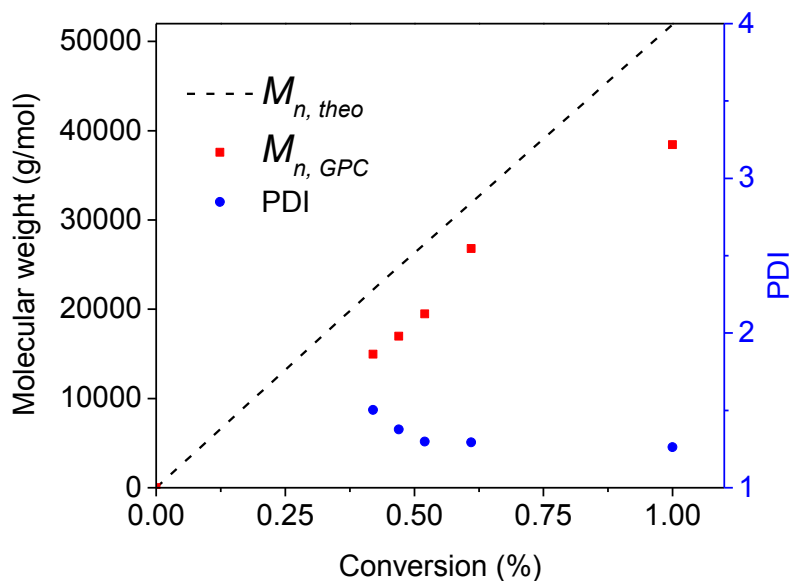
Figure A4.8. Molar mass (red squares) and polydispersity index (blue circles) of star-P*t*BA-4 as a function of conversion during ATRP of *t*BA. The values were determined through GPC using polystyrene standards. The dashed line shows the theoretical M_n value as a function of conversion.
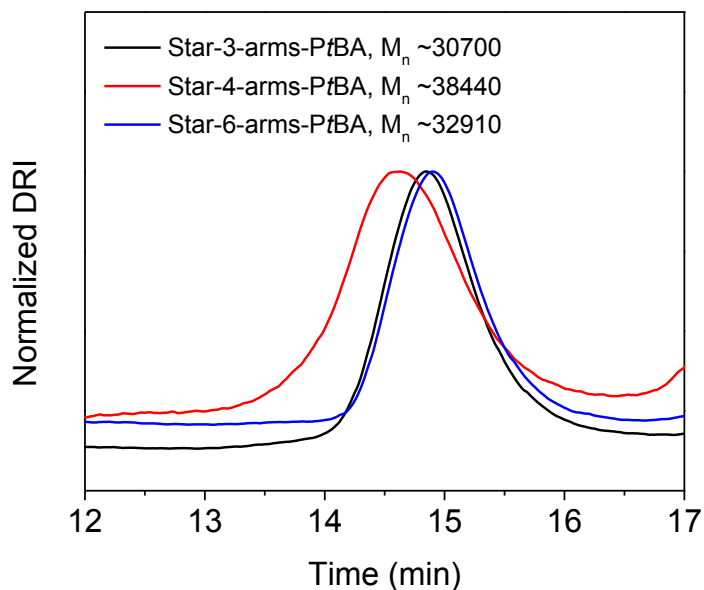
Figure A4.9. GPC chromatograms of star-P*t*BA-3,star-P*t*BA-4, and star-P*t*BA-6. The Y-is the normalized differential refractive index.

The degree of polymerization per arm of star polymer (DP) is 100, 97 and 56 (calculation shown in the footnote of Table A4.1) for star-P*t*BA-3,star-P*t*BA-4, and star-P*t*BA-6, respectively. Table A4.1 lists reaction conditions and conversions for all three polymers.

Table A4.1. Reaction conditions and conversions during star-P*t*BA synthesis by ATRP.

Star polymer	Time (h)	Conv.[%]	$M_{n,theo}$ [g mol^{-1}]	$M_{n,\,GPC}$ [g mol^{-1}]	PDI	DP
P*t*BA-4	1	42	22206	14970	1.503	
	2	47	24766	16970	1.377	
	4	52	27326	19460	1.257	
	8	61	31934	26790	1.293	
	24	100	51902	38440	1.262	100
P*t*BA-3	24	73	37998	30700	1.208	97
P*t*BA-6	24	85	43578	32910	1.079	56

Molar ratio of [I]:[Cu]:[PMDTA] = 1 : 0.5 :0.5
[M] : [I] = 400

$M_{n,\,theo} = \text{Conversion} \times \dfrac{[M]_0}{[I]_0} \times MW_{monomer} + MW_{initiator}$

$M_{n,\,GPC}$ was measured in THF and the literature reported[4] refractive index increment dn/dc = 0.0559 for linear P*t*BAwas used to obtain the molecular weights.

DP (per arm)= $\text{Conversion} \times \dfrac{[M]_0}{[I]_0}$/arm number

Star-PAA-X was synthesized by hydrolysis of the corresponding star-P*t*BA with trifluoroacetic acid in dichloromethane (Figure A4.1). The star-PAA-X precipitates from the reaction medium, and ^{1}H NMR spectra show elimination of essentially all *tert*-butyl groups after 24 h of hydrolysis (Figure A4.10).
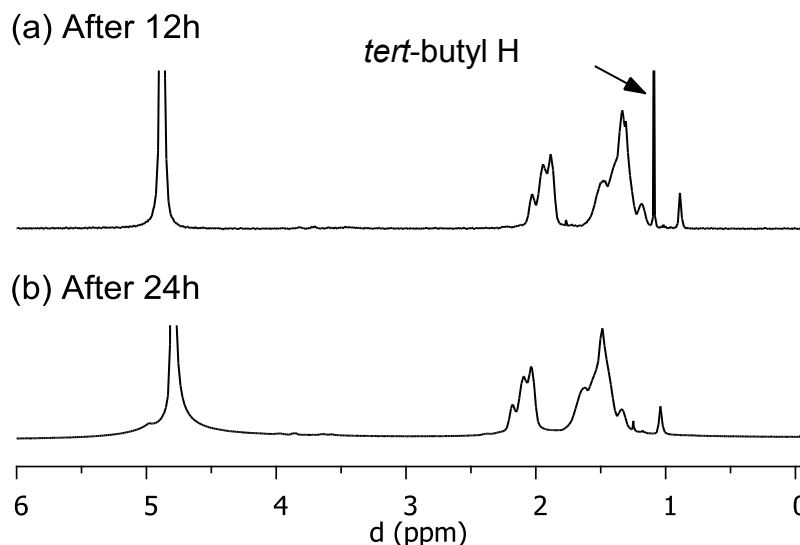
Figure A4.10. ^{1}H NMR spectra of star-P*t*BA-X after acid hydrolysis of *tert*-butyl groups for (a) 12 h and (b) 24 h. Spectra were acquired in D_2O.

Table A4.2. Molecular weights of different star-PAA-X.

Star polymer	Molecular weight (g mol-1)
Star-PAA-3	21,525
Star-PAA-4	29,305
Star-PAA-6	25,333

Molecular weight=(Molecular weight of repeating unit)×DP ×number of arms+FW initiator   Note that molecular weights based on GPC data for star-PTBA-X will be smaller.   These are the theoretical molecular weights.

Peaks corresponding to the initiator core are clearly visible in the ^{1}H NMR spectra of all star-PAA-X polymers, indicating that acid hydrolysis of the *tert*-butyl group does not liberate the initiator core of the star polymer. Previous studies also showed successful hydrolysis of *tert*-butyl functional groups in presence of the star-initiator core.[5]

Molecular weight= (Molecular weight of repeating unit×DP×number of arms) + FW initiator

Eq. A4.1
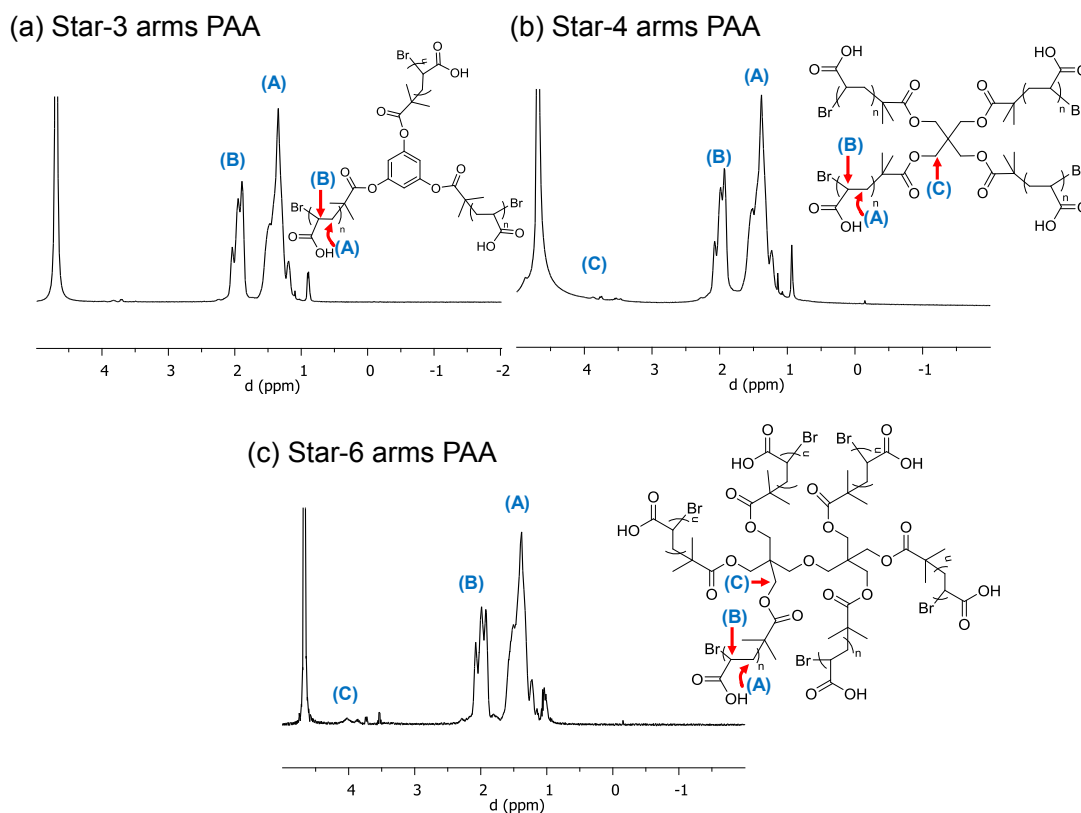
Figure A4.11. ^{1}H NMR spectra of (a) star-PAA-3, (b) star-PAA-4 and (c) star-PAA-6 in D$_2$O.

Similar to star-PAA-4, star-PAA-3 and star-PAA-6 where synthesized via hydrolysis of star-P*t*BA-X, and Figure A4.11 shows ^{1}H NMR spectra. Molecular weights of these polymers were determined using Eq A4.1, which assumes complete hydrolysis. Hammond et al. previously employed this method for determination of molecular weight of star-PAA polymers.[6] This leads to the M$_n$ values in Table A4.2.

A4.3.2. Synthesis and Characterization of Star-poly(*N,N*-dimethylaminoethyl methacrylate) (PDMAEMA).

Similar to synthesis of anionic polyelectrolytes, ATRP was employed to synthesize the cationic poly(*N,N*-dimethylaminoethyl methacrylate) (PDMAEMA) star polymer. We first synthesized the four arm PDMAEMA polymer through room-temperature ATRP of *N,N*-dimethylaminoethyl methacrylate (DMAEMA) from the tetra(2-bromoisobutyryl)pentaerythritol initiator. CuBr and *N,N,N',N'',N''',N'''*-hexamethyltriethylenetetraamine (HMTETA) served as the catalyst and ligand.
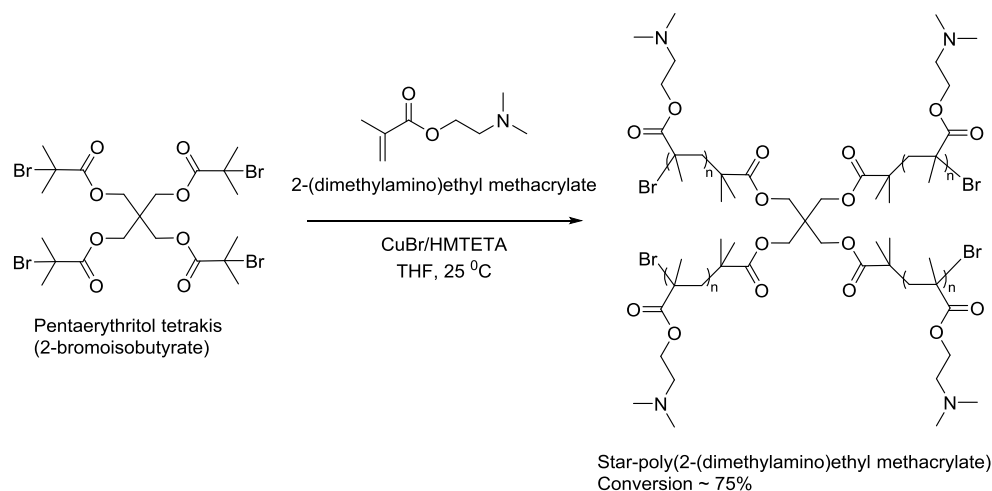
Figure A4.12. Synthesis of 4 arms star-poly(2-(dimethylamino)ethyl methacrylate) using ATRP.

Figure A4.13 shows the NMR spectrum of the final product.
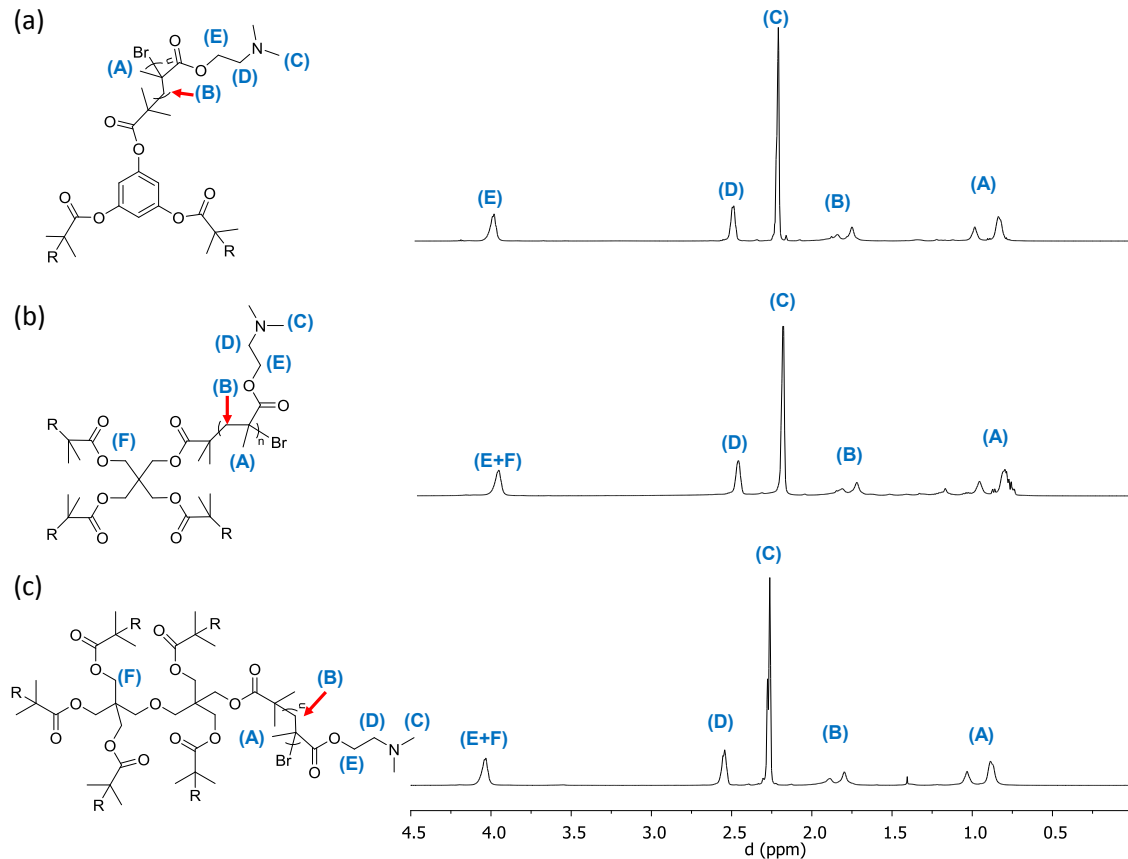
Figure A4.13. ^{1}HNMR spectra of (a) star-PDMAEMA-3, (b) star-PDMAEMA-4 and (c) star-PDMAEMA-6 in CDCl$_3$.

Two distinct peaks for O-CH$_2$- protons for the DMAEMA monomer and the polymer appears around 4.15 and 3.95 ppm regions (**Figure A4.14**). Integral values of these two distinct peaks were used to calculate the percent conversion, similar to the procedure for PtBA. This reaction reaches 71% conversion within 4 h but is sluggish afterward. This could be due to inactivation of the catalyst via monomer reacting with the active catalyst complex. Apart from the high rate during the 4 h period, this reaction provided a very low polydispersity ~ 1.15 (Table A4.3). This is an indication of a well-defined size of the 4-arm star polymers and no star-star coupling.
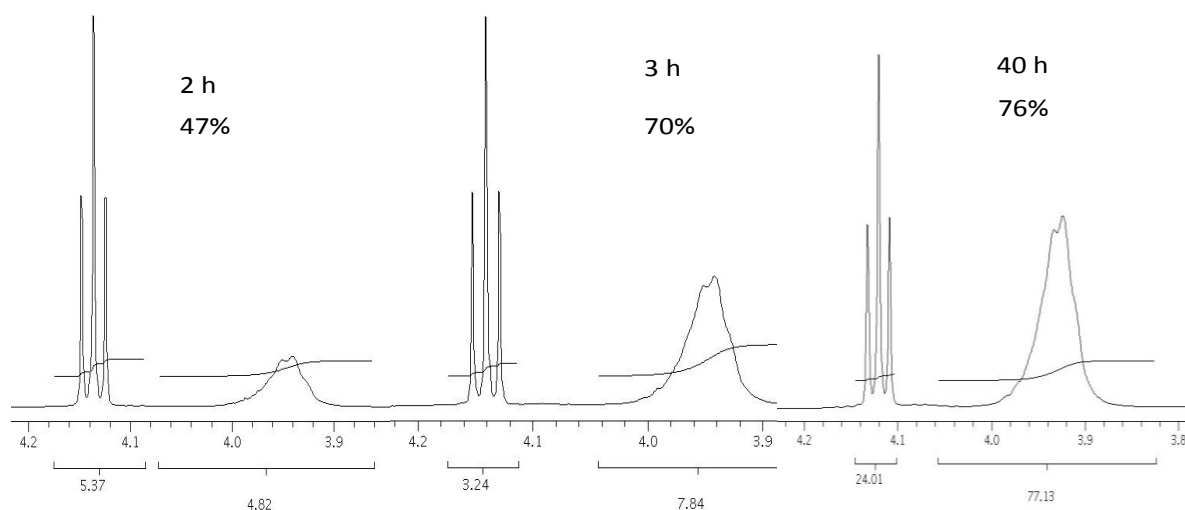
Figure A4.14. ^{1}H NMR spectra (in CDCl$_3$) showing the kinetics of ATRP of DMAEMA using a 4-arm initiator. The figure shows the region between 4.2 and 3.8 ppm in the crude reaction mixture at several times. The bands centered at ~4.15 ppm and 3.95 ppm correspond to O-CH2- protons DMAEMA protons in monomers and polymers, respectively.

When the reaction was conducted synthesis of 3- and 6-arm polymers, the reaction also terminated with conversions around 73-75% (Table A4.3).

Table A4.3. Reaction conditions, conversions, degree of polymerization and molecular weights during star-PDMAEMA-X synthesis by ATRP.

Polymer	Time (h)	Conv.[%]	M_{theo} [g/mol]	M_{GPC}[g/mol]	PDI	DP
PDMAEMA-4	2	47	22899			
	3	70	33746			
	4	71	34218			
	24	76	36576	36551	1.153	57
PDMAEMA-3	24	73	35002	37394	1.131	73
PDMAEMA-6	24	75	36514	37024	1.128	38

Molar ratio of [I]:[Cu]:[PMDTA] = 1 : 0.5 :0.5
[M] : [I] = 300

$$M_{n, theo} = Conversion \times \frac{[M]_0}{[I]_0} \times MW_{monomer} + MW_{initiator}$$

$M_{n, GPC}$ measured in DMF and polystyren standards were used to obtain the molecular weights.

DP (per arm)=[Conversion$\times \frac{[M]_0}{[I]_0}$]/arm number

Furthermore, GPC was used to determine the molar masses of the polymers (Figure A4.15). The symmetry of the refractive index traces indicates that no star-star coupling reaction occurs. Therefore, control of the polymerization process is possible. The reaction conditions and conversions and degree of polymerization for all three polymers are listed in Table A4.3.
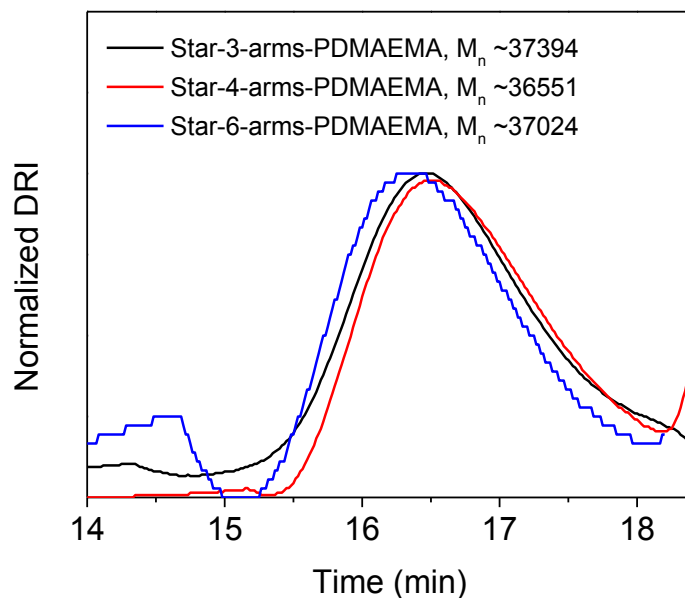
Figure A4.15. GPC traces of 3-, 4- and 6-arm PDMAEMA in DMF.   The Y-axis is normalized differential refractive index.

A4.3.3. Hydrodynamic Diameters (D_h) of the Star Polymers at Various pH Values.

Because star-PAA-X and star-PDMAEMA are weak polyelectrolytes, their degree of ionization and, hence, their hydrodynamic diameter, D_h, will depend on the solution pH. On going from pH 3 to 10, the D_h values of star-PDMAEMA-3 and star-PDMAEMA-4 polymers decrease from ~7.5 to 5 nm. At low pH values, the PDMAEMA arms extend due to electrostatic repulsion between neighboring ammonium groups, but this repulsion decreases at high pH due to deprotonation of amine groups. In contrast, the D_h value for star-PAA-4 increases from 5 to 9 over the same pH range.   Star-PAA-3 shows a similar trend but a smaller value for D_h.   The PAA polymers protonate at low pH to neutralize the polymer and decrease chain extension.   Star-PAA-3 apparently experiences less chain-chain repulsion than star-PAA-4, which leads to a lower Dh value in the 3-arm polymer.
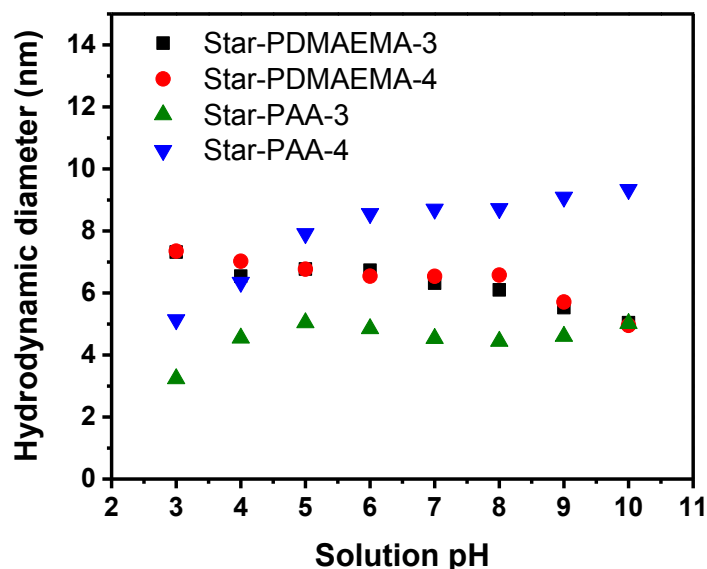
Figure A4.16. Hydrodynamic diameters (D_h) of star-PAA-X and star-PDMAEMA-X as a function of pH. Diameters were determined using light-scattering from solutions containing 1 mg/mL of polymers and are averages of three measurements (STDV±0.01-0.15). Note that star-PAA-X precipitates at pH 2.

A4.3.4. LBL Deposition of (star-PDMAEMA-X/star-PAA-X)$_n$ Films.

We assembled PEMs with 9 different pairs of star-polymer combinations. The substrate was a gold-coated wafer coated with a monolayer of MPA to create a surface with –COOH groups for initial adsorption of PDMAEMA. Figures A4.17-A4.19 show the ellipsometric thicknesses of these layers for different polyelectrolyte pairs as a function of the number of polyelectrolyte bilayers. In general, films containing star-PAA-3 are thinner than those with star-PAA-4 and star-PAA-6, which are similar. The number of arms on PDMAEMA has only a small effect on film thickness.
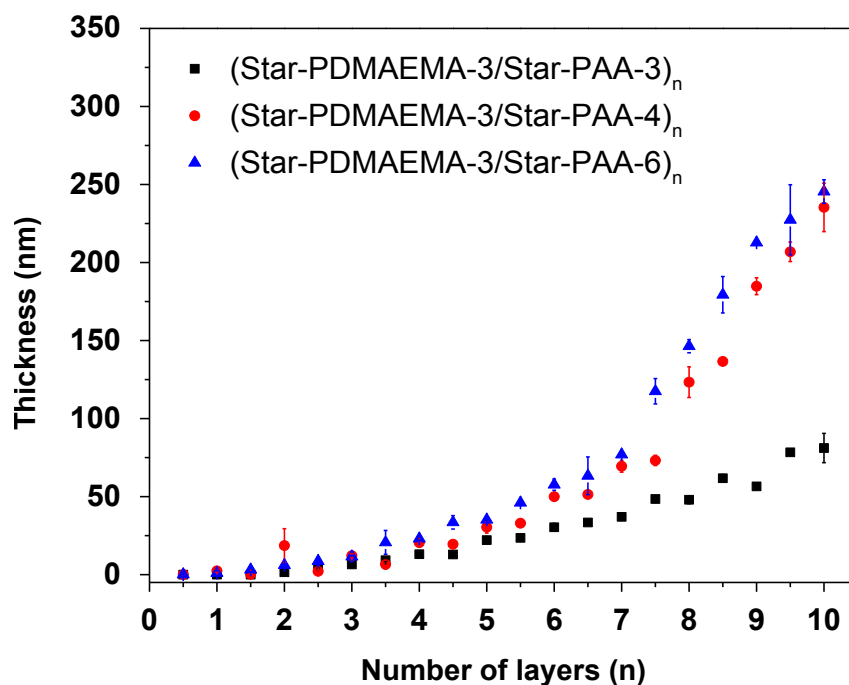
Figure A4.17. Thicknesses of (PDMAEMA-3/PAA-X)$_n$ films adsorbed from polymer solutions adjusted to pH 3.0 and containing 0.5 M NaCl.
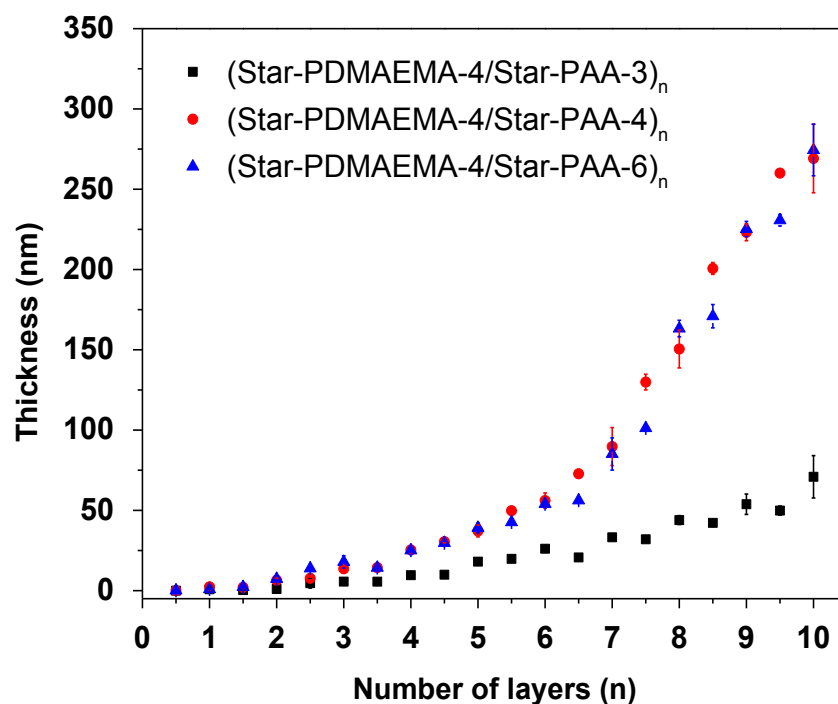
Figure A4.18. Thicknesses of (PDMAEMA-4/PAA-X)$_n$ films adsorbed from polymer solutions adjusted to pH 3.0 and containing 0.5 M NaCl.
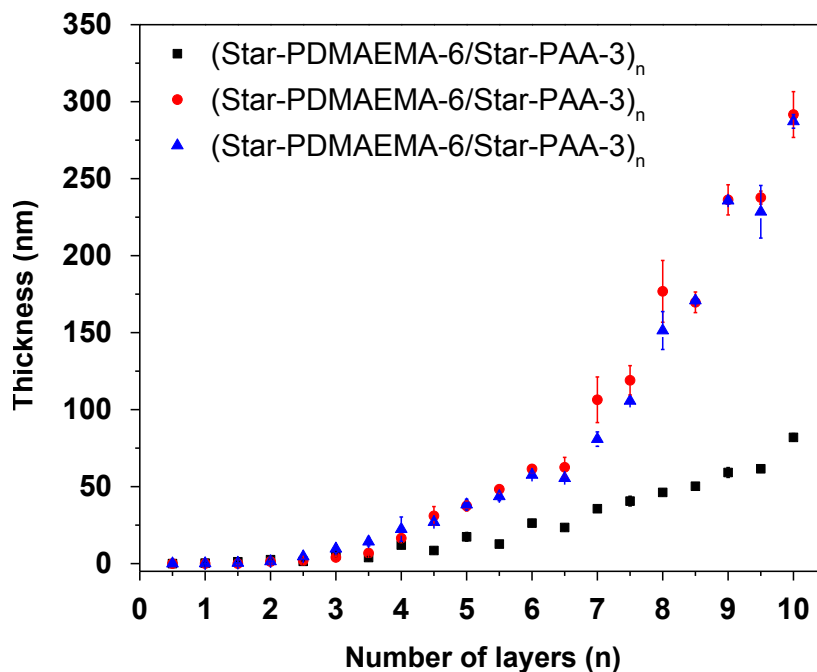
Figure A4.19. Thicknesses of (PDMAEMA-6/PAA-X)$_n$ films adsorbed from polymer solutions adjusted to pH 3.0 and containing 0.5 M NaCl.

A4.3.5. Refractive Index and Porosity Variation of (PDMAEMA-X/PAA-X)$_n$ Films.

The refractive index of the multilayer films was determined from ellipsometry, and the Lorentz-Lorenz effective medium equation,[6,7] equation A5.2, was used to estimate the porosity of each film.

$$P(\%)= \frac{2\left(n_o^2 - n_f^2\right)}{\left(n_o^2 - 1\right) \times \left(n_f^2 - 1\right)} \times 100 \qquad \text{Eq A4.2}$$

In this equation, n_o, n_f, and P are the refractive indices of the star polymers (average refractive index of PDMAEMA and PAA stars is 1.54)[8] and the star/star multilayer film (measured from ellipsometry), and the porosity, respectively. Table A4.4 lists the calculated porosities and refractive index data for (star-PDMAEMA-3/star-PAA-

3)$_n$, (star-PDMAEMA-3/star-PAA-4)$_n$, (star-PDMAEMA-4/star-PAA-3)$_n$, (star-PDMAEMA-4/ star-PAA-4)$_n$ and (star-PDMAEMA-4/star-PAA-6)$_n$ films. Refractive indices for films with 1 to 5 bilayers are low compared to the value for thicker films (1.54), which is consistent for porosity in thinner films. However, the (star-PDMAEMA-3/star-PAA-6)$_n$, (star-PDMAEMA-6/star-PAA-3)$_n$, (star-PDMAEMA-6/star-PAA-4)$_n$ and (star-PDMAEMA-6/star-PAA-6)$_n$ films have high refractive indexes even with fewer (n<5) bilayers. The increased number of arms in PDMAEMA-6 might increase the surface coverage via increasing effective charge cross linking between two polyelectrolytes. The dependence of porosity of the star/star multilayer films on deposition pH shows a similar trend for all films and suggests pore coverage with an increasing number of bilayers.
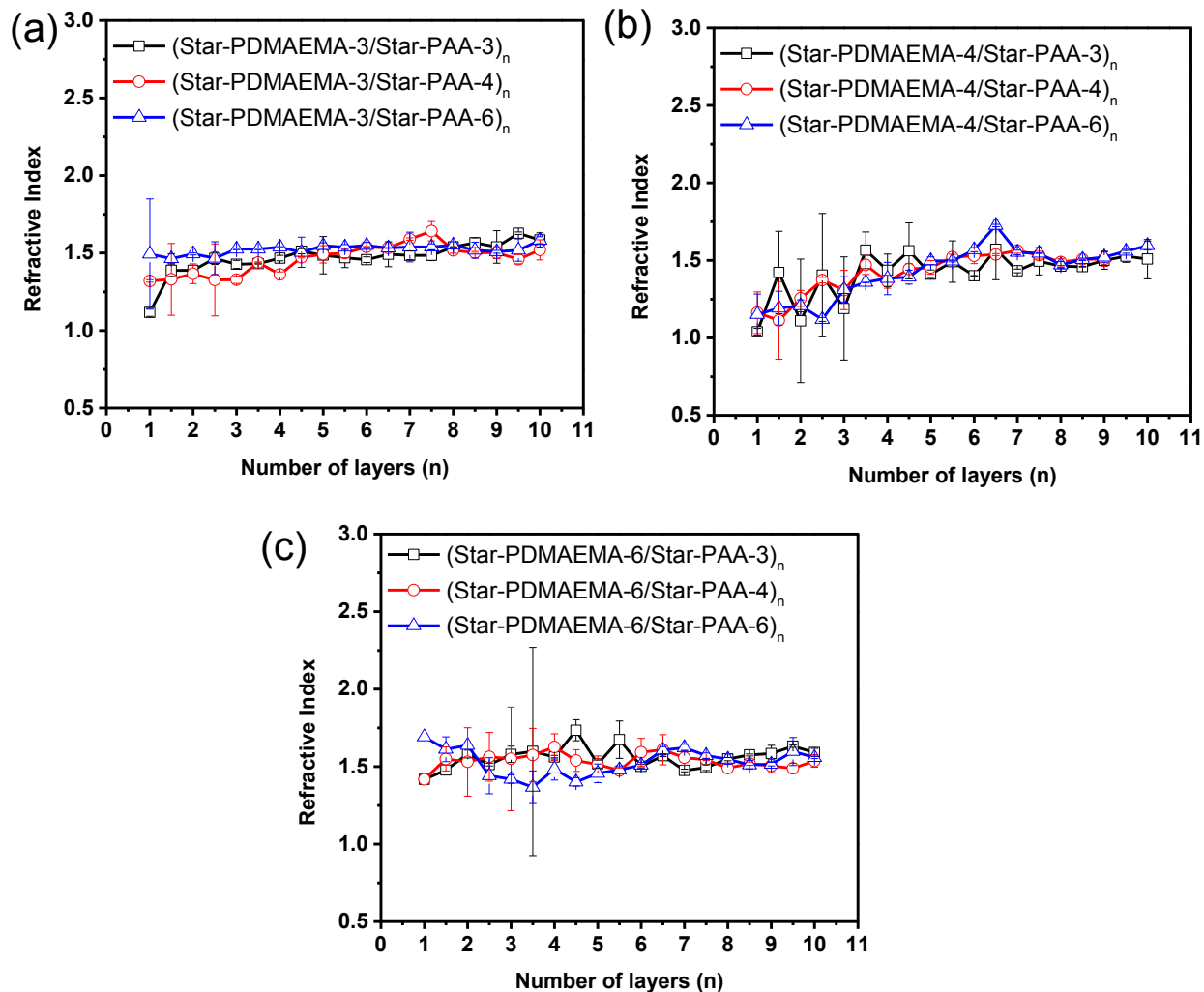
Figure A4.20.Refractive indices (n_f) of s(star-PDMAEMA-X/star-PAA-X)$_n$ films with bilayer number (n) ranging from 1 to 10. Film thickness and refractive index were measured from ellipsometry.

Table A4.4. Porosity of (star-PDMAEMA-X/star-PAA-X)$_n$ films with increasing bilayer number, n.

(n)	Refractive index and Porosity % (P)								
	(PDMAEMA-3/PAA-X)$_n$			(PDMAEMA-4/PAA-X)$_n$			(PDMAEMA-6/PAA-X)$_n$		
	X=3	X=4	X=6	X=3	X=4	X=6	X=3	X=4	X=6
1	1.12 (73)	1.32 (34)	1.49 (7.0)	1.16 (63)	1.04 (91)	1.15 (65)	1.42 (18)	1.42 (18)	1.49 (7.0)
2	1.39 (22)	1.37 (26)	1.48 (6.0)	1.26 (45)	1.11 (75)	1.21 (54)	1.58 (0)	1.53 (1.0)	1.49 (6.0)
3	1.43 (16)	1.33 (32)	1.51 (4.0)	1.31 (35)	1.19 (58)	1.36 (27)	1.57 (0)	1.55 (0)	1.42 (17)
4	1.47 (10)	1.36 (26)	1.54 (0)	1.36 (26)	1.44 (15)	1.44 (14)	1.56 (0)	1.56 (0)	1.48 (7.0)
5	1.49 (7.0)	1.49 (7.0)	1.54 (0)	1.45 (12)	1.41 (18)	1.49 (6.0)	1.52 (3.0)	1.54 (0)	1.46 (11)
6	1.46 (11)	1.54 (0)	1.54 (0)	1.53 (1.0)	1.40 (20)	1.54 (0)	1.50 (5.0)	1.54 (0)	1.51 (4.0)
7	1.49 (7.0)	1.54 (0)	1.54 (0)	1.56 (0)	1.43 (15)	1.54 (0)	1.48(9.0)	1.56 (0)	1.59 (0)
8	1.54 (0)	1.52 (3.0)	1.54 (0)	1.49 (7.0)	1.46 (10)	1.54 (0)	1.54 (0)	1.51 (4.0)	1.54 (0)

245

A4.3.6. Swelling of (star-PDMAEMA-X/star-PAA-X)$_n$ Films.
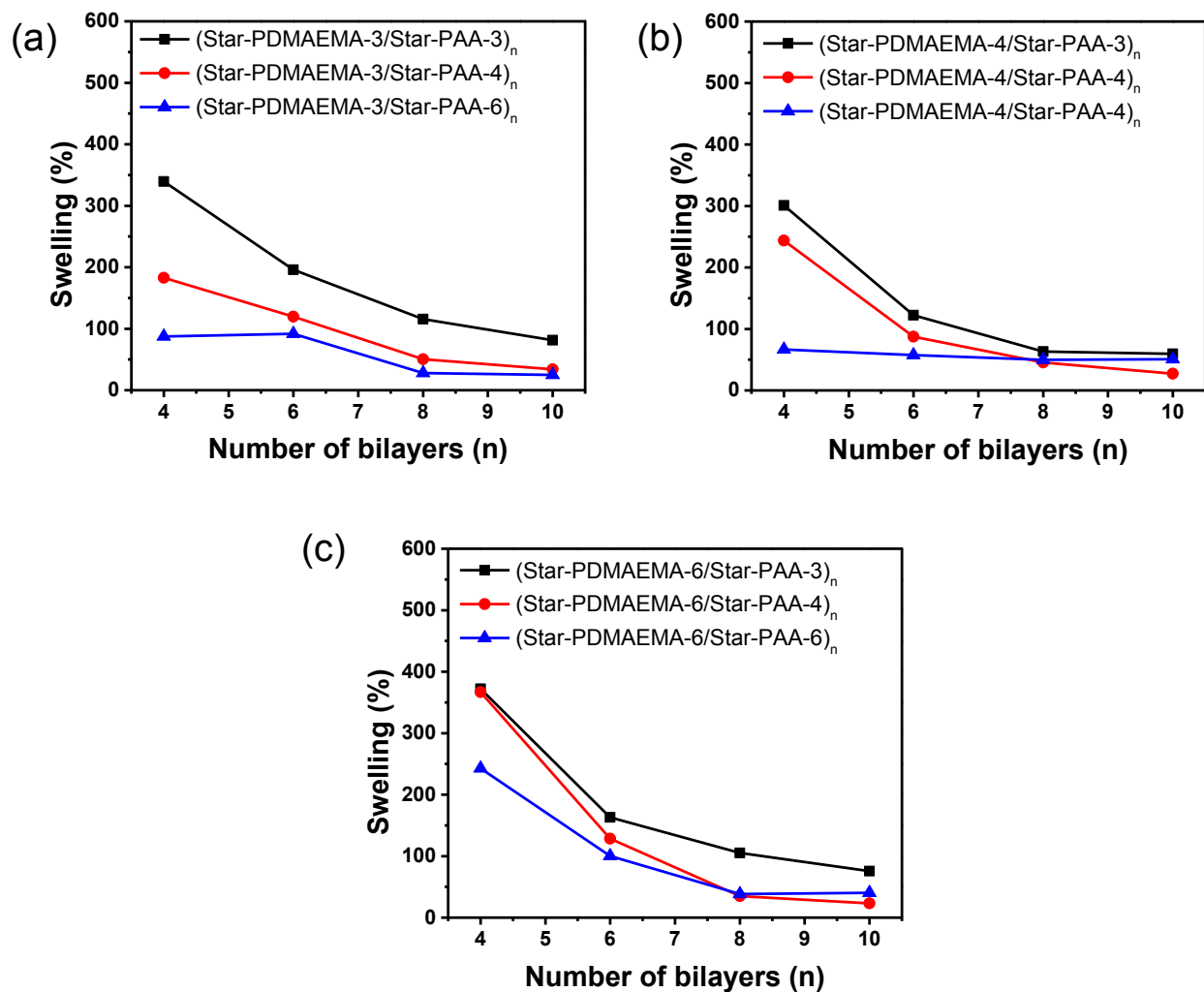
Figure A4.21. Swelling percentages for (star-PDMAEMA-X/ star-PAA-X)$_n$ films (a) 3-3, 3-4, 3-6; (b) star 4-3, 4-4, 4-6 and (c) 6-3, 6-4, 6-6. Numbers indicate sequentially the number of arms in PDMAEMA and PAA.

A4.3.7.Protein Binding to (star-PDMAEMA-6/star-PAA-X)$_n$ Films.
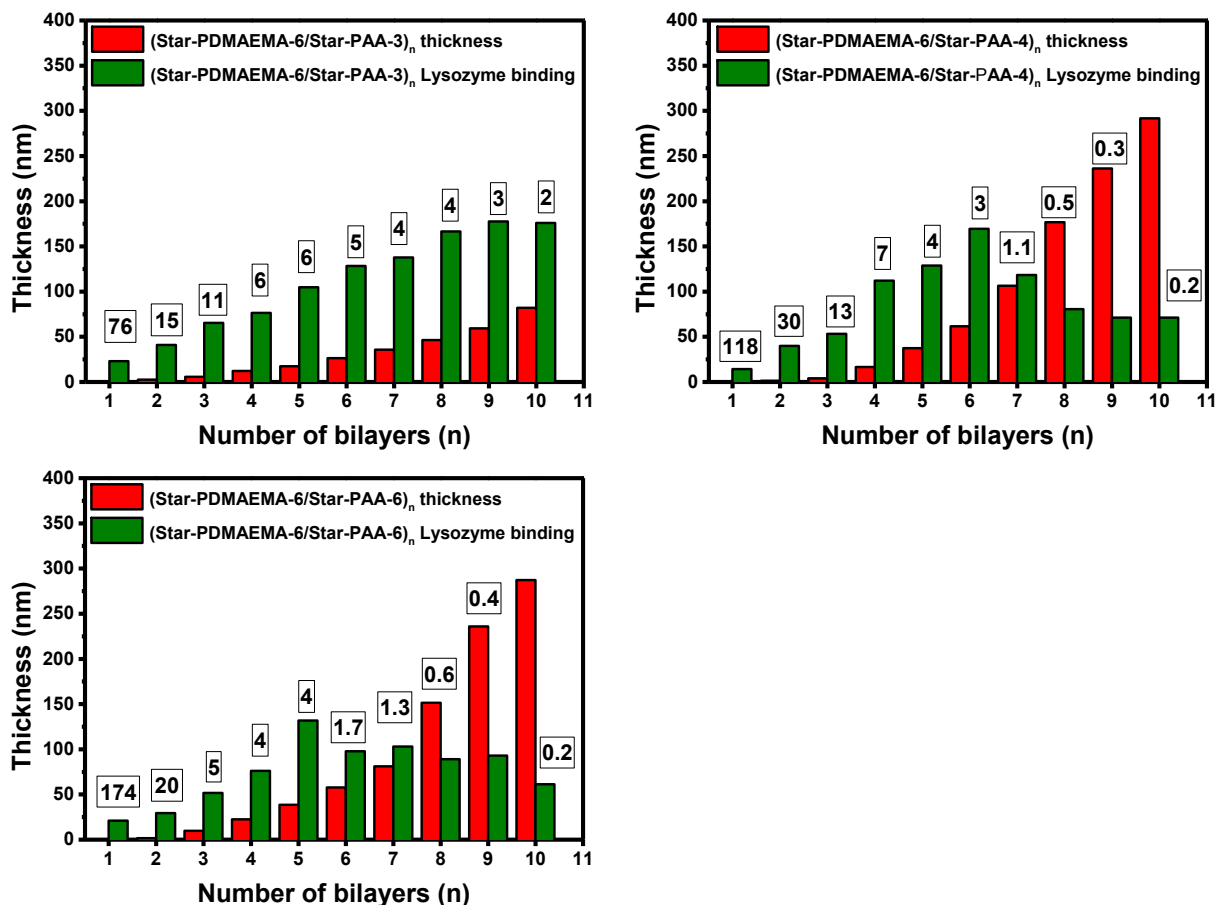
Figure A4.22. Lysozyme binding capacities of (star-PDMAEMA-6/star-PAA-X)$_n$ multilayers (n = 1–10 and X=3, 4 and 6) deposited from polyelectrolyte solutions containing 0.5 M NaCl at pH 3. The numbers above the bars represent the ratios of the lysozyme equivalent thickness to the film thickness. The equivalent thickness is the thickness of spin-coated lysozyme that would give an FTIR absorbance equivalent to that of the sorbed lysozyme.

REFERENCES

REFERENCES

(1)   Jankova, K.; Bednarek, M.; Hvilsted, S. *J. Polym. Sci. Pol. Chem.* **2005**, *43*, 3748-3759.

(2)   Plamper, F. A.; Becker, H.; Lanzendorfer, M.; Patel, M.; Wittemann, A.; Ballauff, M.; Muller, A. H. E. *Macromol. Chem. Phys.* **2005**, *206*, 1813-1825.

(3)   Shim, Y. H.; Bougard, F.; Coulembier, O.; Lazzaroni, R.; Dubois, P. *Eur. Polym. J.* **2008**, *44*, 3715-3723.

(4)   Mendrek, B.; Trzebicka, B. *Eur. Polym. J.* **2009**, *45*, 1979-1993.

(5)   Chen, F.; Liu, G.; Zhang, G. *J. Phys. Chem. B* **2012**, *116*, 10941-10950.

(6)   Kim, B.-S.; Gao, H.; Argun, A. A.; Matyjaszewski, K.; Hammond, P. T. *Macromolecules* **2009**, *42*, 368-375.

(7)   Cho, J.; Hong, J. K.; Char, K.; Caruso, F. *J. Am. Chem. Soc.* **2006**, *128*, 9935-9942.

(8)   Choi, I.; Suntivich, R.; Plamper, F. A.; Synatschke, C. V.; Muller, A. H. E.; Tsukruk, V. V. *J. Am. Chem. Soc.* **2011**, *133*, 9592-9606.

REFERENCES

REFERENCES

(1)   Hammond, P. T. *Adv. Mater.* **2004**, *16*, 1271-1293.

(2)   Decher, G. *Science* **1997**, *277*, 1232-1237.

(3)   Wijeratne, S.; Bruening, M. L.; Baker, G. L. *Langmuir* **2013**, *29*, 12720-12729.

(4)   Yuan, W. Y.; Lu, Z. S.; Li, C. M. *J. Mater. Chem.* **2012**, *22*, 9351-9357.

(5)   Cho, J.; Hong, J.; Char, K.; Caruso, F. *J. Am. Chem. Soc.* **2006**, *128*, 9935-9942.

(6)   Sheng, C. J.; Wijeratne, S.; Cheng, C.; Baker, G. L.; Bruening, M. L. *J. Membr. Sci.* **2014**, *459*, 169-176.

(7)   Jin, W. Q.; Toutianoush, A.; Tieke, B. *Langmuir* **2003**, *19*, 2550-2553.

(8)   Miller, M. D.; Bruening, M. L. *Langmuir* **2004**, *20*, 11545-11551.

(9)   Dotzauer, D. A.; Bhattacharjee, S.; Wen, Y.; Bruening, M. L. *Langmuir* **2009**, *25*, 1865-1871.

(10)   Shchukin, D. G.; Sukhorukov, G. B.; Mohwald, H. *Angew. Chem. Int. Edit.* **2003**, *42*, 4472-4475.

(11)   Ono, S. S.; Decher, G. *Nano. Lett.* **2006**, *6*, 592-598.

(12)   Ning, W. J.; Wijeratne, S.; Dong, J. L.; Bruening, M. L. *ACS Appl. Mater. Inter.* **2015**, *7*, 2575-2584.

(13)   Vogt, C.; Ball, V.; Mutterer, J.; Schaaf, P.; Voegel, J.-C.; Senger, B.; Lavalle, P. *J. Phys. Chem. B* **2012**, *116*, 5269-5278.

(14)   Durstock, M. F.; Rubner, M. F. *Langmuir* **2001**, *17*, 7865-7872.

(15)   Choi, I.; Suntivich, R.; Plamper, F. A.; Synatschke, C. V.; Muller, A. H. E.; Tsukruk, V. V. *J. Am. Chem. Soc.* **2011**, *133*, 9592-9606.

(16)   Kim, B. S.; Gao, H. F.; Argun, A. A.; Matyjaszewski, K.; Hammond, P. T. *Macromolecules* **2009**, *42*, 368-375.

(17)   Fu, G. D.; Yuan, Z. L.; Kang, E. T.; Neoh, K. G.; Lai, D. M.; Huan, A. C. H. *Adv. Funct. Mater.* **2005**, *15*, 315-322.

(18) Lee, B.; Park, Y. H.; Hwang, Y. T.; Oh, W.; Yoon, J.; Ree, M. *Nat. Mater.* **2005**, *4*, 147-151.

(19) Huang, E.; Toney, M. F.; Volksen, W.; Mecerreyes, D.; Brock, P.; Kim, H. C.; Hawker, C. J.; Hedrick, J. L.; Lee, V. Y.; Magbitang, T.; Miller, R. D.; Lurio, L. B. *Appl. Phys. Lett.* **2002**, *81*, 2232-2234.

(20) Zhai, L.; Nolte, A. J.; Cohen, R. E.; Rubner, M. F. *Macromolecules* **2004**, *37*, 6113-6123.

(21) Cho, J.; Quinn, J. F.; Caruso, F. *J. Am. Chem. Soc.* **2004**, *126*, 2270-2271.

(22) Zhang, L.; Zheng, M. A.; Liu, X. K.; Sun, J. Q. *Langmuir* **2011**, *27*, 1346-1352.

(23) Fery, A.; Scholer, B.; Cassagneau, T.; Caruso, F. *Langmuir* **2001**, *17*, 3779-3783.

(24) Hattori, H. *Adv. Mater.* **2001**, *13*, 51-54.

(25) Cebeci, F. C.; Wu, Z. Z.; Zhai, L.; Cohen, R. E.; Rubner, M. F. *Langmuir* **2006**, *22*, 2856-2862.

(26) Sander, M. S.; Gao, H. *J. Am. Chem. Soc.* **2005**, *127*, 12158-12159.

(27) Oekermann, T.; Yoshida, T.; Minoura, H.; Wijayantha, K. G. U.; Peter, L. M. *J. Phys. Chem. B* **2004**, *108*, 8364-8370.

(28) Cho, J.; Hong, J. K.; Char, K.; Caruso, F. *J. Am. Chem. Soc.* **2006**, *128*, 9935-9942.

(29) Guo, Z.; Chen, X.; Xin, J.; Wu, D.; Li, J.; Xu, C. *Macromolecules* **2010**, *43*, 9087-9093.

(30) Yang, S.; Zhang, Y.; Wang, L.; Hong, S.; Xu, J.; Chen, Y.; Li, C. *Langmuir* **2006**, *22*, 338-343.

(31) Connal, L. A.; Li, Q.; Quinn, J. F.; Tjipto, E.; Caruso, F.; Qiao, G. G. *Macromolecules* **2008**, *41*, 2620-2626.

(32) Jankova, K.; Bednarek, M.; Hvilsted, S. *J. Polym. Sci. Pol. Chem.* **2005**, *43*, 3748-3759.

(33) Plamper, F. A.; Becker, H.; Lanzendorfer, M.; Patel, M.; Wittemann, A.; Ballauff, M.; Muller, A. H. E. *Macromol. Chem. Phys.* **2005**, *206*, 1813-1825.

(34) Chen, F.; Liu, G.; Zhang, G. *J. Phys. Chem. B* **2012**, *116*, 10941-10950.

(35)   Shim, Y. H.; Bougard, F.; Coulembier, O.; Lazzaroni, R.; Dubois, P. *Eur. Polym. J.* **2008**, *44*, 3715-3723.

(36)   Harris, J. J.; Bruening, M. L. *Langmuir* **2000**, *16*, 2006-2013.

(37)   Dai, J. H.; Bao, Z. Y.; Sun, L.; Hong, S. U.; Baker, G. L.; Bruening, M. L. *Langmuir* **2006**, *22*, 4274-4281.

(38)   Mendelsohn, J. D.; Barrett, C. J.; Chan, V. V.; Pal, A. J.; Mayes, A. M.; Rubner, M. F. *Langmuir* **2000**, *16*, 5017-5023.

(39)   Hariri, H. H.; Schlenoff, J. B. *Macromolecules* **2010**, *43*, 8656-8663.

(40)   Choi, I.; Suntivich, R.; Plamper, F. A.; Synatschke, C. V.; Müller, A. H. E.; Tsukruk, V. V. *J. Am. Chem. Soc.* **2011**, *133*, 9592-9606.

(41)   Coffinier, Y.; Piret, G.; Das, M. R.; Boukherroub, R. *Comptes Rendus Chimie* **2013**, *16*, 65-72.

(42)   Ke, B. B.; Wan, L. S.; Li, Y.; Xu, M. Y.; Xu, Z. K. *Phys. Chem. Chem. Phys.* **2011**, *13*, 4881-4887.

(43)   Shiratori, S. S.; Rubner, M. F. *Macromolecules* **2000**, *33*, 4213-4219.

(44)   Swanepoel, R. *J. Phys. E Sci. Instrum.* **1983**, *16*, 1214-1222.

(45)   Wong, J. E.; Rehfeldt, F.; Hänni, P.; Tanaka, M.; Klitzing, R. v. *Macromolecules* **2004**, *37*, 7285-7289.

(46)   Ma, Y.; Dong, J.; Bhattacharjee, S.; Wijeratne, S.; Bruening, M. L.; Baker, G. L. *Langmuir* **2013**, *29*, 2946-2954.

(47)   Mustang Membrane Chromatography Starter Kits. http://www.pall.com/main/Biopharmaceuticals/Product.page?id=33053 (accessed July, 19 2015).

(48)   Bhattacharjee, S.; Dong, J.; Ma, Y.; Hovde, S.; Geiger, J. H.; Baker, G. L.; Bruening, M. L. *Langmuir* **2012**, *28*, 6885-6892.

CHAPTER 5. SYNTHESIS OF REDUCED DENSITY POLYMER BRUSHES FOR POTENTIAL PROTEIN-BINDING APPLICATIONS.

5.1. Introduction.

Chain density should directly affect the protein-binding capacity of polymer brushes. As Figure 5.1 suggests, for highly swollen films lower chain densities should lead to increased protein access within the brush and hence greater binding.

(A) Conventional polymer brushes
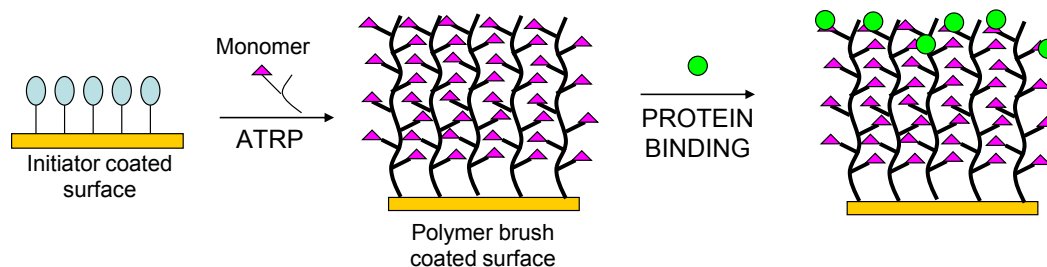
(B) Reduced density polymer brushes
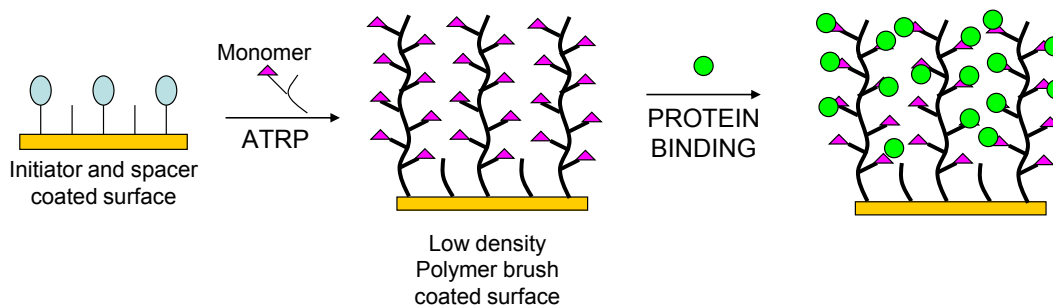
Figure 5.1. Protein binding (a) at the surface of a dense polymer brush and (b) in the interior of a brush with reduced density.[1]

For example, Anuraj et al.[1] prepared poly(MES) brushes in two ways (Scheme 5.1. : direct polymerization of MES and polymerization of poly(HEMA) followed by reaction with succinic anhydride. Although both brushes are poly(MES), the steric crowding should be much greater for the poly(HEMA) reacted with succinic anhydride because the reaction with succinic anhydride adds material to the brush.
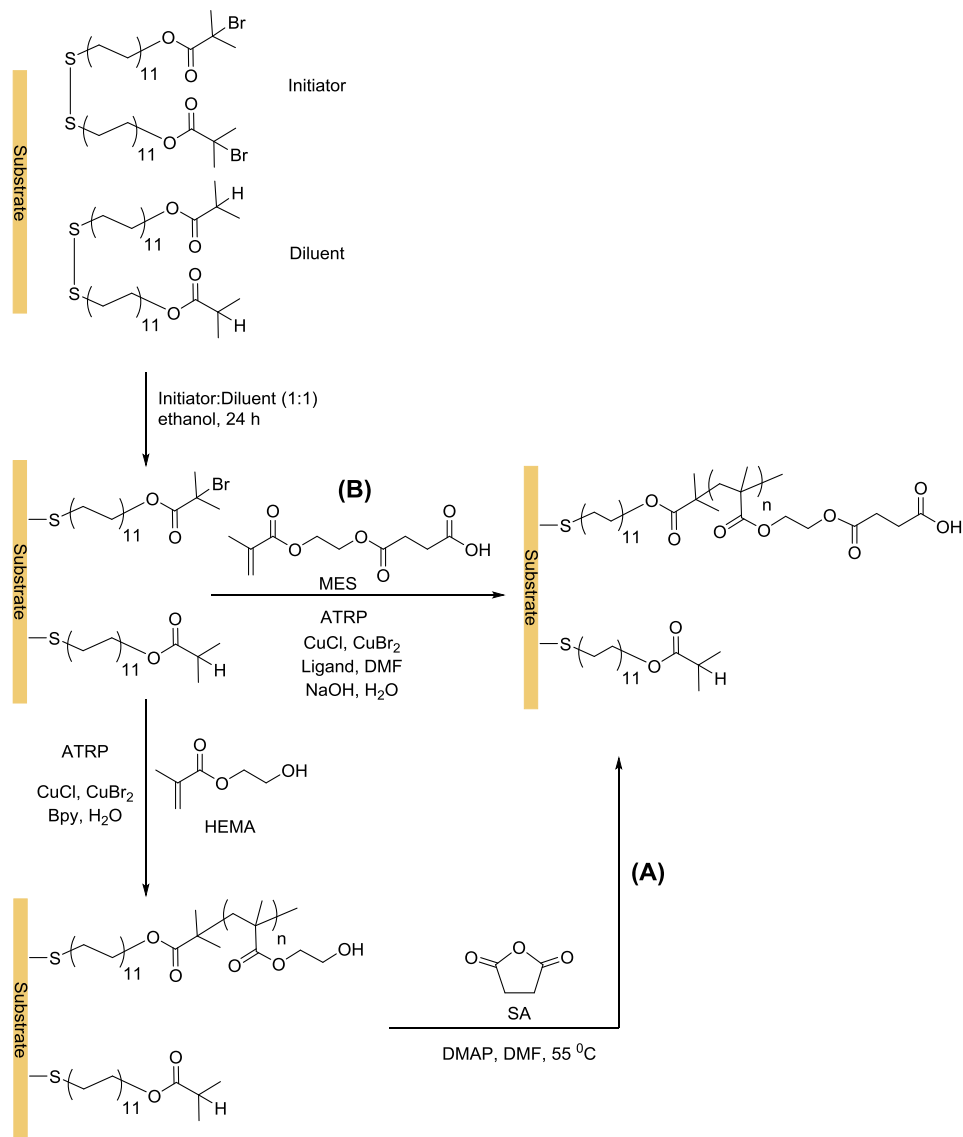
Scheme 5.1. Synthesis of reduced-density polymer brushes from monolayers containing initiator and diluent molecules. Polymerization of MES (reaction B) and polymerization of HEMA followed by reaction with succinic anhydride (SA) (reaction A) both yield poly(MES) brushes with nominally the same formula but different chain spacing.

Interestingly, these two types of poly(MES) bind considerably different protein amounts. Brushes prepared by direct polymerization of MES bind at least twice as much protein as poly(HEMA) derivatized with succinic anhydride, even when using two different initiator densities for brush growth.

There are several ways to grow polymer brushes on a surface. Among these techniques surface-initiated ATRP is especially popular due to the simplicity of the technique and its potential for growing well-defined brushes.[2] ATRP can occur under mild reaction conditions (e.g. room temperature aqueous solutions) with readily available catalysts and monomers. Moreover, with initiators anchored to a substrate, ATRP generates radicals primarily on the surface and minimizes polymerization in solution, which could lead to physisorbed polymers rather than simple chains covalently linked to the substrate.[3]
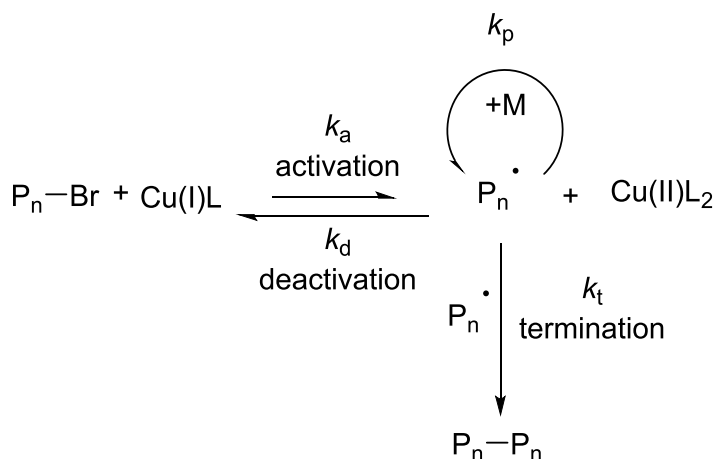
Scheme 5.2. Kinetic scheme for ATRP: pathways for polymerization and radical generation and consumption.[4]

ATRP achieves control over polymerization by maintaining a low concentration of radicals through transfer of a halogen atom between growing chains and metal-ion

complexes (Scheme 5.2). In the activation step, the halogen atom (Cl or Br) transfers from a growing chain to a catalyst, which is typically a Cu(I) species. This step forms a radical on the surface, whereas the reverse reaction will reform the reduced metal-ion species and dormant chain. Because the activation/deactivation equilibrium significantly lies towards the dormant state, the number of active chains (radicals) at a given time is low. This leads to minimal radical termination and relatively constant rates of chain growth. Moreover, fast initiation and rapid equilibrium conversion between active and dormant states also yields low polydispersities among chain molecular weights. The polymerization rate depends on the type and the amount of transition metal catalyst, ligand, solvent and initiator.

When using ATRP to grow polymer brushes, there are several methods for controlling the chain density.[5,6,7,8] The most popular of these methods is the use of an initiator diluent in a self-assembled monolayer to decrease the number of sites available for chain growth (Scheme 5.1). However, initiator densities as low as 1% and 5% of a self assembled monolayer give very low growth rates, and the extent of polymerization is small even after long polymerization times. This resulted in a maximum film thickness of only 15 nm with monolayers containing 1% initiator.[5]
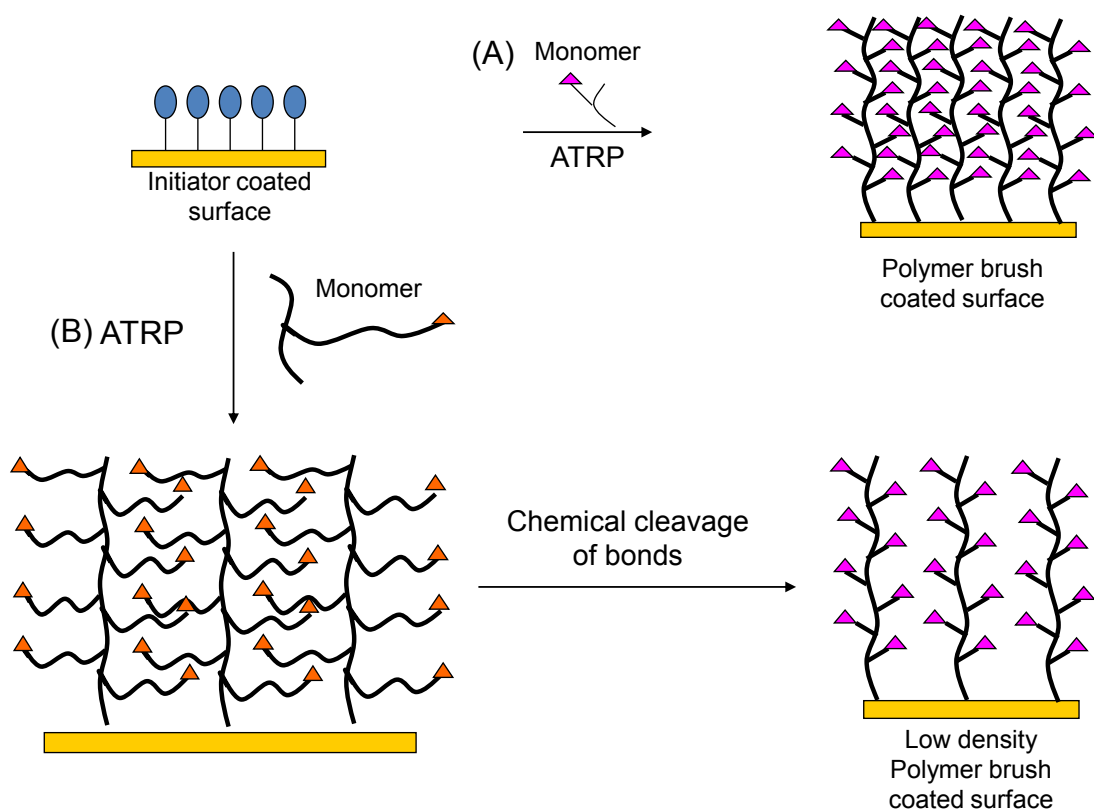
Figure 5.2. Synthesis of (a) high-density polymer brushes using a monomer with a short side chain and (b) reduced density polymer brushes through polymerization of a monomer with a long side chain and subsequent side-chain removal.

We propose polymerization of monomers with a large side chain followed by removal of the side chain to obtain reduced-density polymer brushes that may have high protein-binding capacities compared to conventional polymer brushes (Figure 5.2).[1] This chapter explores the synthesis of such monomers, formation of polymer brushes, cleavage of side chains, and protein capture in these films.

5.2. Experimental.

5.2.1. Materials.

CuBr (99.999%), CuBr$_2$ (99%), 2,2'-bipyridine (bpy, 99%), 1,1,4,7,10,10-hexamethyltriethylenetetramine (HMTETA, 97%), N,N,N',N'',N''-penta methyldiethylenetriamine (PMDETA, 99%), 1,4,8,11-tetraaza-1,4,8,11-tetramethyl cyclotetradecane (Me$_4$Cyclam, 99%), 3-mercaptopropyl-trimethoxysilane (MPS, 95%), 4,4'-dinonyl-2,2'-bipyridine (dnNbpy, 97%), 4-(dimethylamino)pyridine (DMAP, 99%), thionyl chloride (SOCl$_2$, >99%), ethyl α-bromoisobutyrate (EBIB, 97%), 3,6,9-trioxaundecanedioic acid (>70%), 2-(2-(2-methoxyethoxy)ethoxy)acetic acid (Technical grade), methylmagnesium bromide (3.0 M in diethyl ether), and methacryloyl chloride (97%, contains ~200 ppm monomethyl ether hydroquinone as stabilizer) were used as received from Aldrich. 2-Hydroxyethyl methacrylate (HEMA, Aldrich, 98%) and methyl methacrylate (MMA, Aldrich, 99%) were passed through a 10cm long, 0.5 cm diameter column of activated basic alumina and then distilled from calcium hydride to remove inhibitors. The disulfide initiator, 11-[(2-bromo-2-methyl)propionyloxy]undecyl-disulfide,[9] and 2-bromo-2-methyl-N-(3-trimethoxysilyl propyl)propionamide[10] were synthesized using slightly modified versions of literature procedures. Triethylamine (Et$_3$N) was distilled from calcium hydride under a nitrogen atmosphere and stored under nitrogen. Dimethylformamide (DMF, anhydrous, Aldrich, 99.8%), anisole (Aldrich, 99.7%), tetrahydrofuran (THF, Aldrich, 99%) distilled with CaH$_2$, dichloromethane (CH$_2$Cl$_2$), chloroform (CHCl$_3$) and deionized water (Milli-Q, 18 MΩ cm) were used as solvents for reactions and polymerizations. Gold-coated wafers (electron beam evaporation of 200 nm of gold on 20 nm of Cr on Si(100) wafers or sputter coating of 200 nm of gold on 20

nm of Cr on Si(100) wafers) were cleaned in a UV/O$_3$ chamber for 15 min just before use.

5.2.2. Characterization Methods.

A Varian UnityPlus-500 spectrometer was used to record ^{1}H and ^{13}C NMR spectra at room temperature, and the chemical shifts are reported in ppm and referenced to residual solvent signal. Polymer molecular weights were determined by gel permeation chromatography with a multi-angle light scattering detector (GPC-MALLS) at 35 °C using two PLgel 10 μm mixed-B columns in series (manufacturer-stated linear molecular weight range of 500-10×10^6 g/mol). The eluting solvent was THF at a flow rate of 1 mL/min. An Optilab rEX (Wyatt Technology) refractive index detector and a DAWN EOS 18-angle light scattering detector (Wyatt Technology) with a laser wavelength of 684 nm were used to calculate absolute molecular weights. Ellipsometric measurements were obtained with a rotating analyzer spectroscopic ellipsometer (model M-44, J. A. Woollam) using WVASE32 software. When calculating film thicknesses, the angle of incidence was 75° and the refractive index was assumed as 1.50. Reflectance Fourier Transform Infrared (reflectance FTIR) spectra of films were obtained with a Thermo Nicolet 6700 FTIR spectrometer that contained a mercury-cadmium telluride detector and a PIKE grazing angle (80°) attachment.

5.2.3. Synthesis of Monomers with Long Side Chains.

5.2.3.1. Preparation of the Intermediate Diethyl 2,2'-((oxybis(ethane-2,1-diyl))bis(oxy)) diacetate, 3 (Scheme 5.3).[11]

Under a N_2 atmosphere, thionyl chloride (12 mL, 162 mmol) was added to a solution of 3,6,9-trioxaundecanedioic acid (**1**, M_n~250, 14.5 g, 65 mmol) in CH_2Cl_2 (50 mL), and the solution was stirred for 3 h at 40 °C. After evaporation of excess thionyl chloride and CH_2Cl_2 in vacuo, the residue was added dropwise to a 100-ml round-bottomed flask containing ethanol (7 mL, 162 mmol). This mixture was stirred at 40 °C for 3 h, and evaporation of excess ethanol in vacuo afforded **3** (Scheme 5.3) as a pale-yellow liquid with 54% yield (9.7 g, 35 mmol). IR (KBr): 2982, 2876, 1734, 1278, 1032 cm^{-1}. ^{1}H NMR (500 MHz, CDCl$_3$): δ 1.27 (t, J = 7.14 Hz, 3H), 3.69-3.74 (m, PEG-methylenes), 4.14 (s, 2H), 4.21 (q, J = 7.14 Hz, 2H). ^{13}C NMR (125 MHz, CDCl$_3$): 14.11, 61.0, 70.10, 71.24, 170.0.

5.2.3.2. Preparation of Intermediate 1,1'-((oxybis(ethane-2,1-diyl))bis(oxy)) bis(2-methylpropan-2-ol), 4 (Scheme 5.3).[12]

Under a N_2 atmosphere, methyl magnesium bromide (50 mL, 150 mmol) was added to a 500-mL three-necked flask equipped with a reflux condenser and cooled to 0 °C using an ice bath. Compound **3** (7.0 g, 25 mmol) was added dropwise while stirring at 0 °C. The mixture was refluxed for 2 h and completion of the reaction was monitored using proton ^{1}H-NMR spectroscopy. The mixture was cooled to 0 °C using an ice bath,

quenched with distilled water (20 mL), and 2.5 M HCl was added dropwise until the white solid dissolved. After evaporation of excess water in vacuo, the product was extracted into chloroform. Evaporation of chloroform in vacuo gave **4** as a pale yellow liquid in 90% yield (5.0 g, 22.5 mmol). IR (KBr): 3426, 2972, 2874, 1469, 1051 cm^{-1}. ^{1}H NMR (500 MHz, CDCl$_3$): δ 1.19 (s, 12H), 3.34 (s, 4H), 3.65- 3.70 (m, PEG-methylenes), 4.02 (s, 2H). ^{13}C NMR (125 MHz, CDCl$_3$): 26.15, 70.41, 70.79, 71.02, 87.13.

5.2.3.3. Synthesis of Triethyleneglycol-bis-methacrylate (TEGBMA), 6 (Scheme 5.3).

This compound was synthesized according to a published procedure with some modifications.[13] Under a N$_2$ atmosphere, compound **4** (7.0 g, 32 mmol), TEA (9 ml, 64 mmol), DMAP (0.78 g, 6.4 mmol) and methacryloyl chloride (5 mL, 64 mmol) were added to a 100-mL Schlenk flask that contained THF(10 mL) at 0 °C, and the solution was stirred for 24 h at room temperature. Subsequently 5% sodium carbonate (20 mL) was added to the solution to quench the unreacted methacrolyl chloride. The product was extracted in chloroform (10 mL×4) and passed through an alumina column to give **6** as a pale yellow liquid in 70% yield (8.6 g, 22.4 mmol). IR (KBr): 2974, 2872, 1713, 1603, 1115 cm^{-1}. ^{1}H NMR (500 MHz, CDCl$_3$): δ 1.38 (s, 6H), 1.96 (s, 6H), 3.68- 4.28 (m, PEG-methylenes), 5.50 (s, 2H), 6.05 (s, 2H); ^{13}C NMR (125 MHz, CDCl$_3$): 18.58, 23.53, 70.83, 71.47, 76.93, 81.90, 124.94,137.86, 166.94.

5.2.3.4. Preparation of Intermediate 2-(2-(2-methoxyethoxy)ethoxy)acetate, 9 (Scheme 5.4).[11]

Similar to preparation of **3**, reaction of 2-(2-(2-methoxyethoxy)ethoxy)acetic acid (**7**, 12 g, 65 mmol) with thionyl chloride (8 mL, 98 mmol) and ethanol (4 mL, 81 mmol) afforded ethyl 2-(2-(2-methoxyethoxy)ethoxy)acetate, **9,** in 94% yield (12.6 g, 61 mmol). IR (KBr): 2982, 2934, 2834, 1750, 1203, 1116 cm^{-1}. ^{1}H NMR (500 MHz, CDCl$_3$): δ 1.24 (t, J = 7.14 Hz, 3H), 3.34 (s, 3H), 3.50- 3.71 (m, PEG-methylenes), 4.10 (s, 2H), 4.17 (q, J = 7.14 Hz, 2H); ^{13}C NMR (125 MHz, CDCl$_3$): 14.36, 59.16, 60.94, 68.85, 70.67, 70.79, 71.02, 170.60.

5.2.3.5. Preparation of Intermediate 1-(2-(2-methoxyethoxy)ethoxy)-2-methylpropan-2-ol, 10 (Scheme 5.4).[12]

Following the general procedure in 5.2.3.2, reaction of ethyl 2-(2-(2-methoxyethoxy)ethoxy) acetate (12.6 g, 61 mmol) with methyl magnesium bromide (40 mL, 122 mmol) afforded 1-(2-(2-methoxyethoxy)ethoxy)-2-methylpropan-2-ol, **10** in 74% yield (9.3 g, 49 mmol). IR (KBr): 3456, 2974, 2876, 1469, 1109 cm^{-1}. ^{1}H NMR (500 MHz, CDCl$_3$): δ 1.14 (s, 6H), 2.74 (s, 1H), 3.27 (s, 2H), 3.33 (s, 3H), 3.49-3.64 (m, PEG-methylenes); ^{13}C NMR (125 MHz, CDCl$_3$): 26.20, 59.16, 70.42, 70.62, 70.68, 71.24, 72.08, 79.91.

5.2.3.6. Synthesis of 1-(2-(2-Methoxyethoxy)ethoxy)-2-methylpropan-2-yl methacrylate (MEEMPM), 12 (Scheme 5.4).[12]

Similar to preparation of **6**, the reaction of **10** (9.3 g, 49 mmol) with methacrolyl chloride (6 mL, 73 mmol) in the presence of TEA (10 mL, 72 mmol) and DMAP (1.2 g, 9.7 mmol) afforded **12** in 56% yield (7.0 g, 27 mmol). IR (KBr): 2990, 2875, 1720, 1633, 1215 cm^{-1}. ^{1}H NMR (500 MHz, CDCl$_3$): δ 1.45 (s, 6H), 1.86 (s, 3H), 3.34- 3.63 (m, PEG-methylenes), 5.46 (s, 2H), 5.98 (s, 2H); ^{13}C NMR (125 MHz, CDCl$_3$): 18.54, 23.50, 59.21, 70.76, 70.84, 71.39, 72.17, 76.91, 81.81, 124.84, 137.82, 166.84.

5.2.3.7. Synthesis of 2,2-Dimethacroyloxy-1-ethoxypropane (DMOEP), 15 (Scheme 5.5).[14]

Under N$_2$, HEMA (**13**, 20 mL, 160 mmol), 2,2-dimethoxypropane (**14**, 10.1 mL, 82.1 mmol), *p*-TSA (50 mg, 0.3 mmol) and anhydrous benzene (50 mL) were added to a 250-mL Schenk flask, and the mixture was stirred for 24 h at 60 °C in the dark. The crude product was purified by flash column chromatography on silica gel using a mobile phase of 85:14:1 hexane/ethylacetate/TEA. Fractions containing the pure product were pooled, solvent was removed by rotatory evaporation, and the compound was dried overnight under vacuum to afford **15** as a pale yellow oil with 90% yield (47 g, 144 mmol). ^{1}H NMR (500 MHz, CDCl$_3$): δ 1.45 (s, 6H), 1.86 (s, 3H), 3.34-3.63 (m, PEG-methylenes), 5.57 (s, 2H), 6.11 (s, 2H). ^{13}C NMR (125 MHz, CDCl$_3$): 18.54, 23.50, 59.21, 70.76, 70.84, 71.39, 72.17, 76.91, 81.81, 124.84, 137.82, 166.84.

5.2.4. Polymerization of TEGBMA (6) in Solution (Scheme 5.6).[13]

TEGMA (0.3 g, 0.8 mmol) and bpy (9.4 mg, 0.06 mmol) or HMTETA (7.0 mg, 0.03 mmol) were dissolved in EtOH (3 mL) in a 25 ml Schlenk, and the solution was degassed with five freeze-pump-thaw cycles. The solution was frozen under N_2, and CuBr (3 mg, 0.03 mmol) or/and $CuBr_2$ (20 µg, 0.0015 mmol) were added. After three freeze-pump-thaw cycles, ethyl-α-bromoisobutyrate (20 µl, 0.14 mmol) was added, and the mixture was stirred for 24 or 48 h at room temperature. White poly(triethyleneglycol-bis-methacrylate) was precipitated using distilled water, dried in vacuo, and characterized by ^{1}H NMR spectroscopy, gel permeation chromatography (GPC) (see the results and discussion section).

5.2.5. Acid-catalyzed Hydrolysis of poly(TEGBMA) in Solution (Scheme 5.7).[15]

Poly(TEGBMA) ($M_n \sim 7.17 \times 10^5$ g mol^{-1}) was hydrolyzed using aqueous HCl in THF. Specifically, 0.1 g of the polymer was transferred to a glass vial containing 2.5 M HCl in THF (5 mL), and hydrolysis occurred at room temperature for 48 h. After evaporation of THF and water in vacuo, the resulting polymer was characterized using ^{1}H-NMR and FT-IR spectroscopyn (see the results and discussion section).

5.2.6. Surface-initiated Polymerization from Non-cross-linked Initiator on Au-coated Wafers[13,16]

5.2.6.1. Preparation of Non-cross-linked Initiator Monolayers on Au-coated Substrates.

Au-coated Si wafers were cleaned with UV-ozone for 30 min and immersed in 1 mM disulfide initiator, $(BrC(CH_3)_2COO(CH_2)_{11}S)_2$, in ethanol for 24 h to form monolayers of this initiator. The slides were then rinsed with ethanol and dried with N_2.

5.2.6.2. Surface-initiated Polymerization of TEGBMA from Initiators on Au-coated Substrates.

TEGBMA in EtOH (1:1, v:v; 2.2 g, 5.8 mmol of TEGBMA) and bpy (18 mg, 116 µmol) were added to a Schlenk flask under a N_2 atmosphere. The solution was degassed with three freeze-pump-thaw cycles prior to addition of CuBr (5.6 mg, 57 µmol). The reaction mixture was warmed to room temperature with continuous stirring until a homogeneous dark brown solution formed. Under N_2, the monomer/catalyst solution was transferred into a vial containing an initiator-modified Au substrate and kept at room temperature without stirring during polymerization. After a predetermined reaction time, the substrate was removed from the vial, washed with ethanol and dried under a stream of N_2. Surface-inititated methylmethacrylate polymerization was carried out as a model reaction under similar conditions (the same monomer concentration).

Films were characterized using reflectance Fourier Transform Infrared (reflectance FTIR) spectroscopy or ellipsometry.

5.2.6.3. Effect of Solvent on Surface-initiated Polymerization of TEGBMA from Initiators on Au-coated Substrates.

TEGBMA in solvent (TEGBMA/solvent, 1:1, v:v; 2.2 g, 5.8 mmol of TEGBMA) or different solvent combinations (EtOH, MeOH/H_2O, DMF/H_2O) and bpy (18 mg, 116 µmol) were added to a Schlenk flask under a N_2 atmosphere. After three freeze-pump-thaw cycles and addition of CuBr (5.6 mg, 57 µmol) under N_2, surface-initiated polymerization was carried out as described above. In separate experiments surface-initiated methylmethacrylate polymerization occurred under similar conditions as a model reaction.

5.2.6.4. Effect of Addition of Cu^{2+} on Surface-initiated Polymerization of TEGBMA.

TEGBMA/EtOH (1:1, v:v; 2.2 g, 5.8 mmol of TEGBMA), $CuBr_2$ (7.6 mg, 17 µmol) and bpy (18 mg, 116 µmol) were added to a Schlenk flask under a N_2 atmosphere. After three freeze-pump-thaw cycles, CuBr (5.6 mg, 57 µmol) was added, and surface-initiated polymerization was carried out as described above. In separate experiments surface-initiated MMA occurred under similar conditions.

5.2.6.5. Effect of Different Cu-ligand Systems on Surface Polymerization of TEGBMA.

TEGBMA/EtOH (1:1, v:v; 2.2 g, 5.8 mmol of TEGBMA) and different types of ligands (HMTETA and PMDETA) (116 µmol) were added to a Schlenk flask under an nitrogen atmosphere. After three freeze-pump-thaw cycles, CuBr (5.6 mg, 57 µmol) was added to the flask under N_2, and surface-initiated polymerization was carried out as described above. Surface-initiated MMA polymerization occurred under similar conditions.

5.2.6.6. Effect of Different Monomers on Surface-initiated Polymerization.

DMOEP/EtOH or (MEEMPM)/EtOH (1:1, v:v; 5.8 mol of monomer) and bpy or HMTETA (116 µmol) were added to a Schlenk flask under a N_2 atmosphere. After three freeze-pump-thaw cycles, CuBr (5.6 mg, 57 µmol) was added to the solution under N_2, and surface-initiated polymerization was carried out as described above.

5.2.7. Surface-initiated Polymerization from Cross-linked Initiator Films.[17]

5.2.7.1. Immobilization of Initiators on Gold.

Au-coated substrates were immersed in 2 mM methanolic solutions of 3-mercaptopropyl-trimethoxysilane (MPS) for 12 h at room temperature to form a layer on the surface. A more cross-linked, hydroxylated surface was formed by hydrolyzing

the silane monolayer with 0.1 M HCl for 15 h at room temperature. The Au substrates with cross-linked, hydroxylated films were immersed in a 10 mM solution of 2-bromo-2-methyl-*N*-(3–trimethoxysilyl-propyl) propionamide, in toluene at 55 $^{\circ}$C for 12 h to modify the surface with bromide groups that can initiate ATRP. These substrates were rinsed repeatedly with toluene and isopropanol, and then dried under a stream of N_2.

5.2.7.2. Surface-initiated Polymerization of TEGBMA or DMOEP from Cross-Linked Initiator Films.

CuBr$_2$(dnNbpy)$_2$ (3.8 mg, 6 µmol), Me$_4$Cyclam (1.5 mg, 6 µmol) and TEGBMA (1.0 g, 3.0 mmol) or DMOEP (0.9 g, 3.0 mmol)) were added to a Schlenk flask containing 3 mL of a degassed solution of monomer in DMF/anisole ((monomer/DMF/anisole) 1:1:1 v:v:v, [monomer]~1.0 M). Using three freeze-pump-thaw cycles the solution was degassed, and under N_2-purging, CuBr (1 mg, 6 µmol) was added to the mixture, which was then heated with an oil bath to 50 $^{\circ}$C and stirred until it formed a transparent light green solution. Under N_2, the solution was transferred into a vial containing an initiator-modified substrate to start the surface-initiated polymerization. After a predetermined reaction time at 50 $^{\circ}$C, the substrate was removed from the vial, washed with ethyl acetate and THF sequentially, and then dried under a stream of N_2.

5.2.8. Acid-catalyzed Hydrolysis of the Poly(TEGBMA) Film.

TEGBMA films on Au wafers were incubated in a solution of 2.5 M HCl in THF (5 mL), at room temperature for 48 h. After washing with THF and water, the modified films were characterized using reflectance-FTIR spectroscopy.

5.3. Results and Discussion.

5.3.1. Synthesis of Monomers and Polymers with Spacer Arms.

This work presents a convenient synthesis of reduced-density polymer brushes for protein-binding applications. First we employed two different cross-linkable monomers with cleavable side chains to achieve reduced density polymer brushes. Cross-linkable monomers might help to prevent the collapsing of spaced polymer brushes via crosslinking throughout polymerization. However, a non-crosslinkable monomer with a cleavable side chain was also synthesized to fabricate reduced density polymer brushes.

5.3.1.1. Synthesis of TEGBMA, 6.

The novel monomer TEGBMA was prepared as shown in Scheme 5.3 with a 32% overall yield.
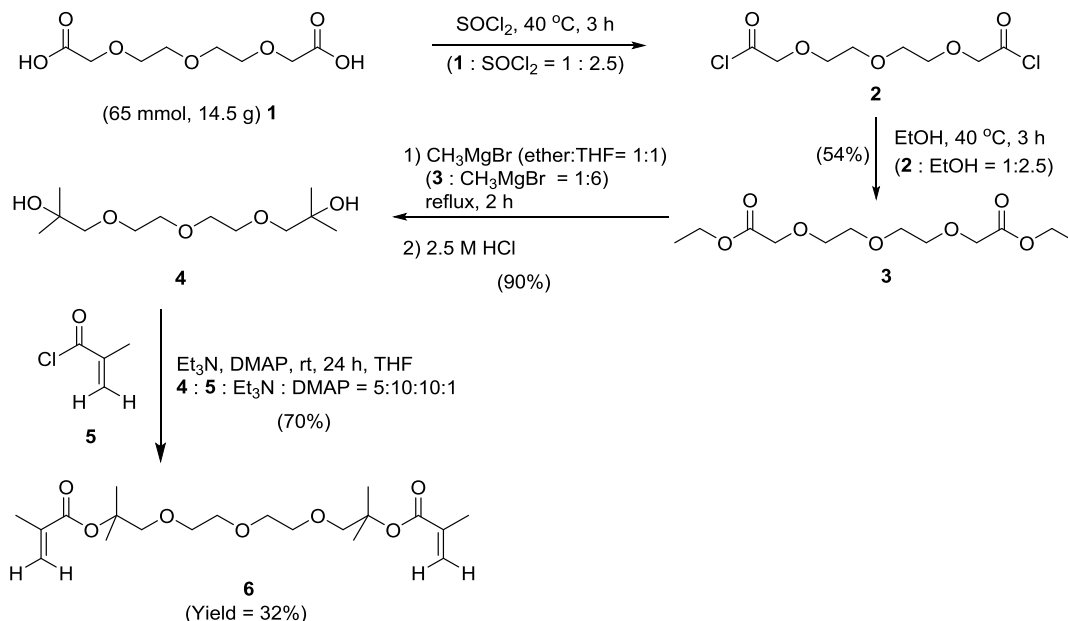
Scheme 5.3. synthesis of a cross-linkable monomer, **6**, with cleavable side chains.

After isolation of compound **6**, the chemical structure of the monomer was confirmed by ^{1}H NMR, ^{13}C NMR and FTIR spectroscopy. Figure 5.3C shows the ^{1}H NMR spectra of TEGBMA, **6,** and intermediate reactants **4** (Figure 5.3B) and **3** (Figure 5.3A). In spectrum C, the peak at 1.49 ppm stems from CH_3 protons adjacent to the ester groups, and the signal at 1.90 ppm results from the CH_3 protons of the methacrylate group. Signals from ethylene protons of the triethyleneglycol backbone appear around 3.65 ppm. The two singlets at 5.50 and 6.02 ppm stem from the vinyl protons of the methacrylate group, and these protons show a shift from 6.05 and 6.51 ppm, respectively, from the spectrum of methacryloyl chloride (not shown).
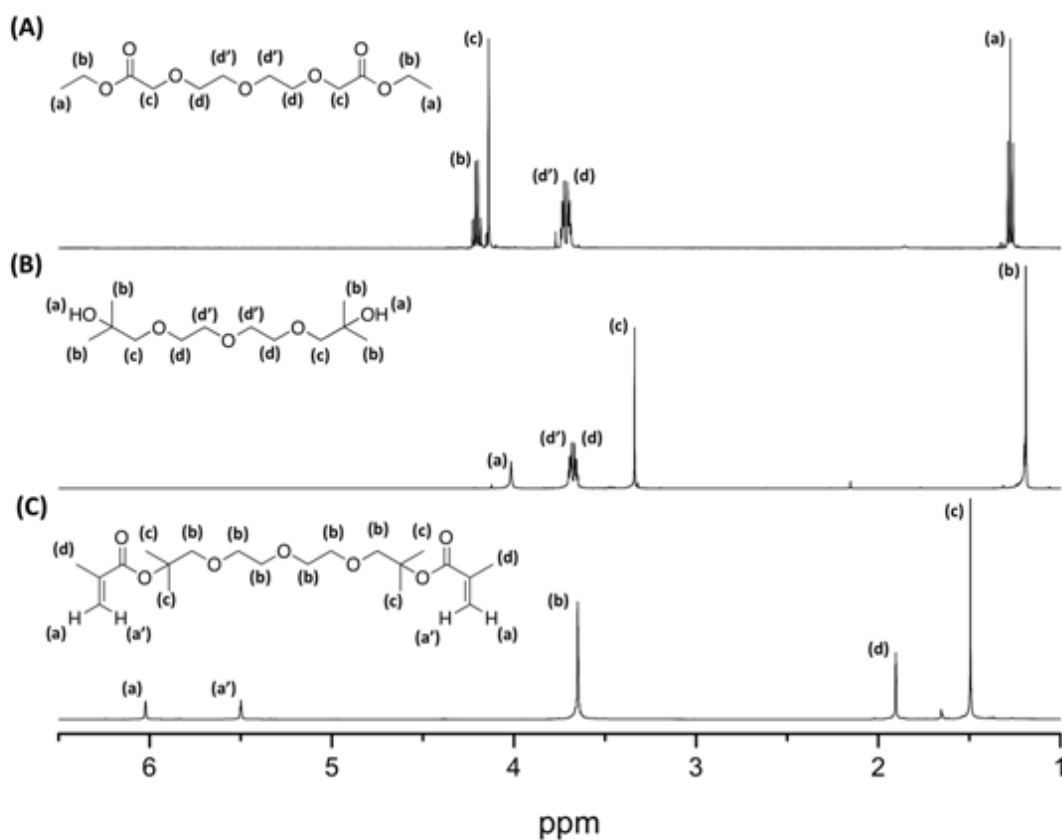
Figure 5.3. ^{1}H NMR spectra of (A) 2,2'-((oxybis(ethane-2,1-diyl))bis(oxy))diacetate, **3**; (B) 1,1'-((oxybis(ethane-2,1-diyl))bis(oxy))bis(2-methylpropan-2-ol), **4**; and (C) TEGBMA **6** in CDCl$_3$

The splitting of the vinyl proton resonances occurs because the conjugation of carbonyl and vinyl groups limits the bond mobility and makes the two protons surrounded by different chemical environments.[18]

5.3.1.2. Synthesis of MEEMPM, 12.

Similar to the synthesis of 6, MEEMPM **12**, was synthesized as shown in the Scheme 5.4 with 41% overall yield. After isolation, the chemical structure of the monomer was confirmed by ^{1}H NMR, ^{13}C NMR and FTIR spectroscopy.
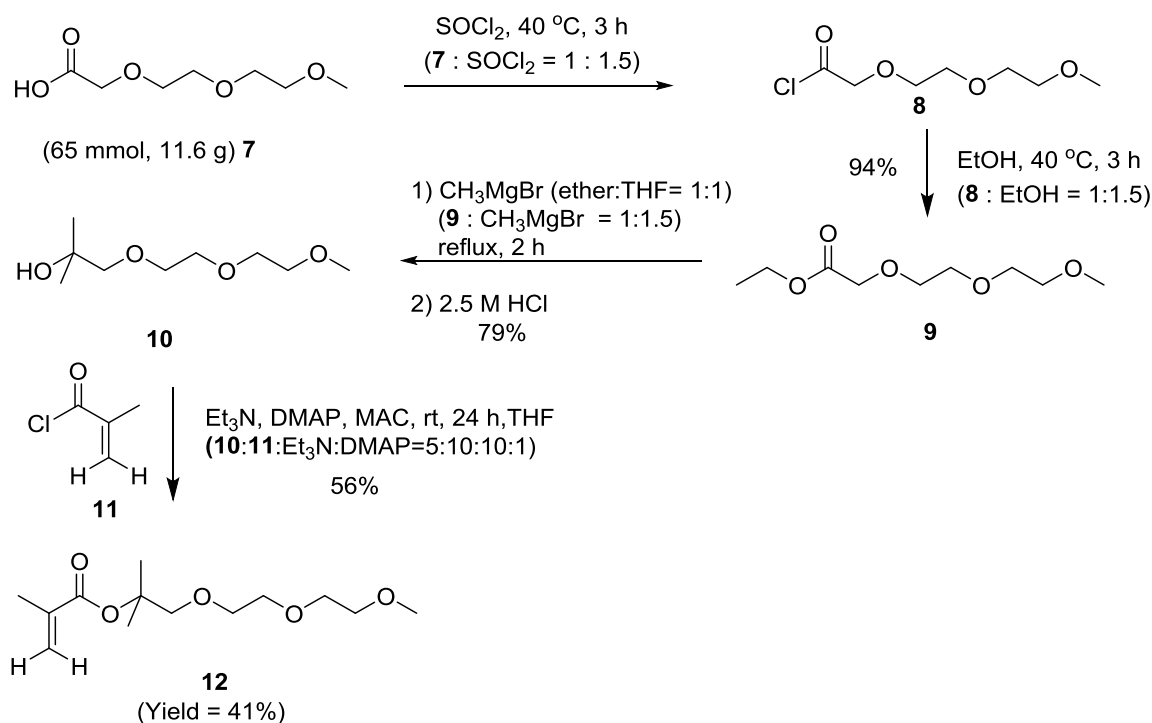
1-(2-(2-methoxyethoxy)ethoxy)-2-methylpropan-2-yl methacrylate

Scheme 5.4. Synthesis of a non-cross-linkable monomer, **12**, with cleavable side chains.

The ^{1}HNMR spectrum of MEEMPM, 12, (not shown) shows a peak at 1.49 ppm due to the protons of CH$_3$ groups adjacent to the ester group and a peak at 1.82 ppm from the CH$_3$ protons of the methacrylate group. The signal of the methyl proton of −

OCH$_3$ appeared around 3.34 ppm, and methylene protons of triethyleneglycol backbone gave signals from 3.35-3.62 ppm as a multiplet. The two singlets at 5.45 and 5.98 ppm result from the vinyl protons of the methacrylate group.

5.3.1.3. Synthesis of DMOEP, 15.

Acid-cleavable monomer 15 (DMOEP) was synthesized as shown in Scheme 5.5 with an isolated yield of 90%.
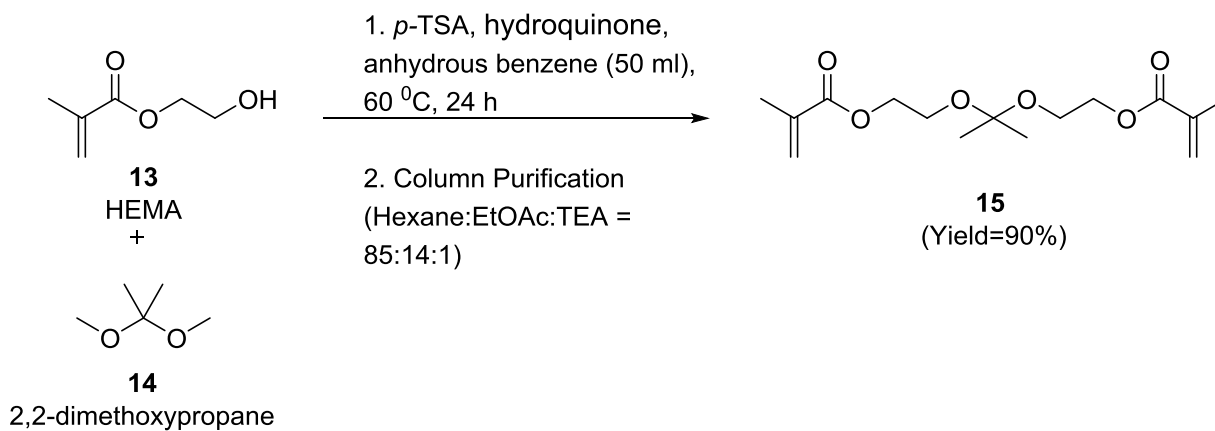
Scheme 5.5. Synthesis of a cross-linkable monomer, **15**, with an acid cleavable ketal moiety in side chain.

The ^{1}H NMR spectrum of DMOEP shows a peak at 1.38 ppm due to the CH$_3$ protons of the $-(O)_2C(CH_3)_2$ group of the backbone of the monomer and a peak at 1.96 ppm from the protons of CH$_3$ group of methacrylate. Methylene protons of the

triethyleneglycol appear around 3.68-4.28 ppm as a multiplet. The two singlets at 5.56 and 6.11 ppm are assigned to the vinyl protons of methacrylate group.

5.3.2. Polymerization of TEGBMA in Solution.

We initially performed polymerization and hydrolysis in solution to give an indication of how these reactions might perform at a surface. Monomer 6 (TEGBMA) served as a model substrate for ATRP in solution. Scheme 5.6 illustrates the polymerization reaction with bromoisobutyrate (EBIB) as the initiator and a Cu/HMTETA catalyst. Due to polymerization, the ^{1}H NMR spectrum of the reaction mixture (Figure 5.4) showed a decrease in the intensity of vinyl proton signals at 5.43 and 5.92 ppm as well as broadening of the peaks from the methylene protons (3.47-3.57 ppm) of the PEG backbone and from the methyl protons adjacent to the ester group (1.39 ppm).

Scheme 5.6. Solution polymerization of TEGBMA (Table 5.1 gives specific conditions).

Based on GPC, poly(TEGBMA) has $M_n = 7.17 \times 10^5$ g mol^{-1} and $M_w/M_n = 2.1$. TEGBMA was also polymerized with the EBIB initiator and a Cu/Bpy catalyst. Table 5.1 summarized polymerization conditions and results.

Figure 5.5 shows the evolution of the ^{1}H NMR spectrum of the reaction mixture for ATRP of TEGBMA using CuBr/HMTETA as the catalyst without the addition of CuBr$_2$. The spectra show a rapid decrease in the intensity of the vinyl proton signals at 5.43 and 5.92 ppm on going from 30 min to 15 h of polymerization, but from 15 h to 24 h these signals hardly change. Moreover, the intensity decline for these signals from 24 to 48 h is insignificant, suggesting termination of polymerization.
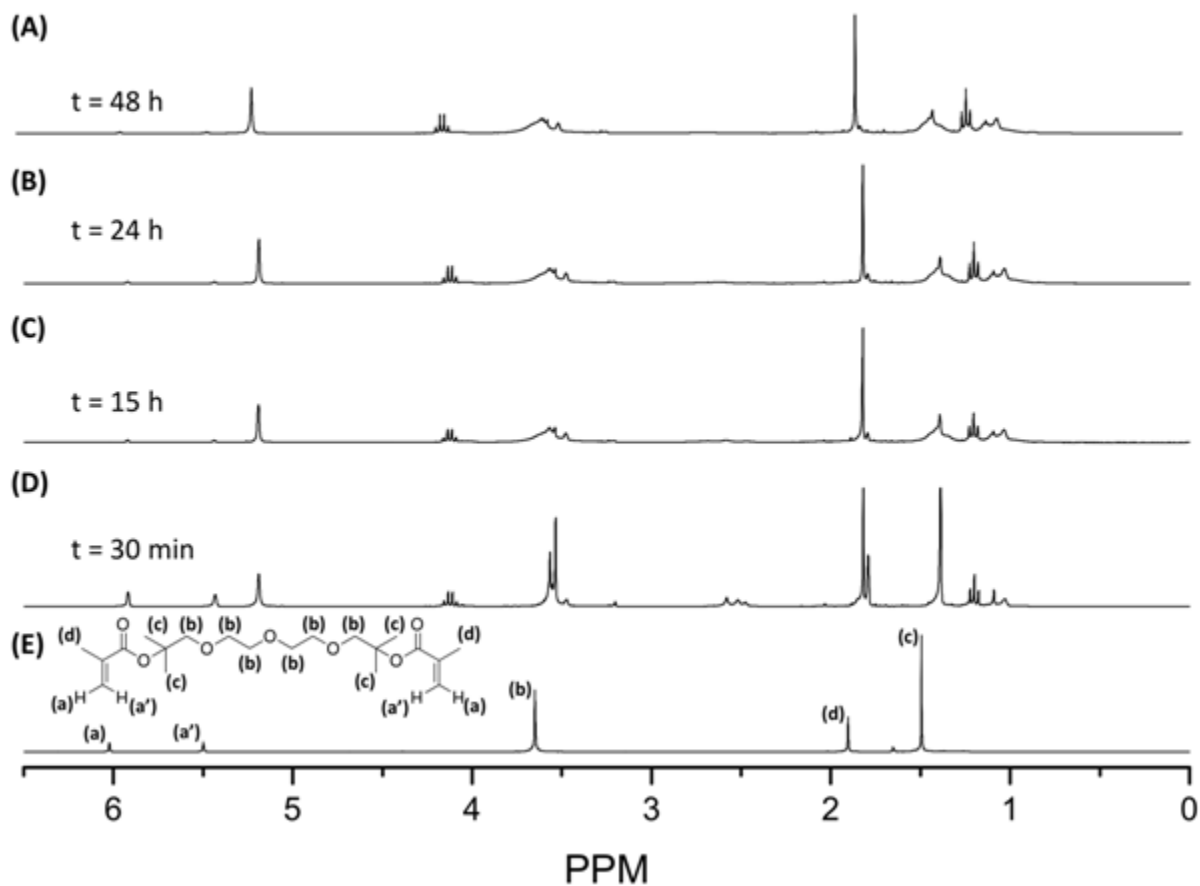
Figure 5.4. Evolution of the ^{1}H NMR spectrum of the reaction mixture for polymerization of TEGBMA by ATRP at 24 °C in CD$_3$CD$_2$OD using EBIB as the initiator and CuBr/HMTETA as the catalyst. The figure shows the spectra after (A) 48 h, (B) 24 h, (C) 15 h and (D) 30 min of polymerization. (E) ^{1}H NMR spectrum of TEGBMA in CDCl$_3$

By comparing the normalized IR absorbance of vinyl groups in poly(TEGBMA) with that of the monomer, we estimate that 25% of the vinyl groups remain unpolymerized in films. This suggests that polymers are about 50% cross-linked, i.e. half the monomers react through both of their vinyl groups. We normalize the absorbance of vinyl groups by dividing by the absorbance of the carbonyl group, and the ratio of the vinyl abosorbance to the carbonyl absorbance is 0.04 for the monomer.

Table 5.1. Solution polymerization of TEGBMA at room temperature using EtOH as a solvent

No	[M]/[I]/[L]/ [Cu(I)]/[Cu(II)]	Ligand(L)	Time(h)	M_n^a, theo (g mol^{-1})	Conversion (%)	C=C /C=O^b	GPC M_n, (g mol^{-1})
1	100:20:10:5:0	Bpy	24	4.82×10^2	13.3	0.18	
2	100:20:10:5:0	Bpy	48	1.45×10^3	56.7	0.21	
3	100:20:10:5:0.25	Bpy	24	9.24×10^2	33.3	0.24	
4	100:20:10:5:0.25	Bpy	48	1.52×10^3	60.0	0.20	
5	100:20:10:5:0	HMTETA	24	1.54×10^3	70.5	0.06	
6	100:20:10:5:0	HMTETA	48	2.40×10^3	100	0.04	7.17×10^5
7	100:20:10:5:0.25	HMTETA	24	1.32×10^3	51.1	0.06	
8	100:20:10:5:0.25	HMTETA	48	2.4×10^3	100	0.06	2.14×10^6

[a] M_n, theo = M_W initiator + M_W TEGBMA monomer $\times [M]_0/[I]_0 \times$ Conversion
[b] Absorbance ratio for the C=C (1639 cm^{-1}) and C=O (1736 cm^{-1}) stretching frequencies

5.3.3. Acid-catalyzed Hydrolysis of Poly(TEGBMA) in Solution.[19]

Hydrolysis of poly(TEGBMA) ($M_n \sim 7.17 \times 10^5$ g mol^{-1}) was carried out in 2.5 M HCl in THF at room temperature, and the hydrolyzed product is most likely poly(methacrylic acid) [poly(MAA)] (Scheme 5.7).
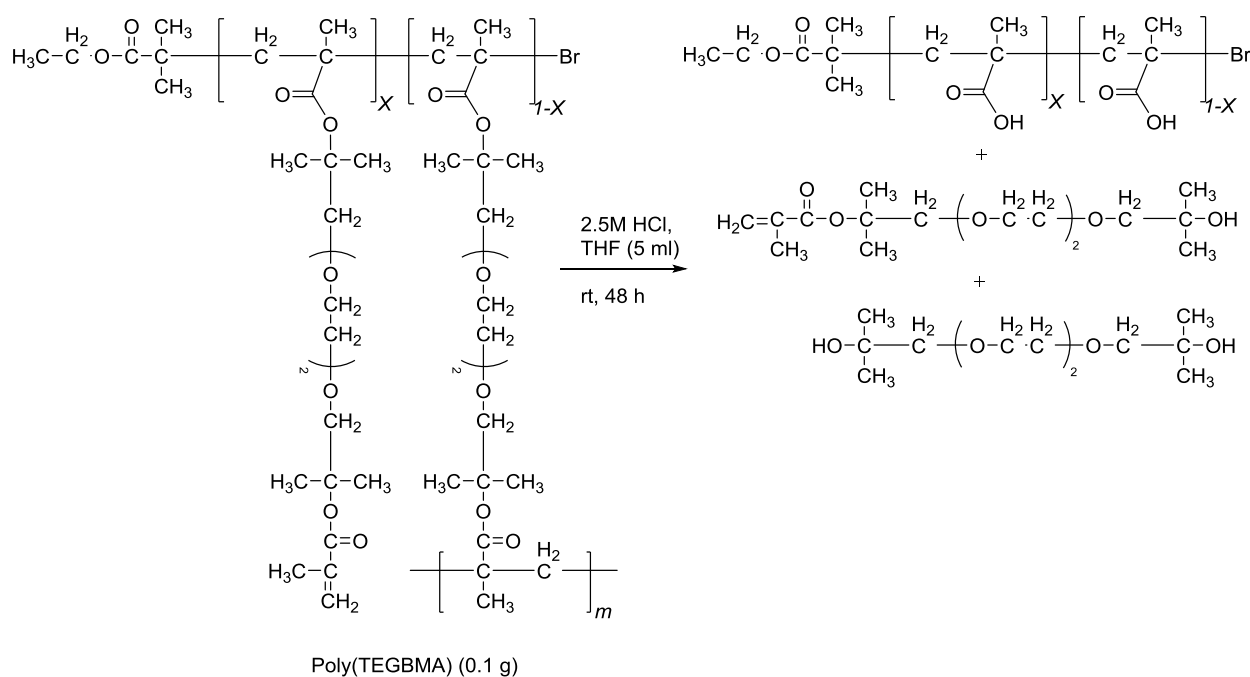
Poly(TEGBMA) (0.1 g)

Scheme 5.7. Acid-catalyzed hydrolysis of poly(TEGBMA).

Figure 5.5 presents the ^{1}H NMR spectra of poly(TEGBMA) before (A) and after (B) hydrolysis. Peaks d, a and a', corresponding to the α-methyl and vinyl protons of TEGBMA monomer, shift to 1.25-1.50 ppm after cross-linking and overlap with the peaks of the α-CH$_3$ ((A)-peak e) and -CH$_2$- ((A)- peak f) belonging to poly(TEGBMA). However, appearance of a new peak corresponding to α-CH$_3$ of poly(MAA) at 0.5-1.3 ppm in the hydrolyzed product (B), indicates that the ester groups of the cross-linker 6

were eliminated to yield the poly(MAA) segment. FT-IR spectra are also consistent with hydrolysis. The hydrolyzed polymer exhibits a broad absorption (2500-3800 cm^{-1}) most likely due to the carboxylic acid groups of poly(MAA) (Figure 5.6). The above results suggest that the hydrolysis reaction fractured polymer through cross-linking points to generate linear poly(MAA) segment (Scheme 5.7).
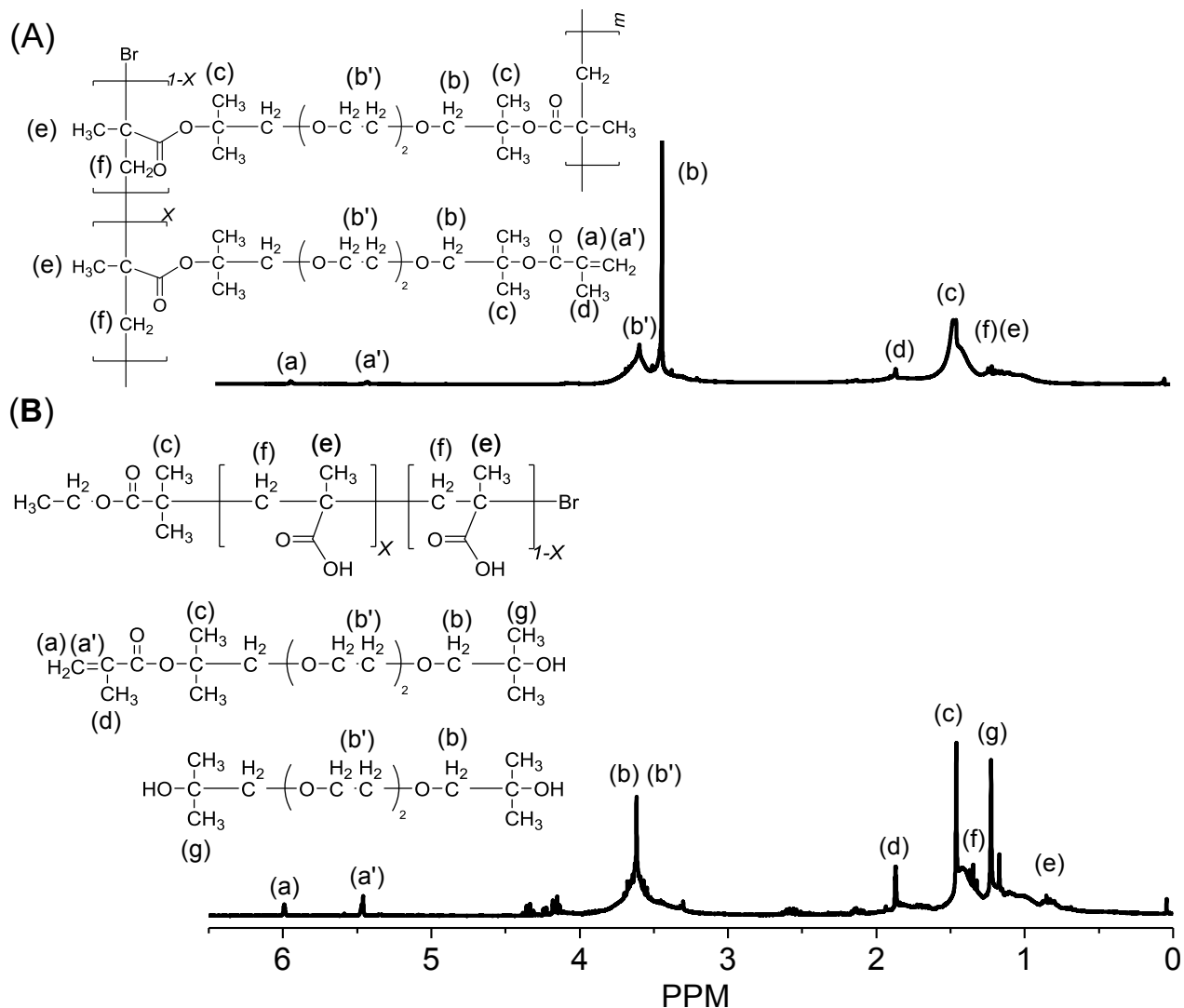
Figure 5.5. ^{1}H NMR spectra of (A) poly(TEGBMA) (Table 5.1, entry 6) in CDCl$_3$ and (B) hydrolyzed poly(TEGMBA).
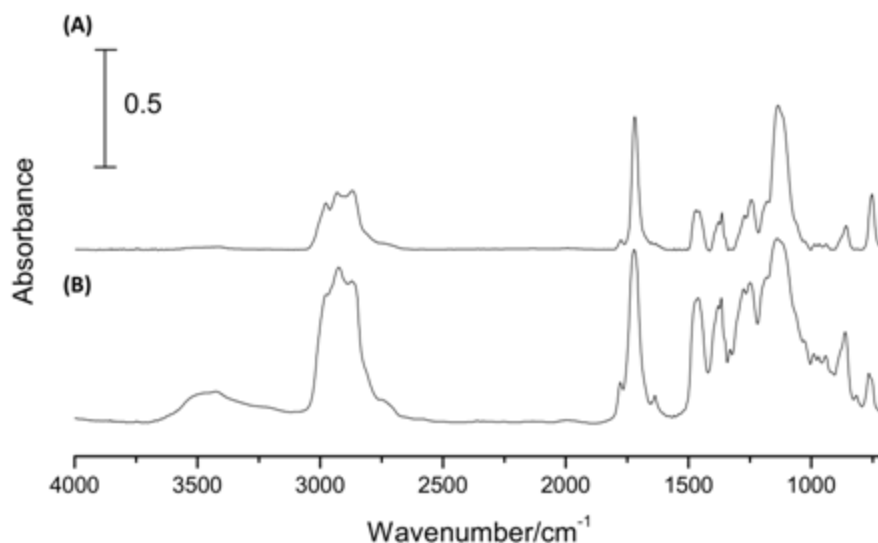
Figure 5.6. FT-IR spectra of (A) poly(TEGBMA) and (B) its hydrolyzed product (B). The OH absorbance (2500-3800 cm^{-1}) suggests the presence of the acid groups of poly(MAA).

5.3.4. Surface-initiated Polymerization from Non-cross-linked-initiators on Au.

5.3.4.1. Surface-initiated Polymerization of TEGBMA; Effect of Solvent and Cu(II) Addition on Polymerization.

Scheme 5.8 shows the pathway for surface-initiated ATRP of TEGBMA from initiator-modified gold surfaces. Immersion of gold-coated wafers in a 1 mM ethanolic solution of the disufide initiator,16, for 24 h leads to the formation of substrate 17. The appearance of a carbonyl peak at 1739 cm^{-1} in the reflectance FTIR spectrum of the monolayer and the monolayer thickness (1.8 nm) confirm initiator attachment.

For surface-initiated polymerization, substrate 17 was immersed for different times in an EGBMA/EtOH mixture containing the CuBr/bpy catalyst system (Table 5.2). The resulting polymer-modified substrate 18 was characterized using ellipsometry and surface-FTIR spectroscopy. As a control MMA was polymerized and characterized similarly. Table 5.2 summarizes the results.

Furthermore, I also performed surface-initiated polymerizations using solvents with different polarities (Table 5.2, entries 1, 3 and 4). Recent literature shows that the rate of ATRP often increases with increasing solvent polarity, presumably because the catalyst becomes more active.[20] Moreover, addition of a deactivating Cu(II) complex to polymerization solutions may help to controls ATRP. In solution ATRP, reaction of Cu(I) with initiator produces the Cu(II) complex. However, because of the amount of initiator on a substrate is small, the concentration of the deactivating Cu(II) complex may be too low to control polymerization from a surface. To ensure a sufficient concentration of deactivating Cu(II) species in the solution, I added 30 mol% of $CuBr_2$ (with respect to CuBr) to the polymerization solution.
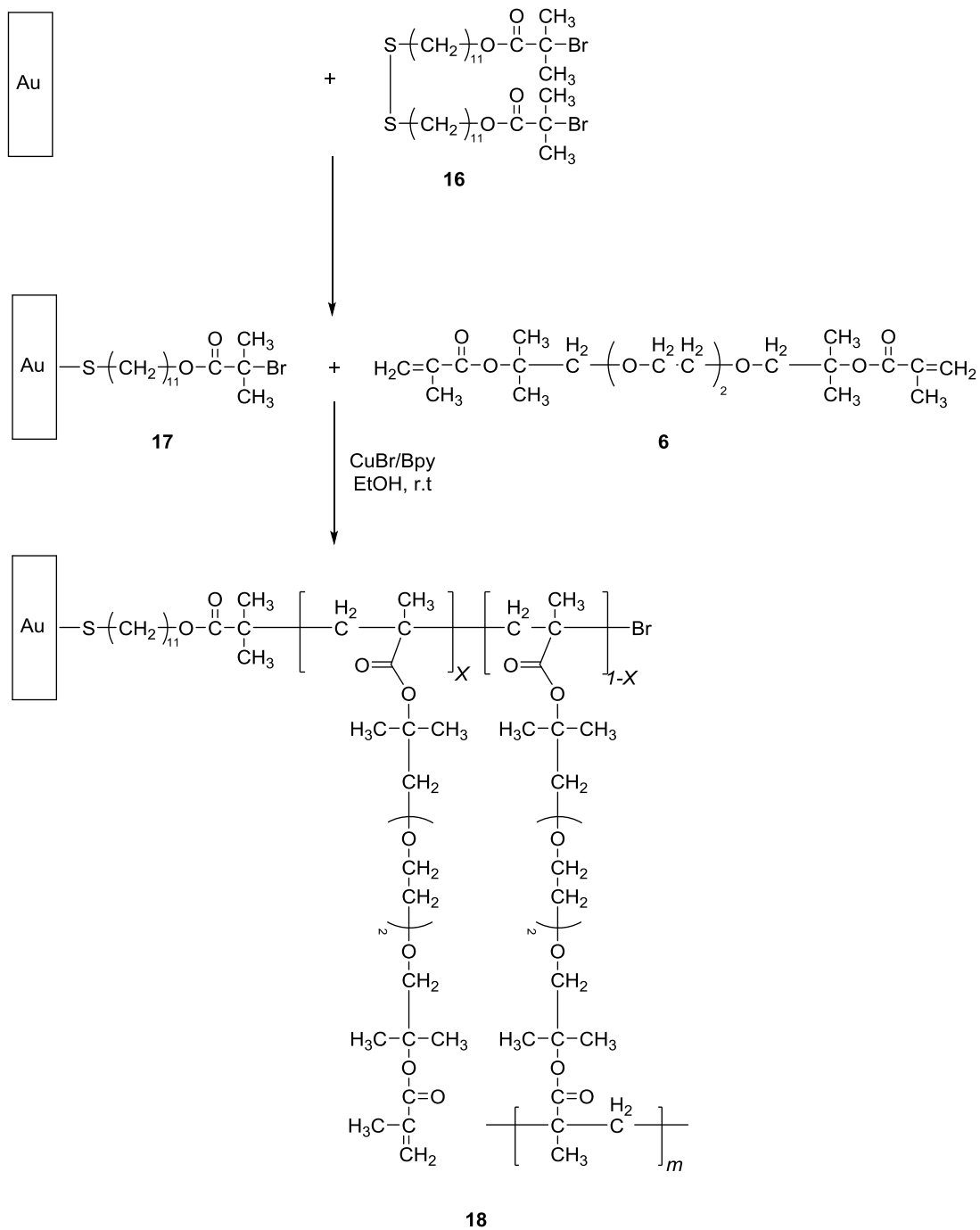
Scheme 5.8. Synthetisof poly(TEGBMA) films on gold surfaces.

Table 5.2. Conditions used for surface-initiated polymerization of TEGBMA and the ellipsometric thicknesses of the resulting films[a]

No	[M]/[L]/ [Cu(I)]/[Cu(II)]	Solvent	Poly(TEGBMA) film thickness (nm)[b]	Poly(MMA) film thickness (nm)[b,c]
1	100:2:1:0	EtOH	0.0	13.3
2	100:2:1:0.3	EtOH	0.0	56.7
3	100:2:1:0	DMF/H_2O	1.2	33.3
4	100:2:1:0	MeOH/H_2O	5.2	60.0

[a]Surface polymerization was carried out with TEGBMA (2.2 g, 5.8 mmol), bpy (18 mg, 116 µmol), $CuBr_2$ (7.6 mg, 17 µmol) or/and CuBr (2.2 g, 5.8 mmol) at room temperature for 12 h. The volume ratio of TEGBMA to solvent was 1:1.
[b]Film thickness was determined using ellipsometry.
[c]As a control methylmethacrylate (MMA) was polymerized under similar conditions.

Use of a CuBr/$CuBr_2$ catalyst system for surface-initiated polymerization of TEGBMA did not increase the thickness of the film compared to polymerization with just a CuBr catalyst (Table 5.2, entry 1). However, the poly(TEGBMA) thickiness increases significantly for ATRP in polar solvents such as MeOH/H_2O. However, the relatively low thicknesses of these films suggests that polymerization terminates in a short time, perhaps due to loss of active catalyst or hindered mass transport of monomers to radicals in the film or loss of active end groups expose to the surface.

5.3.4.2. Effect of Different Cu-ligand Systems on Surface-initiated Polymerization of TEGBMA.

The primary role of the ligand added to an ATRP system is to solubilize the Cu salts and tune the Cu catalyst to achieve well-controlled polymerization. Nitrogen-based ligands generally work well for Cu-mediated ATRP, but the choice of ligand greatly

influences the effectiveness of the catalyst in a specific polymerization. One ligand does not work for every copolymerization; therefore, this work examined three different ligands, bpy, HMTETA and PMDETA (Table 5.3).

Table 5.3. Thicknesses of poly(TEGBMA) formed through surface-initiated polymerization using different solvents and catalyst ligands[a]

No	[M]/[L]/ [Cu(I)]/[Cu(II)]	Solvent	Thickness Poly(TEGBMA) film (nm)[b]		
			[L]=Bpy	[L]= HMTETA	[L]=PMDETA
1	100:2:1:0	EtOH	0.0	1.9	-
2	100:2:1:0.3	EtOH	0.0	0.0	-
3	100:2:1:0	DMF/H$_2$O	1.2	3.0	-
4	100:2:1:0	MeOH/H$_2$O	5.2	8.0	10.0

[a]Surface-initiated polymerization was carried out with TEGBMA (2.2 g, 5.8 mmol) [M], Ligand (116 µmol) [L = Bpy, HMTETA and PMDETA], CuBr$_2$ (7.6 mg, 17 µmol) or/and CuBr (2.2 g, 5.8 mmol) at room temperature for 12 h;
[b]Film thickness was determined using ellipsometry

PMDETA forms more reactive Cu(I) complexes (k_a= 2.7 M^{-1} s^{-1}) than HMTETA (k_a= 0.14 M^{-1} s^{-1}) and bpy (k_a= 0.092 M^{-1} s^{-1}). Hence, the presence of Cu/PMDETA complex gives thicker films in 12 h than polymerization using Bpy and HMTETA ligands (Table 5.3, entry 4). Also, a polar solvent mixture (MeOH/H$_2$O) further improves the thickness from 0 to 5.2 nm (Table 5.3, entries 3 and 4).

5.3.4.3. Effect of Different Monomers on Surface Polymerization.

This set of experiments examined surface-initiated ATRP of DMOEP and MEEMPM using a CuBr catalyst with bpy, HMTETA or PMDETA ligands (Table 5.4).

Table 5.4. Thicknesses of DMOEP and MEEMPM formed through surface-initiated polymerization using different solvents and catalyst ligands[a]

No	Monomer [M]	Solvent	Thickness of the polymer film (nm)[b]		
			[L]=Bpy	[L]=HMTETA	[L]=PMDETA
1	MEEMPM	MeOH/H$_2$O	4.2	5.1	11.3
2	DMOEP	MeOH/H$_2$O	0.0	4.6	7.6

[a]Surface polymerization was carried out with MEEMPM or DMOEP monomer (5.8 mmol) [M] , Ligand (116 µmol) [L = Bpy, HMTETA and PMDETA], and CuBr (2.2 g, 5.8 mmol) at room temperature for 12 h
[b]Film thickness was measured using ellipsometer

Non-cross linkable monomer MEEMPM, 12, shows the highest film thickness upon surface-initiated polymerization using Cu/PMDETA as a catalyst and MeOH/H$_2$O as solvent. The cross-linkable monomer DMOEP, 15, gives thinner films than MEEMPM, perhaps because cross-linking makes films less accessible to incoming monomer. There was no increase in the thickness of poly(MEEMPM) films when polymerization was allowed to occur for an additional 24 h with the conditions given in the entry 1 (Table 5.4) with the ligand PMDETA.

Based on the above results with changes in conditions such as catalyst, solvent and monomers, we couldn't increase the MEEMPM thickness beyond 10-15 nm. For most of the above experiments, we clearly saw solution polymerization during surface polymerization using the disulfide non-crosslinked initiator. This could be due to thiol desorption from the surface, a common limitation to growing thick polymer brushes on Au.[17] Scheme 5.9. shows some pathways that may lead to termination of surface-bound radicals on Au surfaces.

Radical-induced desorption of thiol from growing chains can be initiated over a broad temperature range, and the copper catalyst also may contribute to thiol

desorption. Saha et al[17] observed decreases in film thickness at high Cu concentrations and long reaction times upon modification of polymers on Au using "click chemistry."
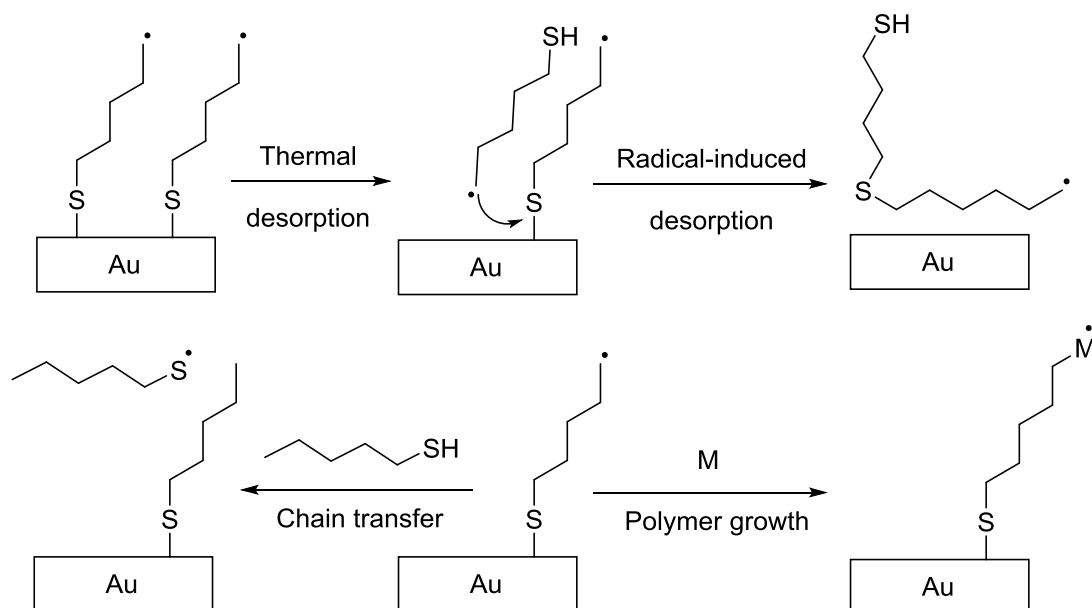
Scheme 5.9. Fate of surface-bound radicals on Au: (top) thermal desorption of surface-bound radicals and desorption induced by reaction of a radical with an Au-S bond, (bottom left) reaction with a chain-transfer agent to terminate polymerization from the bound chain, and (bottom right) polymer growth.

This suggests that Cu is involved in desorption of polymer brushes from Au substrates. Although the copper concentration in ATRP is relatively low, its effect may not be negligible because partial desorption of initiator-containing monolayers from the Au surface would result in a decrease of surface initiator concentration resulting in thin films. If this hypothesis is correct, preventing desorption of thiols from the Au surface could increase film thickness.
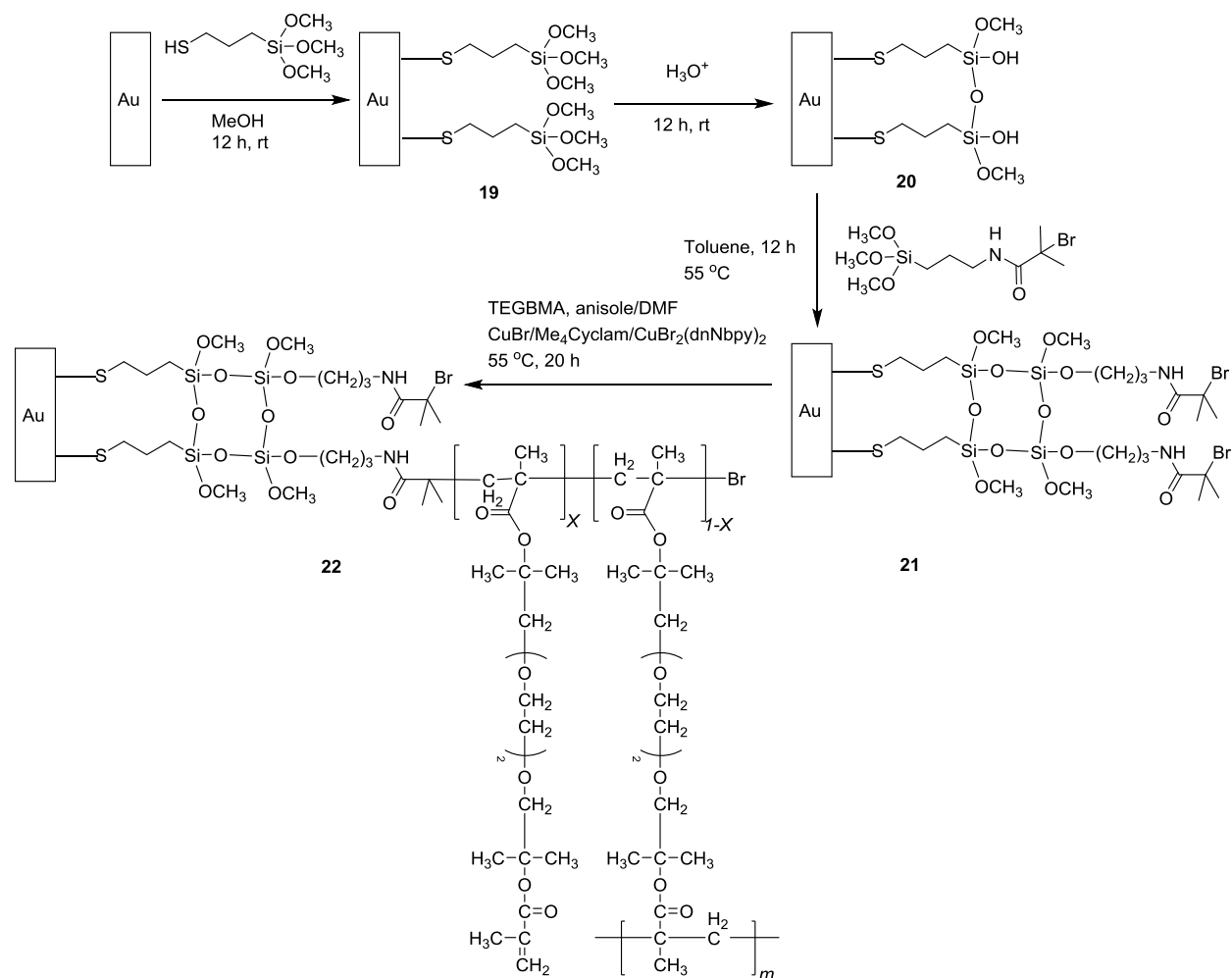
5.3.5. Surface-initiated Polymerization From a Cross-linked Initiator Film.

Scheme 5.10 show the preparation of poly(TEGBMA) and poly(DMOEP) brushes from cross-linked initiator films on Au. After formation of an MPS film, condensation of the methoxysilane groups should give a coating, **19**, with a dense poly(siloxane) network that should stabilize the films. In addition the hydroxylated surface allows subsequent attachment of a trimethoxysilane-ATRP initiator. I prepared the cross-linked initiator surface, 21, using a literature procedure.[21]

The reflectance FTIR spectrum of the MPS layer on Au (Figure 5.7-(A)) shows vibrational bands for MPS (2938 cm^{-1} for overlapping CH$_3$ and CH$_2$ bands, 2846 cm^{-1} for CH$_2$ symmetric stretching, and 1114 cm^{-1} for Si-O-C stretching). After hydrolysis, the methyl stretching band at 2938 cm^{-1} disappears and a peak at 1114 cm^{-1} due to Si-O-C stretching greatly decreases. This is a good indication of complete hydrolysis of the trimethoxysilanes. The 1.2 nm ellipsometric thickness of the hydrolyzed MPS and the IR spectra agree well with literature data (1.0 nm thickness).[17] After substrate 20 reacts with the trimethoxysilane initiator, the film thickness increases to 2.2 nm and amide peaks (1652 and 1548 cm^{-1}) appear in the reflectance FTIR spectrum, consistent with initiator immobilization.

To perform ATRP, substrate **21** was immersed in a solution containing TEGBMA or DMOEP and copper catalyst (CuBr$_2$(dnNbpy)$_2$ and Me$_4$Cyclam) in DMF/anisole. The ellipsometric thickness of poly(TEGBMA) and poly(DMOEP) films grown from the cross-linked initiator were 75 nm and 110 nm, respectively, after 24 h of polymerization. After ATRP, the appearance of a strong carbonyl stretching band around 1750 cm^{-1} and an increase in the intensity of C-O-C stretching around 1100 cm^{-1} confirms film formation

on the surface (Figure 5.7-(E)). Similar results occur for polymerization of DMOEP (Figure 5.7-(D)).

Scheme 5.10. Formation of cross-Linked Initiators on gold surfaces and surface-initiated polymerization of TEGBMA.
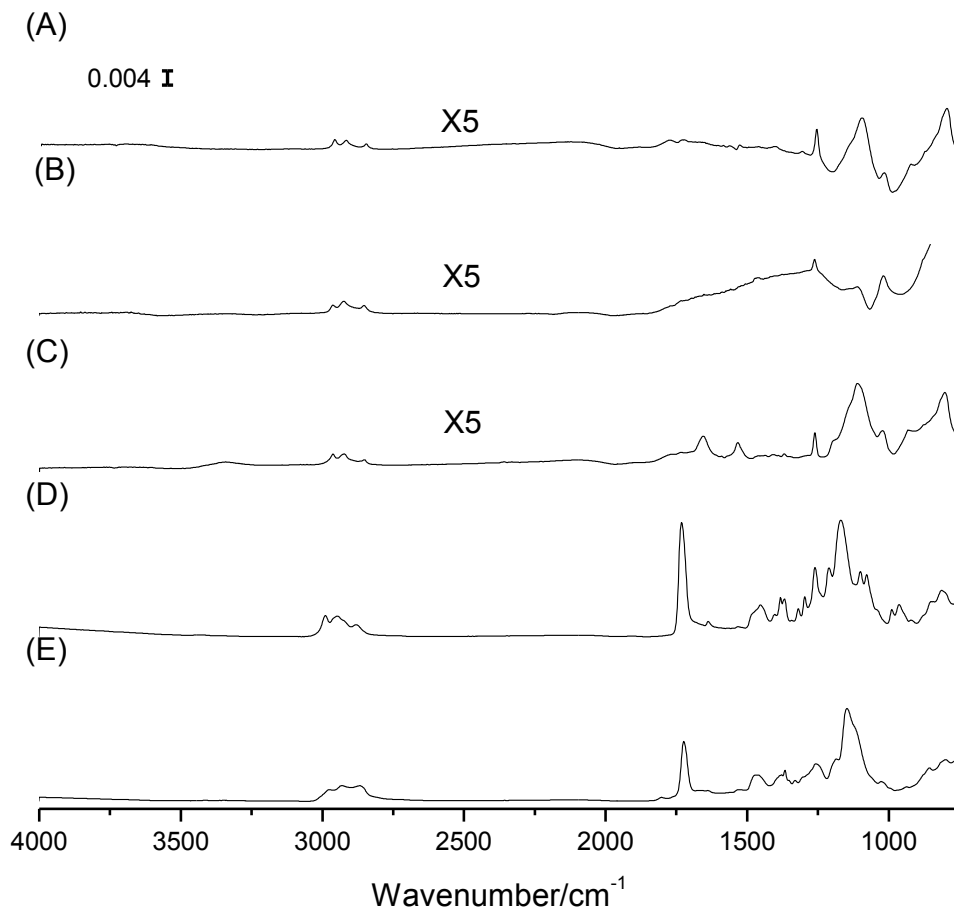
Figure 5.7. Reflectance FT-IR spectra of (A) an MPS layer on a Au-coated wafer, (B) the same layer after condensation of the MPS film to form a poly(siloxane) network, (C) the film in (B) after attachment of the trimethoxysilane-ATRP initiator, and (D) poly(DMOEP) (thickness ~110 nm), and (E) poly(TEGBMA) (thickness ~75 nm), grown from the initiator.

5.3.6. Acid-catalyzed Hydrolysis of the Poly(TEGBMA) Film.

The surface-grafted poly(TEGBMA) Au wafer was incubated in a solution of 2.5 M HCl in THF at room temperature for 48 h. During the hydrolysis, the intensity of the carbonyl-stretching band at 1750 cm^{-1} gradually decreases (Figure 5.8). Additionally,

the carbonyl band broadens and a hydroxyl stretching stretch appears 2500-3500 cm^{-1} region suggesting the formation of poly(MAA).
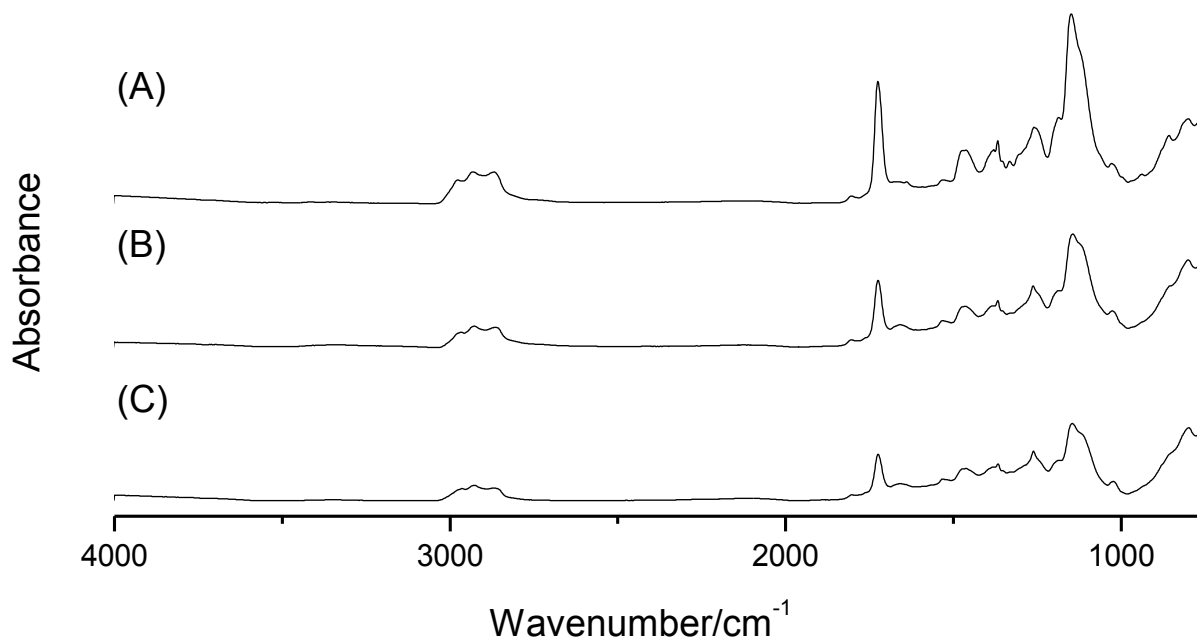

Figure 5.8. FT-IR spectra of a poly(TEGBMA) film on Au before (A) and after hydrolyses in 2.5 HCl for (B) 1.5 h and (C) 4 h.

5.4. Brush Collapse After Hydrolysis.

Growth of the polymer brushes gave ~100 nm-thick films and cleaving the side chain should yield reduced-density polymer brushes with increased distance between polymer brushes. The thickness of poly(TEGBMA) films after cleaving side arms, decreased to 50 nm and upon immersion of the film in a 20 mM phosphate buffer for 1 h, the swollen thickness increases to 55 nm. This is a clear evidence that, upon cleaving the side chains, the polymer brushes collapsed and thus we did not continue studying this system for protein binding applications.

REFERENCES

REFERENCES

(1)   Anuraj, N., 2010, Affinity membranes with functionalized polymer brushes for rapid, high capacity purification of tagged proteins, Michigan State University.

(2)   Singh, N.; Wang, J.; Ulbricht, M.; Wickramasinghe, S. R.; Husson, S. M. *J. Membrane Sci.* **2008**, *309*, 64-72.

(3)   Lee, S. H.; Dreyer, D. R.; An, J.; Velamakanni, A.; Piner, R. D.; Park, S.; Zhu, Y.; Kim, S. O.; Bielawski, C. W.; Ruoff, R. S. *Macromol. Rapid. Comm.* **2010**, *31*, 281-288.

(4)   Kim, J. B.; Huang, W. X.; Miller, M. D.; Baker, G. L.; Bruening, M. L. *J. Polym. Sci. Pol. Chem.* **2003**, *41*, 386-394.

(5)   Bao, Z.; Bruening, M. L.; Baker, G. L. *Macromolecules* **2006**, *39*, 5251-5258.

(6)   He, D.; Ulbricht, M. *J. Membr. Sci.* **2008**, *315*, 155-163.

(7)   Yang, Q.; Kaul, C.; Ulbricht, M. *Langmuir* **2010**, *26*, 5746-5752.

(8)   Wu, T.; Efimenko, K.; Vlcek, P.; Subr, V.; Genzer, J. *Macromolecules* **2003**, *36*, 2448-2453.

(9)   Chen, X.; Dong, B.; Wang, B.; Shah, R.; Li, C. Y. *Macromolecules* **2010**, *43*, 9918-9927.

(10)   Mulvihill, M. J.; Rupert, B. L.; He, R. R.; Hochbaum, A.; Arnold, J.; Yang, P. D. *J. Am. Chem. Soc.* **2005**, *127*, 16040-16041.

(11)   Davis, M. E.; Gonzalez, H.; Hwang, S.; Google Patents: 2013.

(12)   Anzinger, H.; Mutter, M. *Polym. Bull.* **1982**, *6*, 595-601.

(13)   Kitano, H.; Kondo, T.; Suzuki, H.; Ohno, K. *J. Colloid Interface Sci.* **2010**, *345*, 325-331.

(14)   Bhuchar, N.; Sunasee, R.; Ishihara, K.; Thundat, T.; Narain, R. *Bioconjugate Chem.* **2012**, *23*, 75-83.

(15)   Mather, B. D.; Williams, S. R.; Long, T. E. *Macromol. Chem. Phys.* **2007**, *208*, 1949-1955.

(16)   Huang, W. X.; Baker, G. L.; Bruening, M. L. *Angew. Chem. Int. Ed.* **2001**, *40*, 1510–1512.

(17)   Saha, S.; Bruening, M. L.; Baker, G. L. *ACS App. Mat. Int* **2011**, *3*, 3042-3048.

(18)   Jin, L.; Agag, T.; Yagci, Y.; Ishida, H. *Macromolecules* **2011**, *44*, 767-772.

(19)   Ruckenstein, E.; Zhang, H. M. *Macromolecules* **1999**, *32*, 3979-3983.

(20)   Kim, J.-B.; Bruening, M. L.; Baker, G. L. *J. Am. Chem. Soc.* **2000**, *122*, 7616-7617.

(21)   Huang, W. X.; Skanth, G.; Baker, G. L.; Bruening, M. L. *Langmuir* **2001**, *17*, 1731-1736.

CHAPTER 6. ACHIEVENTS AND FUTURE WORK.

6.1. Achievements.

Chapter 2 describes a simple, rapid and direct procedure to deposit polymer films that bind His-tagged proteins. Two different polymers, PDCMAA and CMPEI, containing IDA ligands were synthesized and applied for membrane modification. Remarkably, 10-bilayer PAH/PDCMAA films are 1 μm thick, and these coatings have a very high Cu^{2+} binding capacity (~2.5 mmol/cm^3 of film, or 2.5 M).[1] When deposited on the surface of porous membranes, PAH/PDCMAA films function as highly selective facilitated-transport membranes with a Cu^{2+}/Mg^{2+} selectivity around 50.[2] For protein sorption, these films must also swell in water to provide enough space for protein-ligand interactions. Unfortunately, PAH/PDCMAA films do not swell sufficiently for extensive protein capture, perhaps because of the hydrophobic backbone of the polymer. Therefore we applied CMPEI for membrane modification. Sequential adsorption of PAH and CMPEI leads to membranes that bind Ni^{2+} and capture ~60 mg of His-tagged ubiquitin per mL of membrane, and this capacity is higher than for commercially available bead systems.[3] Such membrane can purify His-tagged protein directly from cell extracts.[4]

Minimizing metal-ion leaching is also important in purifying His-tagged proteinw. Thus, chapter 3 describes synthesis of a series of polymers containing N_α, N_α-bis(carboxymethyl)-L-lysine (tethered NTA). Due to the high cost of commercial NTA derivatization agents, this method established an important alternative route to synthesize these polymers at low cost. Sequential adsorption of PAH and NTA-

containing PEs leads to membranes that bind Ni^{2+} and capture $\sim$40 mg of His-tagged ubiquitin per mL of membrane. This capacity is higher than that for commercially available systems. Such membranes can purify His-tagged protein directly from cell extracts. Moreover, these polymer films show less metal-ion leaching than coatings containing IDA ligands.

With both CMPEI and NTA-containing polymers, we tried to increase film swelling through introduction of charged groups in films.   High swelling should improve permeation of protein into PEMs. Introduction of porosity is another approach to enhance the kinetics of protein binding in polyelectrolyte films. Chapter 4 describes the development of porous films through adsorption of star polymers. Under appropriate deposition conditions, LBL adsorption of these star polymers leads to highly porous films that bind as much as 10-20 multilayers of lysozyme, which is $\sim$5-fold greater than lysozyme binding to $(PAA/PAH)_n$ films at the same pH.[5]   Sequential adsorption of PDMAEMA-X and PAA-X leads to membranes that capture $\sim$120 mg of lysozyme per mL of membrane, which is higher than the capacity of commercially available systems (40-50 mg/mL).

Chapter 5 describes efforts to reduce the areal density of polymer-brushes and increase their aqueous swelling, which should enhance the kinetics and amount of protein binding. Removal of side chains after polymerization should reduce brush chain density and provide the space necessary to capture large amounts of protein. Growth of the polymer brushes gave 75-100 nm-thick films, but unfortunately upon cleaving the side chains, the polymer brushes collapsed to prevent further functionalization.

However, this synthetic strategy is an interesting method for fabricating brushes with increased distances between polymer chains.

6.2. Future Work.

6.2.1. Proposed Method to Improve Swelling of Polymer Films.

Chapters 2 and 3 describe polymer films containing two different ligands, IDA and NTA. Introduction of fixed net charge into such films enhances swelling, which should increase the space inside the film for improved protein permeation (Figure 6.1).
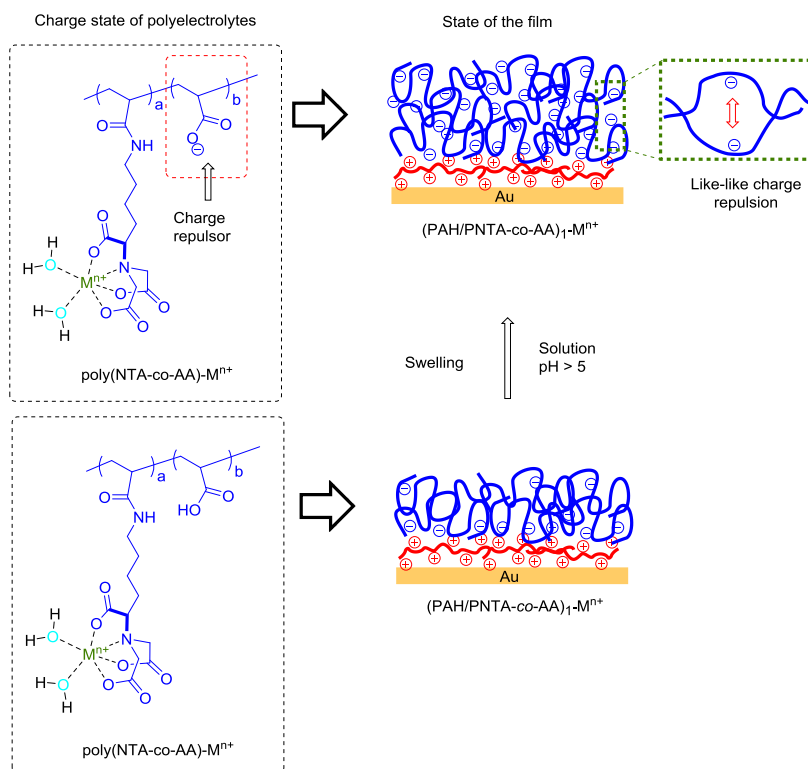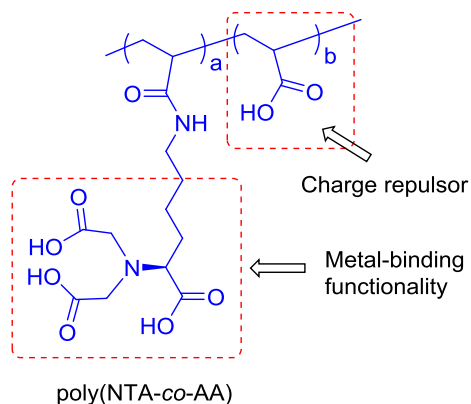

Figure 6.1. Schematic representation of like-like charge repulsion-induced swelling of a PNTA-*co*-AA polymer at high pH.
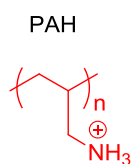
However, in the case of PNTA-*co*-AA we achieved this high swelling by making modification to the anionic polymer architecture. This should only improve the swelling of anionic layer of the film (Figure 6.2A and C). Thus, here we suggest the design of new polyanions and polycations containing hydrophilic backbones to improve the swelling in both layers as shown in Figure 6.2B and D. We assume that the oxygen-rich backbone will attract water molecules to the system and enhanced swelling of both polymers. The following sections contain some proposed syntheses of polymers that should form highly swollen polymer films.
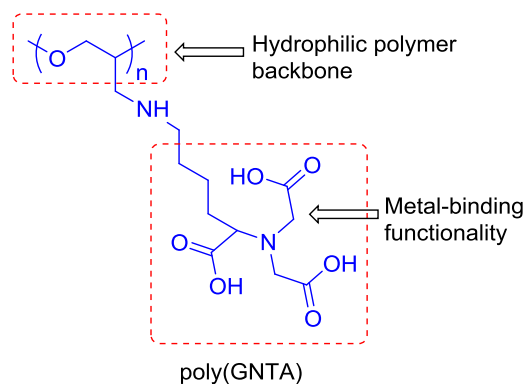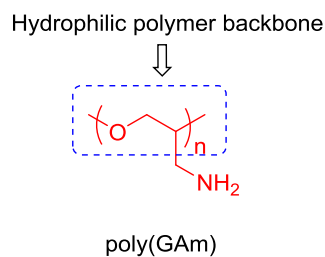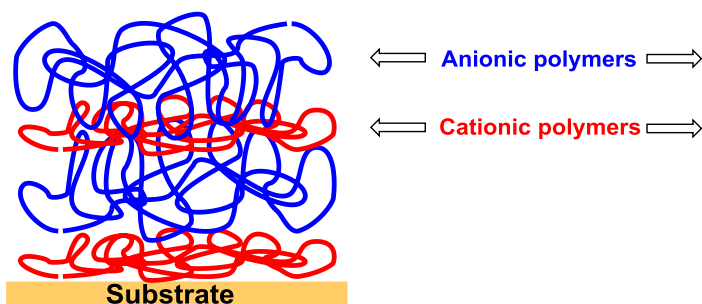
**Figure 6.2.** Structures of (A) poly(NTA-*co*-AA) anionic polymer and PAH, (B) poly(GNTA) and poly(GAm), (C) (poly(NTA-*co*-AA)/PAH)$_n$ films in pH 7.4 buffer and (D) (poly(GNTA)/poly(GAm))$_n$ in pH 7.4 buffer.

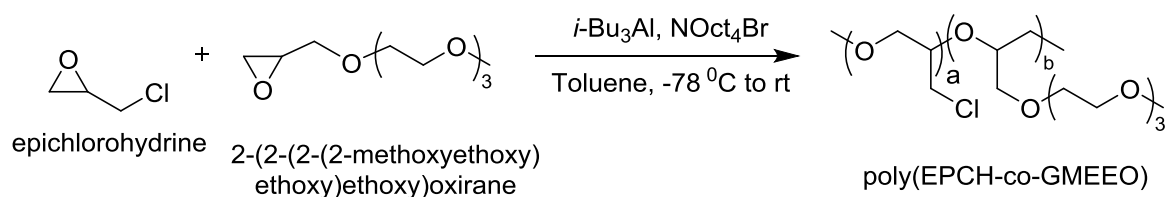### 6.2.1.1.Synthesis of Poly(epichlorohydrin) Backbone [poly(EPCH)].

Synthesis of poly(epichlorohydrin) poly(EPCH) was carried out according to the previously published literature procedure[7] with some modifications (Scheme 6.1). First, dry epichlorohydrin (8.64 ml, 0.11 mol, [EPCH] = 3M) was dissolved in dry Toluene (23 ml) in a 200-mL Shlenck flask. Initiator (NOct$_4$Br)(0.17 g, 0.31 mmol) was added, and the reaction was stirred under N$_2$ for 5 min prior to three freeze-pump-thaw cycles. The reaction mixture was cooled with liquid nitrogen and catalyst i-Bu$_3$Al (1.72 ml, 1.7 mmol) was added using a syringe. Conversion was monitored using ^{1}H NMR spectroscopy. At the end of the reaction, a few drops of ethanol were added to quench the reaction. Toluene was removed by rotary evaporation, the resulting polymer was washed with 3% V/V HCl in ethanol, and the final product was dried under vacuum. The yield was 9.0 g (88%). ^{1}H NMR (CDCl$_3$, δ ppm): 3.58-3.67 (br, 1H), 3.69-3.79 (br, 4H).
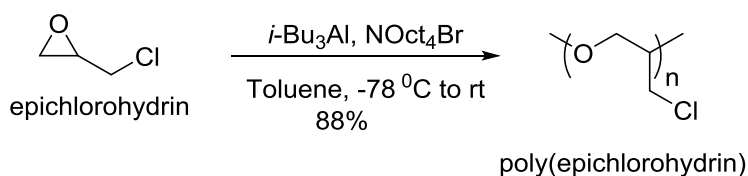
Scheme 6.1. Scheme for synthesis of poly(epichlorohydrin).

6.2.1.2. Proposed Synthesis of Poly(epichlorohydrin-*co*-glycidyl methoxyethoxyethoxy-oxirane) backbone [poly(EPCH-*co*-GMEEO)].

Poly(EPCH-co-GMEEO) can be synthesized in a procedure similar to that described above.[7] Epichlorohydrin and 2-(2-(2-(2-methoxyethoxy)ethoxy)ethoxy)oxirane can be copolymerized under the conditions shown in the Scheme 6.2 to get the desired polymer backbone.

Scheme 6.2. Scheme for synthesis of poly(EPCH-*co*-GMEEO).

6.2.1.3. Proposed Synthesis of Poly(glycidyl-*N,N* bis-(carboxymethyl)-L-lysine) [poly(GNTA)].
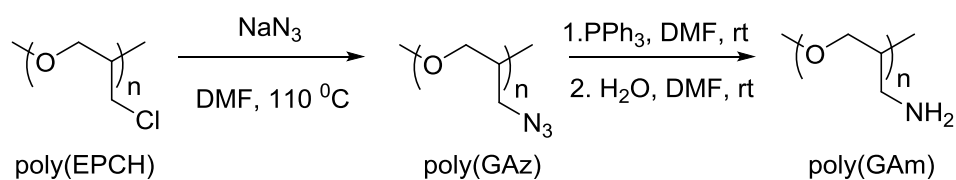
Poly(GNTA) can be synthesized as shown in Scheme 6.3 by simply reacting poly(ephichlorohydrine) with *N,N*-bis-(carboxymethyl)-L-lysine (Aminobutyl NTA) under basic conditions.
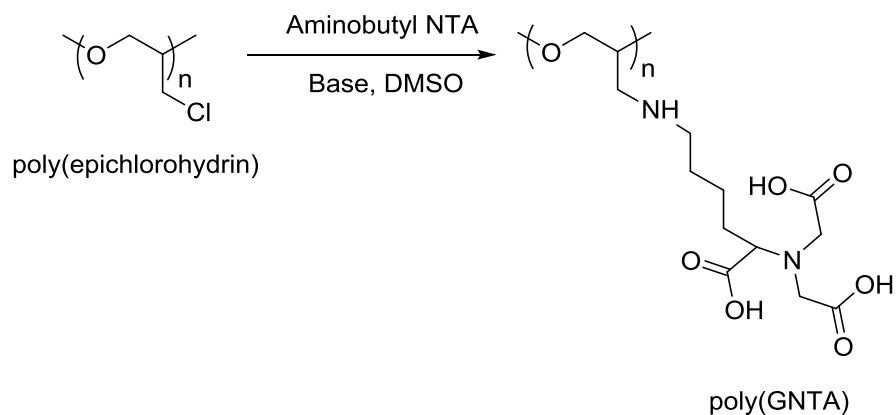
Scheme 6.3. Scheme for synthesis of poly(GNTA).

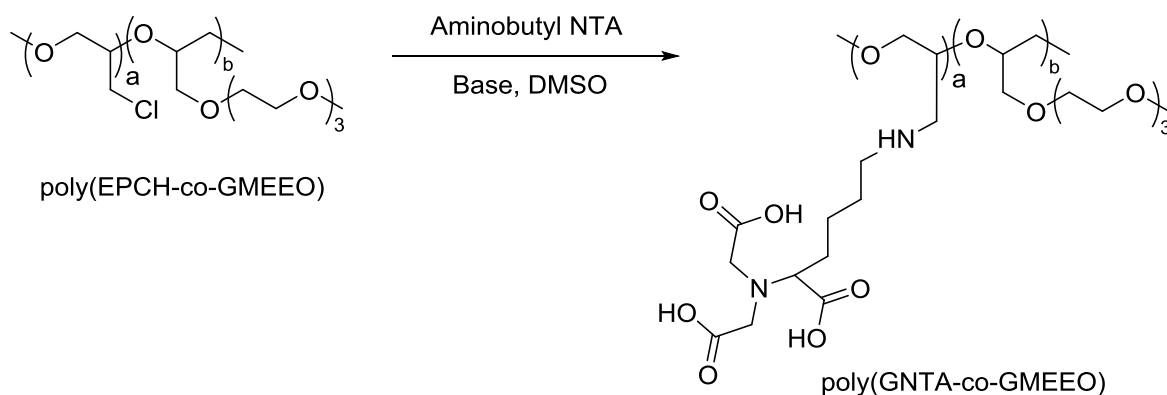### 6.2.1.4. Proposed Synthesis of Poly(glycidyl amine) [poly(GAm)].

Synthesis of poly(GAm) is already published in literature.[8] First poly(glycidyl azide) was synthesized as shown in Scheme 6.4. The resulting polymer, poly(GAz), was reacted with triphenyl- phosphine and water to get the final product poly(GAm).

Scheme 6.4. Scheme for synthesis of poly(GAm).

6.2.1.5. Proposed Synthesis of Poly(glycidyl-*N,N*-bis-(carboxymethyl)-L-lysine-*co*-glycidyl methoxyethoxyethoxyoxirane) [poly(GNTA-*co*-GMEEO)].

Poly(GNTA-*co*-GMEEO) can be synthesized as shown the Scheme 6.5 by simply reacting poly(EPCH-*co*-GMEEO) with *N,N*-bis-(carboxymethyl)-L-lysine (Aminobutyl NTA) under basic conditions.

poly(EPCH-co-GMEEO)

Aminobutyl NTA

Base, DMSO

poly(GNTA-co-GMEEO)

Scheme 6.5. Scheme for synthesis of poly(GNTA-co-GMEEO).

6.2.1.6.Proposed Synthesis of Poly(glycidylamine-*co*-glycidyl methoxyethoxyethoxy-oxirane) [poly(GAm-*co*-GMEEO)]

Poly(GAm-*co*-GMEEO) can be synthesized via a scheme similar to a literature procedure (Scheme 6.5).[8] First the azide intermediate can be synthesized by reacting poly(EPCH-*co*-GMEEO) with sodium azide under the condition shown in the Scheme

303

6.5. The resulting poly(GAz-*co*-GMEEO) can be undergo further reaction to give the desired product, poly(GAm-*co*-GMEEO).

poly(EPCH-co-GMEEO)　　　　　　poly(GAz-co-GMEEO)　　　　　poly(GAm-co-GMEEO)
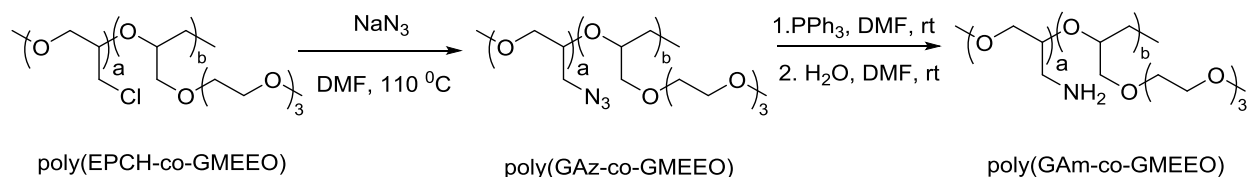
Scheme 6.6. Scheme for synthesis of poly(GAm-*co*-GMEEO).

6.2.2. Improving Porous Star-polymer Films for His-tagged Protein Binding, and a Proposed Method for Convenient Preparation of Highly Nanoporous PEMs.

The main problem with porous star-PAA/star-PDMAEMA films is their instability at pH 7.4 and, presumably, at higher pH values as well. This instability may stem from some deprotonation of PDMAEMA that begins around neutral pH. Quaternization of PDMAEMA will give the polymer in Figure 6.3A, and the permanent charge on this compound may enhance the stability of star-polymer films at neutral and high pH.
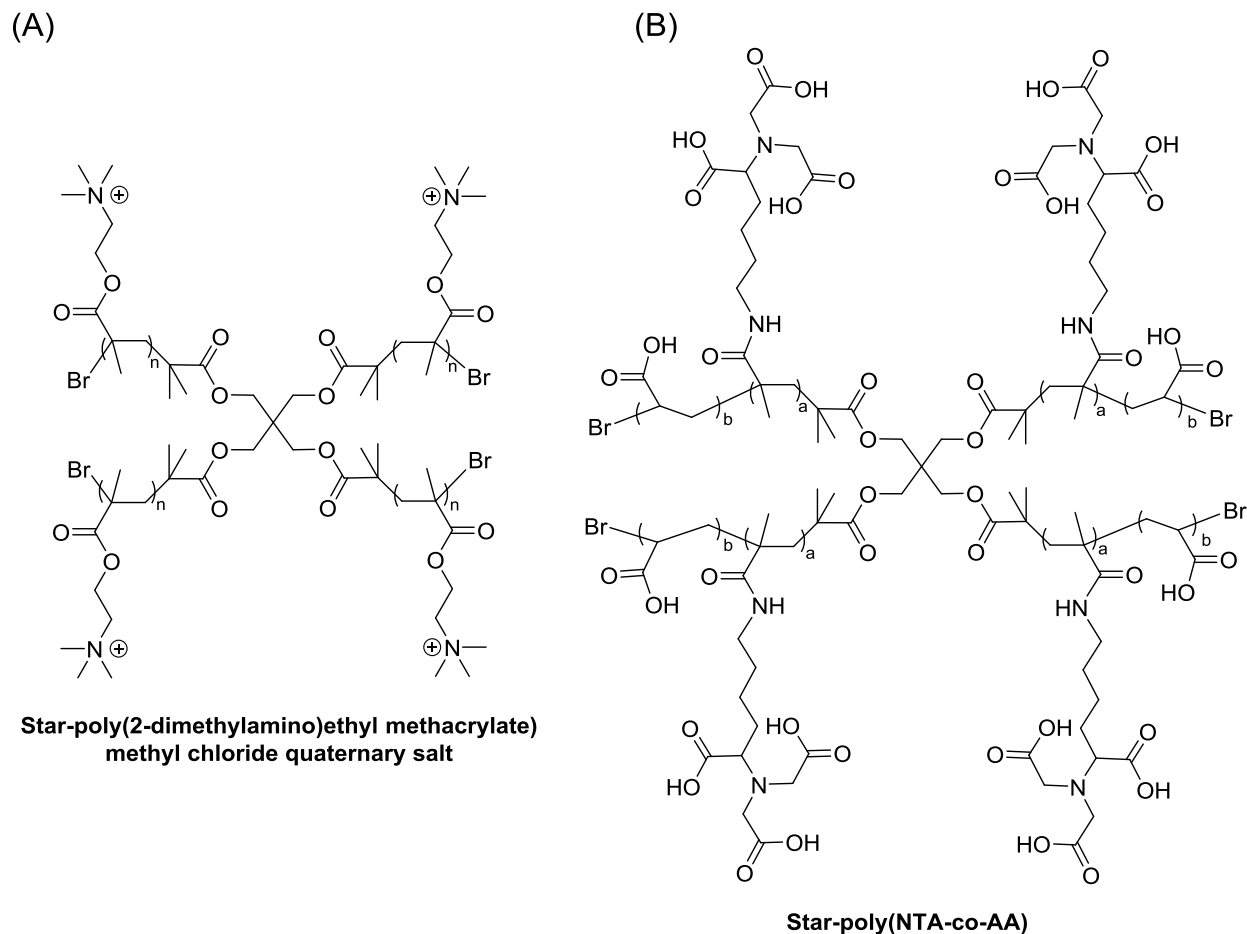
(A)

(B)

Figure 6.3. (A) Star-poly(2-trimethylamino)ethyl methacrylate) methyl chloride quaternary salt and (B) Star-poly(NTA-*co*-AA).

We also hope to employ star-polymer films for His-tagged protein binding. For this application, coupling of star-PAA with aminobuyl NTA will give the polymer in Figure 6.3B. Films prepared with these polymer will for metal-ion complexes to capture His-tagged protein.

The synthesis of star polymers requires multiple steps, and the porosity of star polymer films is not yet sufficient to greatly improve the surface area of the film. To overcome these challenges, we may apply film-formation techniques developed by

Chang Ming Li et al.[9] They showed that layer-by-layer adsorption of PAA (M_w 100000) and branched, high-molecular-weight PEI (BPEI, M_w= 750000) yield thick films when adsorption occurs at high pH for PEI and low pH for PAA. The thickness of these films increases exponentially with the number of layers. More importantly, the films show a highly nanoporous structure with well-defined double-scaled pore sizes (200 nm and nanopores 30 nm). After construction of the films, we could derivatize them with aminobutyl NTA to create films that bind His-tagged protein. High porosity should increase the kinetic and amount of protein binding.

REFERENCES

REFERENCES

(1)   Wijeratne, S.; Bruening, M. L.; Baker, G. L. *Langmuir* **2013**, *29*, 12720-12729.

(2)   Sheng, C.; Wijeratne, S.; Cheng, C.; Baker, G. L.; Bruening, M. L. *J Membrane Sci* **2014**, *459*, 169-176.

(3)   HisTrap FF crude for faster purification of histidine-tagged protein. http://www.gelifesciences.com/webapp/wcs/stores/servlet/ProductDisplay?categoryId=11448&catalogId=10101&productId=19665&storeId=11787&langId=-1 (accessed July 16, 2015).

(4)   Ning, W.; Wijeratne, S.; Dong, J.; Bruening, M. L. *Acs Appl Mater Inter* **2015**, *7*, 2575-2584.

(5)   Ma, Y.; Dong, J.; Bhattacharjee, S.; Wijeratne, S.; Bruening, M. L.; Baker, G. L. *Langmuir* **2013**, *29*, 2946-2954.

(6)   Uhlig, K.; Madaboosi, N.; Schmidt, S.; Jager, M. S.; Rose, J.; Duschl, C.; Volodkin, D. V. *Soft Matter* **2012**, *8*, 11786-11789.

(7)   Carlotti, S.; Labbé, A.; Rejsek, V.; Doutaz, S.; Gervais, M.; Deffieux, A. *Macromolecules* **2008**, *41*, 7058-7062.

(8)   Meyer, J.; Keul, H.; Möller, M. *Macromolecules* **2011**, *44*, 4082-4091.

(9)   Yuan, W.; Li, C. M. *Chemical Communications* **2010**, *46*, 9161-9163.